이학박사 학위논문

Assessment of biogeochemical fate of organic pollutants in marine ecosystems and identification of their ecotoxicological responses by the first principles modeling

해양생태계 내 유기오염물질의 생지화학적 거동 평가 및 제일원리기법에 기반한 생태독성 반응 규명

2022년 8월

서울대학교 대학원

지구환경과학부

김 태 우

Assessment of biogeochemical fate of organic pollutants in marine ecosystems and identification of their ecotoxicological responses by the first principles modeling

지도 교수 김 종 성

이 논문을 이학박사 학위논문으로 제출함

2022년 8월

서울대학교 대학원

지구환경과학부

김 태 우

김태우의 이학박사 학위논문을 인준함

2022년 8월

위 원 장 _____ (인)

부위원장 _____ (인)

위 원 _____ (인)

위 원 _____ (인)

위 원 _____ (인)

ABSTRACT

The marine environment is subject to a broad range of adverse impacts from anthropogenic activities. Among the marine environment, an intertidal zone maintains a balance as a buffer between the land and the sea from the introduction of organic pollutants, including nutrients (total nitrogen, TN; total phosphorus, TP), hydrocarbons (oil and polycyclic aromatic hydrocarbons, PAHs), alkylphenols (APs+APEOs), and styrene oligomers (SOs). The fate of organic pollutants in the marine environment is highly dependent on their physicochemical properties. Due to their hydrophobicity and particle reactivity, many organic pollutants have concentrations in sediments that are several orders of magnitude greater than those in the surrounding water. As a result, sediments are frequently regarded as the final destination for pollutants in the environment. Thus, it is crucial to estimate the restoration capacity and ecotoxicological effect of organic pollutants in the marine environment to maintain environmental services. Until this study, the restoration ability of organic pollutants in the intertidal zone was not quantitatively known, and the chemical, toxicological and ecological reactions occurring during the restoration process were not predicted. In this study, the ecological processes occurring in sediments being purified were identified quantitatively using an enhanced integrated sediment quality triad (SQT) approach with an enclosed experimental scale study (mesocosm). Additionally, using an in silico study, by examining the physico-chemical properties of organic pollutants, the causes of the restoration and ecotoxicity were analyzed. For evaluating the specific recovery of the benthic community health from the organic pollutants, instrumental analysis, bioassays, and investigation of the benthic community structure were also implemented.

The mudflat sediments significantly removed waterborne organic pollutants to background levels in ~2 and 6–7 days for TP and COD (chemical oxygen demand), respectively. This rapid removal of organic matters by natural sediments could be attributed to the microbe community degrading the corresponding pollutants. The temporal trend and removal efficacy for COD and TP were found to be similar between the bare tidal flat and salt marsh. Meantime, it was noteworthy that the salt marsh removed waterborne DIP much more quickly and efficiently, implying a high affinity of the halophyte on dissolved forms of organic matters. Of note, sedimentary organic sink prevailed in a defaunated condition under the lesser bioturbation effect.

Physical and biological remediation techniques were compared to natural attenuation for the removal of residual oil using a 60-day mesocosm experiment with SQT. First, physical treatment of hot water + high pressure flushing maximally

removed residual oils (max=93%), showing the greatest recovery among the SQT variables (mean=72%). Physical cleanup generally involved adverse effects such as depression of the microphytobenthic community during the initial period. Next, biological treatments, such as fertilizer, emulsifier, enzyme, and augmentation of the microbes, all facilitated the removal of oil (max=66%) enhancing the ecological recovery. Natural attenuation with "no treatment" showed a comparable recovery to the other remediations (max=54%). During the experimental periods, the dynamics of the benthic community were presented. Artificial remediation techniques showed a better efficacy as indicated by the SQT parameters (mean=47%). Natural restoration was also often as efficient as most active restoration alternatives and was cost-effective while minimizing the impacts on benthic communities.

Contaminated sediments were transplanted into the site tidal flats to confirm the PTS specific restoration in the tidal flat and their ecotoxicological effects. A 60-day in situ mesocosm study was implemented to quantify the restoration capacity using the SQT. Contaminated sediments recovered rapidly through bio-irrigation and phytoremediation (max. recovery: 71.2%). Machine learning classified the sedimentary qualities of the natural restoration process into four groups. During the 60-day sediment recovery period the benthic community changed through four stages. The reduction of parent compounds of PTSs (high molecular weight PAHs, STs, and APEOs) progressed primarily through bio-irrigation and phytoremediation. The results show that the presence of macrofauna and macrophytes in the tidal flat can promote the degradation of parent compounds with a rapid reduction of toxicity.

The influence of the dipole-driven orientation and the resulting directional configuration of the organic pollutants on the predicted reactivity to the media (seawater, sediment, and marine organisms) were investigated. Using physico-chemical properties calculated by ab initio density functional theory, directional reactivity factors (DRF) were devised as the main indicators of reactivity, linking the interaction between the organic pollutants and the media. The directional reactive model was applied to predict the variation of the aryl hydrocarbon receptor (AhR)-mediated toxic potencies among homologues of chrysene with structural modifications such as the number of constituent benzene rings, methylation, and hydroxylation. The results of this study explain why the toxic responses of the parent and metabolites of the organic pollutants were different. Moreover, the results of the predictive models were consistent with the empirical potencies determined by the use of the H4IIE-*luc* transactivation bioassay. An experiment-free approach based on first principles would provide an analytical framework for estimating the molecular reactivity in silico and complements conventional empirical approaches for studying

molecular initiating events in adverse outcome pathways.

Because the advanced DRF model was calculated for the interaction between organic pollutants and media, quantitatively calculations for the dynamical mechanism were used for applying the potential toxicity prediction model. Using molecular dynamics (MD) analysis, given the possibility of AhR-organic pollutants binding (conjugated state), it was confirmed that the directional reactive binding factor (DRBF) could be a mechanistic predictive index linking molecular ligand-receptor binding to in vitro toxicity. The DR model accurately estimated the toxic potency of a set of 16 similar PAHs, as confirmed by the H4IIE-*luc* bioassay. The first application of DRF to the prediction of potential toxicity implies that the physico-chemical properties of organic pollutants can be a major driving factor in the reaction with a medium, and the in silico method will provide important basic data for predicting the restoration and ecotoxicity of organic pollutants in the future. To summarize the above study results, first, the concentration of organic pollutants introduced into the intertidal zone showed a rapid decrease in the initial stage overall, and the decomposition of the parent material proceeded actively. Second, with the decrease of the concentration of the organic pollutants, the potential toxicity of the sediment also decreased rapidly, and the rate of decrease was faster than the decrease of the concentration of the organic pollutants. Third, the benthic cluster recovered exponentially, and there was a difference in each recovery rate according to the trophic level. Fourth, it was confirmed that the differences in chemical, toxicological, and ecological recovery were affected by the physicochemical properties of the organic pollutants. Finally, the DRF in this study could be developed into a DRBF predicting the potential toxicity and corresponded to the results of the in vitro bioassay. An integrated approach for understanding the restoration capacity and ecotoxicological effects of organic pollutants in this study can be useful for interpreting the chemical, toxicological, and ecological responses. In the future, to systematically manage coastal waters with severe contamination of benthic sediments, continuous development of ecological risk assessment techniques is required. In the future, to reconsider the value of ecosystem services in the intertidal zone of Korea and systematically manage coasts, the above interdisciplinary approach is continuously needed.

Keywords: Organic pollutants, Restoration capacity, Ecotoxicological effect, Benthic community, Seidment quality triad, Density functional theory

Student Number: 2018-39302

TABLE OF CONTENTS

LIST OF ABBREVIATIONS

1HC	1-hydroxychrysene
1MC	1-methylchrysene
2HC	2-hydroxychrysene
2MC	2-methylchrysene
3HC	3-hydroxychrysene
3MC	3-methylchrysene
Ace	Acenaphthene
Acl	Acenaphthylene
AhR	Aryl hydrocarbon receptor
Aluminum	Al
ANCOVA	Analysis of covariance
ANN	Artificial neural networks
Ant	Anthracene
AOPs	Adverse outcome pathways
APs	Alkylphenols
ARNT	AhR nuclear translocator
B3LYP	Becke three-parameter Lee-Yang-Parr
BaA	Benzo[*a*]anthracene
BaC	Benzo[*a*]chrysene
BaP	Benzo[*a*]pyrene
BAT	Best available technique
BbC	Benzo[*b*]chrysene
BbF	Benzo[*b*]fluoranthene
BcC	Benzo[*c*]chrysene
BghiP	Benzo[*g*,*h*,*i*]perylene
BkF	Benzo[*k*]fluoranthene
BT	Bare tidal flat
BTm	Bare tidal flat + macrofauna
C. sinensis	*Cyclina sinensis*

CGenFF	CHARMM General Force Field
Chl-*a*	Chlorophyll a
Chr	Chrysene
COD	Chemical oxygen demand
DahA	Dibenzo[*a*,*h*]anthracene
DbdC	Dibenzo[*b*,*d*]chrysene
DBF	Directional binding factor
DdpC	Dibenzo[*def*,*p*]chrysene
def2-TZVPP	polarized triple-zeta valence
DFT	Density functional theory
DIP	Dissolved inorganic phosphorus
DM	Dipole moment
DOS	Density of state
DR	Directional reactive
DRBF	Directional reactive and binding factor
DRE	Dioxin-responsive element
Ea	Economic availability
EA-IRMS	Element analyzer-isotope ratio mass spectrometer
EC50	Half-maximal effective concentration
EM	Effective microbes
Ep	Environmental performance
expDRF	Exponential DRF
F2	Fraction 2
F3	Fraction 3
Fe	Iron
FE	Fertilizer + emulsifier
FEM	Fertilizer + emulsifier + microbe
FL	Flushing
Fla	Fluoranthene
Flu	Fluorene
FMeM	Fertilizer + multi-enzyme + microbe
FMO	Frontier molecular orbitals

GC-MSD	Gas chromatograph equipped with a mass selective detector
GEq	Gravel equivalent
Glu	Glutamate
H4llE-*luc*	H4llE-luciferase
HCL	Hydrochloric acid
DahA	Dibenzo[*a*,*h*]anthracene
DbdC	Dibenzo[*b*,*d*]chrysene
DBF	Directional binding factor
HI	Hydrocarbon index
His	Histidine
HMs	Heavy metals
HMW	High molecular weight
HOMO	Highest occupied molecular orbital
HOPG	Highly oriented pyrolytic graphite
HW/HP	Hot water-high pressure
IcdP	Indeno[*1*,*2*,*3*-*cd*]pyrene
IRFMN	Instituto di Ricerche Farmacologiche Mario Negri
ITOPF	International Tanker Owners Pollution Federation
LBD	Ligand binding domain
LFEM	Linear free energy model
LOE	Line of evidence
LUMO	Lowest unoccupied molecular orbital
M. japonicus	*Macrophthatmus japonicus*
MA	Manual hand wiping
MAUT	Multi-attribute utility theory
mCd	Degree of contamination index
MD	Molecular dynamic
MDL	Method detection limit
MO	Molecular orbital
MOA	Mode of action
MPB	Microphytobenthos
Nap	Naphthalene

NEXAFS	Near edge X-ray absorption fine structure
NT	No treatment
OM	Organic matter
OUT	Operational taxonomic unit
P. australis	*Phragmites australis*
PAHs	Polycyclic aromatic hydrocarbons
PAS	Per-Arnt-Sim
PCBs	Polychlorinated biphenyl
Phe	Phenanthrene
PHL	Restoration half-life
PME	Particle-Mesh-Ewald
PTSs	Persistent toxic substances
Pyr	Pyrene
QIIME	Quantitative Insights into Microbial Ecology
QSAR	Quantitative structure activity relationship
RDP	Ribosomal Database Project
rRNA	Ribosomal ribonucleic acid
SM	Salt marsh
SMA	Special management area
SMm	Salt marsh + macrofauna
SOM	Self-organizing map
SOs	Styrene oligomers
SQT	Sediment quality triad
STs	Stryene trimers
Ta	Technical applicability
TCDD	2,3,7,8-Tetrachlorodibenzo-*p*-Dioxin
TDDFT	Time dependent density functional theory
TN	Total nitrogen
TOC	Total organic carbon
TP	Total phosphorus
TPH	Total petroleum hydrocarbons
TPLMS	Total pollution load management system

UCM	Unresolved complex mixture
V. fischeri	Vibrio fischeri
VA	Vibrational amplitude

LIST OF TABLES

LIST OF FIGURES

CHAPTER 1.

INTRODUCTION

1.1. Backgrounds

An intertidal flat in a marine environment maintains a balance between the land and the sea. This characteristic, such as the role of the buffer zone, can make the intertidal flat easily exposed to a variety of threats from land and sea (e.g., rapid development, damming and modification of a large river, and oil spill accidents) (Kim et al., 2020) (Figure 1.1). Industrial, agricultural, and other anthropogenic activities have led to the introduction of thousands of pollutants, most of them synthetic organic pollutants, into the marine environment (Yang et al., 2020; Yoon et al., 2020; Hwang et al., 2021). A fraction of these organic pollutants are chemicals that have become a major concern in the marine environment because of their persistence, toxicity, bioaccumulation tendency, and susceptibility to long-range transport. Traditionally, much attention has been given to a few families of nutrients such as total phosphorus (TP), total nitrogen (TN), and other organic materials that are oxidized (denoted as chemical oxygen demand, COD) (Kim et al., 2020; Kwon et al., 2022). In recent years, land-driven persistent toxic substances (PTSs) have been the major cause of pollution. PTSs such as polycyclic aromatic hydrocarbons (PAHs), alkylphenols and alkylphenol ethoxylates (APs+APEOs), heavy metals (HMs), and styrene oligomers (SOs) are primarily targeted due to their ecotoxicity (carcinogenic and endocrine disrupting effects) and have negative effects on the marine ecosystem (Yoon et al., 2019). Of note, after a sudden event such as an oil spill, total petroleum hydrocarbons (TPH) are also considered one of the most markedly harmful substances nowadays (Hong et al., 2020; Yim et al., 2020; Kim et al., 2022).

Tidal flats provide essential marine ecosystem services, including not only shoreline protection but also water quality improvement (Table 1.1) (Okata et al., 2021). An imbalance between the loads of organic pollutants and natural restoration capacity in the tidal flats could change the role of sediments from a source of nutrients to a purifier (Kim et al., 2020). The activities of various marine organisms, such as bacterial degradation, bio-irrigation by macrofauna, and phytoextraction in the tidal flat, promote the cycling of organic pollutants in the sediment (Kwon et al., 2022). While previous studies on the role of tidal flats have mainly focused on various media (sediment, seawater, and fauna) and cycles of material, there are few studies that have quantitatively revealed the contribution and effect of various

restoration processes involved in the removal of organic pollutants (Kim et al., 2020).

Predicting the results of restoration capacity for organic pollutants in an intertidal flat is not only very important but also very difficult. Understanding and predicting the ecological responses of the load of organic pollutants necessitate the use of multiple and complementary approaches (Lee et al., 2019, Lee and Khim, 2022). The reason is partly because it involves changes in chemical, toxicological, and biological variations. That is why the sediment quality triad (SQT) approach is useful to identify the status of contaminated sediments, and this approach comprises an independent assessment of the ecotoxicological risk. The traditional SQT method has been improved with technological advances in chemical, toxicological, and ecological factors, going through many phases so far. Advances in chemical and toxicological technologies have enabled indirect confirmation of the effects of contaminated sediments. On the other hand, as for ecological components, there have been developments to confirm the ecotoxicological effect of bacteria on macrofauna up to now, but studies that confirm all marine benthic organisms are still insufficient (Figure. 1.2). Additionally, until now, SQT did not account for changes in contaminated sediments during the restoration process because it mainly focuses on the transient sediment status of original and degraded ecosystems (Figure. 1.3).

Furthermore, the causality for all these variables, on average, was difficult to identify because they were time- and site-dependent and depended on inferential data (Lee et al., 2019). Experiments can reveal causality and the underlying mechanisms, but they are inevitably simplifications of the studied systems, particularly when conducted on small spatial and temporal scales. A more integrated approach that encompasses these different methods is needed, together with larger-scale experiments that can support realistic levels of biocomplexity: microcosm–mesocosm studies (Kim et al., 2022).

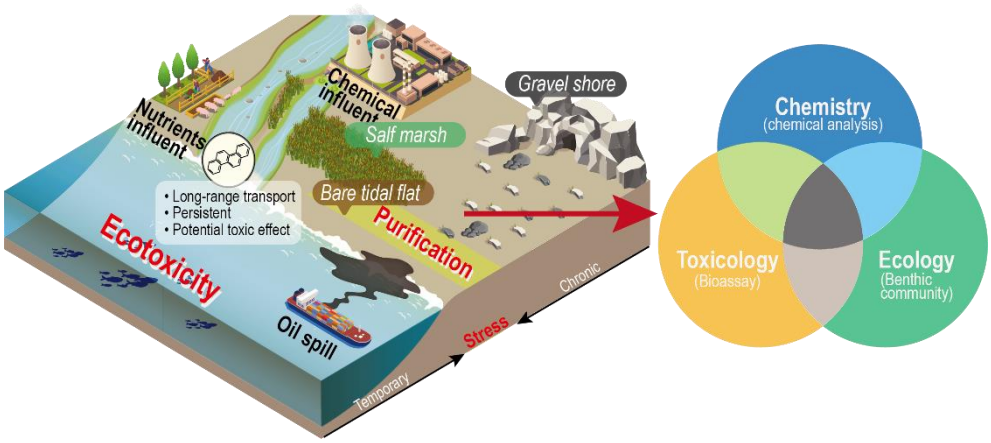

Figure 1.1.
Illustration of sources of various pollutants in the coastal environment and a tidal flat as a role of buffer zone.

Table 1.1.

[a] List of ecosystem services provided by intertidal flat.

Service category	Service	Specific content of services provided
Provisioning	Food provision	Supplying seafood as food
Regulating	Water quality improvement	Organic matter decomposition
	Global warming mitigation	Carbon storage in organism and sediment
Cultural	Recreation	Marine leisure
	Environmental education	Environmental education
	Research	Research
	Historical site	Festivals and rituals
	Relaxation	Rest and relaxation
Supporting	Species conservation	Existence of diverse species

[a] Okada et al. (2021)

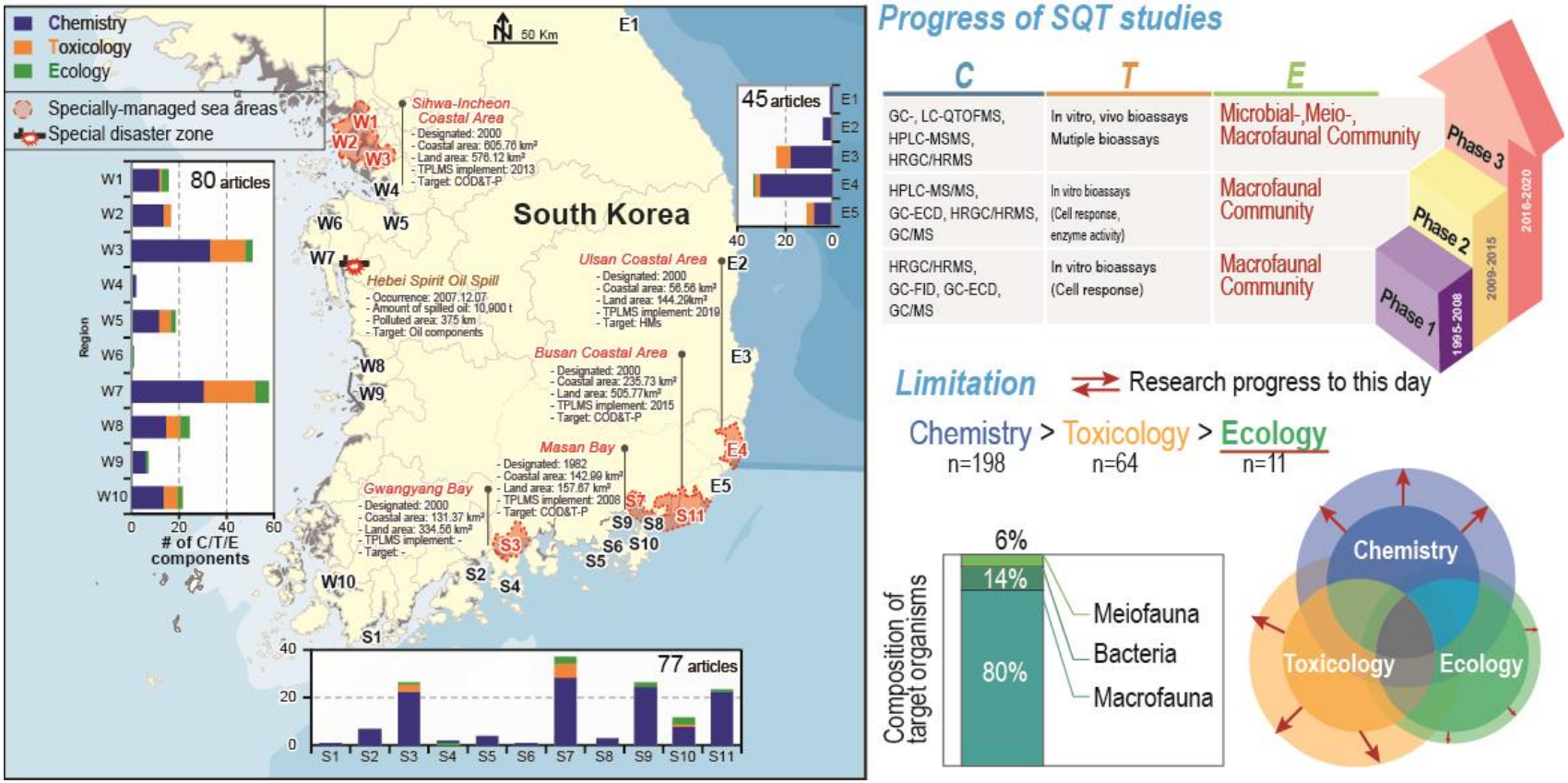

Figure 1.2.
Study efforts of SQT approach: lack of ecological approach (modified from Lee et al., 2022)

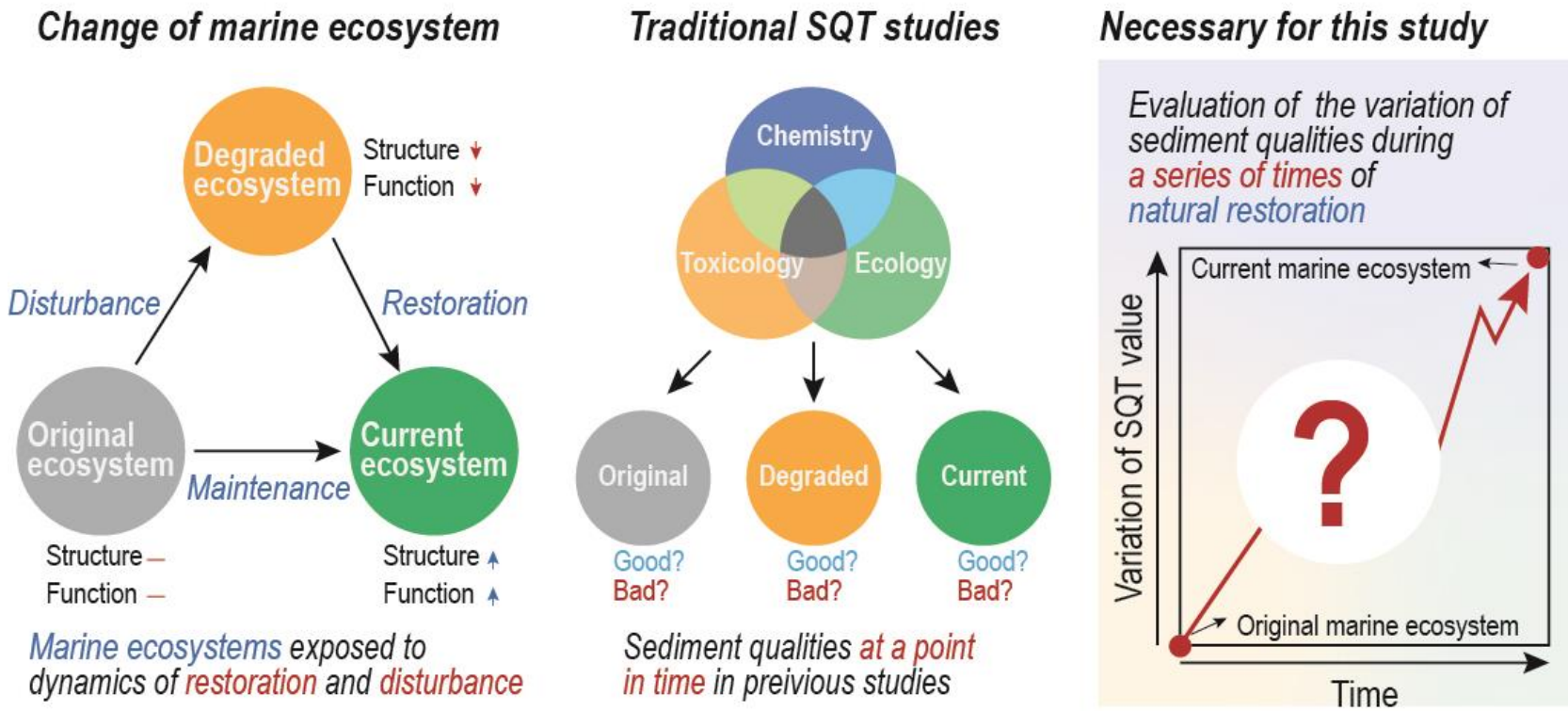

Figure 1.3.
Study efforts of SQT approach: lack of the time seires SQT studies

Once organic pollutants enter the water column in a marine environment through a continuous and/or temporary influx, they undergo a series of environmental processes that are related to the marine carbon cycle (Figure 1.4). The fate of organic pollutants in the marine ecosystem depends to a great extent on their physico-chemical characteristics (Kim et al., 2019) (Figure 1.5). Their hydrophobicity and particle reactivity result in the concentrations of many organic pollutants in sediments being several orders of magnitude higher than those in the overlying water (Shi et al., 2021). As such, sediments are often considered a terminal sink for pollutants in the environment. It is well known that organic pollutants accumulated in sediments adversely impact benthic ecosystems in a variety of ways (Kim et al., 2017, Yoon et al., 2019, Yoon et al., 2021, Park et al., 2022).

The concentration of organic pollutants increases at some of the steps in the food chain. An issue that has received increasing attention during the last few decades is the effect of organic pollutants on the first steps of the trophic web, phytoplankton, bacteria, and zooplankton. This process, which exposes animals at high trophic levels in the food web to doses, can affect such things as endocrine disruption, altered neurological development, immune system modulation, and carcinogenesis (Kim et al., 2019, Lee et al., 2020, Yoon et al., 2022, Cha et al., 2021, Cha et al., 2022 Lee et al., 2022). Accumulated organic pollutants can have ecotoxicological effects on cells, tissues, and even communities within marine organisms (Figure 1.6).

Various investigations of the physico-chemical properties of organic pollutants have been performed for identifying the impact of organic pollutants in advance (Kim et al., 2020). Knowledge of the physicochemical properties of potential chemical alternatives is a requirement of the alternative assessment process for two reasons. First, the inherent hazard of a chemical, such as its capacity to interfere with normal biological processes and its physical hazards and environmental fate (degradation and persistence) are determined by its intrinsic physicochemical properties and the system with which it is interacting. For organic and inorganic chemicals, these intrinsic properties are determined by molecular structure, while for materials, they are determined by composition, size, structure, and morphology. Second, physicochemical properties can be used to eliminate from consideration

chemicals that are likely to exhibit particular physical or toxicological hazards. As important as these data are, obtaining them is relatively fast and inexpensive and can be readily done at the initial stages of the alternative assessment.

For example, in toxicology, toxicity testing is under increasing pressure to meet several competing demands: i) test a large number of existing chemicals, many of which lack basic toxicity data; ii) test an increasing number of new chemicals and novel materials; and iii) reduce the cost and time required for chemical safety evaluation (Lee et al., 2019, Lee et al., 2020, Kim et al., 2020). However, despite the obvious advantages of in vitro assays for the determination of toxicological profiles of sediments, results of in vitro bioassays can explain only a small portion of the overall toxic potencies in extracted samples and are limited with respect to predicting the in vivo toxicity. Therefore, methods for predicting toxicity using the molecular characteristics of organic pollutants are being developed rather than bioassays that have no choice but to depend on the characteristics of cells and animals. From cell-based in vitro studies to high-throughput computational techniques, these newer approaches focusing on both hazard identification and the physico-chemical properties of organic pollutants have led to new understandings about the potential impacts of chemicals on the environment.

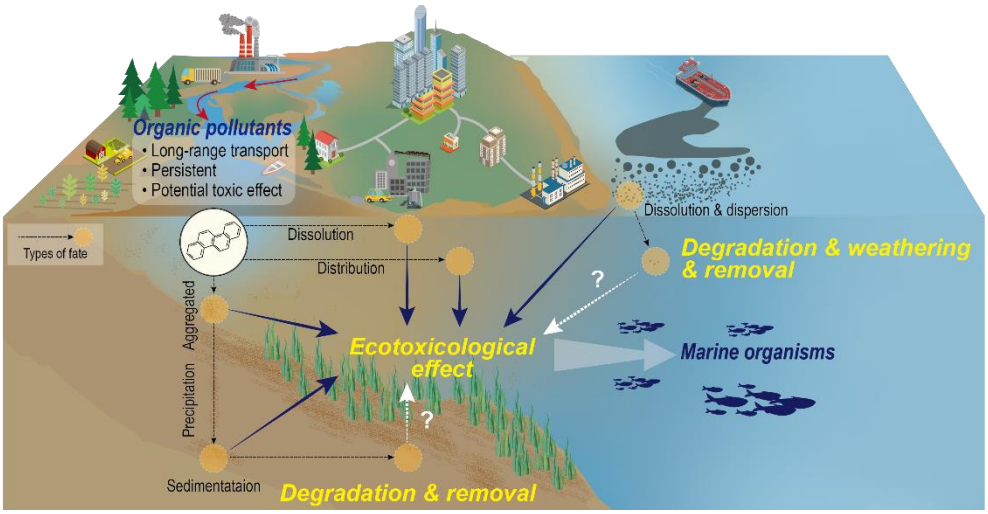

Figure 1.4.
Fate of organic pollutants in the marine environment.

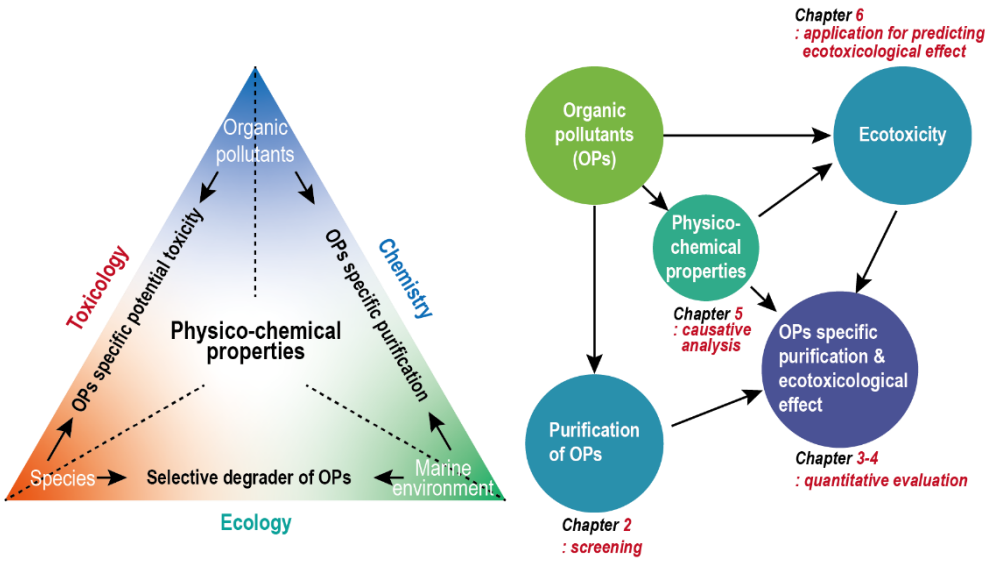

Figure 1.5.
Effect of physico-chemical properties of organic pollutants to their fate in marine environment.

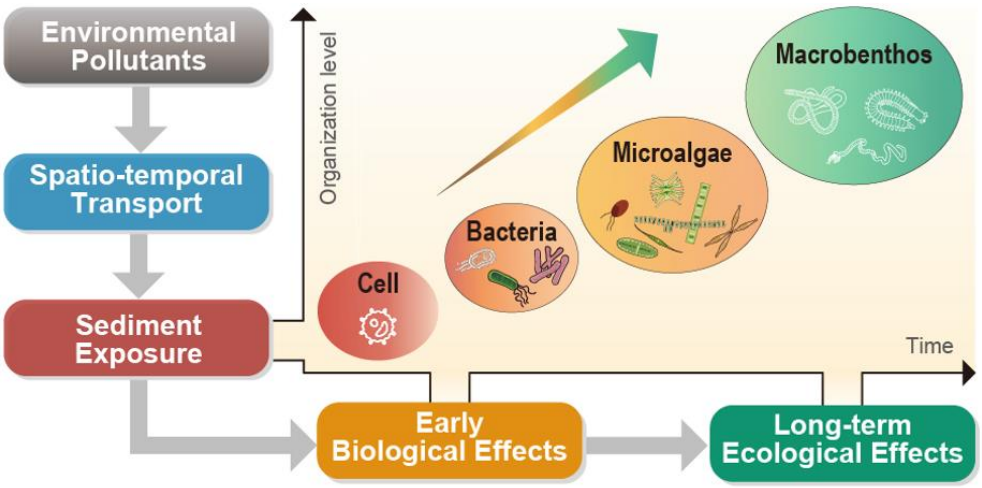

Figure 1.6.
A stepwise effect of environmental pollutants from cell to macrobenthos community.

In recent years, many computational models (e.g., in silico) have been developed for the prediction of ecotoxicity (Kim et al., 2020, Cha et al., 2022). In silico methods encompass a wide variety of computational tools: databases for storing data about chemicals, their toxicity, and chemical properties; molecular descriptors; simulation tools for systems biology and molecular dynamics; and modeling methods for toxicity prediction (Table 1.2). To understand the reaction between toxicants and bio-organisms, understanding the basic mechanisms by which those physico-chemical properties come about has been emphasized. Among the various properties, their electronic states, which are a result of the behavior of electrons, could be determined first in consideration. Representatively, first-principles theory (calculation) is an essential tool for predicting a significant portion of the properties of a given material by determining the electronic states in materials. The electronic states are calculated entirely from the atomic species and their positions in the compounds using computation. Empirical parameters are not necessary to obtain results in agreement with experiments; certain materials could be calculated with confidence. In other words, first-principles, which are often synonymous with density functional theory (DFT), could be used to understand existing compounds in advance of experimentation and predict the optimal composition (Forrest et al., 2014, Kim et al., 2020).

Overall, in this dissertation, the chemical, toxicological, and ecological responses of organic pollutants that occur during the restoration process were observed. Moreover, by broadly using physicochemical properties that define intrinsic reactivity, the phenomena were interpreted by understanding the interactions in the intertidal zone. Additional studies of the physicochemical properties of organic pollutants to interpret and discuss the causes of complicated interactions can be used to understand or predict the restoration in the intertidal zone for organic pollutants and their ecotoxicological effects, quantitatively.

Table 1.2.

The molecular descriptor used in the prediction toxicity of organic pollutants through in silico methods

Dimensional (D) descriptor	Examples
0D descriptors	Atom types, molecular weight, bond types
1D descriptors	Counts of atom types, counts of hydrogen bond donors or acceptors, number of rings, number of functional groups by type (element composition)
2D descriptors	Mathematical representations by graph theory or calculated values such as lipophilicity or topological polar surface area (topological PSA, number of H-bond acceptors, number of H-bond donors, logP, logD, solubility, number of rotatable bonds, number of molecular fragments, E-state index, topological index)
3D descriptors	Geometrical descriptors or polar surface area (polar surface area, molecular surface area, molecular volume)

1.2. Objectives

This dissertation evaluated the restoration capacity in marine ecosystems and the ecotoxicological effects of organic pollutants by in silico to in situ study and presented the results in Chapters 2 to 6. Key questions that required resolving or clarification, along with specific objectives and workflow, are stated as follows (Table 1.3 and Figure 1.7):

1. **Chapter 2**

   Evaluation of the natural restoration capacity of tidal flat sediments for organic matter- and nutrient-stressed water (TP, TN, and COD) using an indoor microcosm (experimental scale: < 1 m^2).

2. **Chapter 3**

   Various remediation techniques for removing residual oil on rocky shores after oil spill events and examining the effectiveness of each technique with an indoor mesocosm (experimental scale: > 3 m^2).

3. **Chapter 4**

   Evaluation of the natural restoration capacity of a tidal flat for organic pollutants in sediments and the change in the health of the benthic community during the restoration with an in-situ mesocosm (experimental scale: > 10 m^2).

4. **Chapter 5**

   The fate of organic pollutants on the toxicity response and bio-physical communication model estimating their potential toxicity using an in-silico study (experimental scale: < 10^{-11} m).

5. **Chapter 6**

   A novel probabilistic approach to the fate of organic pollutants on binding to receptors of cells by developing a bio-physical communication model that estimates their potential toxicity using an in-silico study (experimental scale: < 10^{-11} m).

Finally, conclusions, including a summary, environmental implications and limitations, and future research directions are provided in Chapter 7.

Table 1.3.

Summary of the key questions that have not been resolved or clarified in previous researches on the natural restoration capacity and ecotoxicity of organic pollutants in the marine environment. Approaches and objectives for each Chapter are suggested.

Subject		Key question	Ch.	Approach & Target
I	Screening restoration capacity of nutrients	**Quantification** of restoration capacity of tidal flat to nutrient in seawater? *(Bare tidal flat vs. salt marsh)*	**2**	**In door microcosm** Nutrient (TP, TN, and COD)
II	Evaluation of the change of SQT values during the restoration from oil spill	**Effectiveness** of natural restoration capacity to oiled sediment? *(Natural attenuation vs. remediation techniques)*	**3**	**In door mesocosm** Residual oil (TPH, UCM)
III	Evaluation of the change of SQT values during the restoration in the contaminated sediment by PTSs	Increase of restoration capacity by **bio-irrigation and phytoremediation** in tidal flat? *(Bio-irrigation vs. phytoremediation)*	**4**	**In situ mesocosm** PTSs (PAHs, APs, and SOs)
IV	Determination of reactivity of parent PAHs and their metabolites	Any **driving factors** in ecotoxicological effects when PTSs response to organism? *(Physico-chemical properties of organic pollutants)*	**5**	**In silico/ computation** PTSs (PAHs)
V	Application of reactivity of PAHs to predict biological activity	**Possibility** of ecotoxicological effects when PTSs response to organism? *(From statistical approach to probabilistic prediction)*	**6**	**In silico/ computation** PTSs (PAHs)

Chapter	Target	Period	Objectives	Approach
2	Nitrogen, phosphorus	14 d	Screening restoration capacity of tidal flat sediment for nutrients	*Effect analysis*
3	Iranian heavy crude oil	60 d	Evaluation of the change of SQT values during the restoration rom oil spill	
4	PAHs, APs, SOs, HMs	60 d	Evaluation of the change of SQT values during the restoration in the contaminated sediment by PTSs	
5	PAHs	< 3 d	Determination of reactivity of parent PAHs and their metabolites	*Causative analysis*
6	PAHs	< 7 d	Application of reactivity of PAHs to predict biological activity	

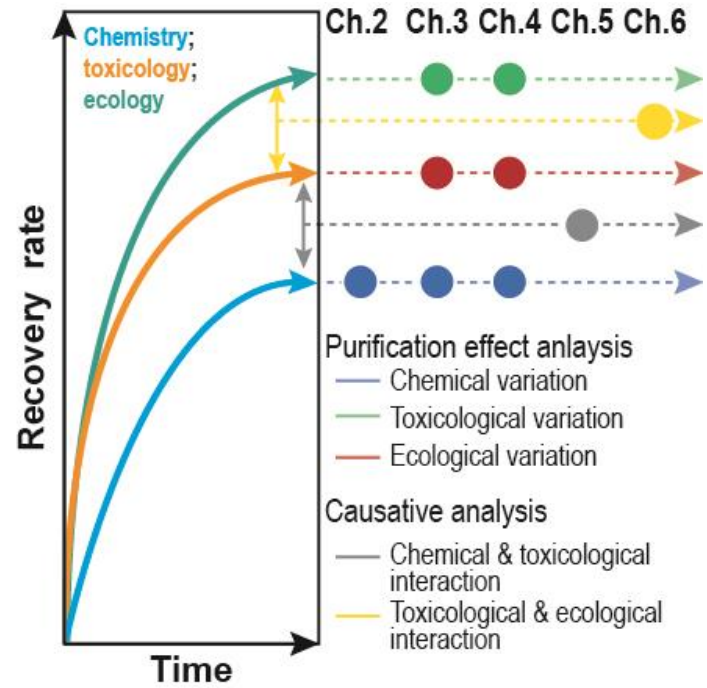

Figure 1.7.
Schematic plot for overview, target, and objectives in this study.

CHAPTER 2.

NATURAL RESTORATION CAPACITY OF TIDAL FLATS FOR ORGANIC MATTERS AND NUTRIENTS: A MESOCOSM STUDY

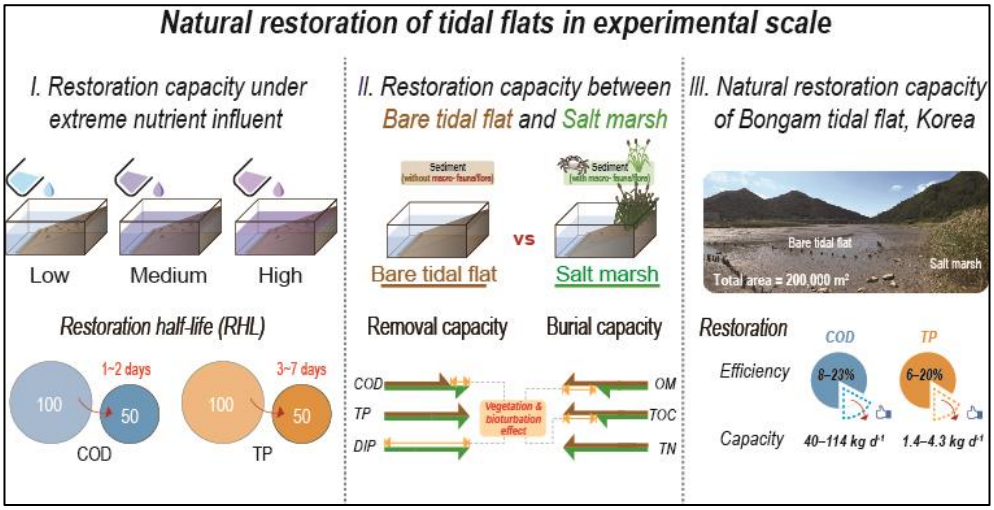

This chapter has been published in Marine Pollution Bulletin.
Kim, T., Noh, J., Kwon, B.-O., Lee, C., Kim, B., Kwon, I., Hong, S., Chang, G. S., Chang, W. K., Nam, J., Khim, J. S. Natural purification capacity of tidal flats for organic matters and nutrients: A mesocosm study. *Marine Pollution Bulletin* 2020, **154**, 111046. https://doi.org/10.1016/j.marpolbul.2020.111046

2.1. Introduction

Marine environments are currently experiencing intense pressure from anthropogenic driving forces due to high settlements along coastlines. Accordingly, increasing shortage of space and resources on land would cause the socio-economic demands for overexploitation to expand (Atkins et al., 2011; Borja and Dauer, 2008). Especially, tidal flat, where is the closest from the land, is one severely polluted region by discharge of various industrial and domestic effluents. Since marine sediment has been suggested as a final sink for organic pollutants, their continuing inputs to coastal areas can produce a wide range of deleterious effects on various marine lives. Such anthropogenic impacts include coastal eutrophication, harmful algal blooms, and declining aquaculture production and fisheries (Lee et al., 2018a; Hong et al., 2010). Thus, the role and function of tidal flat or salt marsh in the marine environment have been the subjects of recent intensive research in aspect of tidal flat's pollution control (Koo et al., 2011; Winberg et al., 2007; Yamochi, 2008).

Tidal flat is recognized as active buffer zone in the transport of nutrients and organic compounds between land and sea (Levin et al., 2001). Population growth, urbanization, and industrialization would augment organic matter and nutrient loads to the tidal flats. Imbalance between the pollutant loads and natural restoration capacity in tidal flats could change the role of coastal sediments from a source of nutrients to a purifier. The role of sediments in organic matter and nutrient cycling has been highlighted primarily from the standpoint of carbon and nutrient turnover (Hu et al., 2006). For example, the role of sediment microbes to degrade organic matters has been known to contribute the overall restoration function of tidal flats (Yagi and Terai, 2001). Several studies relating to the tidal flat restoration or artificial construction have also confirmed the ability of tidal flats to restorate the contraminated sediment by land-driven pollutants and nutrients (Hou et al., 2003; Lee et al., 1998). The results rekindled recent interest in restoration and protection of the tidal flat of Tokyo-Yokohama Bay in Japan (Hong et al., 2010) and the Atlantic and Pacific coasts as well as one along the Gulf of Mexico in USA (Turner et al., 2004). After restoration and protection of these tidal flats, some positive effects on increasing the distribution of living organisms and root biomass were documented (Furukawa, 2013).

Since the early 1980s, the Korean Ministry of Oceans and Fisheries have designated the so called "special management area (SMA)" to protect the marine environment and ecosystem under significant risk by environmental deterioration (MMAF, 2002). The SMA includes terrestrial areas that primarily contribute to marine pollution. Five coastal areas in Korea have been designated as SMAs to date, and Masan Bay was the first designated SMA in 1982 (Lee et al., 2016). To improve the water quality in SMAs, the Korean government has launched the Total Pollution Load Management System (TPLMS) and first applied it to Masan Bay in 2008. TPLMS contributed to the reduction of nutrients by sewer system improvement, technical upgrading of the two wastewater treatment plants (WWTPs), and an intensive river clean-up (Chang et al., 2012). However, despite substantial efforts, the concentrations of chemical oxygen demand (COD) and total phosphorus (TP), which are the water quality targets, have remained unchanged (Park et al., 2018). This issue drove the Korean government to implement various actions for enhancing the water-quality elements from prevention to post-treatment. Bongam tidal flat, situated in Masan Bay SMA, has received increasing public attention as it is the only tidal flat located in a trading port and has been damaged by the construction of industrial and housing complexes since the 1960s. Significant efforts have been recently devoted to restore the deteriorated Bongam tidal flat from industrialization and urbanization (Lee et al., 2020).

In the present study, we designed an enclosed experimental ecosystem (viz., mesocosm) to evaluate the restoration capacity of tidal flat sediments for waterborne organic matters and nutrients. Mesocosm has been suggested to have the potential to serve as a powerful tool for testing and expanding our understanding of the mechanisms that drive ecological dynamics in the coastal zone. The present study specifically aimed to 1) evaluate the restoration capacity of a tidal flat under extreme nutrient exposure, 2) compare removal rate of organic matters and nutrients between bare tidal flat and salt marsh, and 3) provide natural restoration capacity of the Bongam tidal flat of Korea, along with a mini-review.

2.2. Materials and Methods

2.2.1. Study design and development of mesocosm system

A mesocosm system was developed to simulate and control the tidal cycle of the intertidal area. A system consisted of three compartments; 1) one aquarium with sloped bare tidal flat and salt marsh bed, 2) the other aquarium serving as a reservoir of water during the tidal cycle, and 3) pump which controls the water transfer rate between two aquariums. From the aquarium containing the influent, the water is transferred to a sedimentary aquarium for 4 h and stays there for 2 h. The water was then transferred to the reservoir aquarium for 4 h. The two aquariums were mounted in a thermal water bath, where the temperature was maintained at 18 °C using a temperature control system (Table 2.1).

Two separate experiments were designed and conducted depending on the topic. First experiment aimed to evaluate the restoration capacity of organic matters and nutrients by the bare tidal flats. Three treatments (low, medium, and high groups) with varying initial waterborne concentrations of organic matters and nutrients were tested (Figure 2.1). The concentration gradients of organic pollutants were adjusted by having the sediment spiked with the standard materials (Glucose; KH_2PO_4, Sigma Aldrich). Of note, the initial COD concentrations in the low, medium, and high treatments were set to ~10, 15, and 40 mg L^{-1}, respectively. TPs in the corresponding treatments were set to ~0.1, 0.2, and 0.25 mg L^{-1}. Of note, the initial COD and TP given in the low treatment were about twice greater than those measured in influent water flowing into Bongam tidal flat in Masan Bay (Figure 2.2). Seawater sampling was carried out daily during 14 days of experiment to monitor the water quality (COD and TP).

Second experiment utilized the organic enriched sediments collected from study area, in order to address the restoration capacity of tidal flats (Figure 2.3). In particular, we focused on the evaluation of natural restoration in absence of faunal activities (viz., bioturbation) and under vegetated environment. Two treatments were tested; one for the defaunated sediment, simulating the bare tidal flat, and the other for the vegetated one, modifying salt marsh system. Of note, eight Phragmites australis plants covering one-third of the sloped sediment area (0.2 m^2) were transplanted to modify the natural vegetated density in the upper intertidal flat of study area. During the 6 days of experiment, both seawater and sediment samples were collected twice every day, considering tidal cycle (viz., inflow and outflow) and general water and sediment qualities are monitored, as described below.

2.2.2 Sampling and data analyses

Sediments and seawater samples collected from mesovcosm treatments (Figure 2.4) were analyzed following the standard methods described elsewhere (APHA-AWWA-WPCF, 1981; Lee et al., 2019). First, sediment samples were analyzed for total organic carbon (TOC), TP, and total nitrogen (TN). The sediment was decalcified with 10% hydrochloric acid (HCl), washed twice with deionized water, and freeze-dried for TOC determination. The TOC and TN were measured using an Elemental Analyzer-Isotope Ratio Mass Spectrometer (EA-IRMS) (Elementar, Gmbh, Hanau, Germany). The water samples were analyzed for various parameters, including, COD_{Cr}, TP, and dissolved inorganic phosphorus (DIP). T-test was carried out to determine the significant difference between the mesocosm experiments using Sigma Plot (Version 10.0, Chicago, IL).

Table 2.1. Comparison of physico-chemical properties of sediment and inflow water in mesocosm experiments on the bare tidal flat and salt marsh.

Media	Content	Bare tidal flat		Salt marsh	
		Results	SD	Results	SD
Seawater	Temperature (°C)	17.9	1.37	17.4	1.41
	pH	7.80	0.12	7.86	0.19
	Dissolved oxygen (mg L^{-1})	7.85	1.54	7.47	1.12
	Salinity (‰)	19.7	2.24	19.9	2.87
Sediment	Temperature (°C)	18.1	1.11	17.7	1.23

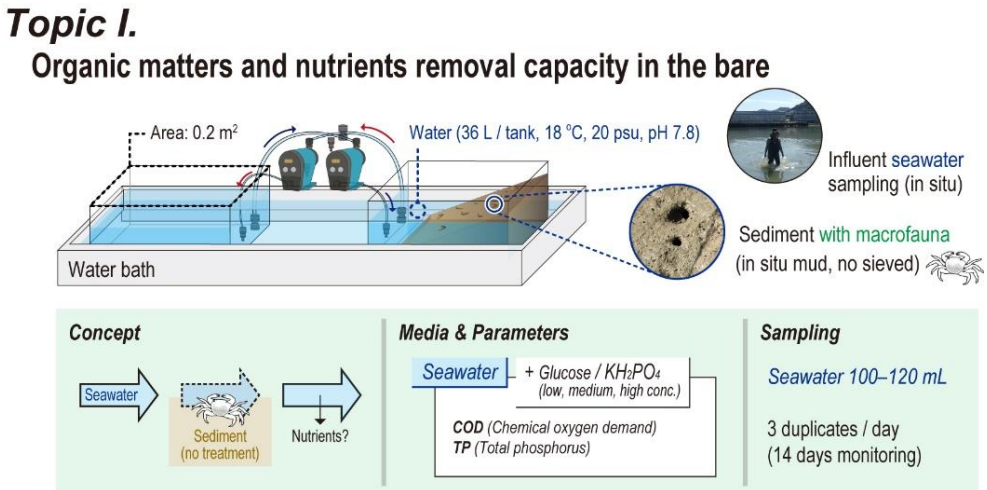

Figure 2.1.
Overview of workflow and experimental design for the evaluation of restoration capacity in bare intertidal flat and salt marsh by use of mesocosm experiments (1).

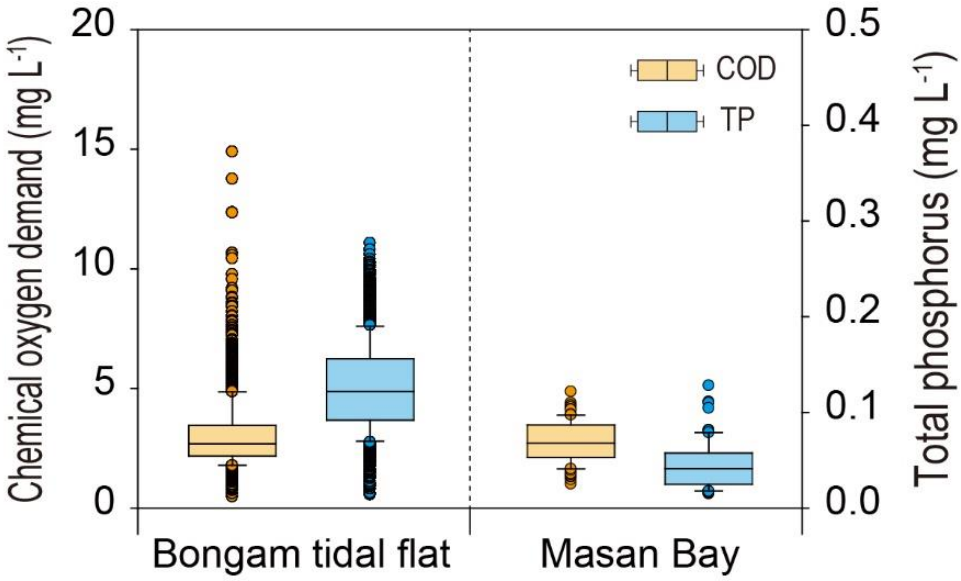

Figure 2.2.
Mean concentration of chemical oxygen demand (COD) and total phosphorus (TP) measured in seawater in Bongam tidal flat and Masan Bay from January to August, 2018. The data from MEIS (http://www.meis.go.kr).

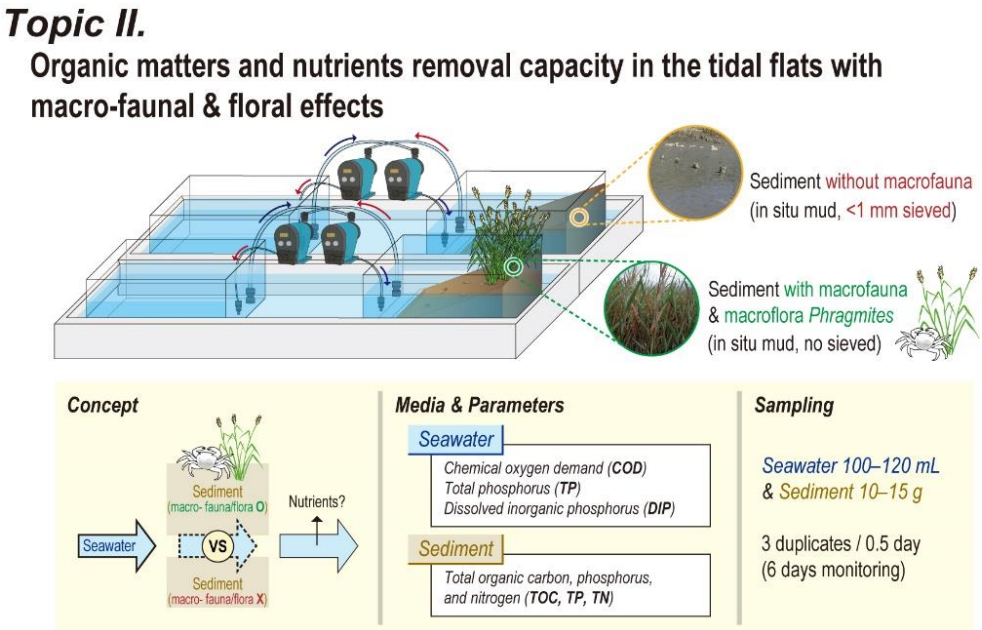

Figure 2.3.
Overview of workflow and experimental design for the evaluation of restoration capacity in bare intertidal flat and salt marsh by use of mesocosm experiments (2).

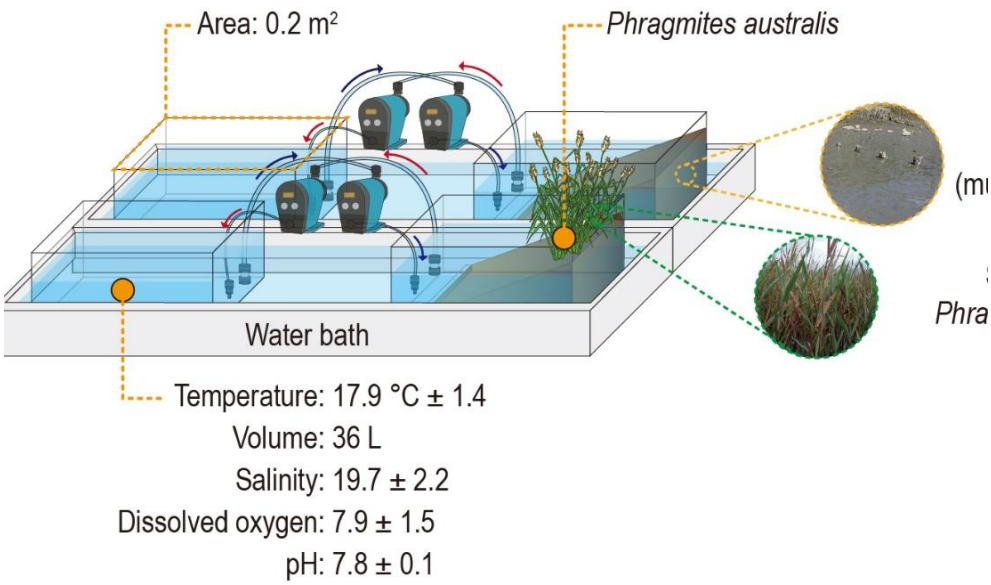

Figure 2.4.
Summary of the experimental conditions and description of mesocosm in this study

3. Results and Discussion

2.3.1. Natural restoration under waterborne organic matters and nutrients in tidal flat

Three concentration gradients in the mesocosm were designed to determine how much organic matters and/or nutrients can be purified in seawater and sediment under extreme concentration exposures (Figure 2.5). The initial concentration of COD was 10.3 mg L^{-1}, 15.6 mg L^{-1}, and 39.7 mg L^{-1}, respectively, and total phosphorus was set to 0.09 mg L^{-1}, 0.21 mg L^{-1}, and 0.26 mg L^{-1}. A day after the exposure (D + 1), the removal rates of COD were obtained to be 7.7 and 8.4% in the low and medium groups, respectively, while the high group exhibited much larger removal rate of 48.1%. The COD concentration in the low group tended to decrease continuously, and on 13th day (D + 13), the lowest concentration was detected. In the medium and high groups, there was a significant tendency of COD decrease from D + 1 to D + 2. After that, the saturation state began to occur until D + 14 in both groups. The lowest concentration was detected in the medium group at D + 14 and in the high group at D + 13. The initial concentration of COD was halved after 1–2 days in the high group (Restoration half-life, RHL). Consequently, it was confirmed that 47.2, 71.2, and 77.7% of COD were removed during 14 days in the low, medium, and high groups, respectively. TP showed a similar tendency as COD. At the low group, the concentration steadily decreased, and the saturation was reached on D + 3 (0.04 mg L^{-1}). The medium group showed the greatest reduction on D + 2 and the saturated state after D + 4 (RHL = 5 days). The greatest decrease was observed on D + 1 in the high group, and the concentration tended to remain constant from 0.07 ± 0.02 mg L^{-1} after D + 6 (RHL = 7 days). The removal rate in TP was determined to 52.4%, 64.7%, and 71.7% in low, medium, and high groups, respectively. Organic matters and nutrients which were targeted in this study, initially decreased rapidly and remained constant over time. Such a trend was clearly identified when the exposure concentration was high. The core of the tidal flat's restoration capacity is the ability of microorganisms to remove organic matters and nutrients introduced into tidal flats.

Tidal flats provide sedimentary layers with oxygen through disturbance, submergence, and exposure of the surface sediments from water, enabling the more effective aerobic decomposition process. The decomposition of land-based organic matters thus becomes very active in the tidal flats (Howes et al., 1984; Jørgensen, 1977). Bioturbation of sediments through marine organism movements increases oxygen content in sediment-water interface. It could cause an increase in the restoration for nutrients such as denitrification (Harada et al., 2014; Allen and Vaughn, 2009). And also, there are many studies on the removal of nutrients by microorganisms, and effective microbes (EM) have been developed for purifying the water quality. Lee et al., 2018 reported that *Verrucomicrobiaceae* and *Planctomycetia*, which are known to dominate in sludge and influent from treatment halophytes, showed relatively high abundance in Masan Bay (ElNaker et al., 2018). *Verrucomicrobiaceae* can be shown to grow and degrade nutrients at the early stage of exposure to high concentrations of nutrients according to this study. And, it is well known that Planctomycetia plays an important role in the biogeochemical cycle in the marine environment, and rapidly uptake and degrade the nutrients (Zhang et al., 2019). The reduction of organic matters and nutrients at the initial stage can result in the deposition of organic particles present in the influent to the sediment during the exposure time and the use of microorganisms in the organic particles and nutrients. However, the amount of organic matters and nutrients that microbes can uptake is limited, and if organic matters and nutrients are adsorbed at non-biological adsorption sites, microbes can no longer use them. In addition, change in the chemical composition in the sediment-water mixture due to microbes eventually leads to the equilibrium of organic matter and nutrient degradation (Kahl et al., 1993; Zhang and Huang, 2011).

Topic I.

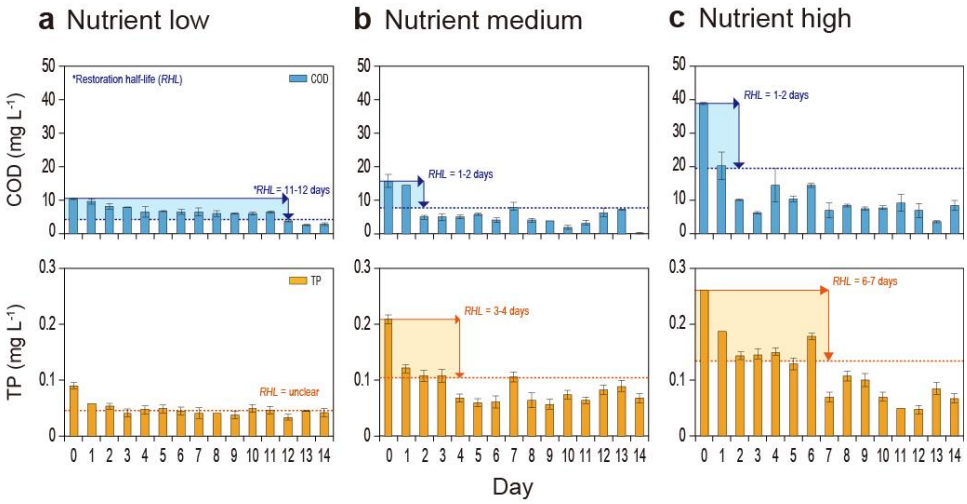

Figure 2.5.

Comparisons of restoration capacity in the sediment for water quality (COD and TP) depending on the gradients of initial concentrations of organic pollutants given by three groups; low, medium, and high. After initial waterborne exposure of organic matters and nutrients, concentrations of target water quality were daily monitored during the 14 days of experiments. Line over bars indicates the restoration half-life (RHL) of organic matters and nutrients.

2.3.2. Comparison of restoration capacity between bare and vegetated sediment

We investigated whether the presence of halophytes can enhance the restoration of organic matters and nutrients in the water (Figure 2.6 and Table 2.2). The experiments were conducted in the same environmental condition after sieving to minimize the influence of bioturbation. P. australis were selected and transplanted into the mesocosm for comparison with bare tidal flat. COD, TP, and DIP were parameters indicating water quality parameters (Figure 2.6). During the experiment periods, water and sediment samples were collected and analyzed. In the bare tidal flat, on average, 5.20, 0.20, and 0.02 mg L^{-1} of removal capacity in COD, TP, and DIP were obtained, respectively, from the renewal treatments (i.e., total of 11 samples at 12 h intervals for 6 days). Same orders, for the salt marsh, 6.50, 0.17, and 0.14 mg L^{-1} of removal in COD, TP, and DIP were obtained, respectively. Based on accumulated amounts of DIP and COD indicated greater capacity in salt marsh treatments compared to the that of bare tidal flat. Remarkably, 7 times efficiency observed for DIP in salt marsh sediments (0.14 mg L^{-1}) than bare tidal flats (0.02 mg L^{-1}). Despite greater removal capacity of both DIP and COD in salt marsh experiments, similar accumulated removal capacities were observed in TP treatments (Figure 2.6). On the other hand, OM, TOC, and TN showed reversal trends compared to the water parameters, at the end of experiments, the amounts of sediment parameters increased in all treatments (Figure 2.7). For COD, TP, and DIP in the bare tidal flat treatments, on average, 3.40, 3.50, and 0.47 mg L^{-1} of accumulation capacity were obtained, respectively, whilst 1.40, 1.80, and 0.39 mg L^{-1} of accumulation capacity were obtained in salt marsh, respectively. Accumulation capacities for OM and TOC in bare tidal flat treatments indicated approximately over doubled compared to that of salt marsh treatments. There was no distinctive trend between bare tidal flat and salt marsh for TN. Altogether, these results suggest that organic matters and nutrients in the form of particles can be decomposed and removed more efficiently than those in the dissolved state after the accumulation of organic matters.

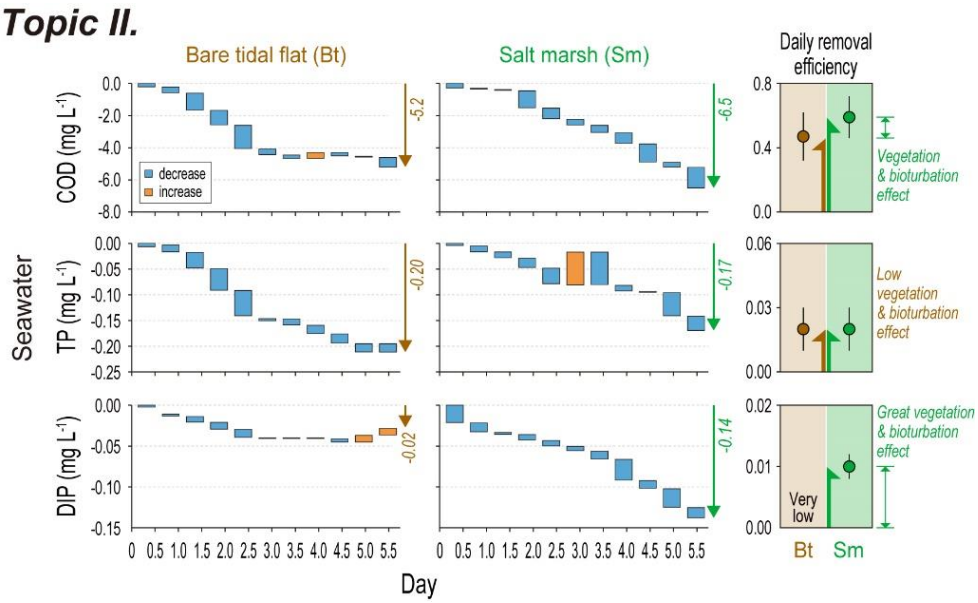

Figure 2.6.

Comparison of the restoration capacity for COD, TP, and DIP in seawaters of the bare tidal flat and the salt marsh by use of mesocosm experiments.

Table 2.2. Restoration capacity of bare tidal flat versus salt marsh in experimental scale studies.

Compounds	Experimental set	[a] Removal rate (%) in each experiment											Average (%)
		1	2	3	4	5	6	7	8	9	10	11	
COD	Bare tidal flat	7.1	10.3	28.7	18.8	22.5	16.2	13.1	-14.3	8.1	2.2	24.1	12.4
	Salt marsh	8.1	1.4	2.2	31.9	18.0	9.6	12.2	17.1	31.9	8.3	36.3	16.1
TP	Bare tidal flat	6.3	9.3	20.3	23.8	22.0	3.5	11.1	9.0	10.1	14.5	-24.1	9.6
	Salt marsh	6.4	12.2	11.3	16.6	23.3	-31.6	27.4	9.6	0.9	11.3	26.6	10.4
DIP	Bare tidal flat	4.1	5.8	8.6	7.7	11.5	1.1	2.2	2.2	5.1	-21.1	-14.6	1.2
	Salt marsh	5.1	5.2	9.1	7.1	8.2	4.4	1.4	4.4	18.9	5.1	14.9	7.6

[a] C_e: Initial concentration of COD, TP and DIP; C_i: the concentration of COD, TP and DIP after exposure 6 h; Equation: $100 - (C_e \div C_i) \times 100 = removal$ rate (%)

Figure 2.7.
Comparison of the burial amounts of OM, TOC, and TN in sediments of the bare tidal flat and the salt marsh by use of mesocosm experiments.

Organic matters and nutrients are mainly removed by adsorption and sedimentation, as well as intake by environmental organisms (Imfeld et al., 2009). It is also reported that iron (Fe) and aluminum (Al) present in the tidal flat promote the precipitation of phosphorus. Phosphorus is known to react rapidly with inorganic components such as Al, Fe, and Ca, as well as sediments (Nichols, 1983). The concentrations of COD and TP can decrease due to sedimentation and the microbial response to organic matters and nutrients after the influent flowed into the aquarium, but no significant difference in removal rate of COD and TP was found between the bare tidal flat and salt marsh in this study. Previous studies have emphasized the role of vegetation in the fate of phosphorus in tidal flat or wetland (Fisher and Acreman, 2004). The presence of vegetation distributes the flow velocity of water, which encourages sedimentation of suspended particles. Halophytes assimilate phosphorus to meet their nutritional requirements. And also, since the activity of microbial is more active than the bare tidal flat, decomposition of precipitated organic matter occurs a lot (Dai et al., 2009; Duarte et al., 2009). In addition, halophytes can influence the redox potential, which is an important determinant of the exchange of phosphorus between the sediment and water column (Chen and Barko, 1988). Especially, *P. australis* is one of the most distributed plants in marine ecosystem over the world including South Korea (Park et al., 2013). Many previous studies have identified what *P. australis* plays in the marine environment, and one of them has reported its restoration ability. *P. australis* could incorporate nitrogen and phosphorus into its tissues and promote phosphorus absorption onto the tidal flat by the release of oxygen from the roots (Wathugala et al., 1987). Therefore, *P. australis* in the salt marsh can make result in a relatively high removal efficiency of DIP compared to the bare tidal flat (Tables 2.3 and 2.4).

Table 2.3. Average influent and effluent concentration of COD, TP, and DIP in seawater, and content of OM, TOC, and TN in sediment (bare tidal flat).

Media	Target[a]		Day 1	Day 2	Day 3	Day 4	Day 5	Day 6	Day 7	Day 8	Day 9	Day 10	Day 11	Total	Mean
Seawater	COD	Influent	2.74	3.83	3.84	5.10	6.32	2.44	2.16	1.98	2.67	2.34	2.99	36.41	3.31
		Effluent	2.54	3.44	2.74	4.14	4.90	2.10	1.91	2.31	2.47	2.29	2.41	31.25	2.84
		Variation	-0.20	-0.39	-1.10	-0.96	-1.42	-0.34	-0.25	0.33	-0.20	-0.05	-0.58	-5.16	-0.47
	TP	Influent	0.13	0.15	0.15	0.18	0.22	0.15	0.09	0.20	0.20	0.11	0.07	1.65	0.15
		Effluent	0.12	0.13	0.12	0.14	0.17	0.15	0.08	0.19	0.18	0.09	0.09	1.46	0.13
		Variation	-0.01	-0.01	-0.03	-0.04	-0.05	-0.01	-0.01	-0.02	-0.02	-0.02	0.02	-0.20	-0.02
	DIP	Influent	0.05	0.06	0.07	0.13	0.08	0.04	0.00	0.04	0.06	0.04	0.05	0.63	0.06
		Effluent	0.05	0.06	0.07	0.12	0.07	0.04	0.00	0.04	0.06	0.05	0.06	0.61	0.06
		Variation	0.00	0.00	-0.01	-0.01	-0.01	0.00	0.00	0.00	0.00	0.01	0.01	-0.02	0.00
Sediment	OM	Influent	6.85	6.24	5.73	5.37	6.42	5.14	6.24	8.67	6.13	5.87	6.10	68.76	6.25
		Effluent	6.91	6.40	6.14	5.89	6.77	5.23	6.55	8.64	7.44	6.12	6.02	72.11	6.56
		Variation	0.06	0.16	0.41	0.52	0.35	0.09	0.31	-0.03	1.31	0.25	-0.08	3.35	0.30
	TOC	Influent	0.88	0.74	1.43	1.56	1.36	1.14	0.88	0.74	1.21	1.11	1.36	12.42	1.13
		Effluent	1.43	1.39	1.92	1.86	1.41	1.42	1.39	1.22	1.41	0.98	1.47	15.91	1.45
		Variation	0.55	0.65	0.49	0.30	0.05	0.28	0.51	0.48	0.20	-0.13	0.11	3.48	0.32
	TN	Influent	0.03	0.05	0.06	0.04	0.07	0.05	0.07	0.04	0.06	0.06	0.05	0.58	0.05
		Effluent	0.07	0.08	0.07	0.07	0.13	0.09	0.14	0.08	0.15	0.10	0.07	1.05	0.10
		Variation	0.04	0.03	0.01	0.03	0.06	0.04	0.07	0.04	0.09	0.04	0.02	0.47	0.04

[a] Each unit of target compounds was mg L^{-1} (COD, TP, DIP) and % (OM, TOC, TN).

Table 2.4. Average influent and effluent concentration of COD, TP, and DIP in seawater, and content of OM, TOC, and TN in sediment (salt marsh).

Media	Target[a]		Day 1	Day 2	Day 3	Day 4	Day 5	Day 6	Day 7	Day 8	Day 9	Day 10	Day 11	Total	Mean
Seawater	COD	Influent	3.59	3.64	2.23	3.60	3.94	3.64	3.76	3.87	3.60	3.25	3.66	38.78	3.53
		Effluent	3.30	3.59	2.18	2.45	3.23	3.29	3.30	3.21	2.45	2.98	2.33	32.31	2.94
		Variation	-0.29	-0.05	-0.05	-1.15	-0.71	-0.35	-0.46	-0.66	-1.15	-0.27	-1.33	-6.47	-0.59
	TP	Influent	0.08	0.09	0.09	0.14	0.14	0.20	0.23	0.13	0.15	0.42	0.10	1.76	0.16
		Effluent	0.07	0.08	0.08	0.11	0.10	0.26	0.17	0.12	0.15	0.37	0.08	1.59	0.14
		Variation	0.00	-0.01	-0.01	-0.02	-0.03	0.06	-0.06	-0.01	0.00	-0.05	-0.03	-0.17	-0.02
	DIP	Influent	0.07	0.05	0.03	0.10	0.07	0.12	0.09	0.13	0.05	0.06	0.08	0.85	0.08
		Effluent	0.04	0.04	0.03	0.09	0.06	0.12	0.08	0.10	0.04	0.04	0.07	0.71	0.06
		Variation	-0.02	-0.01	0.00	-0.01	-0.01	-0.01	-0.01	-0.03	-0.01	-0.02	-0.01	-0.14	-0.01
Sediment	OM	Influent	6.57	7.03	6.40	6.43	5.91	5.97	5.19	5.93	6.02	5.13	6.93	67.51	6.14
		Effluent	7.20	7.54	6.76	6.35	5.97	6.38	5.93	5.72	6.21	5.14	5.71	68.90	6.26
		Variation	0.63	0.51	0.36	-0.07	0.06	0.41	0.73	-0.21	0.19	0.01	-1.22	1.40	0.13
	TOC	Influent	0.88	0.74	1.11	1.33	0.98	1.14	1.75	0.99	1.65	1.41	1.21	13.20	1.20
		Effluent	1.39	0.98	1.42	1.41	1.00	1.24	1.75	1.14	1.77	1.56	1.34	15.00	1.36
		Variation	0.51	0.24	0.31	0.08	0.02	0.10	0.00	0.15	0.12	0.15	0.13	1.80	0.16
	TN	Influent	0.07	0.11	0.06	0.05	0.11	0.03	0.07	0.05	0.04	0.04	0.05	0.68	0.06
		Effluent	0.14	0.14	0.07	0.07	0.14	0.07	0.11	0.08	0.09	0.07	0.09	1.07	0.10
		Variation	0.07	0.03	0.01	0.02	0.03	0.04	0.04	0.03	0.05	0.03	0.04	0.39	0.04

[a] Each unit of target compounds was mg L^{-1} (COD, TP, DIP) and % (OM, TOC, TN).

2.3.3. Restoration capacity in Bongam tidal flat, Masan Bay

Removal efficiency of COD in the salt marsh and the bare tidal flat was determined to be 7.9% and 22.5%, and that of TP was 6.4% and 20.2%, respectively. In order to quantitatively evaluate the restoration performance of the Bongam tidal flat, we calculated the removal amount of COD and TP by considering the average water quality in Masan Bay (3.50 mg L^{-1} for COD and 0.13 mg L^{-1} for TP), the width of the mesocosm (0.2 m^2), the volume of inflow (36 L), and the exposure time (6 h) during the experiment period of 14 days (Table 2). The removal of COD and TP was expressed in g m^{-2} h^{-1} according to the equation below and converted to the amount during the day (Eq. 1):

$$\text{Restoration capacity} = \frac{CRV}{ST} \quad \cdots\cdots (1)$$

where C is the mean concentration of COD or TP in Masan Bay (mg L^{-1}), R is the removal efficiency (%), V is the volume of water inflow (L), S is the width of the sediment (m^2), and T is the exposure time (h). The restoration capacity of the Bongam tidal flat in Masan Bay determined from the equation was 0.1–0.3 g m^{-2} day^{-1} for COD and 0.002–0.007 g m^{-2} day^{-1} for TP. Applying this to the entire area of the Bongam tidal flat, the removal amount of COD and TP was estimated to be 20–57 kg day^{-1} and 0.5–1.5 kg day^{-1}, respectively (Table 2.5). The values are smaller than the removal amount of organic matters and nutrients in Saemangeum tidal land reported by You and Kim (1999). However, in terms of efficiency, the removal rate of the Bongam tidal flat in this study is greater. In the case of the Saemangeum tidal flat, the area is 400 km^2, while the Bongam has a total tidal flat area of ~0.2 km^2, which is considerably small compared to the Saemangeum (Lee et al., 2020; Ryu et al., 2011). Therefore, it should be advised that even if the retoration rates between the tidal flats do not vary greatly, there could be a large difference in the actual restoration amounts between tidal flats. Of note, we provided the estimated restoration capacities of COD and TP for the Korean tidal flats during the past 30 years.

Table 2.5 Evaluation on the restoration capacity of pollutants in Bongam tidal flat, Korea.

Target analysis	[a] Concentration ($mg\ L^{-1}$)	[b] Range of restoration efficiency (%)	[c] Amount of removal ($g\ m^{-2}\ hr^{-1}$)	[c] Restoration capacity in Bongam tidal flat ($kg\ day^{-1}$)
COD	3.5	7.9 – 22.5	0.2 – 0.6	40.3 – 113.8
TP	0.1	6.4 – 20.2	0.01 – 0.02	1.4 – 4.3

[a] Mean values in Masan Bay (2018) from National Maritime Environmental Information Integration System (MEIS), [b] Removal efficiency in this study, [c] exposure time: 6 h; volume of seawater in experiment: 36 L, area of sediment in the mesocosm: 0.2 m^2, [d] applying area of 200,000 m^2 in Bongam tidal flat.

2.3.4. Comparison to other mesocosm studies for restoration capacity of tidal flats

Previous mesocosm studies have mainly designed the experiments to replicate wetlands with relatively few experiments for bare tidal flat (Figure 2.8). Among the studies conducted using in situ mesocosms, the average of maximum COD removal rate for vegetated one was reported to be 100%. On the other hand, the in-lab mesocosm experiments showed the removal rate of 74% for the bare tidal and 94% for the salt marsh on maximum (Figure 2.8a), which are much different from the COD results in this study (29% and 36%, respectively).

The different removal efficiency between in situ and in-lab experiments indicates the influence of various environmental and non-environmental factors. In the case of TP, the in situ mesocosm experiment showed 89% of the maximum removal rate, while 39% was obtained from the in-lab mesocosm. In this study, the bare tidal flat and salt marsh resulted in the removal rate of 23% and 27%, respectively, from in-lab experiments (Figure 2.8b). The relatively low restoration capacity of phosphorus in the tidal flat reflects that phosphorus is more stable than organic matters in environment (Suzumura and Ingall, 2004), which is in accordance with other studies reporting the higher removal efficiency of TP in the presence of vegetation than in bare condition (Figure 2.8b). We note that previous studies on the role of vegetation in ecological restoration were usually conducted in the fields of P. australis or transplanted mesocosms (Table 2.6). P. australis is one of the dominant halophytes in the tidal flats and wetlands, and it has been reported that these halophytes contribute to the restoration by up taking phosphorous or nitrogen (Romero et al., 1999).

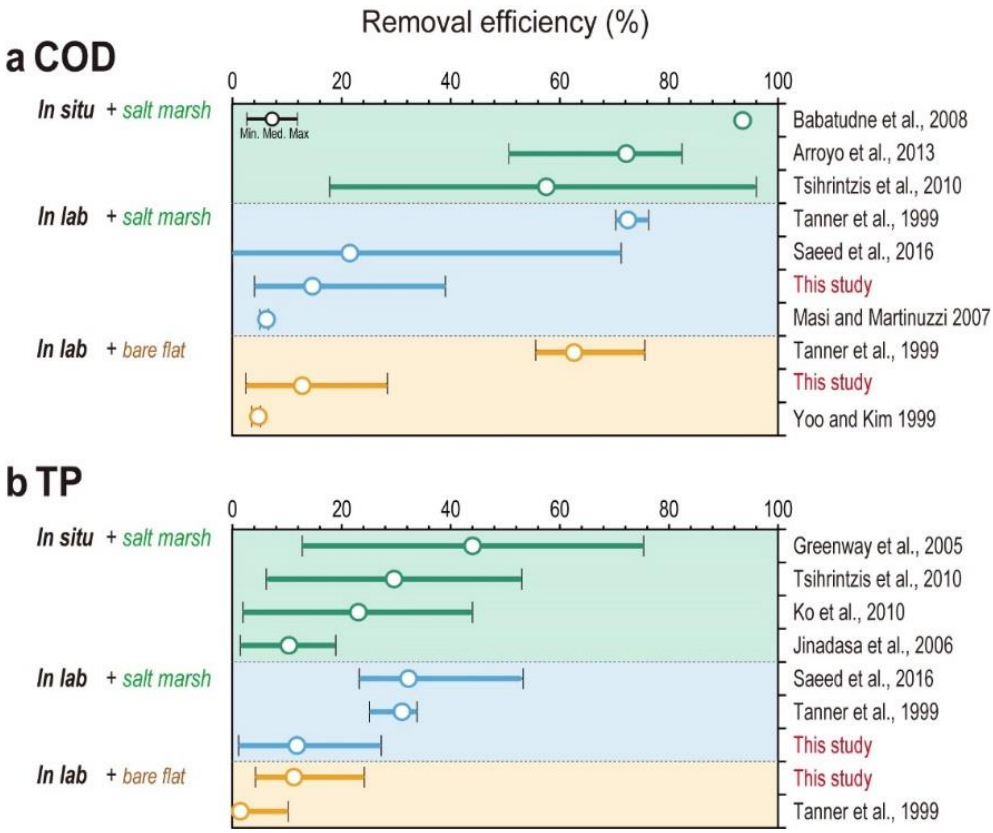

Figure 2.8.
Mini review on the studies evaluating removal efficiency of COD and TP by the tidal flats based on the in situ and laboratory mesocosm experiments, the present study included as for a comparison.

To conclude, recent reconsideration of marine ecosystem services has led a growing interest in the restoration or construction of tidal flat and wetland as a countermeasure for land-driven pollution (Kimura et al., 2002). The restoration capacity of tidal flats has been confirmed through mesocosm experiments and emphasizes the importance of not only the restoration capacity but also other values such as aesthetic and economic values in tidal flat (Kim, 2013). This study focused on the restoration capacity for organic pollution by in situ sediments under conditions of bare intertidal flat and salt marsh. There are many international studies focusing on the restoration for the load of organic matters and nutrients from artificial wetlands rather than natural tidal flats. Also, Meuleman et al. (2003) and Austin and Lohan (2005) suggested a vertical-flow constructed wetland model for the treatment of wastewater. There are several other models, such as the reed-bed treatment system and gravel-bed wetland mesocosm. Since the mechanism of restoration that occurs in the tidal flat is diverse, the shape and results of mesocosm might differ depending on which mechanism was focused on in each study (Hasanudin et al., 2004). For example, it is suggested to use an approach for microbial communities in the sediment to accurately identify the restoration mechanisms in the tidal flat ecosystem (Jones et al., 2005; Kim et al., 2012). In particular, ignoring the microbial community may cause a biased and even erroneous identification of natural restoration capacity in the tidal flat. Thus, not only chemical data but also biological data are needed to quantitatively confirm the restoration capacity and its mechanism in the tidal flat. The difference of the natural restoration results seems to be due to the design and function of the mesocosm. To understand and address the natural remediation capacity of tidal flats, it will be necessary to determine various mechanisms and functions being unsolved in the future.

Table 2.6. Various previous studies for evaluating the restoraiton capacity in tidal flat using mesocosm.

In situ/ lab	Configuration	Target compound	Removal rate		Plant	Reference
			Min.	Max.		
In situ	Salt marsh	COD	-	93.3	*Phragmites australis*	Babatunde et al., 2007
			50.8	82.4	*Iris pseudacorus*	Arroyo et al., 2013
			18.0	96.1	*Phragmites australis* *Arundo donax*	Tsihrintzis et al., 2010
lab	Salt marsh		-	9.0	*Phragmites australis*	Masi and Martinuzzi 2007
			0.0	71.4	*Phragmites australis*	Saeed et al., 2016
			71.0	77.0	*Schoenoplectus validus*	Tanner et al., 1999
			1.4	36.3	*Phragmites australis*	This study
	Bare tidal flat		54.0	74.0	-	Tanner et al., 1999
			5.2	6.5	-	Yoo and Kim 1999
			2.1	28.6	-	This study
In situ	Salt marsh	TP	1.4	19.0	*Scirpus grassus* *Typha angustifolia*	Jinadasa et al., 2006
			6.2	53.1	*Phragmites australis* *Arundo donax*	Tsihrintzis et al., 2010
			1.9	44.0	*Typha orientlis* *Phragmites communis*	Ko et al., 2010
			12.5	75.0	*Phragmites australis*	Greenway 2005
lab	Salt marsh		-36.8	87.0	*Carex virgata,* *Schoenoplectus tabernaemontani* *Cyperus ustulatus* *Juncus edgariae*	Saeed et al., 2016
			25.0	34.0	*Schoenoplectus validus*	Tanner et al., 1999
			0.9	27.4	*Phragmites australis*	This study
	Bare tidal flat		-3.0	10.0	-	Tanner et al., 1999
			3.5	23.7	-	This study

2.4. Conclusions

There has been significant and increasing interest in the restoration capacity of organic matters and nutrients in the natural tidal flat. Nowadays, artificial tidal flat and constructed wetland are considered an effective option to control the non-point sources of organic pollutants from the land. As part of the present study, we reported the restoration capacity of a tidal flat in the extreme nutrient exposure and identified the removal effiency between the bare tidal flat and the salt marsh with the expectation of how much organics can be removed in Bongam tidal flat. Further, we summarized the results of in situ and lab-mesocosm studies, including the data from present work. The mini-review confirmed great variations in restoration capacity cross habitats and region, indicating the various mechanisms of purifying target materials. Ecosystem services and functions (viz., aesthetic, restoration) provided by the tidal flat should be recognized following the adaptive management and restoration. Finally, further work is necessary to develop enhanced mesocosm systems and address more profound mechanisms of natural restoration capacity and pathways in the tidal flats.

CHAPTER 3.

BEST AVAILABLE TECHNIQUE FOR THE RECOVERY OF MARINE BENTHIC COMMUNITIES IN A GRAVEL SHORE AFTER THE OIL SPILL: A MESOCOSM-BASED SEDIMENT TRIAD ASSESSMENT

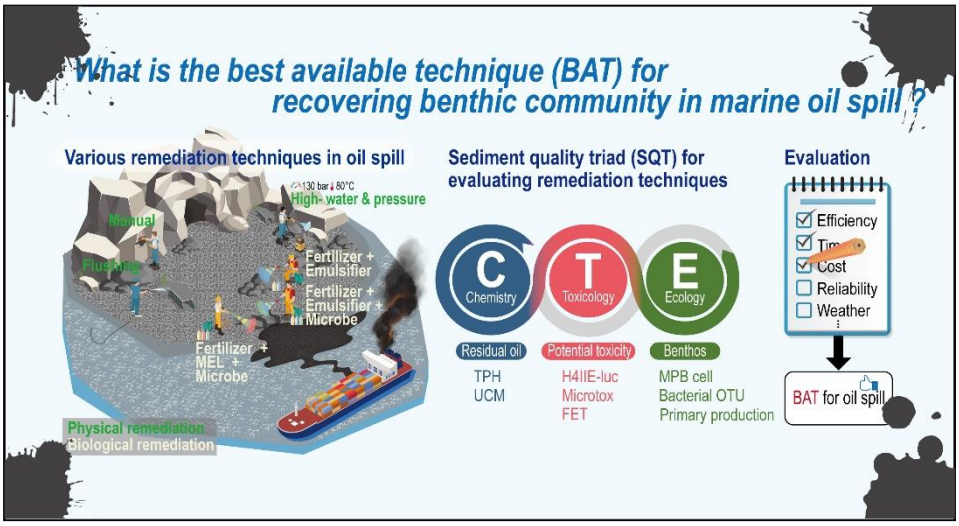

This chapter has been published in Journal of Hazardous Materials.
Kim, T., Lee, C., Lee, J., Bae, H., Noh, J., Hong, S., Kwon, B.-O., Kim, J. J., Yim, U. H., Chang, G. S., Giesy, J. P., Khim, J. S. Best Available Technique for the Recovery of Marine Benthic Communities in a Gravel Shore after the Oil Spill: A Mesocosm-based Sediment Triad Assessment. *J. Hazard. Mater.* 2022, 435, 128945.
https://doi.org/10.1016/j.jhazmat.2022.128945

3.1. Introduction

Oil spills can result in a wide range of adverse ecotoxicological effects on marine ecosystems, across diverse habitats of tidal flats, sandy beaches, and gravel shore (EPA, 1993; ITOPF, 2011). Spilled oils could reach and easily penetrate nearshore bottoms, varied though depending on the sedimentary environments such as mud content, sediment particle size, or organic and oxygen content. Permeation of oil into substrata could subsequently result in persistent, residual oil in surface and/or subsurface layers (Moore, 2016). Remaining, deeper subsurface oils can affect abundances and diversity of marine organisms (Hayes et al., 2010; Nixon et al., 2018, Yim et al., 2020). For example, after the Hebei Spirit spill in South Korea and the Exxon Valdez spill in Alaska, it took over 6 and 20 years, respectively, for benthic communities to recover and return to pre-spill status (Dave and Ghaly, 2011; Li et al., 2016).

Various techniques for remediation have been developed and employed to cleanup spilled oil (Azubuike et al., 2016; Dhaka et al., 2021). On hard bottoms, physical cleanups, such as hand wiping and hot water/high pressure flushing are essential for initial removal of stranded oils (ITOPF, 2011). Some biological treatments, which generally include applications of fertilizers (Nikolopoulou et al., 2007), emulsifier (Feng et al., 2006), multi-enzyme (Das et al., 2011) or augmenting microbial communities (Gao et al., 2011) are useful for longer-term cleanups. Typically, the primary focus on these methods of cleanup are rapid removals of spilled oils, but not considering receptor-oriented recovery of populations or communities (Siva et al., 1979). Historically, less attention has been paid to recovery of benthic organisms. For example, hot water/high pressure flushing, used in response to the Exxon Valdez spill, effectively removed stranded oils on hard surfaces, but severely damaged epibenthos (Mearns et al., 1993). Following the Torrey Canyon spill, use of dispersants caused unintended, greater toxicities to many organisms (Wardrop, 1991). Thus, a choice of timely method selection would be of great significance in effective cleanup implementation as oil spill response.

An intertidal zone with hard bottoms typically has great biodiversity, and its characteristics, including varying slopes, overhangs, and various textures of surfaces where various marine organisms can live. Spilled oil can penetrate hard bottoms as a function of porosity related to gravel type and size. Finally, oil that penetrates gravel can form a relatively permanent surface or subsurface layer (Moore, 2016). Selection of the most appropriate techniques for remediation of hard bottom communities is challenging. For example, variations in oceanographic conditions, such as tide, current, geomorphology, sediment facies all influence spatiotemporal distributions and fates of sedimentary residual oils. Accessibility to the impacted shoreline, in particular, has to be considered. On the shore, oil frequently coats hard surfaces such as rocks and gravel during the tidal range, accumulating in rock pools and cracks. Typically, the oil does not remain static, but is moved along the coast, eventually stranding in a safe spot. Access to the shorelines can be challenging at times, and special attention must be paid to worker safety in slippery areas, as well as to the hazards of waves and tides. In particular, the low load bearing qualities of such shorelines impede both vehicle and personnel transportation. That is the reason why relatively mobile techniques and equipment would be used to remove oil (ITOPF, 2011).

Since responses of benthic communities are important to overall recovery of marine ecosystems, remediation methods should be carefully chosen considering a number of factors. Thus, application of SQT assessment adopting lines of evidence approach, can be used to select the best available technique (BAT) for the remediation of sedimentary contamination by spilled oils. SQT is composed of three key components: chemical exposure (chemistry line of evidence (LOE)), toxicological effect (toxicology LOE), and benthic community health (ecology LOE) (Chapman, 1990, 1996). A single strategy or method cannot provide strong evidence for sediment toxicity, as causation cannot be established without integrating the three components. Nowadays, the ecological LOE contains a diverse array of benthic community, including microbiota and meiofauna (Khim et al., 2018; Lee et al., 2018b, Lee and Khim, 2022). From a chemical perspective, total petroleum hydrocarbon (TPH) and unresolved complex mixture (UCM) could be targeted (Yim

et al., 2012). Second, toxicity tests sensitive to polycyclic aromatic hydrocarbons (PAHs) and weathered PAHs should be conducted; The H4llE-luc bioassay (Martínez-Gómez et al., 2010), microtox® and fish embryo test (Lee et al., 2018a) have also been shown to be useful. Finally, ecological endpoints for multiple taxonomic groups relating to the benthic communities, such as diversity of the microbiome (Bourlat et al., 2013), microphytobenthos (MPB), and macrofauna can be monitored to determine potential ecological risks from oil spills (Lee et al., 2019a; Mohr et al., 2005). Overall, the integrated SQT approach is useful to accurately assess overall recovery of benthic communities in the vicinity of spills.

Enclosed experimental ecosystems, such as indoor mesocosms provide useful tools for examining effectiveness of cleanup and remediation. A recent mesocosm study successfully demonstrated the most appropriate biological methods for remediation of oil from soft bottoms and recoveries of marine benthic communities (Lee et al., 2019a). Here, as a continuing, but more in-depth effort, we evaluated physical and biological remediations, targeting recoveries of hard-bottom communities. The study adopted the advanced SQT approach, with multiple measures of chemical, toxicological, and ecological indicators across eight endpoints: 1) TPH, 2) UCM, 3) fish embryo mortality, 4) bacterial inhibition, 5) aryl hydrocarbon receptor (AhR) mediated potency, 6) MPB cell, 7) bacterial operational taxonomic unit (OTU), and 8) benthic primary production. Finally, the BAT for remediation of oil spills was carefully determined and discussed considering all eight indexes of the SQTs.

3.2. Materials and Methods

3.2.1. Sample preparation

To simulate the gravel-covered coastal zone affected by oil spills, gravel with a diameter of 6.5 cm or less was collected from Gimhae on the southern coast of South Korea. We focused on the contamination of the gravels from oil exposure; therefore, the media used in the experiment were only composed of gravel. Collected gravel was introduced to seawater for 30 days in order to recruit marine organisms before

initiating experiments (Figure 3.1). Gravel was exposed to Iranian Heavy Crude oil (details in Table 3.1 of the Supplementary materials) at a volume ratio of 1:10 (oil: gravel) and was homogenized with a polytetrafluoroethylene stick. Gravel was shaken with oil until surfaces of gravel were evenly coated (physical remediation: set -1 d and biological remediation: set -30 d). In general, whilst, physical remediation is used to remove oil during the initial phases of remediation of oil spills, biological remediation can be applied to accelerate natural attenuation during the final phases of cleanup. Therefore, by setting the different weathering periods in each remediation, this study provided a more realistic simulation exposure of the gravel shore to oil.

3.2.2. Mesocosm experimental setting

The artificial tide system was designed to simulate tides on gravel-covered shores (Figire 3.2). The tide control system was composed of three compartments: 1) one water storage tank with a dimension of 200 × 90 × 41 cm (W × L × H) and a capacity of ~700 L on the top (for thermal and dissolved oxygen control); 2) a set of 10 experimental aquariums with 45 × 35 × 40 cm per aquarium in the middle (to control water level, tidal cycle, and light condition); and 3) one wastewater tank with 200 × 70 × 80 cm in dimension and ~100 L of capacity at the bottom. Temperature was maintained constant (18–19°C) by use of the temperature control system. The volume of gravel in the aquarium portion of the mesocosm was identical to that of the gravel shore near where the mesocosm was installed. Natural seawater was supplied to experimental aquariums at 40 L for 12 h so that the gravel pile could be gradually submerged from the lower layer to the upper layer. This daily of horizontal supply and discharge of seawater at a 12 h interval, mimicking an in situ tidal condition, was repeated during the experimental period of 60 days without high-energy tidal action. The irradiance reaching the gravels was measured to be approximately 380–425 μmol m^{-2} s^{-1} from each aquarium's LED lamps (20 watts per lamp or aquarium).

Among the remediation techniques proposed by the International Tanker Owners Pollution Federation (ITOPF), 6 techniques were applied during the

experiments (Figure 3.1) (ITOPF, 2011). In particular, considering the applicable physical remediation techniques in a gravel and/or rocky shore from the manual of ITOPF, we chose the techniques which can be used in an indoor scale experiment (Table 3.2) possibly. They included 3 physical techniques; manual hand wiping (MA), flushing (FL), and hot water-high pressure (HW/HP). We analyzed the pressure in each remediation technique with (MA: 30 bars, FL: 20 bars, and HW/HP: 130 bars) by the in-line pressure gauge kit in each machine. Total 4 products were used in the biological remediation (fertilizer: oleophilic fertilizer, S200; emulsifier: Tween 80; multi-enzyme: Oil Spill Eater II; microbe: mixture (*Alcanivorax* sp., *Roseovarius* sp., *Corynebacterium variabilis*, *Dietzia* sp., *Sphingomonas yanoikuyae*, *Kyotococcus sedentarius*, *Bacillus aquimaris*, *Novosphingobium*, *Pentaromativorans*, and *Yarrowia lipolytica*)). To evaluate the mixed effects of biological remediation, 3 combined biological techniques; fertilizer + emulsifier (FE), fertilizer + emulsifier + microbe (FEM), and fertilizer + multi-enzyme + microbe (FMeM) were selected. In addition, natural attenuation during which no active treatments were applied (NT) was used to simulate responses to seawater circulation alone.

All treatments were applied at times equivalent to low tide, according to the tidal cycle in the area (34° 59.578'N, 128° 40.393'E) where the mesocosm was installed. Physical treatments were employed initially (0 d) and biological treatments were applied at the first low tide time on days 0, 15, 30, 45, and 60 d (Table 3.3). Advantages and disadvantages of selected techniques are listed in Table 3.4.

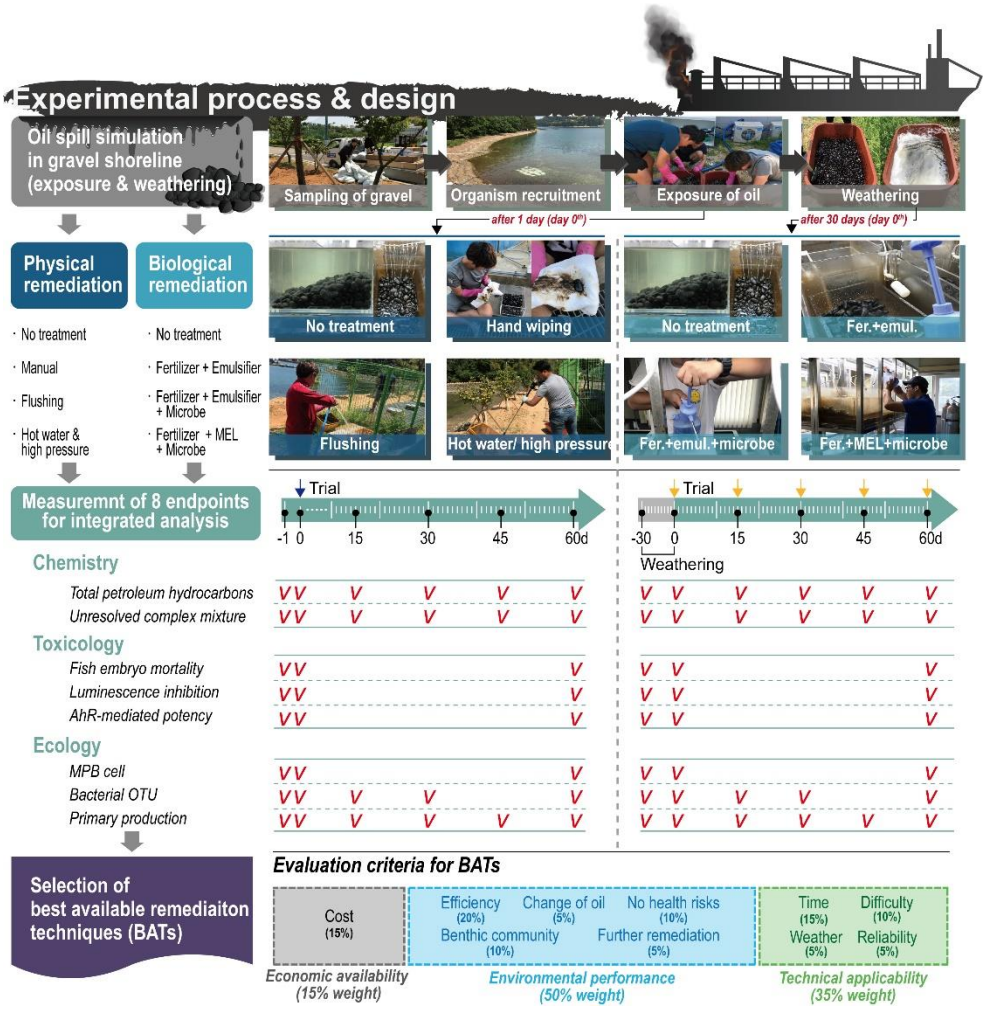

Figure 3.1

Schematic of physical and biological remediation techniques, experimental conditions, and sampling design of this study

Table 3.1.
General properties of Iranian Heavy Crude oil used in this study

Properties	Unit	Value
Density (15°C)	g mL-1	0.9
API Gravity	API	30
Dynamic Viscosity	mPa.s	20
Surface Tension (15°C)	mN/M	26
Interfacial Tension (15°C, 33psu)	mN/M	22
Sulphur Content	% w/w	1
Water Content	% w/w	< 0.025
Total Petroleum Hydrocarbons (TPH)	µg g-1	300,000
Unresolved Complex Mixture	µg g-1	190,000
n-Alkane	µg g-1	40,000
Total 16 PAHs	µg g-1	396
Total alkylated PAHs	µg g-1	12,216

Graphical design of indoor experiment

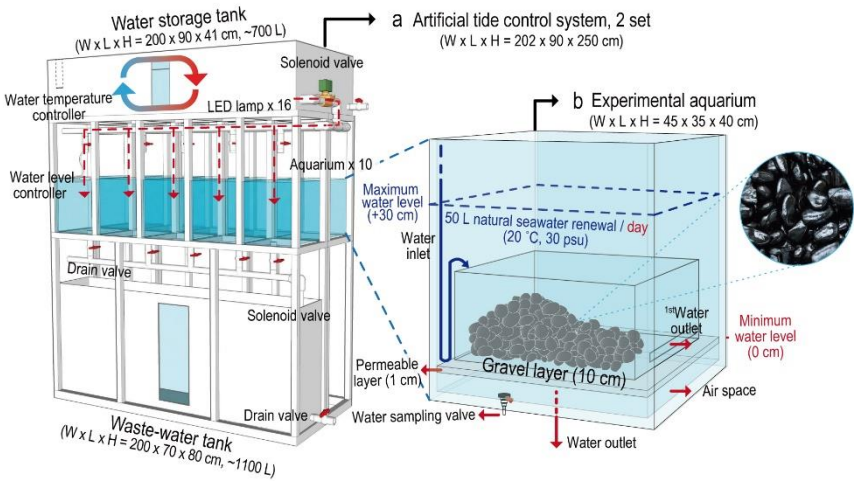

Figure 3.2
Schematic of the artificial tide control system. (a) artificial tide control system, and (b) experiment aquarium.

Table 3.2. Applicable techniques for cleaning oil in gravel and/or rocky shore (ITOPF, 2011)

Approach	Rocks and boulders		Gravels and pebbles	
	Accessible	Inaccessible	Accessible	Inaccessible
Stage 1	Skimmers/pumps, vacuum trucks, flushing	Manual, Manual & sorbents	Skimmers/pumps, vacuum trucks, flushing	Manual, manual & sorbents
Stage 2	Pressure washing, sorbent materials, natural cleaning	Natural cleaning, hand wiping	Flushing, surf/cobble washing, mechanical, natural cleaning	Natural cleaning, hand wiping
Stage 3	Natural cleaning, pressure washing, sand blasting	Natural cleaning	Natural cleaning, surf/cobble washing, sand blasting	Natural cleaning

Table 3.3
Summary of the experimental conditions and description of remediation techniques in this study

Experimental conditions			
Salinity	28 – 30		
Dissolved oxygen	> 80%		
pH range	7.9 – 8.2		
Experimental duration (d)	90		
Gravel size	Φ <60 mm		
Crude oil	Iranian Heavy Crude oil		
Volume ratio (gravel:oil)	10:1		
Remediation	**Techniques**	**Description**	**Reference**
Physical- and biological remediation	Manual	Oil absorbent, handling, <30 bar	ITOPF, 2011
	Flushing	Spraying for 10 min, <20 bar	ITOPF, 2011
	Hot water & high pressure	M1002 DS, spraying for 3 min, 130 bars	ITOPF, 2011
	Fertilizer	Oleophilic fertilizer; S200, 15 mL per treatment	Nikolopoulou et al., 2007
	Multi-enzyme liquid	Oil Spill Eater II, 15 mL per treatment	Das and Chamdram, 2011[14]
	Emulsifier	Tween 80, 15 mL per treatment	Feng et al., 2011
	Microbe solution	Microbial solution (bacteria mixture; *Alcanivorax* sp., *Roseovarius* sp., *Corynebacterium variabilis, Dietzia* sp., *Sphingomonas yanoikuyae*, *Kyotococcus sedentarius*, *Bacillus aquimaris*, *Novosphingobium*, *Pentaromativorans*, and *Yarrowia lipolytica*), 50 mL per treatment	Gao and Zaki, 2011

Table 3.4
Advantage and disadvantage of various remediation techniques for oil removal

Remediation techniques	Advantage	Disadvantage
Physical		
[a)] Manual	Application of all kind of oil No maintenance required Effective as final clean up	Moderate expensive Labour intensive Weather condition dependent
[b)] Flushing	Application of all kind of oil Cost effective Less labour intensive	Moderate expensive Threaten for marine organism Weather condition dependent
[b)] Hot water & high pressure	Application of all kind of oil Quick Less labour intensive	Moderate expensive Threaten for marine organism Possibility of second oil contamination Weather condition dependent
Biological		
[a)] Fertilizer	Application of all kind of oil No maintenance required Less labour intensive	Moderate Expensive Disrupting balance of nutrient and pH Oil dependent Indigenous bacteria dependent
[a)] Emulsifier	Effective on wide range of oil Accelerating the degradation Less labour intensive	Potential toxicity Expensive Second pollution
[a)] MEL	Non-aggressive No maintenance required Environmentally friendly	Slow recovery Expensive Oil dependent
[c)] Microbe solution	Non-aggressive Accelerating the degradation Environmentally friendly	Slow recovery Expensive Required maintenance

Data from [a)] Dave and Ghaly, 2011, [b)] Baker, 1995 and [c)] Gudi et al., 2016

3.2.3. Instrumental analysis of residual TPH and UCM in gravel

The analytical procedures for TPH and UCM in gravel followed methods used in previous studies (Yim et al., 2005, Yim et al., 2011). In brief, 120–140 g oil-contaminated gravel was mixed with anhydrous sodium sulfate (Sigma-Aldrich, St. Louis, MO) to remove water, and surrogate standard (*o*-terphenyl) was added. The samples were ultrasonically extracted for 15 min with 150 mL dichloromethane (Burdick & Jackson, Muskegon, MI), with three repeats. The extracts were concentrated to 1 mL under a gentle stream of nitrogen gas, and the internal standard (5α-androstane) was added. TPH and UCM were calculated by using an Agilent 7890 gas chromatograph equipped with a flame-ionization detector (Agilent Technologies, Santa Clara, CA) (Wang et al., 1994).

3.2.4. Zebrafish (Danio rerio) embryo test

In order to clarify efficiencies of each remediation, bioassays were conducted at three times, including an initial oil exposure (-30 d), first application of each remediation (0 d), and final stages (60 d). Oil-contaminated gravel was extracted by DCM, and the extracts were substituted with dimethyl sulfoxide (~10 mg oil-contaminated gravel equivalent (GEq) mL^{-1}). Before the solution was exposed to embryos, embryos with no abnormality in differentiation were selected. Using 12-well plates, the experiment was performed on 12 individuals with three repetitions. Individuals were exposed for 96 h in a culture system that was maintained at a constant temperature (26 °C). Every day, the mortality of each individual and developmental effect rates (spinal curvature and cardiac edema) were checked with a microscope (Lee et al., 2018a).

3.2.5. Vibrio fischeri (V. fischeri) biossay

The *V. fischeri* bioassay was used to evaluate the potential toxicity of residual oil in gravel. Organic extracts from gravel were exposed to *V. fischeri*, confirming the effect of residual oil on the inhibition of luminescence using N-TOX (model 200; NeoEnBiz Inc., Bucheon, Korea), which is a commercial toxicity assessment kit (~10 mg GEq mL^{-1}). The *V. fischeri* bioassay was conducted following the standard method specified by the Ministry of Maritime Affairs and Fisheries of South Korea (Lee et al., 2019b; Lee et al., 2019c).

3.2.6. H4IIE-luciferase transactiviation bioassay

The H4IIE-*luc* bioassay was performed to detect AhR-mediated potencies in oil-contaminated gravel according to previously published methods (Hong et al., 2012). In brief, trypsinized cells (~7.0×10^4 cells mL^{-1}) were seeded in 96-well plates and incubated for 72 hours. The plates were then dosed with the appropriate standards (2,3,7,8-tetrachlorodibenzodioxin; 0.1% dose), samples (raw; 0.1% dose (~0.1 mg GEq mL^{-1})), and solvent controls (0.1% dimethylsulfoxide) for 72 hours. After 72 hours exposure, the results were expressed as relative luminescence units that were quantified using a Victor X3 multi-label plate reader (PerkinElmer, Waltham, MA).

3.2.7. Identification of MPB individual

Considering that organisms have different rates of response rate to temporal variation of oil contamination, each data point is given as a different color, according to the endpoints (Yim et al., 2017). Because the lower the trophic levels respond more rapidly and responses to sedimentary contamination are complex, data points were assigned in this study in the following order: bacteria (n = 5) > MPB cells (n = 3), and meiofauna (n = 3). Because estimates of primary production were derived from the results of functions in various benthic organisms, we collected more data points than for other biological variables.

Oil-contaminated gravel was collected in triplicate from each experimental aquarium. For diatom separation from gravel, 5% formalin solution was added to the collected gravels (5 of about 100 pieces of gravel in each aquarium) and thoroughly

shaken. Only the supernatant was decanted into a beaker. After adding 10 mL distilled water to the remaining gravel, the water-gravel mixture was sonicated for 5 seconds. The supernatant was removed from the submerged samples, and 30 mL distilled water and 10 mL hydrochloric acid were added for the acid treatment. Samples, containing MPB cells, were heated and cooled to be neutralized for species identification and cell counting (until counting max of 100 cells) (Bae et al., 2020).

3.2.8. Bacterial metagenomic analysis

The bacterial community was analyzed by extracting total genomic DNA from gravel, using a PowerSoil® DNA Isolation Kit (MoBio Laboratories, Solana Beach, CA). Sequencing was conducted using the Illumina MiSeq Platform with 16S rRNA gene amplicons. The amplicons of V34 were prepared using the forward primer (16S_341F: TCG TCG GCA GCG TCA GAT GTG TAT AAG AGA CAG CCT ACG GGN GGC WGC AG) and the reverse primer (16S_805R: GTC TCG TGG GCT CGG AGA TGT GTA TAA GAG ACA GGA CTA CHV GGG TAT CTA ATC C). Quantitative Insights into Microbial Ecology was used to analyze the sequence data. Using the UCLUST algorithm, sequences were clustered by OTUs at a 97% identity threshold (Edgar et al., 2010). Taxonomic information was delegated by aligning sequences with the data from Ribosomal Database Project (RDP) (Cole et al., 2014).

3.2.9. Measurements of benthic primary production

Primary production of benthic algae was measured in each experimental aquarium (three times) using a Diving-PAM fluorometer (Walz, Effeltrich, Germany) (Perkins et al., 2001). The maximum relative electron transport rate (rETRm) was determined as the product of Fq'/ Fm' and irradiance (Sakshaug et al., 1997). Fq' and Fm' denote the proportion of harvested photons driving photosynthesis and the light-adapted maximum fluorescence, respectively.

3.2.10. Multi-attribute utility theory (MAUT) analysis for selection of the best available technique for remediation of oil

MAUT analysis is a decision-making approach in multi-criteria decision analysis (MCDA). Various data were used as nine assessment factors (main 3 criteria: economic availability (Ea), environmental performance (Ep), and technical applicability (Ta)) within MAUT analysis. Each criterion was scaled from 0 (worst) to 1 (best) based on the average result. The best available remediation assessment was determined by use of MAUT, which was based on three previously proposed criteria (Dave and Ghaly, 2011; Zheng et al., 2019) *Ea* in terms of cost (relative inexpensive), and *Ep* in terms of efficiency, effect on oil (physical and chemical change of properties), potential toxicity, recovery of benthic community, and further treatment (no further treatment required), and *Ta* in terms of time (removal of oil within days), weather (favorable for application of method), reliability (the method works the majority of the time), and level of difficulty (easy to maintain and operate) (Figire 3.3). Each criterion was weighted (15% for economic availability, 50% for environmental performance, and 35 % for technical applicability).

3.2.11. Statistical analysis

Data analyses were carried out using IBM SPSS software (version 23.0; SPSS Inc., Chicago, IL). The difference of recovery and reduction rate among each treatment was analyzed by analysis of covariance (ANCOVA). In all statistical analyses, p values less than 0.05 were considered to be statistically significant. Principal component analysis (PCA) to visualize the similarity between selected endpoint (concentrations of TPH and UCM, HI, and primary production) and bacterial abundance.

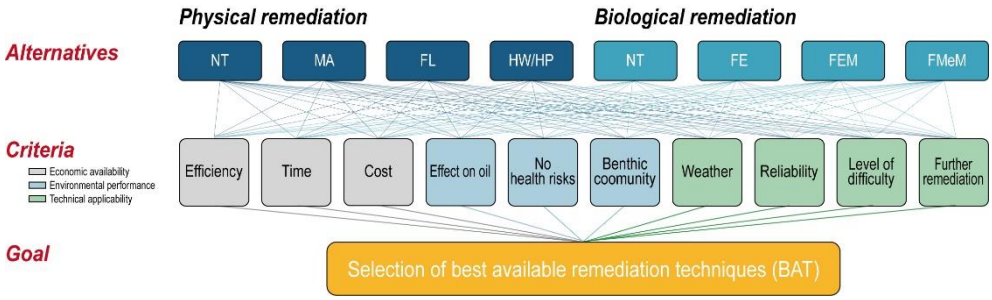

Figure 3.3
Proposing criteria for the best available techniques (BATs) in physical and biological remediation against the oil spills.

3.3. Results and Discussion

3.3.1. Physical and biological remediations

Each efficiency was determined to increase (ecology) and/or reduction rate (chemical and toxicity) as compared to the initial stage in order to evaluate the effect of using remediation techniques (Figure 3.4). Physical remediation after exposure of oils to gravels resulted in time-dependent, recovery of all three components of the SQT, but efficiencies of recovery varied among the eight endpoints. Removal of hydrocarbons of 78–93% occurred within 60 days (Figure 3.4a and 3.5a). After 60 d, rates of reduction of hydrocarbons of several treatments were significantly different from that of NT (MA: $p < 0.05$, FL: $p < 0.05$, and HW/HP: $p < 0.01$). Physical remediation seemed to mitigate toxicity of residual oil with an average reduction rate of 71% (MA: 72%; FL: 67%; and HW/HP: 73%) compared to the initial stage (-1d), which was significantly greater than that of NT (52% and $p < 0.05$) (Figure 3.4a). Adverse effects on measures of ecosystem structure were observed soon after applications of physical remediation. In particular, the HW/HP treatment caused the greatest negative effects on ecological endpoints (mean=-79%) on the -1 d (Figure 3.6a). However, the rate of recovery of structure of the benthic community increased as the seawater exchange promoted recruitment of micro-benthic organisms. Treatment MA resulted in the greatest (298%) recovery of the benthic community, followed by HW/HP (273%) and FL (266%) at the end of experiment (60 d), which almost doubled compared to that of NT (161%) (MA: $p < 0.05$, FL: $p < 0.05$, and HW/HP: $p < 0.05$).

Biological remediation, which was applied for 30 d, during which weathered oil was present on gravel (set treatment day as 0 d). Rate of removal of TPH was 49%, greater than NT when biological remediation techniques were applied. Removal of TPH of 50–66% was observed after 90 d (-30 d to 60 d) (Figure 3.4b and 3.5b). Greatest reduction of toxicity of 62%, was observed for treatment FMeM, followed by FEM and FE, with reductions of 57% and 48%, respectively. Recovery of the benthic invertebrate community was greater with increases of all three ecological endpoints observed during the weathering period (Figure 3.6b). On 60 d,

the greatest ecological recovery of 346%, was observed for treatment FMeM followed by FEM and FE with improvements of 267% and 220%, respectively.

Reduction of residual oil was proportional to physical pressure given to each treatment. For example, reduction was greatest for treatment HW/HP (130 bars), followed by MA (30 bars), FL (20 bars), and NT (Table 3.5). Of the biological remediation treatments, TPH and UCM were reduced to the least concentrations by treatment FMeM, which indicated that combined use of fertilizers and augmenting the microbial community was effective at breaking down residual oil. However, compared to physical techniques, biological techniques resulted in more gradual reduction in TPH and UCM. This could be due to fertilizer, MEL, and microbe solutions stimulate growth of existing bacteria that were capable of degrading petroleum, which results in time-lagged promoting the natural degradation (Kim et al., 2005).

Reduction in toxicity, including mortality of embryos and AhR-mediated potency in gravel, was observed with the reduction of TPH after physical treatments (Figure 3.4c, Tables 3.6, and 3.7) ($p < 0.05$). Embryo stages of development in fish have been found to be sensitive to exposure to oil, which especially includes various dioxin-like compounds, causing AhR activity (Johann et al., 2020). The *V. fischeri* bioassay is less sensitive to reduction of residual oil during the 90 days of experiment. For example, inhibition of luminescence relatively small responses (<50%), compared to fish embryo mortality (~100%), even when the concentration of TPH and UCM were greatest during the initial period. Results of previous studies have found that toxicity of oil to bacteria depends on constituents of the mixture other TPH or UCM (Brils et al., 2002; Adams, 2015). Toxic potency of residual oils decreased over 90 days (Figure 3.4d, $p < 0.05$) when biological treatments were applied. For treatment FE, AhR-mediated potency did not decrease from 0 d to 60 d, even though TPH decreased (Tables 3.5 and 3.6). This is in accordance with the results reported by Johann et al. suggesting that emulsifier contributes to greater toxicity compared to native oils (Johann et al., 2020). Indeed, the emulsifier does not appear to effectively remove the dioxin-like compounds affecting the AhR activity at the moment (Bach et al., 2005).

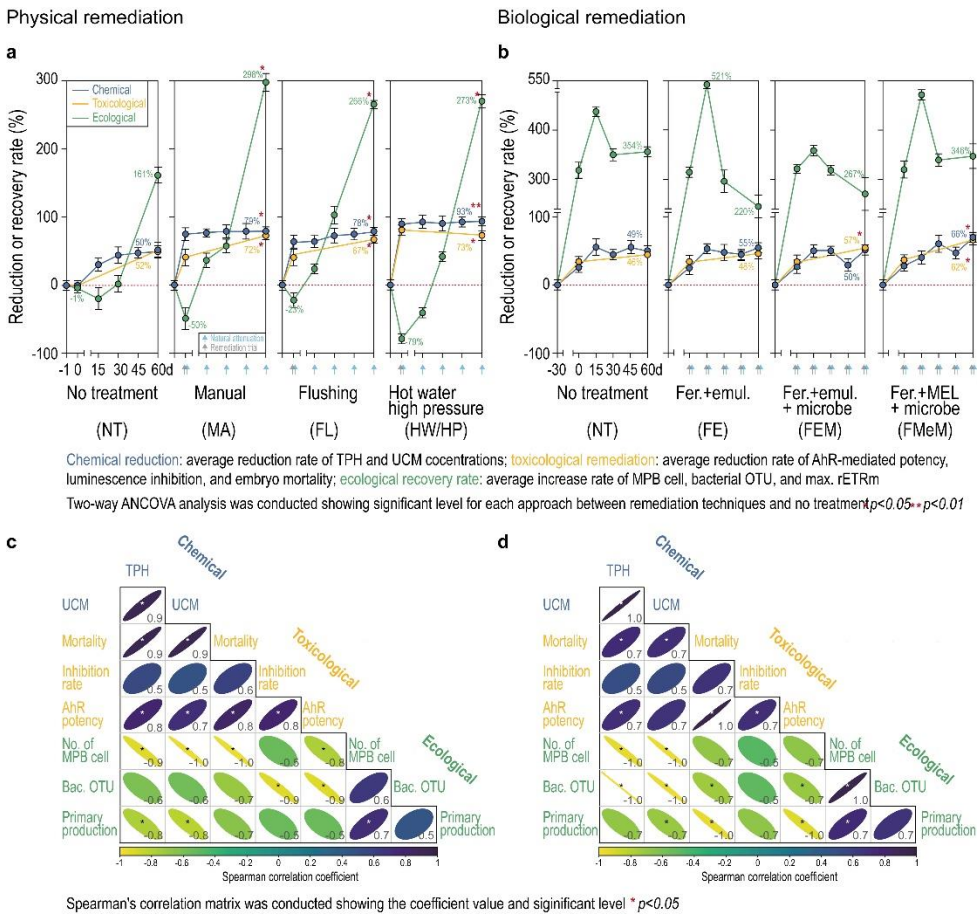

Figure 3.4

Chemical–and toxicological reduction rate and ecological recovery rate after implementation of each remediation techniques (physical and biological remediation).

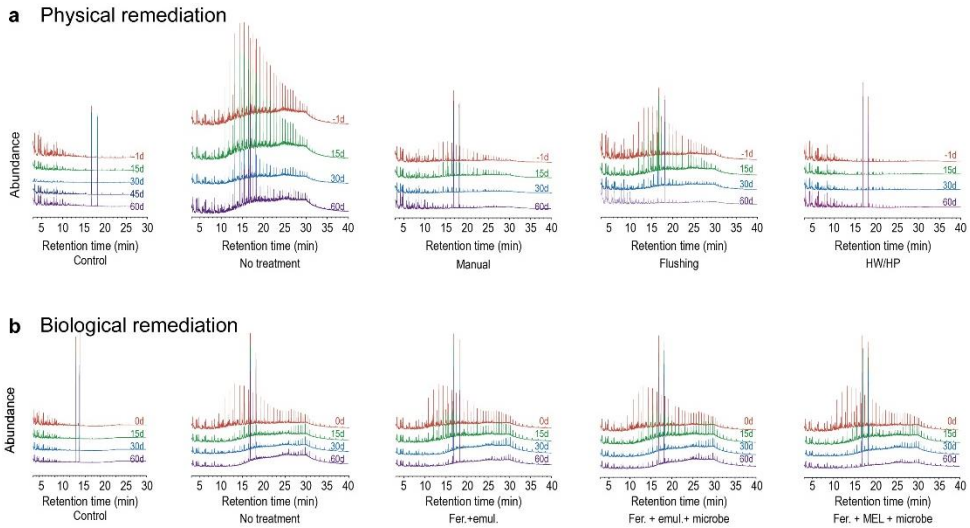

Figure 3.5

Overall chromatograms obtained from gravel samples in each physical and biological remediation techniques for oil removal from day 0 to 60 d.

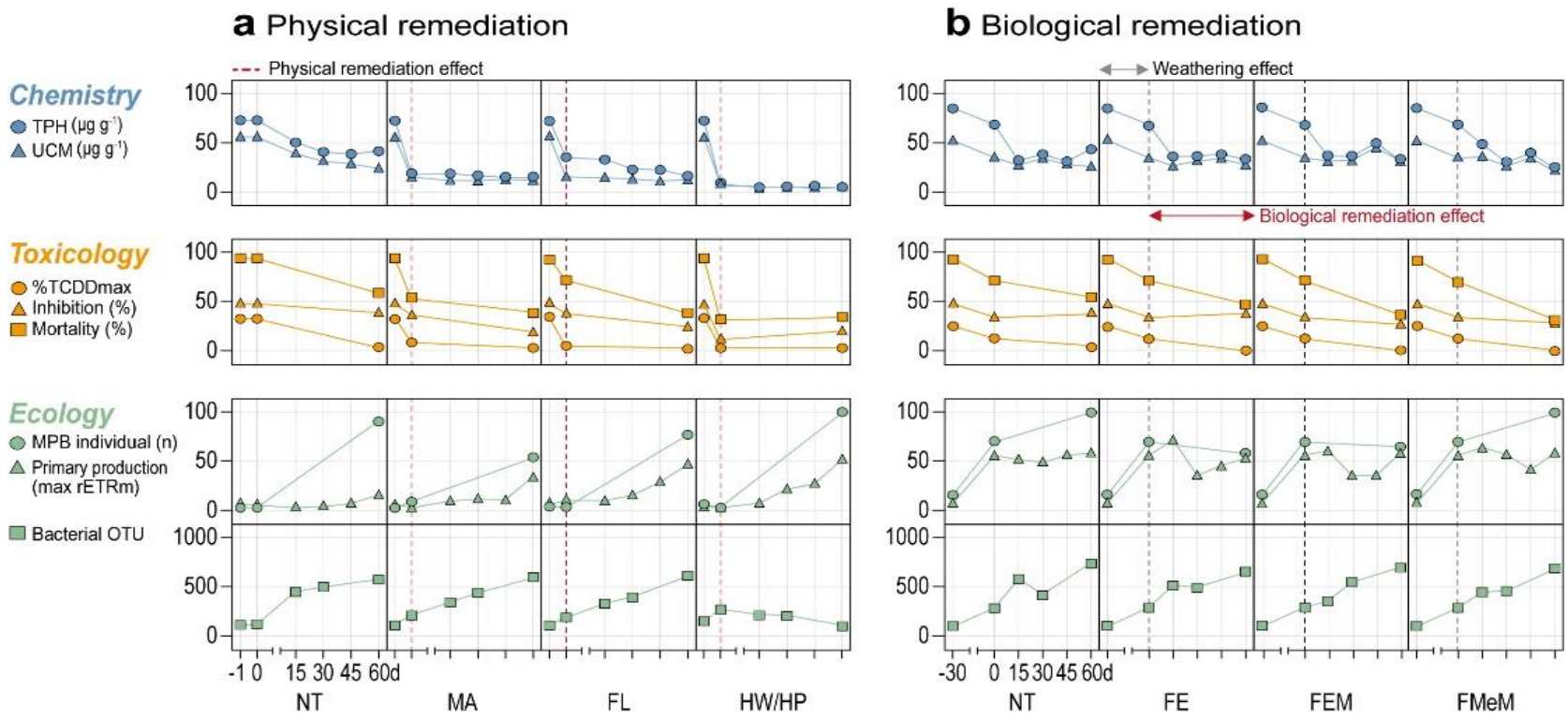

Figure 3.6

Temporal variation in TPH and UCM concentrations (µg g^{-1}), zebra fish embryo mortality (%), Vibrio fischeri luminescence inhibition rate (%), AhR-mediated potency (%TCDDmax), MPB cell (n), primary production (P.P) (max rETRm), and bacterial OTUs measured in the experiments periods. Eight remediation techniques were implemented including control.

Table 3.5.
Temporal variation of sedimentary TPH and UCM concentration in the 60–90 days including positive controls.

Remediation techniques	**Compounds**											
	TPH (ug g^{-1})						UCM (ug g^{-1})					
Physical	**-1 d**	**0 d**	**15 d**	**30 d**	**45 d**	**60 d**	**-1 d**	**0 d**	**15 d**	**30 d**	**45 d**	**60 d**
NT	70	70	51	41	39	42	56	56	39	31	29	24
MA	70	18	19	16	15	15	56	11	14	11	11	10
FL	70	30	33	24	23	17	56	23	26	19	15	15
HW/HP	70	8	5	6	5	9	56	3	2	2	1	1
Control	1	1	0.6	0.3	1	1	0.4	0.4	0.2	0.7	0.5	0.6
Biological	**-30 d**	**0 d**	**15 d**	**30 d**	**45 d**	**60 d**	**-30 d**	**0 d**	**15 d**	**30 d**	**45 d**	**60 d**
NT	86	68	73	33	39	32	52	35	58	27	35	28
FE	86	68	46	36	36	38	52	35	68	28	32	34
FEM	86	68	36	37	36	50	52	35	27	31	32	45
FMeM	86	68	44	48	30	39	52	35	41	36	26	35
Control	1	1	1	0	0	0	0.2	0.2	0.2	0.1	0.1	0.1

NT: no treatment; MA: manual; FL: flushing; HP: hot water & high pressure; FE: fertilizer + emulsifier; FEM: fertilizer + emulsifier + microbe; FMeM: fertilizer + MEL + microbe

Table 3.6.
Evaluating developmental effect (spinal curvature and cardiac edema) and mortality of the residual oil exposure on zebrafish embryo (in vivo bioassay).

Remediation techniques	Spinal curvature (%)			Cardiac edema (%)			Mortality (%)		
Physical	**-1 d**	**0 d**	**60 d**	**-1 d**	**0 d**	**60 d**	**-1 d**	**0 d**	**60 d**
NT		42	36		58	44		94	14
MA	42	28	14	58	42	14	94	72	10
FL		8	6		8	6		53	13
HW/HP		8	3		3	3		31	33
Biological	**-30 d**	**0 d**	**60 d**	**-30 d**	**0 d**	**60 d**	**-30 d**	**0 d**	**60 d**
NT			36			36			55
FE	3	19	3	3	17	3	69	72	50
FEM			19			17			44
FMeM			31			36			39

NT: no treatment; MA: manual; FL: flushing; HP: hot water & high pressure; FE: fertilizer + emulsifier; FEM: fertilizer + emulsifier + microbe; FMeM: fertilizer + MEL + microbe

Table 3.7.

Evaluating AhR mediated potency of the residual oil by H4llE-*luc* (in vitro bioassay)

Remediation techniques	%TCDD$_{max}$		
Physical	**-1 d**	**0 d**	**60 d**
NT	48.3±8.1	48.3±8.1	39.3±6.6
MA		37.1±6.1	20.3±2.7
FL		38.6±8.2	24.8±5.5
HW/HP		12.1±2.1	19.8±4.3
Biological	**-30 d**	**0 d**	**60 d**
NT	47.9±5.8	38.6±6.8	43.8±12.2
FE			48.7±2.1
FEM			38.5±1.1
FMeM			34.0±1.5

NT: no treatment; MA: manual; FL: flushing; HP: hot water & high pressure; FE: fertilizer + emulsifier; FEM: fertilizer + emulsifier + microbe; FMeM: fertilizer + MEL + microbe

Ecological endpoints of SQT, initially included four targets, including MPB, bacteria, meiofauna, and primary production, generally encompassing key benthic taxonomic groups. Due to small numbers of individuals detected in control treatment (Figure 3.7), meiofauna were not utilized to calculate rates or efficiencies of recovery. For physical treatments, MPB cells decreased within a day of removal of oil, although chemical concentrations of TPH and UCM decreased dramatically (Figure 3.6a, 3.8a, and Table 3.8). This could be simply due to physical disturbance along with removal of oil from surfaces of gravel. MPB cells increased after 60 d during experiments, which confirms recolonization by MPB cells following proliferation after exposure to oil was less. This phenomenon was observed for all physical treatments, but HW/HP showed relatively good recovery of MPB. Similar to physical treatment, the MPB cells after 0 d) and/or 60 d in biological treatments showed significantly greater numbers of MPB cells compared to the initial exposure to oil (-30 d) (Figure 3.6b). Application of emulsifiers was an effective at reducing residual oil, but adversely affected the MPB community (Figure 3.4d, $p < 0.05$). For example, treatments FE and FEM, which contained emulsifiers, resulted in lesser numbers of MPB cells at the end of biological treatments even though concentrations of TPH and UCM decreased during that period. Toxic constituents of the emulsifiers affected the MPB community which offset the beneficial effects of dispersing residual oil (Hook and Osborn, 2012). In general, MPB species observed at the end of physical and biological treatments were dominated by a few taxa, including *Navicula* sp., *Amphora* sp. and *Nitzschia* sp. (Figure 3.8 and 3.9), genera that have been reported to be resistant to effects of oil (Partrick and Palavage, 1994).

Changes in the bacterial community were observed during physical and biological remediations, that resulted in greater numbers of bacterial OTUs more quickly. In particular, rapid increase of bacterial OTUs during NT indicated faster recovery under natural conditions (Figure 3.6a). During treatment with HW/HP, recovery of bacterial OTUs after 60 d was not clearly observed, and was eventually less than that initially (factor change: <1). Indices of bacterial diversity for HW/HP were less than those for other treatments. For instance, the Chao1 index decreased over 90 d (Table 3.9). The lesser *HI* (n17C/pristane and n18C/phytane) observed for

treatment HW/HP resulted in a decrease in biodegradation of oil by bacteria (Figure 3.10a). A combination of high temperature and pressure during the HW/HP treatment was the most effective in reducing concentrations of residual oil, but also resulted in adverse effects on natural bacteria (De Vogelaere et al., 1994). Some previous studies reported that the HW/HP method could damage directly to the habitat in which the marine organism lives, both in the short- and long-term periods (Paine et al., 1996; Pezeshki et al., 2000).

The number of bacterial OTUs in biological treatments also increased over 90 d of experiments, with final values being five-fold greater than initially stage (-30 d) (Figure 3.6b). Oil-degrading bacteria were more abundant in biological treatments than physical treatments, (Table 3.9). In marine environments exposed to oil spills, abundances of hydrocarbon-degrading bacteria rapidly expand (Love et al., 2021). Relatively lesser and slow breakdown of residual oils in biological treatments than physical treatments minimize this response (Figure 3.10b).

Primary production in the benthic environment, monitored in the remediation experiments to assessed functioning of microorganisms under the oil exposed environments tended to increase during both physical and biological remediations. Benthic, primary production increased 2- to 6-fold in all treatments over 60 d and was significantly ($p < 0.05$) and negatively correlated with concentrations of TPH and UCM (Figure 3.4c and 3.4d), increasing as the amount of oil decreased. However, 30 days of pre-seawater exchange before the actual biological treatments resulted in the greatest benthic primary production across all biological treatments. Greater primary production was attributed to recruitment of MPB and bacteria during continuous seawater inputs and consumption of hydrocarbon by oil-degrading bacteria (Valentine et al., 2015).

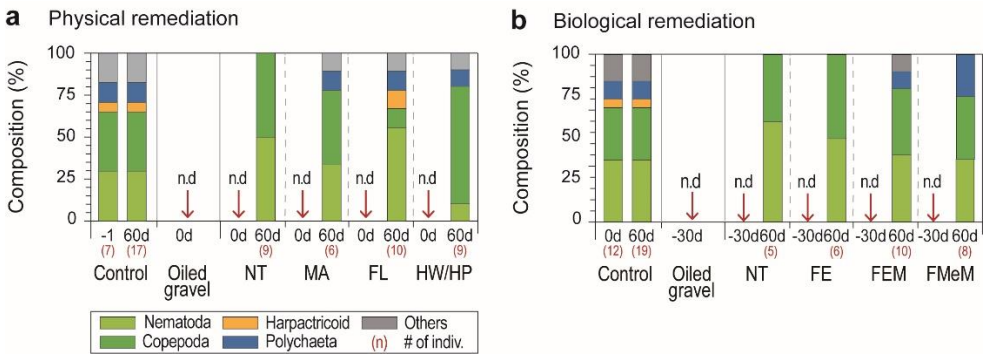

Figure 3.7
Observed meiofauna and its composition in each treatment during the experiment.

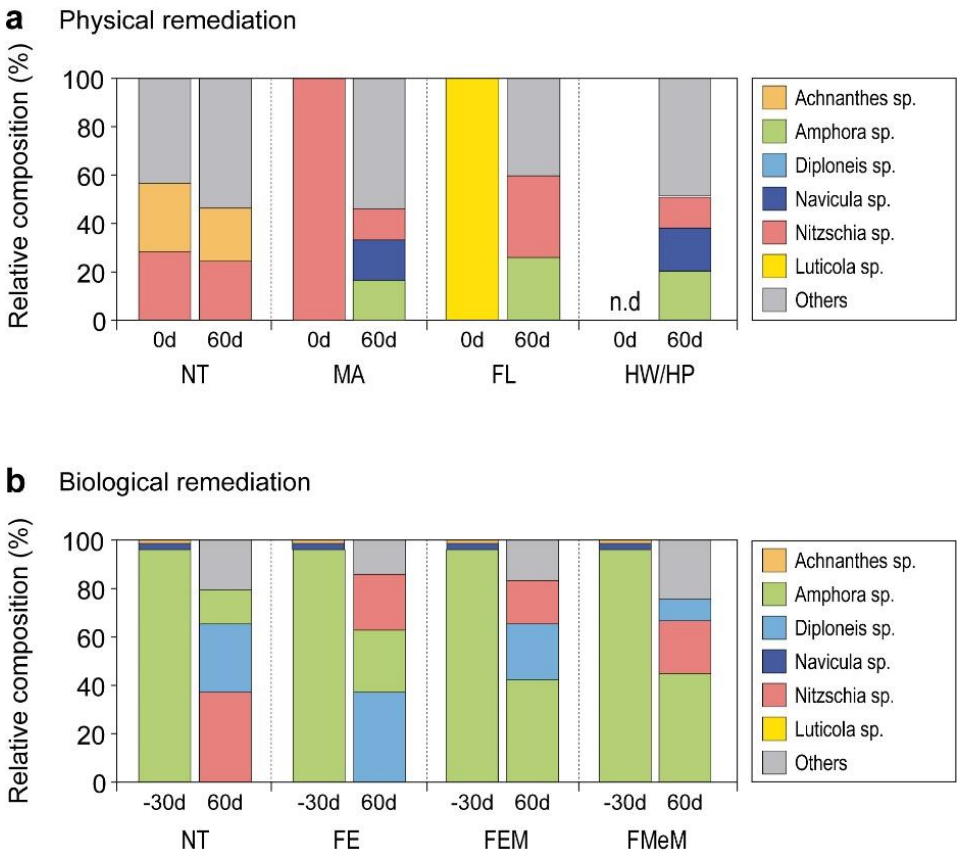

Figure 3.8
Relative composition and abundance of the dominant diatom species in each treatment during the experiment.

Table 3.8. Temporal changes of the number of diatoms in each treatment

Remediation techniques	Number of diatom		
Physical	**-1d**	**0d**	**60d**
Control	100	100	77
NT	18	18	75
MA	18	1	100
FL	18	7	52
HW/HP	18	1	90
Biological	**-30d**	**0d**	**60d**
Control	16	100	100
NT	16	72	100
FE	16	72	54
FEM	16	72	68
FMeM	16	72	100

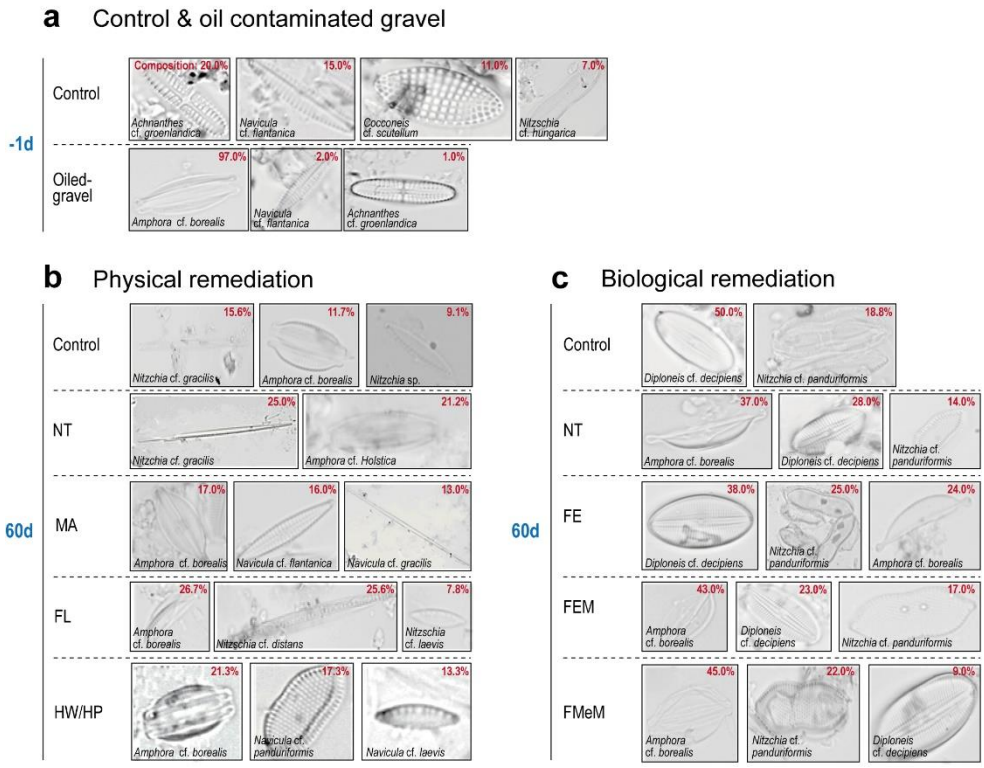

Figure 3.9
Images of dominant species of diatom in each treatment

Table 3.9.
Shannon and Simpson diversity index, and Chao1 index for each of the sampling in physical and biological remediation techniques

Remediation techniques	Diversity and richness index of bacteria														
	Shannon					Simpson					Chao1				
Physical	**-1 d**	**0 d**	**15 d**	**30 d**	**60 d**	**-1 d**	**0 d**	**15 d**	**30 d**	**60 d**	**-1 d**	**0 d**	**15 d**	**30 d**	**60 d**
NT	5.5	5.5	5.5	5.7	6.2	0.9	0.9	0.9	1.0	1.0	132	132	469	524	592
MA	5.5	6.6	5.4	4.9	5.5	0.9	1.0	0.9	0.9	0.9	132	233	360	455	612
FL	5.5	6.7	4.7	5.9	5.3	0.9	1.0	0.9	0.9	0.9	132	203	352	418	620
HW/HP	5.5	4.2	4.4	5.7	5.2	0.9	0.9	1.0	0.9	0.9	132	255	200	198	94
Control	3.7	3.7	4.5	4.9	6.4	0.8	0.8	0.8	0.9	1.0	387	387	721	538	229
Biological	**-30 d**	**0 d**	**15 d**	**30 d**	**60 d**	**-30 d**	**0 d**	**15 d**	**30 d**	**60 d**	**-30 d**	**0 d**	**15 d**	**30 d**	**60 d**
NT	1.8	5.2	6.1	4.7	5.8	0.4	0.9	1.0	0.9	0.9	142	306	673	523	839
FE	1.8	5.2	6.1	5.1	5.8	0.4	0.9	1.0	0.9	1.0	142	306	519	600	699
FEM	1.8	5.2	4.6	5.3	5.8	0.4	0.9	0.9	0.9	1.0	142	306	471	601	791
FMeM	1.8	5.2	5.6	5.0	5.9	0.4	0.9	0.9	0.9	1.0	142	306	516	575	731
Control	8.0	8.0	7.5	4.6	7.7	1.0	1.0	1.0	0.7	1.0	1443	1443	1412	1173	1181

NT: no treatment; MA: manual; FL: flushing; HP: hot water & high pressure; FE: fertilizer + emulsifier; FEM: fertilizer + emulsifier + microbe; FMeM: fertilizer + MEL + microbe

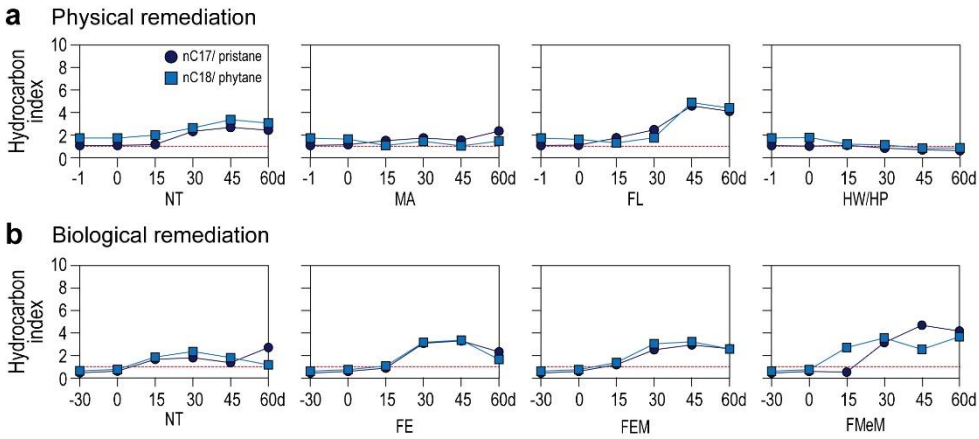

Figure 3.10
Temporal variations of nC17/ pristine and nC18/ phytane in the oil-contaminated gravel in each treatment

3.3.2. Dynamics in bacterial communities

Relative abundances of bacterial 16S rRNA gene sequences discriminatively revealed variation in relative compositions of bacterial communities. This information was used to address dynamics in structures of bacterial communities during exposure to and weathering of oil (Figure 3.11). On average, three phyla (Proteobacteria, Bacteroidetes, and Firmicutes) accounted for more than 85% of bacterial communities during both physical and biological treatments (Figure 3.12). For physical treatments, the principal component analysis (PCA) showed that abundances of bacterial phyla are interrelated with residual oil (TPH and UCM), *HI* (nC17/pristine and nC18/phytane), and primary production in the correlation matrix (Figure 3.13). Results of PCA suggested that the two principal components collectively accounted for 58.8% of the total variance. Actinobacteria, Bacteroidetes, Cyanobacteria, Firmicutes, and Proteobacteria were grouped with the concentrations of the residual oil (represented by Groups I–III). Three classes of Proteobacteria were specifically grouped with respect to different endpoints. First, beta-proteobacteria was positively loaded with residual oil, while alpha-proteobacteria were grouped with *HI* and primary production, which indicated biodegradation and functional recovery. In comparison, gamma-proteobacteria did not load to any endpoints.

Temporal variation between the groups was observed and was a of concentrations of residual oil and hydrocarbons (aliphatic) for each physical remediation technique (Figure 3.14). Bacterial Group I included Bacteroidia, Bacilli, Clostridia, beta-proteobacteria, and others, including unknown classes from Actinobacteria and Cyanobacteria, and generally consisted of early oil-degrading bacteria which changed in response to aliphatic hydrocarbons in TPH (Figure 3.14b). Group II included gamma-proteobacteria exclusively which have multiple oil-derived hydrocarbons, both aliphatic and aromatic, degrading metabolic activities; genera included *Pseudoaltermonas*, *Alcanivorax*, *Thalassolituus*, and *Cycloclasticus*. For HW/HP treatment, relatively small abundance of bacteria associated with degradation of oil was detected because a large amount of oil was initially removed. In particular, the FL treatment seemed to promote the rapid removal of residual oil as well as natural degradation by bacteria when *HI* increased.

Samples dominated by Group III had greater *HI* and primary production later in the experiment period. The results showed that a greater availability of residual aromatics supported greater degradation of hydrocarbons and increased primary production by *Sulfitobacter* and *Erythrobacter* as phototrophic bacteria despite the effect of overall reduction in the amount of hydrocarbons. Results of previous studies have shown changes in bacterial communities during degradation of oil might be attributed to a preference by various bacteria for hydrocarbon degradation intermediates as sources of carbon (Lea-smith et al., 2015; Uribe-Flores et al., 2019). Changes in structures of bacterial communities would be dependent on compositions of hydrocarbons present in oil during process of degradation of oil, in the order of alkanes, cycloalkanes, aromatics, resins, and finally asphalt (Dubinsky et al., 2013).

Changes in bacterial communities also occurred in response to lessening concentrations of hydrocarbons with increasing *HI* and primary production during biological treatments. Results of PCA ordination showed that the two principal components collectively accounted for 81.5% of total variance (Figure 3.13b). Changes in structures of bacterial communities were strongly associated with experimental periods. Bacteria in Group I, which mainly degrade aliphatic compounds decreased in response to a gradual decrease in TPH (Figure 3.14c). After 30 d of pre-exposure (-30 d to 0 d), the relative abundance of Group II noticeably increased. *Alcanivorax*, *Salegentibacter*, *Muricauda*, and *Marinicella* in gamma-proteobacteria were the prominent degraders of hydrocarbons (aliphatic and aromatic hydrocarbons) and more prevalent than any other taxa detected (Figure 3.14d). Bacteria in Group III began to dominate the community after 30 d. In particular, these bacteria included *Roseovarius* and *Erythrobacter*, which are psychrophilic photosynthetic organisms in addition to *Dietzia*. Appearances of these bacteria is indicative of a community optimized for degradation of complex organic matter and they dominated the community in the treatments in which microbial communities were augmented and enhanced, either directly or with fertilization.

In contrast to physical treatments, biological treatments had relatively great amounts of residual oil, which resulted in the dominance of aliphatic compound-degrading bacteria in Group II (30 d to 60 d). Biological remediations influenced

compositions and enriched bacterial populations with the ability to use dispersed compounds as the growth substrates (Kleindienst et al., 2015). Furthermore, these treatments enhanced abundances and expressions of oil-degrading bacteria, such as *Alcanivorax* and *Roseovarius* (Tremblay et al., 2017; Procópio et al., 2020). Together, biological treatments and proliferation of oil-degrading bacteria from seawater input collectively contributed to the overall reduction of residual oils in a combined manner.

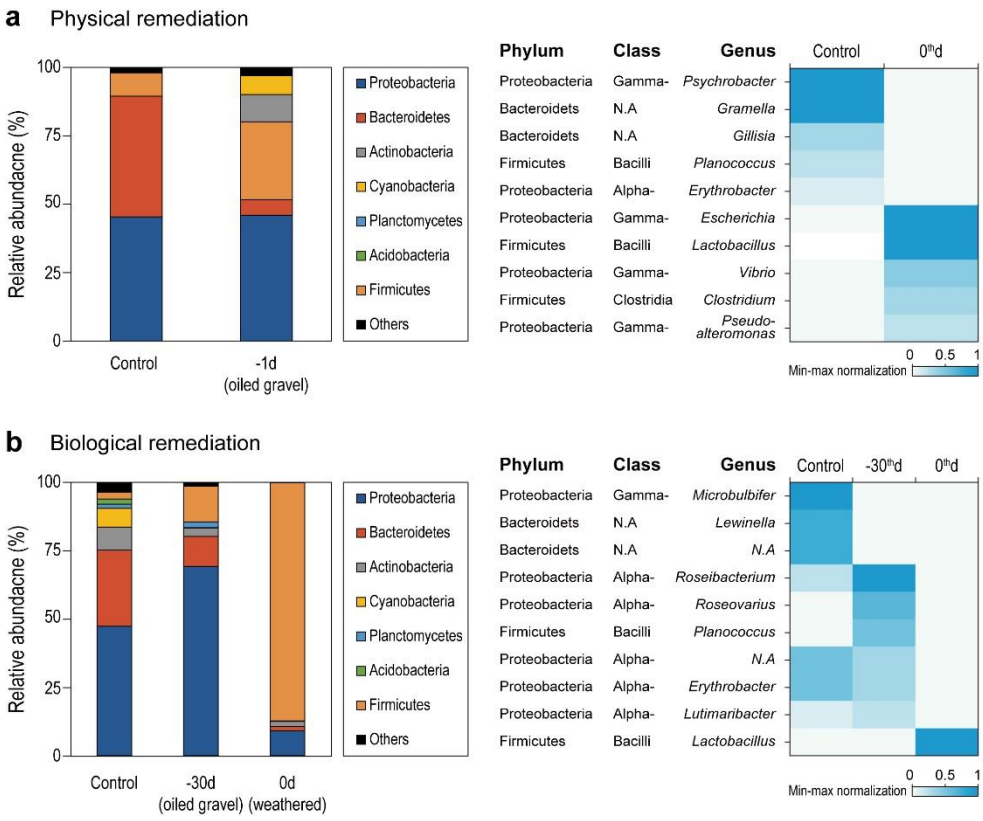

Figure 3.11

Relative composition of bacterial community and dominant genus in the control and oil- contaminated gravel. (a) Negative control and oil-contaminated gravel, (b) negative control, oil-contaminated gravel, and oil-weathered gravel.

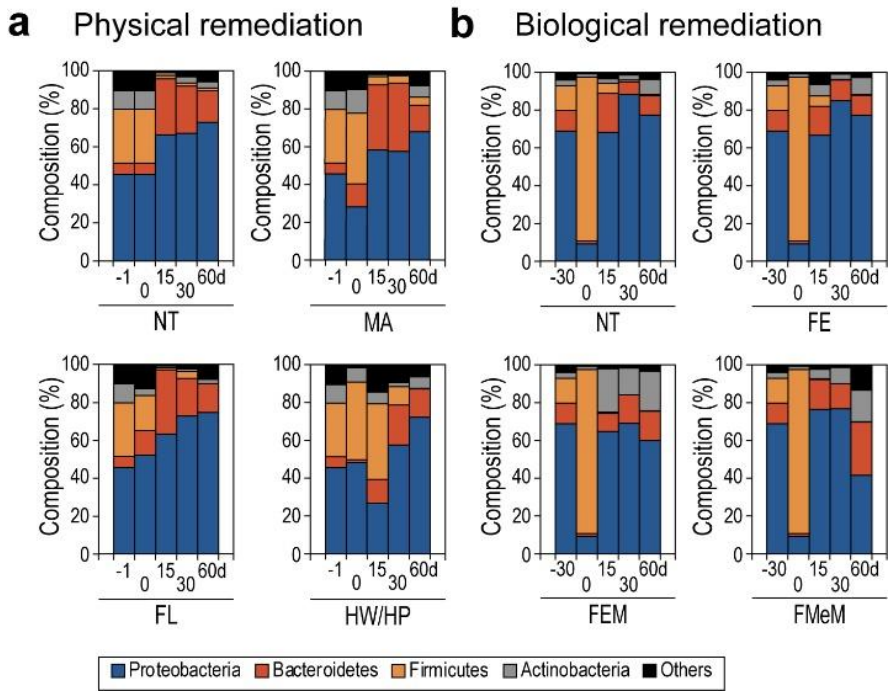

Figure 3.12
Relative composition of bacterial community and dominant genus in each treatment from day 0d to 60 d and -30 d to 60 d.

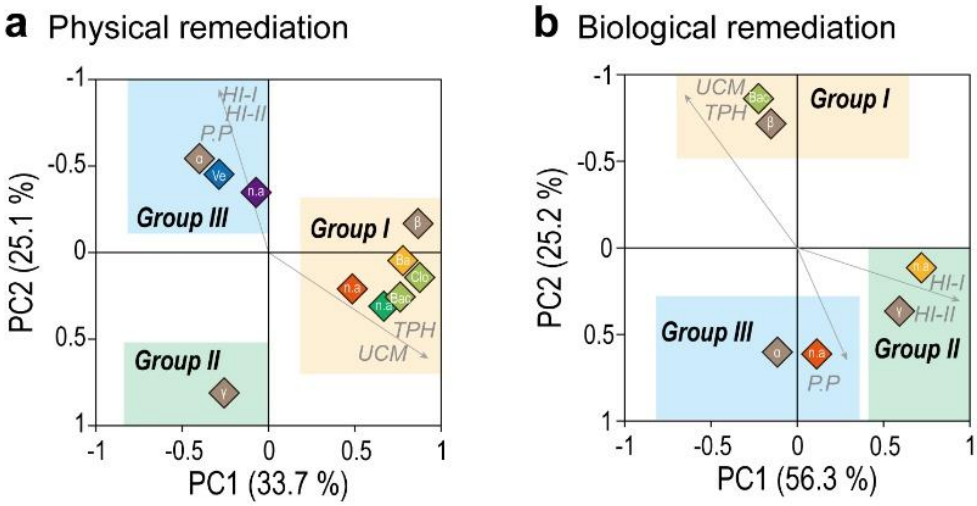

Figure 3.13

Principal component analysis (PCA) ordination between the selected endpoint (TPH and UCM concentration, hydrocarbon index, and primary production) representatives of Group I–III (Diamond colored with red: *Actinobacteria*; yellow: *Bacteroidetes*; green: *Cyanobacteria*; light green: *Firmicutes*; brown: *Proteobacteria*; purple: N.A) (n.a: unknown; Ba.: *Bacteroidia*; Bac.: *Bacilli*.; Clo.: *Clostridia*; α: *Alphaproteobacteria*; β: *Betaproteobacteria*; γ: *Gammaproteobacteria*; Ve.: *Verrucomicrobiae*).

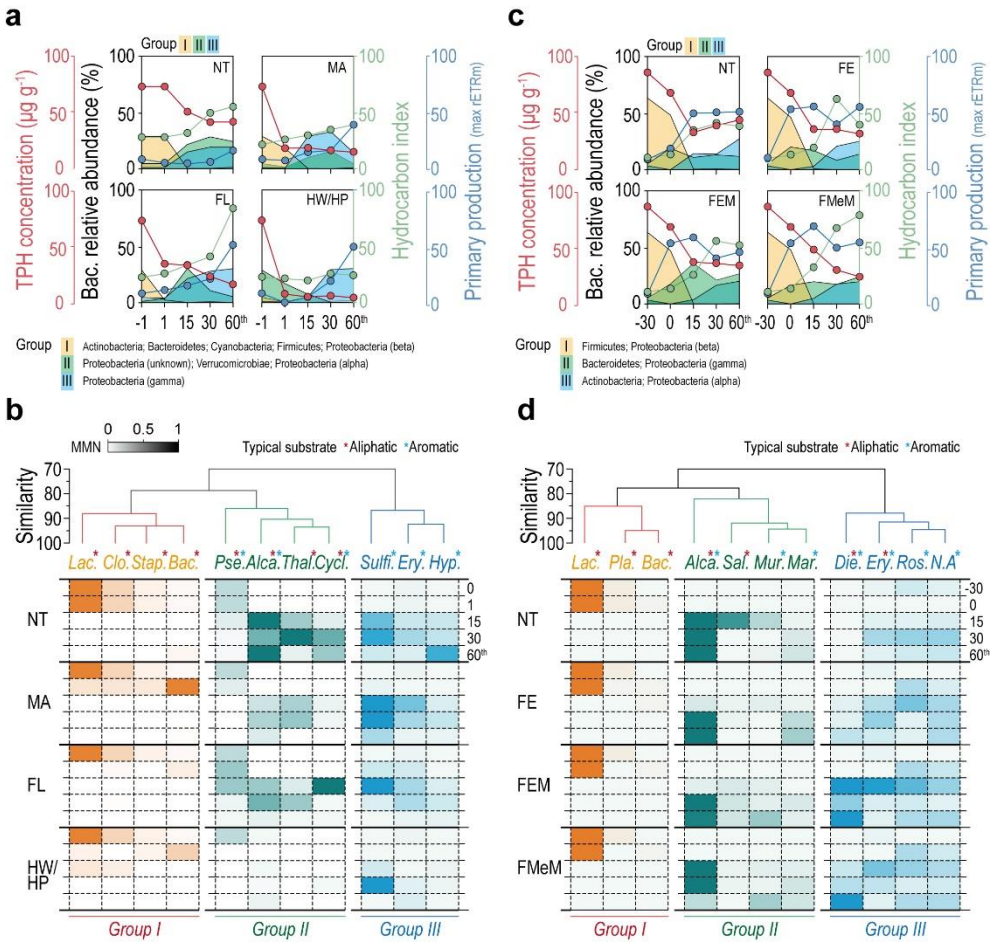

Figure 3.14

Temporal variation of the most abundant bacteria in each treatment (a: physical remediation and b: biological remediation) and heat map showing changes to bacterial genera over the experiment periods (c: physical remediation and d: biological remediation). Genus name is provided for genera with over 3% of the relative abundance to the total for each remediation (*Lac.*: *Lactobacillus*; *Clo.*: *Clostridium*; *Stap.*: *Staphylococcus*; *Bac.*: *Bacillus*; *Pse.*: *Pseudoalteromonas*; *Alca.*: *Alacanivorax*; *Thal.*: *Thalassolituus*; *Cycl.*: *Cycloclasticus*; *Sulfi.*: *Sulfitobacter*; *Ery.*: *Erythrobacter*; *Hyp.*: *Hyphomonas*; *Pla.*: *Planococcus*; *Sal.*: *Salegentibacter*; *Mur.*: *Muricauda*; *Mar.*: *Marinicella*; *Die.*: *Dietzia*; *Ros.*: *Roseovarius*; and *N.A.*: unknown).

3.3.3. Effectiveness of remediation techniques

To evaluate the effectiveness of various methods of physical and biological remediation, ratios of eight target endpoints to negative control values (clean gravel) were determined (Figure 3.15 and 3.16). The results (-30 d, 0 d, 1 d, 30 d, and 60 d) were used to determine the recovery from the implementation of remediation treatments and oil weathering, and to confirm the long-term effects. The HW/HP treatment showed the greatest recovery effectiveness (72%), since the initial implementation for 60 d, followed by MA (68%), NT (54%), and FL (53%) (Figure 3.15a). Except for MPB biomass and primary production, bacterial richness was adversely affected by HW/HP at 60 d (Figure 3.16). After 60 d of all treatments, except for HW/HP, ecological endpoints first recovered rapidly, followed by toxicological endpoints. Although physical oil removal negatively influenced the marine life at the beginning of treatment, physical treatments accelerated the long-term recovery. In particular, ecological endpoints recovered by the MA treatment (100%) reached similar level to the control values. While the recovery of chemical endpoints was relatively great in the HW/HP treatment compared to other treatments, ecological endpoints showed little recovery. Furthermore, the HW/HP treatment had a lesser effectiveness for toxicological endpoints on 60 d (55.3%) compared to 0 d (79.2%), indicating certain unknown effect. When HW/HP treatment was implemented to wash oil-contaminated gravel, the washed oil appeared to penetrate into the deeper layers of sediment and caused potential toxicity (Street, 2011; Walther III, 2014). Overall, although physical treatments were initially effective at removing oil, the oil could remain beneath the surface and cause further adverse effects on surrounding environments.

Weathering oil-contaminated gravel for 30 d before biological treatments given generally increased the recovery of chemical, toxicological, and ecological endpoints, with mean efficiency of >30% (Figure 3.15b). After 90 d, total recovery efficiency reached 47% in the FMeM treatment, which was greatest among the biological treatments. In the previous study, as in one of the series of this study, a combination of microbes was effective for remediation of the sedimentary contamination by oil. Interestingly, "no treatment" showed comparable recovery to

others, indicating natural attenuation can promote soft bottom benthic community health (Lee et al., 2019a). Alternatively, the combined use of emulsifiers reduced both potential toxicity and residual oil, but adversely affected marine benthic organisms (Lönning et al., 1976). Primary production was less in the mixed solution with emulsifier at 60 d compared to 0 d (Figure 3.16). Results of a previous study demonstrated that primary producers are sensitive to biological treatments (Hsiao et al., 1978). In particular, potential toxic effects by dioxin-like substances would increase after implementing the techniques, resulting in negative effects of emulsifiers on benthic organisms, including primary producers (Couillard et al., 2005; Rahsepar et al., 2016). Unlike physical techniques, the poor efficiency for reducing the total amount of residual oil could be attributed to incomplete removal of the residual oil by the dilution of the mixed solution due to seawater inflow. Overall, the present results suggested that residual oil cannot be removed completely by a sole application of biological techniques, but it is desirable to use physical techniques prior to implementation of biological treatments (Fox, 1996).

3.3.4. Best available remediation techniques

Decision-making in response to spilled oil entails balancing economic constraints with the need to remove as much oil as possible from the spilled site while minimizing the environmental effects of the remediations used, thus optimizing environmental protection in the short and long term (Etkin, 2005). Natural attenuation is often as efficient as most active restoration alternative and is cost-effective while minimizing the impacts of active remediation (Jahn and Robillard, 1997). Results of the study presented here also indicated that no treatment was effective for long-term recovery of the area in which oil was spilled. While natural recovery has less effect on the environment compared to active remediations, it would be difficult to implement in areas, which are more heavily affected by oil spills. Accordingly, natural recovery might be suitable for the areas exposed to small quantities of oil spills and high energy tides (Etkin, 2002). An appropriate remediation technique should be carefully selected in a way to promote both short- and long-term recoveries while securing the immediate remediation at golden time.

In order to evaluate the best available techniques, we considered three main criteria, including economic availability, environmental performance, and technical applicability. The three criteria were subdivided into a total of 9 factors (Table 3.10). For physical remediation, the criteria with greater scores were different from treatment by treatment (Figure 3.17a and Table 2). NT scored great in the economic availability category (0.15), which focuses on the lesser cost of removing residual oil. Various physical techniques used for remediation of oil are effective in restoring benthic ecosystems, but seem to be relatively more expensive for operating them compared to NT. Based on performance, treatment MA showed the greatest score (0.30). While MA had relatively lesser scores for economic availability, it scored well for environmental performance and technical applicability. Therefore, in comprehensive consideration of all three categories, MA was evaluated as the BAT among physical techniques tested during the present investigation (Figure 3.17a). The HW/HP treatment was ranked next to MA because of a lesser score for technical applicability.

Based on the MAUT analysis, FMeM treatment scored greater in all categories compared to other biological techniques (Figure 3.17a and Table 3.11). Other techniques scored similarly in environmental performance and technical applicability (0.18–0.27), but FMeM scored the greatest in environmental performance (0.45) because of a quick reduction of oil. The NT scored great in economic availability (0.15) but little in environmental performance and technical applicability, because of its relatively poor ability to remove residual oil and may incur additional remediation cost. However, on exposed shorelines with high-energy tides, the majority of oil is expected to be cleared within a seasonal cycle. Natural cleaning is similar to flushing in principle, but relies on the natural energy of the waves to give far larger quantities of water than could be delivered by pumps. Future research is needed to settle the high-energy tide system in the mesocosm system, and determine its potential for removing oil. Overall, based on biological techniques tested, FMeM was deemed to be the BAT. However, these biological technologies do not rapidly remove a large amount of residual oil in a short-time period, so they need to be employed in conjunction with physical techniques (Zengel et al., 2015).

Assuming an oil spill occurred on a gravel shoreline, the BAT could be selected by multiplying each previously obtained score from the MAUT analysis (Figure 3.17b). When evaluating various remediation techniques in this study, the most effective remediation for oil was calculated as "MA + FMeM", which scored 0.46. The "HW/HP + FMeM" received a comparable score of 0.44, but a penetration of washed oil into the substrate layer and thus long-term adverse effects on the benthic community would be required. While employing various remediation techniques in this study, although various other factors, including labor requirement, workplace safety, and the post management should be included in evaluating each technique, quantitative studies were insufficient to include all of them. Therefore, the result of this study may not be suitable to all oil spill situations.

Physical remediation is conducted to recover sedimentary contamination by oil at initial stage. Biological remediation is applied to promote health of benthic communities (Tuler et al., 2007). Physical and biological remediation treatments should be applied differently depending on the habitat characteristics of the spilled site and it is recommended that the remediation technique suggested in this study would be applied to a gravel covered coast with an environmental sensitive index (ESI) of “6A” (Table 3.12) (Michel, 2013). When the oil spilled from sea is introduced to the coast, MA treatment proposed in this study can limit the spread of pollution by reducing the risk of oil landfilled in the coast by the wave or the wind (POSOW, 2013). In general, a combination of physical and biological techniques is well known to effectively remedy the oil spills (Byroade et al., 1981; Reed et al., 1995; Chen et al., 2019). According to the results of this study, the use of the initial implementation of MA and the use of FMeM treatment can promote the recovery of benthic community health avoiding further adverse effects. Further study to conduct the experiment as successive combining between physical and biological remediation is necessary for applying to in situ oil spill response. Final cleanup should be recommended to begin only as successive after the initial cleanup of the large-scale accumulated oil has been completed and all threats of new significant deposits have been removed (Venosa et al., 2004).

Table 3.10.
Modified evaluation criteria from Dave and Ghaly (2011) for marine oil spill remediation techniques.

Criteria		Definition	Score
Economic availability	Cost	Relatively inexpensive	15
Environmental performance	Efficiency	a) 95-99% removal	20
	Health	a) Reduction rate of potential toxicity	10
		a) Recovery of benthic community	10
	Change of oil	Do not change physical/chemical characteristics of oil	5
	Further treatment	No further treatment required	5
Technical applicability	Time	a) Removes contaminant within days	15
	Level of difficulty	Easy to maintain and operate	10
	Weather	Favourable for application of method	5
	Reliability	The method works the majority of the time	5

[a)] Scoring from data in this study.

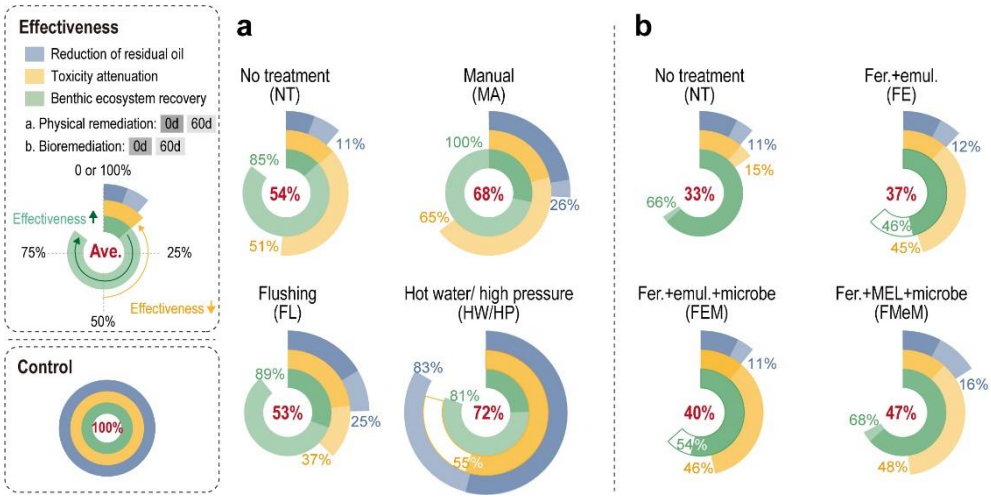

Figure 3.15.

Comparison of effectiveness based on integrated approaches with eight target elements. The integrated approaches included: 1) reduction of residual oil (TPH and UCM concentration), 2) toxicology attenuation (mortality, luminescence inhibition, and $\%TCDD_{max}$), and 3) benthic ecosystem recovery (MPB cell, bacterial community richness, and primary production). Each element was calculated using the ratio to negative control (see Data Analysis section for details).

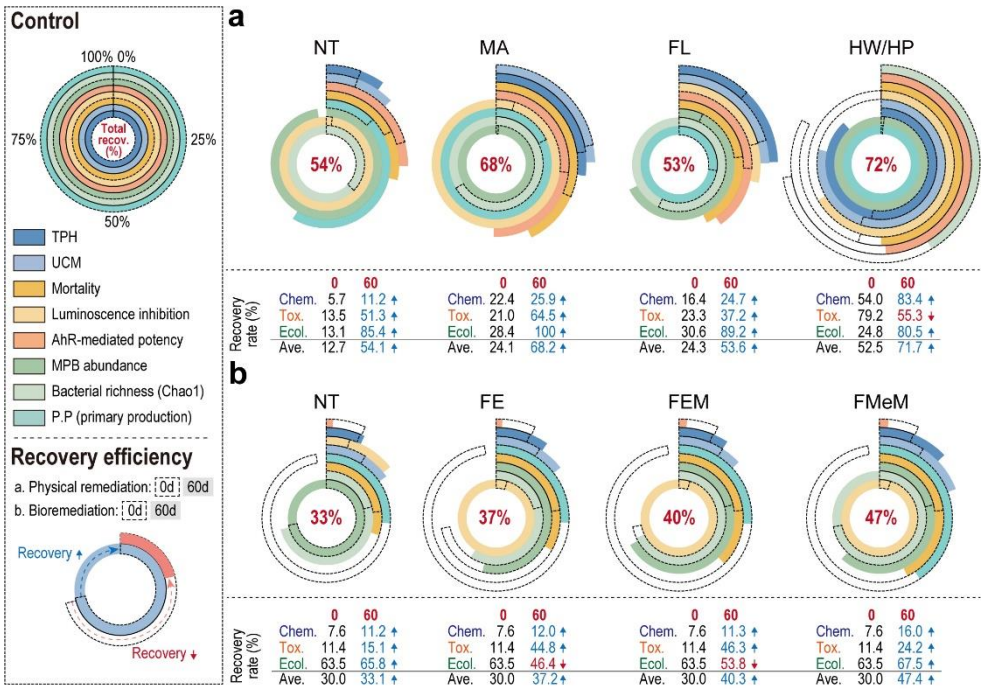

Figure 3.16
Comparison of efficiency by the integrated approaches with eight target elements in each remediation.

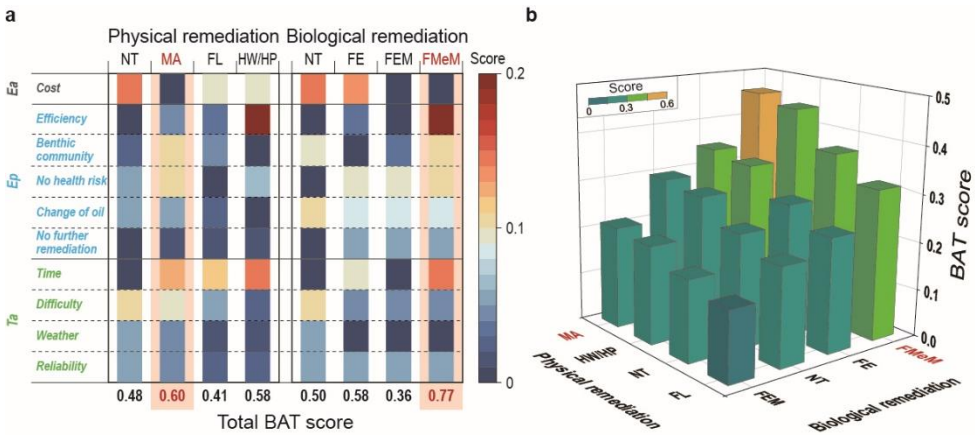

Figure 3.17

Score diagram of the best available techniques (BATs). (a) Total score calculated from ten criteria using multi-attribute utility theory (MAUT) analysis for each technique. (b) Evaluation of combined physical and biological remediation techniques based on multiplying each score in the oil spill simulation.

Table 3.11.
Multi-attribute utility theory (MAUT) analysis for selecting the best available techniques for oil spill response.

Remediation techniques	Method	[a)] Ea	Rank	[b)] Ep	Rank	[c)] Ta	Rank	Ea+Ep	Rank	Ea+Ta	Rank	Ep+Ta	Rank	Ea+Ep+Ta	Rank
Physical	NT	**0.15**	**1**	0.13	3	0.20	4	0.28	3	**0.35**	**1**	0.33	3	0.48	3
	MA	0.00	4	**0.30**	**1**	**0.30**	**1**	0.30	2	0.30	4	**0.60**	**1**	**0.60**	**1**
	FL	0.09	2	0.11	4	0.21	2	0.21	4	0.30	2	0.32	4	0.41	4
	HW/HP	0.09	2	0.28	2	0.21	2	**0.37**	**1**	0.30	2	0.48	2	0.57	2
Biological	NT	**0.15**	**1**	0.15	4	0.20	3	0.30	3	0.35	2	0.35	4	0.50	3
	FE	0.14	2	0.18	3	0.27	2	0.31	2	**0.40**	**1**	0.45	2	0.58	2
	FEM	0.00	3	0.18	2	0.18	4	0.18	4	0.18	4	0.36	3	0.36	4
	FMeM	0.00	3	**0.45**	**1**	**0.32**	**1**	**0.45**	**1**	0.32	3	**0.77**	**1**	**0.77**	**1**

[a)] Ea (economic availability): cost (relatively inexpensive); [b)] Ep (environmental performance): efficiency (95–99% removal rate of residual oil); health (reduction rate of potential toxicity and recovery of benthic community); change of oil (do not change physical/chemical characteristics of oil); necessity for further treatment (no further remediation required); [c)] Ta (technical applicability): time (removal of contaminant within days); level of difficulty (easy to maintain and operate); weather (favorable for application of method); reliability (the method works the majority of the time).

Table 3.12.
Environmental sensitive index (ESI) types for estuarine settings modified from NOAA (2013).

ESI no.	Estuarine
1A	Exposed rocky shores
1B	Exposed, solid man-made structures
1C	Exposed rocky cliffs with boulder talus base
2A	Exposed wave-cut platforms in bedrock, mud, or clay
2B	Exposed scarps and steep slopes in clay
3A	Fine- to medium-grained sand beaches
3B	Scarps and steep slopes in sand
3C	Tundra cliffs
4	Coarse-grained sand beaches
5	Mixed sand and gravel beaches
6A	**Gravel beaches (granules and pebbles)**
6B	Riprap
7	Exposed tidal flats
8A	Sheltered scarps in bedrock, mud, or clay
8B	Sheltered, solid man-made structures
8C	Sheltered riprap
8D	Sheltered rocky rubble shores
8E	Peat shorelines
8F	None
9A	Sheltered tidal flats
9B	Vegetated low banks
9C	Hypersaline tidal flats
10A	Salt- and brackish-water marshes
10B	Freshwater marshes
10C	Swamps
10D	Scrub-shrub wetlands; mangroves
10E	Inundated low-lying tundra

3.4. Conclusions

In conclusion, the present study successfully analyzed and demonstrated the integrated aspects of the efficiency of various remediation techniques in relation to early and long-term recovery of a gravel shore. Much environmental and technical science research has been under taken recently to better understand the evaluation of efficiency in the physical and biological remediation techniques. For removing the residual oil more effectively and eco-friendly, application of appropriate remediation techniques to be suitable the targeted shoreline is required. The selection of the techniques cannot be determined unless considering economic availability, environmental performance, and technical applicability. With experimental results, further study of encompassing economic, social, technical, and environmental aspects is needed to oil contaminated shoreline. The results provide guidelines on the techniques best suited for recovering an oil-contaminated gravel shore while facilitating the recovery of adversely affected benthic ecosystems, elsewhere.

CHAPTER 4.

DETERMINING CHARACTERISTICS OF SEDIMENT QUALITY WITH MACHINE LEARNING TO EVALUATE THE NATURAL RESTORATION IN CONTAMINATED TIDAL FLAT SEDIMENT FOR PERSISTENT TOXIC SUBSTANCES

This chapter has been in preparation.
Kim, T., Kim, J., Kwon, I., Lee, J., Bae, H., Jin, G., Park, S. Y., Noh, J., Lee, C., Hong, S., Kwon, B.-O., Song, S. J., Chang, G. S., Giesy, J. P., Khim, J. S. Determining characteristics of sediment quality with machine learning to evaluate the natural restoration in contaminated tidal flat sediment for persistent toxic substances.

4.1. Introduction

Coastal pollution by persistent toxic substances (PTSs) in sediments among tidal flats is primarily from human activities associated with population growth and expansions of industrial and commercial developments (Hong et al., 2012). The fate of PTSs in marine ecosystems depends to a great extent on their physicochemical characteristics. Due to their hydrophobicity and particle reactivity, concentrations of many PTSs are often several orders of magnitude higher in sediments compared to concentrations in the overlying waters. As such, sediments are often a sink for pollutants in aquatic environments (Bae et al., 2017). The ultimate fate of sediment associated pollutants in a given environment is determined by the physicochemical properties of the pollutants, diagenetic processes within the sediments and the physical stability of that particular environment. It is well known that PTSs accumulated in sediments adversely impact benthic ecosystems in a variety of ways (Lee et al., 2017; Khim et al., 2018).

The role of tidal flat in natural restoration has been highlighted primarily from the standpoint of hydrocarbon and nutrients turnover (Hu et al., 2006). Imbalance between the PTSs loads and natural restoration capacity in tidal flats could change the role of coastal sediments from a source of nutrients to a purifier. Recent reconsideration of marine ecosystem services has led a growing interest in the restoration or construction of tidal flat and wetland as a countermeasure for land-driven pollution (Kim et al., 2020). The restoration capacity of tidal flats has been highlighted through various mesocosm experiments (Kim, 2013). Since the mechanisms of remediation in tidal flats are diverse and complicated, study for quantification of restoration capacity on each process has been insufficient (Hasanudin et al., 2004).

Representatively, there are bio-irrigation and phytoremediation process of natural restoration in tidal flat. Irrigation by macrofauna (denoted bio-irrigation) leads to an increased exchange of solutes between the porewaters and overlying water. One of the major effects of infaunal irrigation is to extend the oxidized zone to depth within the sediments (Fenchel 1996) which stimulates aerobic and subtoxic

(i.e., metal reduction) decomposition processes (Banta et al. 1999, Hansen & Kristensen 1998, Thamdrup et al. 1994). Macrophytes have been shown to play important roles in marsh biogeochemistry through their active and passive circulation of elements. Active uptake of elements into macrophyte tissue may promote immobilization in macrophyte tissues, as seen in wetlands constructed for wastewater treatment (Kadlec and Knight, 1996) and in the use of wetland macrophytes in phytoremediation. Phytoremediation is considered an effective and preferred cleanup option for moderately contaminated areas. These two processes are known to contribute to the overall restoration function of tidal flats by increasing the activity of bacteria (Yagi and Terai, 2001).

Mesocosms have been employed as research tools in both terrestrial and aquatic systems and to study environmental phenomena at both small and large spatial scales. Mesocosm experiments are commonly used as physical models of ecosystems (Ahn and Mitsch 2002) and provide researchers with a controlled and replicable framework (Kemp et al. 1980, Banse 1982, Odum 1984) that can be applied in numerous scientific disciplines. Mesocosm experiments have some inherent limitations that should be considered. Small-scale mesocosm experiments may have reduced ecological complexity relative to the ‘‘reference’’ ecosystem (Ahn and Mitsch 2002). And, a complex array of interactions found in natural ecosystems cannot always be simulated by mesocosms (Clements et al., 1988; Carpenter, 1996; Schindler, 1998). To overcome these issues, we designed an over 1-m diameter mesocosm system which closely mimicked larger scale, whole field experiment and set them up in a natural tidal flat for simulating an actual circumstance (e.g., weather, physico-chemical properties of seawater).

Our recent mesocosm studies successfully demonstrated the most appropriate biological methods for evaluating natural restoration capacity in aspect of soft bottom benthic community recovery (Lee et al., 2018; Kim et al., 2020). Here, as a continuing effort, the present study evaluated the natural restoration capacity in contaminated sediment among tidal flat. The study adopted the advanced sediment quality triad (SQT) approach, with multiple measures of chemical, toxicological, and ecological indicators; 1) PTSs concentration (polycyclic aromatic hydrocarbons

(PAHs); alkylphenols (APs); styrene oligomers (SOs); heavy metals (HMs)), 2) aryl hydrocarbon receptor (AhR) mediated potency, 3) bacterial OTU, 4) microphytobenthic (MPB) and 5) meiofauna individuals, 6) chlorophyll-*a* (chl-*a*). For evaluating the restoration status, and analyzing benthic community characteristics, we employed the self-organizing map (SOM; also called Kohonen map or topology preserving feature map), which is a kind of artificial neural networks (ANN) method which is capable of clustering, classification, estimation, prediction, and data mining. The present study insights on the method-dependent and endpoint-specific remediation efficiency in a rarely studied restoration capacity of tidal flat for PTSs and benthic communities.

4.2. Materials and Methods

4.2.1. Sample preparation and In situ mesocosm experimental setting

Core sediments near Lake Sihwa in Incheon, Korea were sampled for transplantation (Figure 4.1). The concentrations of PTSs (PAHs, APs, and SOs) in the sediments were 2300 ng g^{-1}, 2000 ng g^{-1}, and 500 ng g^{-1}, respectively. After sampling the experimental sediment near an industry area, the sediments were transplanted in the mesocosm. Contaminated sediments were transplanted to a height of 12–15 cm above the in-situ sediments. Mesocosms (1.6 m inner diameter) were constructed using rubber that formed the base of the structures and covered with 1×1 mm mesh to prevent macrofauna from adding to them. In addition, a total of three valves were installed according to the lowest, average, and highest seawater levels in the tidal flat so that seawater could only flow through the valve. In situ mesocosms included three habitat types: bare tidal flat (BT), bare tidal flat + biota (BTB), salt marsh (SM), and salt marsh + biota (SMB). To reflect a field marine ecosystem, the treatments were added with organisms (*Cyclina sinensis* (C. *sinensis*) and *Macrophthatmus japonicus* (M. *japonicus*)) and vegetation (*Phragmites australis* (P. *australis*)) to correspond to the nature of the habitat. Sampling was conducted 11 times (0 h, 2 h, 6 h, 12 h, 1 d, 2 d, 3 d, 7 d, 14 d, 30 d, and 60 d). We employed a sediment quality triad approach (SQT) (chemistry, toxicology, and ecology) to evaluate the natural restoration capacity of PTSs in each habitat type. Experimental conditions and descriptions of each remediation technique are presented in Figure 4.2 and Table 4.1

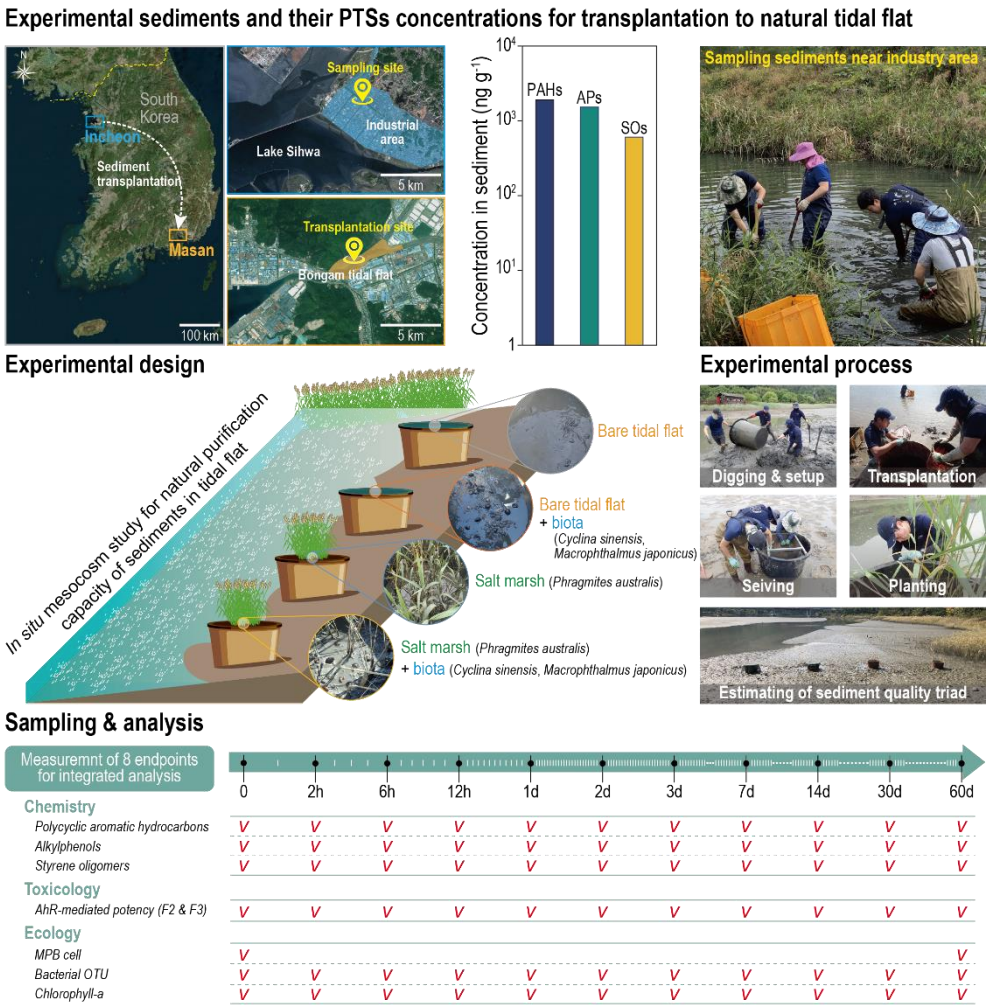

Figure 4.1

Schematic of physical and biological remediation techniques, experimental conditions, and sampling design of this study.

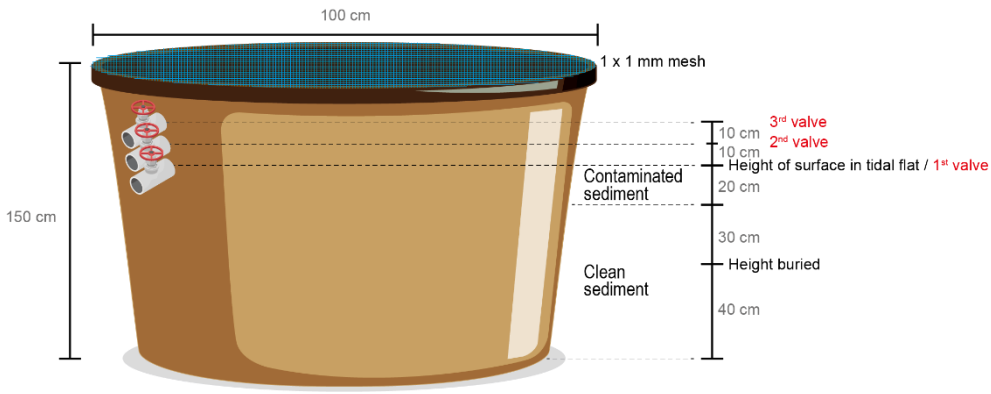

Figure 4.2
Experimental design for mesocosm system.

Table 4.1. Density of habitat of organisms used in this study

Scientific name	Density of habitat (ind. m^{-2})										
	1st	**2nd**	**3rd**	**4th**	**5th**	**6th**	**7th**	**8th**	**9th**	**10th**	**Ave.**
Cyclina sinensis	12	6	13	7	6	9	7	8	11	9	9.9
Macrophthalmus japonicus	9	5	4	7	8	6	4	9	11	7	7.4
Phragmites australis	72	56	34	64	56	32	48	73	101	87	41.9

4.2.2. Persistent toxic substances analysis (PAHs, APs, and SOs)

Measurements of PTSs including polycyclic aromatic hydrocarbons (PAHs), alkylphenols (APs), styrene oligomers (SOs), heavy metals (HMs) in sediment were conducted by following the procedures in previous studies (Yoon et al., 2019). Sediment samples were prepared to analyze PAHs, Aps and SOs following an existing method, with minor modifications [Ref, Ref]. In brief, Freeze-dried sediment samples were extracted using an accelerated solvent extractor (Dionex ASE 350, Thermo Scientific, Salt Lake, UT), following an existing method with minor modifications (Yuan et al., 2020). In brief, 10 g sediment was placed in a 33 mL stainless steel cell, and extraction was performed with dichloromethane (DCM, Burdick & Jackson, Muskegon, MI) at 120 °C, with an extraction time of 10 min for one cycle. All samples were spiked with 100 ng of four surrogate standards before extraction for quality control. The extracts were collected in pre-cleaned 60-mL glass vials, and were concentrated to about 1 mL by N_2 gas flow (TurboVap LV, Biotage, Uppsala, Sweden). To desulphurize the mixture, activated copper powder (Merck, Darmstadt, Germany) was added for 1 h. The extracts were purified through an open column chromatography packed with 8.0 g activated silica gel (70–230 mesh, Sigma-Aldrich).

The aromatic fraction was collected by eluting 60 mL hexane:DCM (8:2, v/v) for PAHs and SOs analysis, and 60 mL DCM:acetone (6:4, v/v) for APs analysis. The eluent was concentrated to 1 mL under N2 gas flow, and 100 ng of internal standard (2-fluorobiphenyl, ChemService) was added. We quantified PAHs and APs using an Agilent 7890A gas chromatograph equipped with a mass selective detector (GC-MSD) (Agilent Technologies, Santa Clara, CA). Method detection limits (MDLs) were determined as standard deviations 3.707 times that of standard samples. The ranges of MDLs were 0.27–0.90 ng g^{-1} for PAHs and SOs, and 0.10–0.91 ng g^{-1} for APs. Recoveries for the five surrogate standards and standard reference material 1944 were generally acceptable: 72%–121% (mean = 90%) and 80%– 126% (mean = 106%).

4.2.3. H4IIE-luciferase transactivation bioassay

Fractions (F2: semi-polar and F3: polar) were substituted with dimethyl sulfoxide (DMSO), followed by concentrating them to 1 mL (~10 mg contaminated sediment equivalent (SEq) mL^{-1}) (Lee et al., 2020). H4IIE-*luc* bioassay were employed for testing acute toxicity of the residual PTSs in the sediment (Lee et al., 2019). The H4IIE-luc bioassay was performed to detect AhR-mediated potencies in oil-contaminated gravel according to previously published methods. In brief, trypsinized cells (~7.0×104 cells mL−1) were seeded in 96-well plates and incubated for 4 h. The plates were then dosed with the appropriate standards (Benzo[*a*]pyrene, (BaP); 0.1% dose), samples (raw; 0.1% dose (~0.1 mg SEq mL-1)), and solvent controls (0.1% DMSO) for 4 h. After 4 h exposure, the results were expressed as relative luminescence units that were quantified using a Victor X3 multi-label plate reader (PerkinElmer, Waltham, MA).

4.2.4. Bacterial metagenomic analysis

The bacterial community was analyzed by extracting total genomic DNA from gravels on 0th to $60d^{th}$ using a PowerSoil® DNA Isolation Kit (MoBio Laboratories, Solana Beach, CA, USA). Sequencing was conducted using the Illumina MiSeq Platform with 16S, rRNA gene amplicons. The V3 and V4 regions of the bacterial 16S ribosomal gene were amplified using Illumina primers and barcoded adapters. Quantitative Insights into Microbial Ecology (QIIME) was used to analyze the sequence data. Using UCLUST, sequences were clustered by operational taxonomic units (OTUs) at a 97% identity threshold. Taxonomic information was delegated by aligning sequences with the data from Ribosomal Database Project (RDP).

4.2.5. Identification of diatom individual

Samples was collected from each experimental aquarium, with triple replicates per aquarium. For diatom separation from gravel, 5% formalin solution was added to the collected gravel samples and shaken. Only the supernatant was decanted into a beaker. After adding 10 mL distilled water to remaining sediment, the water-sediment mixture was sonicated for 5 seconds. The supernatant was removed from the submerged samples, and 30 mL distilled water and 10 mL hydrochloric acid (HCl) were added for the acid treatment. Finally, the gravel samples were heated and cooled to be neutralized for observation and identification.

4.2.6. Identification of meiofauna individual

The meiofaunal samples were obtained using a plastic core with a surface area of 10 cm^2 in a depth of 0–3 cm. The pooled meiofaunal samples were fixed with 5% formaldehyde solution, and separated by flotation (Heip et al., 1985) and centrifugation (Burgess, 2001) using a colloidal silica solution (LudoxHS-40, Aldrich Chemical Company). The procedure was repeated three more times to ensure that all organisms had been extracted from the sediment. All meiofauna individuals were identified to the highest taxonomic level following Higgins and Thiel (1988), and counted under a stereomicroscope.

4.2.7. Measurements of benthic primary production

Surface sediments (at 0–5mm depth) were collected using a syringe core (inside diameter=1.5 cm) to measure chlorophyll a (Chl-*a*) concentration as a proxy for MPB biomass. Added a 10 ml 100% acetone in approximately 7 cm^3 volumes of sediment sample in a 50 ml conical and vortexed. The pigments in the sample are eluted for 24h in refrigerator maintained at 4 °C in the dark. Samples were then centrifuged at 3000 rpm for 5 min. The 3 ml of supernatant solution of the centrifuged sample was placed in quartz cuvette by using a pipette. The absorbance of the solution was measured at 750, 665 nm using a spectrophotometer before and after acidification with 2 drops of 1N HCl. The concentration of Chl-*a* (mg m^{-2}) in the sediment was measured and calculated by the Lorenzen (1967) method.

4.2.8. Self-Organizing Map (SOM)

Self-organizing map (SOM) was used to classify characteristics of samples in each treatment during the experimental periods (~60 d). The SOM is an efficient means of creating maps of multidimensional and complex data to approximate the probability density function of the input data in a more comprehensive fashion (Kohonen, 1990). In the SOM network, the output layer consisted of computation nodes (j) in low dimension (conveniently 2). Assuming input data consisting of four parameters, the value of a parameter, i, is expressed as a vector, xi, and was given to the input layer of the SOM. In the network each computation node, j, is connected to each node, i, of the input layer. The connectivity is represented as the weights, $w_{ji}(t)$, between input and output nodes, adaptively changing in each iteration of calculation, t, until convergence is reached. Initially, the weight is randomly assigned in small values. Each neuron of the network computes the summed distance between the weights and the distance, $d_j(t)$, at output node, *j*, and the network is calculated as shown below (Eom et al., 2014):

$$d_j(t) = \sum_{i=0}^{N-1} \left(x_i - w_{ji}(t)\right)^2$$

The input data matrix consists of four behavior parameters (concentration of PTSs, index of HMs, AhR-mediated potency, bacterial OTU, number of species in diatom, abundance of meiofauna, and chlorophyll-*a*) as variables and 44 movement segments (i.e., 11 (time series) × 4 (treatments) = 44) as sample units (Figure 4.3).

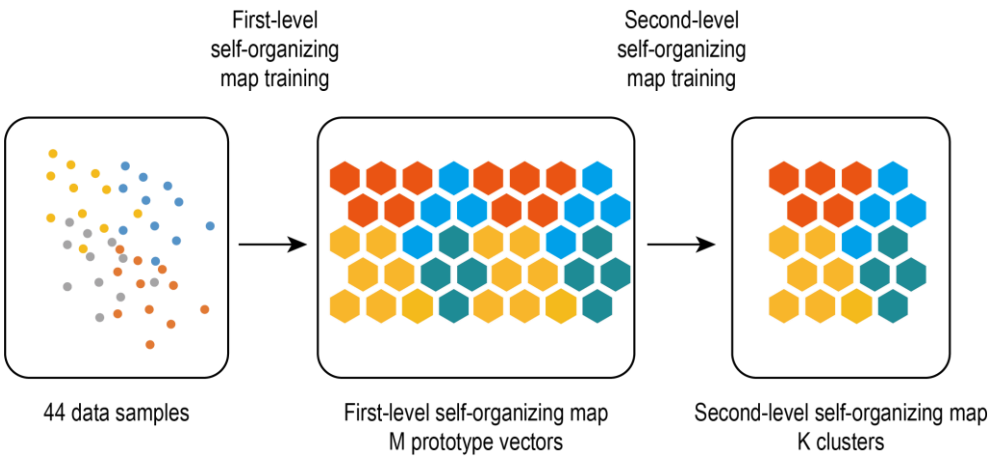

Figure 4.3
Diagram representing SOM clustering process

4.2.9. K-means clustering via principal component analysis (PCA)

The proposed model is designed and implemented by combing the benefit of applying PCA, K-means and Logistic regression. This methodology (Ding and He, 2004) is then proposed by using PCA to transform the initial set of features, thereby solving the problem of correlation, which makes it difficult for the classification algorithm to find relationships among the data. The PCA application helps to filter out irrelevant features, thereby lowering the training time, cost, and increases model performance. After performing PCA analysis, the result is then passed for unsupervised clustering using K-means because of the ability of k-means to address outliers. The K-means cluster result is cleaned, and logistic regression is applied to build our supervised classification for the dataset.

4.2.10. Statistical analysis

Data analyses were carried out using IBM SPSS software (version 23.0; SPSS Inc., Chicago, IL, USA). The difference of recovery and reduction rate among each treatment was analyzed by Analysis of covariance (ANCOVA). In all statistical analyses, p values less than 0.05 were considered to be statistically significant. Principal component analysis (PCA) to visualize the similarity between selected endpoint (TPH, UCM, HI, and primary production) and bacterial abundance.

4.3. Results and Discussion

4.3.1. Chemical, toxicological, and biological responses in natural restoration process of tidal flat

The average initial (0 h) concentrations of PAHs, APs, and SOs in the contaminated sediments were 2450 ng g^{-1}, 2150 ng g^{-1}, and 550 ng g^{-1}, respectively (Figure 4.4 and Table 4.2). After the sediments transplanted were exposure to the environment, the concentrations of PAHs, APs, and SOs decreased rapidly. Thereafter, in the treatments without macrofauna (BT and SM), the concentration of PTSs decreased slowly until 60 d, but the treatments with macrofauna (BTB and SMB) showed concentration fluctuations. The concentration in 60 d was lower than that of the treatments without macrofauna. In degree of contamination index (mC_d) (Kowalska et al., 2018) for heavy metals (calculated using data for Zn, Cd, Pb, Cr, and Cu, raw data showed in Figure 4.5), all treatments showed "moderate contamination" ($2 < mC_d < 4$) at the initial stage (0 h). For 60 days (0 h–60 d), the index decreased stepwise, and finally indicated "very low" ($mC_d < 1.5$) in all treatments except BT. Mixing of sediments by bio-irrigation from macrofauna activity can drastically change the composition of electron acceptors deep within sediment through reoxygenation with promoting the degradation of PTSs. In unperturbed, organic carbon–enriched sediment, heterotrophic bacterial metabolism rapidly depletes oxygen, limiting its availability to the top few millimeters of sediment (Montgomery et al., 2008). PTSs degradation or absorption enhancement by macrophyte was also investigated since it is known that macrophyte exudates are a significant source of organic nutrients and inorganic compounds. Macrophytes have a more direct effect on contaminant levels via phytoextraction, which concentrates PTSs (e.g., heavy metals) from the environment into macrophyte tissues (Shrestha et al., 2019).

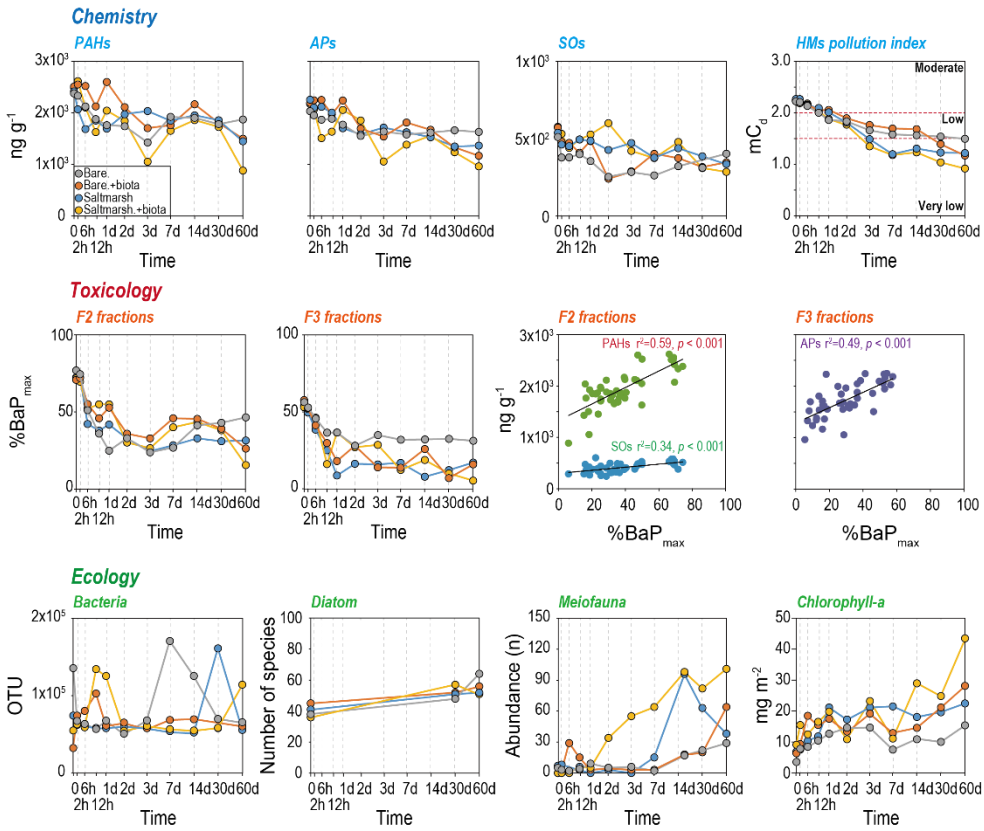

Figure 4.4

Chemical and toxicological reduction rate and ecological recovery rate after implementation of each treatment.

Table 4.2. Temporal variation of sedimentary PTSs concentration in each treatment for the ~60 days

Target PTSs & treatments	Concentration (ng g^{-1})										
	0h	**2h**	**6h**	**12h**	**1d**	**2d**	**3d**	**7d**	**14d**	**30d**	**60d**
PAHs											
BT	2379	2332	2123	1877	1761	1740	1426	1922	1902	1781	1872
BTB	2509	2551	2520	2124	2599	2110	1704	1760	2166	1816	1499
SM	2416	2069	1685	1850	1693	1971	2035	1846	1952	1857	1449
SMB	2494	2616	2104	1626	2044	1843	1052	1652	1859	1724	885
APs											
BT	511	378	379	399	355	253	285	263	321	312	403
BTB	571	479	472	409	483	241	289	402	374	316	346
SM	538	462	451	495	486	427	472	377	438	386	336
SMB	576	531	440	495	527	600	421	375	479	310	285
SOs											
BT	2022	1943	1858	1877	1761	1547	1629	1573	1610	1654	1622
BTB	2182	2232	2240	1960	2228	1688	1533	1804	1665	1325	1162
SM	2243	2092	2106	1993	1693	1577	1706	1615	1518	1341	1359
SMB	2161	2055	1503	1626	2044	1843	1052	1376	1550	1232	959

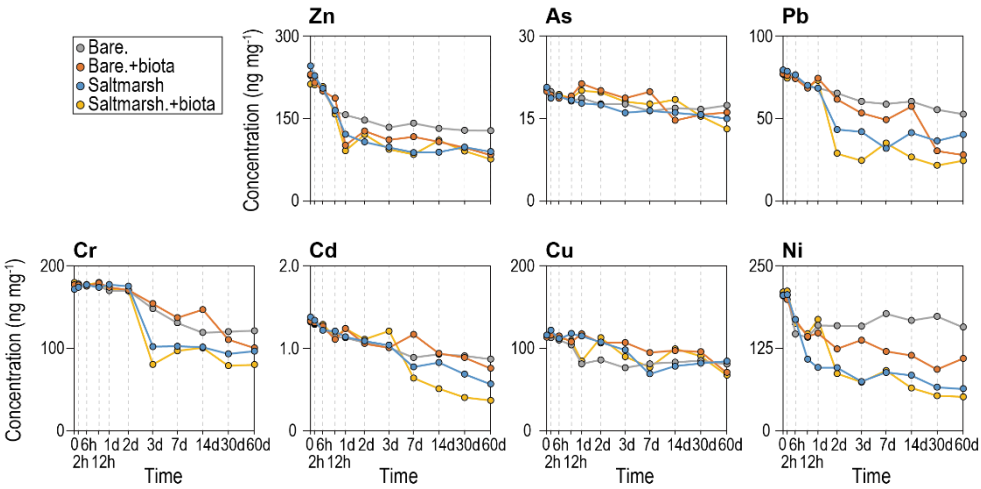

Figure 4.5
Overall temporal variation of heavy metal concentrations obtained from samples in each treatment from day 0d to 60d.

Among silica gel fractions from the sediments, greater AhR-mediated potencies were observed in the fractions of F2 (mid-polar compounds) and F3 (polar compounds) at the initial stage (0 h) (Figure 4.4). Variations of AhR-mediated potency showed a decrease during 60 d, which was consistent with the PTSs concentration (Table 4.3). After the sediment transplantation, the AhR potency decreased until 3 d, and increased from 7d in F2 fractions. AhR-mediated potency of F2 fractions was decreased the most in the treatments with macrofauna. The F3 fraction showed a faster reduction in AhR-mediated potency than the F2 fraction. Most AhR-mediated responses appeared to be caused by the aromatic compounds associated with the residual PTSs in the sediments. In a strong correlation between the AhR potency and target PTSs in each fraction, PAHs, SOs, and APs showed R^2 = 0.59, 0.34, and 0.49, respectively, indicating that PAHs contributed significantly to AhR mediated potency. Results of the present study were consistent with previous finding showing that AhR agonists in the fractions were degraded or transformed to lesser toxic chemicals during the contaminated sediment purified (Lee et al., 2018). In particular, the rapid and high potential toxicity reduction in the treatments with macrofauna and macrophyte can be seen because of the more degradation of the contributed substances in F2 (high molecular PAHs: HMW and styrene trimers: STs) and F3 (nonylphenol – and octylphenol: NP/OP) (Biliard et al., 2006; Ohyama et al., 2001; Acir & Guenther, 2018).

Table 4.3. Evaluating AhR mediated potency in the sediments from each treatment by H4llE-*luc* (in vitro bioassay)

Fractionations & treatments	AhR mediated potency (%BaP_{max})										
	0h	**2h**	**6h**	**12h**	**1d**	**2d**	**3d**	**7d**	**14d**	**30d**	**60d**
F2											
BT	76.9	74.5	51.1	35.9	24.9	32.9	23.8	26.8	41.3	42.9	46.4
BTB	70.8	72.0	55.1	45.8	52.8	35.8	32.8	45.8	45.5	39.0	26.2
SM	72.4	72.5	42.1	37.8	41.8	32.7	24.5	28.4	32.8	30.9	31.5
SMB	71.7	69.6	52.2	54.9	54.9	30.1	26.5	40.1	43.4	38.1	15.5
F3											
BT	56.4	52.8	45.7	36.6	36.6	28.0	35.0	32.0	32.1	32.5	31.2
BTB	57.7	52.5	41.3	29.8	18.1	28.1	14.0	13.8	25.9	7.0	15.9
SM	54.2	49.6	38.5	25.1	8.7	16.4	15.9	16.9	8.0	12.3	17.1
SMB	53.0	51.9	46.3	16.1	36.6	27.1	28.6	12.4	18.8	10.0	5.4

Bacterial OTU showed dynamical changes during the experimental periods (Figure 4.4 and Table 4.4). 0.5×10^5 OTU was generally detected in all treatments, but the period when the OTU increased was different. In the treatments with biota (BTB and SMB), OTU increased more than 2 to 3 times during the 6 h–1 d period. Whilst, in the treatments without macrofauna (BT and SM), the OTU values showed rapidly increase after 3 d. Unlike the change of bacteria OTU, the number of species in diatom and abundance of meiofauna increased steadily from the initial stage (0 h). In the SMB, a marked increase in the abundance of meiofauna was observed, and the highest value of Chl-*a* was also detected. In BO and SO groups, the amount of Chl-*a* more than twice as high as in the initial stage (0 d) means that the transplanted contaminated sediments are gradually recovered, indicating environment for benthic organisms can live has been created.

Bio-irrigation has been linked to dramatic changes in both the composition and metabolic activity of the sedimentary bacterial assemblage. Macrofaunal burrows harbor unique assemblages of bacteria that mineralize PTSs more rapidly than those from adjacent nonborrowed sediment (Montgomery et al., 2008). The influence of benthic macrofauna on the biomass, spatial distribution, and production rate of MPB (diatom in this study) not only results from their feeding activity (i.e., grazing pressure) but also depends on their effects on organic matter mineralization rates and nutrient cycling, mainly through sediment bio-irrigation (Swanberg 1991; D'Hondt et al., 2018). On the other hand, through their bio-irrigation activity, the two species (C. *sinensis* and M. *japonicus*) may have a positive effect on MPB photosynthesis and growth by enhancing remineralization processes and nutrient fluxes across the benthic interface (Thrush et al., 2006; Sandwell et al., 2009; Lohrer et al., 2010; Donadi et al., 2013; Volkenborn et al., 2016; Eriksson et al., 2017). Altogether, bioturbation processes (i.e., both sediment reworking and bio-irrigation) increase the incorporation and regeneration rates of organic carbon within the benthic compartment, thereby stimulating nutrient fluxes across the sediment-water interface where microbenthic primary producers can assimilate them for photosynthesis under optimal conditions (Eriksson et al., 2017; Hope et al., 2020).

Table 4.4. Temporal variation of benthic community in each treatment for the ~60 days

Target (unit) & treatments	Spatial variations										
	0h	**2h**	**6h**	**12h**	**1d**	**2d**	**3d**	**7d**	**14d**	**30d**	**60d**
Bacteria (OTU)											
BT	1.4e+5	6.7e+4	6.4e+4	5.7e+4	6.8e+4	5.1e+4	6.8e+4	1.7e+5	1.3e+5	7.0e+4	6.6e+4
BTB	3.2e+4	7.4e+4	8.0e+4	1.0e+5	6.1e+4	6.5e+4	5.8e+4	6.9e+4	7.0e+4	5.8e+4	6.0e+4
SM	7.4e+4	6.2e+4	6.0e+4	5.8e+4	5.8e+4	6.0e+4	5.9e+4	5.4e+4	5.2e+4	1.6e+5	5.6e+4
SMB	5.5e+4	6.3e+4	5.9e+4	1.3e+5	1.3e+5	5.5e+4	6.1e+4	5.7e+4	5.5e+4	5.8e+4	1.1e+5
Diatom (# of species)											
BT	38	n.a	n.a	n.a	n.a	n.a	n.a	n.a	n.a	48	64
BTB	45	n.a	n.a	n.a	n.a	n.a	n.a	n.a	n.a	52	56
SM	41	n.a	n.a	n.a	n.a	n.a	n.a	n.a	n.a	51	52
SMB	36	n.a	n.a	n.a	n.a	n.a	n.a	n.a	n.a	57	51
Meiofauna (abundance)											
BT	5	3	2	4	9	5	6	2	17	22	29
BTB	0	2	29	15	3	5	3	3	18	20	64
SM	7	8	0	3	0	3	0	15	96	63	38
SMB	0	0	0	6	5	34	55	64	98	82	101
Chlorophyll-*a* (mg m^{-1})											
BT	3.6	7.8	8.5	10.5	12.7	14.6	14.7	7.6	10.9	10.0	15.4
BTB	6.4	9.4	18.5	15.5	17.5	13.4	19.2	12.9	14.6	21.1	28.2
SM	6.9	7.6	10.4	11.8	21.2	17.3	21.2	21.5	18.1	19.6	22.5
SMB	9.1	15.5	12.5	16.5	19.8	10.9	23.2	11.1	29.0	24.9	43.5

4.3.2. Time series clustering in evaluating the recovery of each treatment with the self-organizing map (SOM) using machine learning

We built a SOM for evaluating the recovery of each treatment to create an integrated analysis including chemical, toxicological, and ecological data in spatial samples in this study. Considering the number of samples and unexplained variance, total 4 superclasses (groups) were chosen (Figure 4.6a). The results of the clustering of SOM prototypes into superclasses showed 0.23 (S_i) in average (Figure 4.6b). In particular, the cells (C1, C2, C5) in Group I showed the highest S_i value ($S_i = 0.36$), which meant that it held the longest distance between other groups. A spatial gradient was observed for all of the samples (Figure 4.6c); Group I (total 10): BT^{0h}, BT^{2h}, SM^{0h}, SM^{2h}, BTB^{0h}, BTB^{2h}, BTB^{6h}, BTB^{1d}, SMB^{0h}, and SMB^{2h}; Group II (total 13): BT^{6h}, BT^{12}h, SM^{6h}, SM^{12h}, SM^{1d}, SM^{2d}, SM^{3d}, BTB^{12h}, BTB^{7d}, SMB^{6h}, SMB^{12h}, SMB^{1d}, and SMB^{2d}; Group III (11): BT^{1d}, BT^{2d}, BT^{3d}, BT^{7d}, BT^{14d}, BT^{30d}, BT^{60d}, SM^{30d}, BTB^{2d}, BTB^{3d}, and BTB^{14d}; Group IV (10): SM^{7d}, SM^{14d}, SM^{60d}, BTB^{30d}, BTB^{60d}, SMB^{3d}, SMB^{7d}, SMB^{14d}, SMB^{30d}, and SMB^{60d}. This result, along with sampling date and various results (Figure 4.1 and 4.4), collectively suggesting the decrease of PTSs and their toxicity, and recovery of benthos community in response to times going by.

Each group had various characteristics, which showed the difference of recovery in chemistry (reduction rate of PTSs), toxicology (reduction rate of AhR-mediated potency), and ecology (increase of benthos community health) from the initial stage (0h) (Figure 4.6d). Common characteristics of the Group I samples are that the concentration and potential toxicity of PTS are low, and the ecological community is not well restored. In Group II, III, and IV, the recovery of all factors increased. PTSs decreased by 40% and latent toxicity by 54%, and benthic community increased by 2.9 times in Group IV, which indicated more recovered from the initial stage than other groups. Change of groups in each treatment varied according to their habitat types. All treatments except BT had the characteristics of Group IV at 60 d. Interestingly, Samples in BTB moved more frequently between groups than those of BT, but as a result, it had the characteristics of Group IV finally.

Both SM and SMB recovered quickly, unlike non-saltmarsh treatments, and SMB had the characteristics of Group IV after the 3 d.

Approach for benthic ecosystem health approach from multipollutant has a variety of methods (Pearce et al., 2014). There is an integrated analysis in evaluating the marine ecosystem health that considers SQT associated with the recovery from the contaminated environmental status (Lee et al., 2018). Combining between SQT and machine learning, one promising solution is to use classifications or groupings to characterize aspects of the sediment quality (Pearce et al., 2014). To achieve this goal, we presented an approach for identifying a 'reasonable' number of classes that emphasized aspects of classification representativeness and considered potential statistical power by using a SOM. This strategy found a 4-superclass system as an attractive solution for this data as it provided a balance between variance explained and potential sample size. SOM is to be an attractive framework for classifying day types for ambient sediment quality characterization because the approach produces classifications equivalent to traditional techniques with the benefit of a map that provides an organized visualization of class profiles (Eom et al., 2014). This additional feature of SOM promotes understanding of potentially complex interclass relationships that could prove useful in evaluating the recovery of marine ecosystem settings requiring larger classification systems.

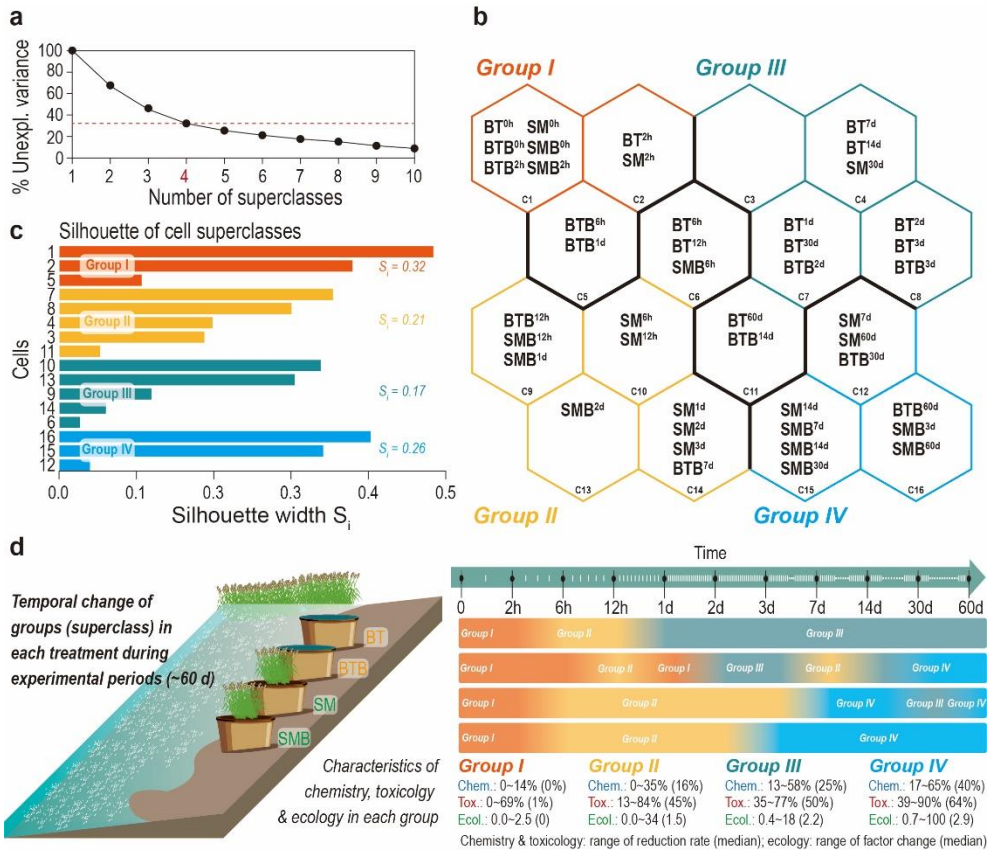

Figure 4.6

A novel approach combining self-organizing map and SQT for evaluating restoration capacity of tidal flat for contaminated sediments. (a) Number of superclasses for related characteristics of samples. (b) Silhouette plot for verification of distance between each cell. (c) Self-organizing map showing each temporal sediment quality in treatments. (d) Temporal change of groups in each treatment during experimental periods and characteristics of each groups.

4.3.3. Effect of macrofauna (*C. sinensis* and *M. japonicus*) and salt marsh (*P. australis*) on the change of benthic community using K-means clustering: PCA

To evaluate the effect of macrofaunal and macrophyte to the variation of benthic community, the treatments with the same characteristics (BO: BTB + SMB, BX: BT+SM, SO: SM+SMB, and SX: BT+BTB) were integrated, and then the relationship between the communities was compared. *K*-means clustering via principal components analysis (PCA) indicated the relationship between benthic organisms.

The first two axis of the PCA, which was conducted to visualize the multivariate variability of z-standardized data, explained 75.9% of the variation (Figure 4.7a-1). As indicated in the plot, four clusters were observed according to the sampling periods on the PCA diagram (A1: 0 h; A2–A3: 2 h–14 d; A4: 30 d and 60 d). Group A1 was assigned showing the significant correlation with *Paralia sulcata*. Group A2, which mainly included BO^{2d}–BO^{14d}, can mainly be related with *Chloroflexi* in bacteria, Polychaeta and Amphipoda in meiofauna. Nematoda strongly showed the correlation with Group A3, showing in the intermediated sampling dates in BX. Finally, Group A4 identified the samples with *Campilobacterota*, *Thalassinema nitzschioides*, *Cyclotella* cf. *stylorum*, and Copepoda. Changes of groups over time depended on the presence or absence of macrofauna in the treatments (BO vs. BX). In particular, in the treatments group with macrofauan (BO), there were many changes in benthic community structure.

In Figure 4.7a-2, the PCA explained a proportion of variance (i.e., 48.7% and 30.5% for axes 1 and 2, respectively). The results also revealed that four clusters were identified with the sampling periods (B1: 0 h, B2–B3: 2 h–14 d, and B4: 30 d, 60 d). Group B1 was clustered showing *Paralia sulcate* was dominant at the initial stage (0 h). Group B2 including mainly SO^{6h}–SO^{3d} showed the positive correlation between *Chloroflexi* and Amphipoda. During the almost experimental periods, in SX, Nematoda strongly was dominant, indicating Group B3. Group B4 identified the samples with *Campilobacterota*, *Cyanobacteria*, *Bacteroidota*, *Cyclotella* cf. *stylorum*, and *Delphineis* sp..

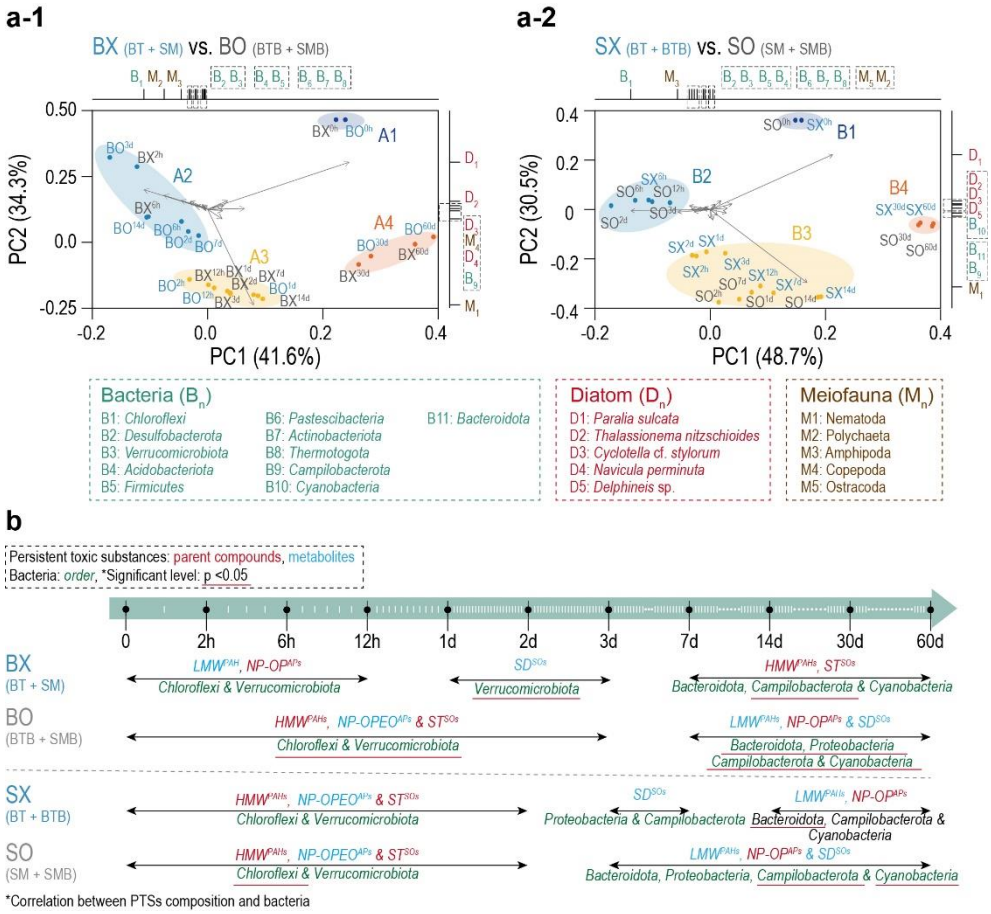

Figure 4.7

Temporal change of benthic community in each treatment. (a) Principal component analysis (PCA) ordination between benthic communities including bacteria, diatom, and meiofauna. (b) Changes of PTSs composition according to dominant bacteria in each treatment group.

Marine organisms either stabilize or destabilize the sediment with facilitating or inhibiting effects on shoreline succession (Reise, 2002). Our study provides experimental evidence that macrofauna have the potential to ecologically change a habitat in a depositional coastal environment. Change of dominant benthic organisms (**meiofauna**: Polychaeta and Amphipoda → Copepod; **diatom**: *Paralia sulcata* → *Cyclotella* cf. stylorum and *Navicula perminuta*; **bacteria**: *Chloroflexi* → *Campilobacterota*) showed that biological irrigation can enhance native PTSs biodegradation and promote the emergence of several benthic communities by increasing the sediment quality (Drira et al., 2018; McQuoid & Nordberg, 2003; Saros & Anderson, 2015; Chen et al., 2019; Speirs et al., 2019; Wang et al., 2022). Effect of the benthic community by transplanting the macrophyte promoted a change of bacterial communities but did not make significant difference between SX and SO groups in meiofauna communities. Treatments in 30 d with the macrophyte rapidly seemed to acquire diatom communities of similar composition and diversity to those in those of status in 60 d, indicating relatively rapid recovery of MPB communities at the level of major taxonomic groups. However, it is not clear that the results are from the effect of phytoremediation (Figure 4.8). Except for the early appearance of *Chloroflexi* in the SO group, the benthic community was changed similarly to that of the SX group. The data imply that provision of structural heterogeneity in tidal flat structure might speed change of MPB and bacterial communities, not suggesting notable effect fr om seeding of halophyte (Tolhurst et al., 2020).

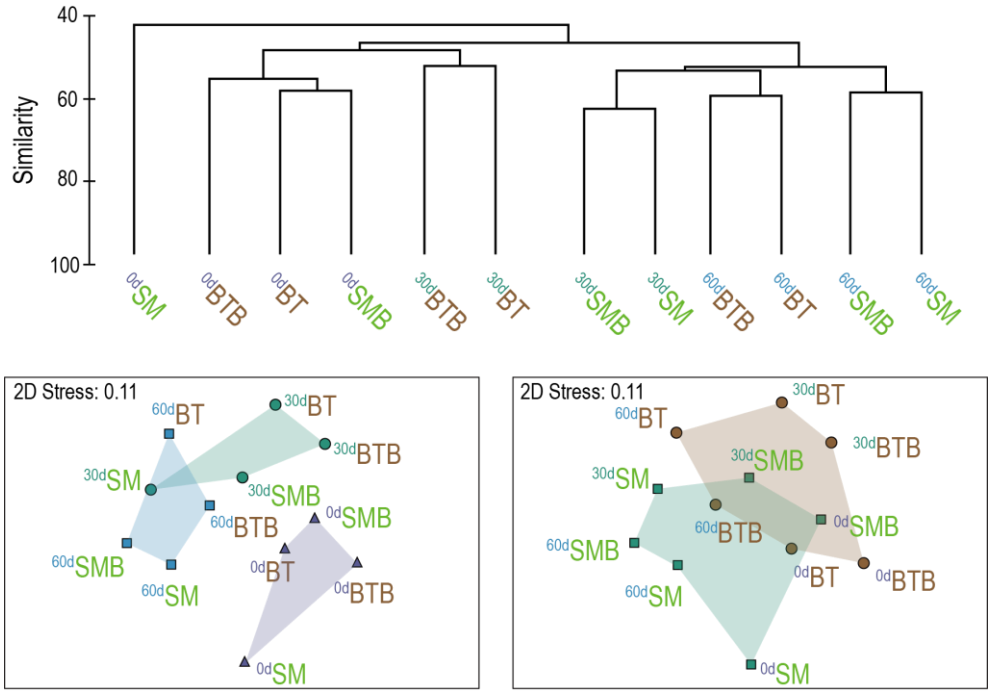

Figure 4.8
Hierarchical clustering and dendrogram from data of meiofauna in each treatment.

4.3.4. Correlation between composition of PTSs and bacterial community in each treatment groups

Change of bacterial community at each group (BX, BO, SX, and SO) are shown in Figure 4.9a. Among the bacteria detected in the samples, we selected the order, which showed over 1% of community, and analyzed the relationship between PTSs components (parent and metabolites compounds) and them (Figure 4.9b). *Chloroflexi*, and *Verrucomicrobia* showed positive correlations with LMW^{PAHs} and $NP\text{-}OP^{APs}$ from 0 h to 12 h in the BX without biota. Thereafter, as the amount of SD^{SOs} increased relative to 1d–3d, *Verrucomicrobia* also increased further ($p < 0.05$) (Figure 4.10). In 7 d–60 d, *Bacteroidota*, *Campilobacterota* ($p < 0.05$), and *Cyanobacteria* showed a positive correlation with parent substances such as HMW and ST^{SOs}. In BO, In BO, parent compounds (HMW^{PAHs}, $NP\text{-}OP^{APs}$, and ST^{SOs}) in the sediment were increased in the early stage (0h–3d), and a positive correlation was shown with *Chloroflexi* and *Verrucomicrobia* ($p < 0.05$). During 7 d–60 d, the composition of *Bacteroidota*, *Proteobacteria*, *Campilobacterota* and *Cyanobacteria* increased with metabolites increased ($p < 0.05$). In the SX group, three bacterial groups varied according to the composition of PTSs during the experiment period. Among them, at 14 d-60 d, *Bacteroidota* significantly increased with metabolites such as LMW^{PAHs} and $NP\text{-}OPEO^{APs}$ except SD^{SOs}. Whilst, in the SO group, similar to BO group, *Chloroflexi* increased with the increase of parent compounds (HWM^{PAHs}, $NP\text{-}OP^{APs}$, and ST^{SOs}), and *Campilobacterota* and *Cyanobacteria* increased significantly along with metabolites (LMW^{PAHs}, $NP\text{-}OPEO^{APs}$, and SD^{SOs}) during 3 d–60 d period.

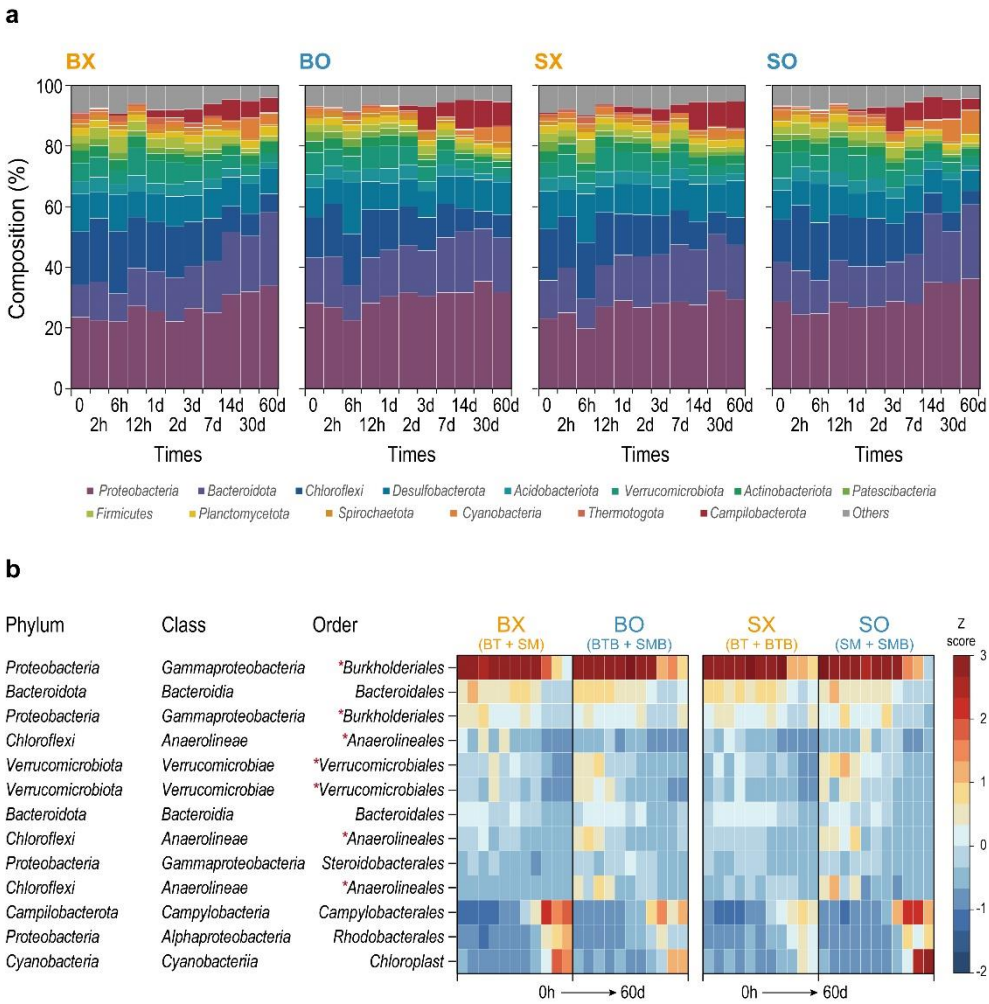

Figure 4.9

Temporal change of bacteria composition in each treatment. (a) The bacterial phyla of sediment change over time in each treatment. (b) Over 1% bacterial order in the bacterial community detected in the sediments among each treatment.

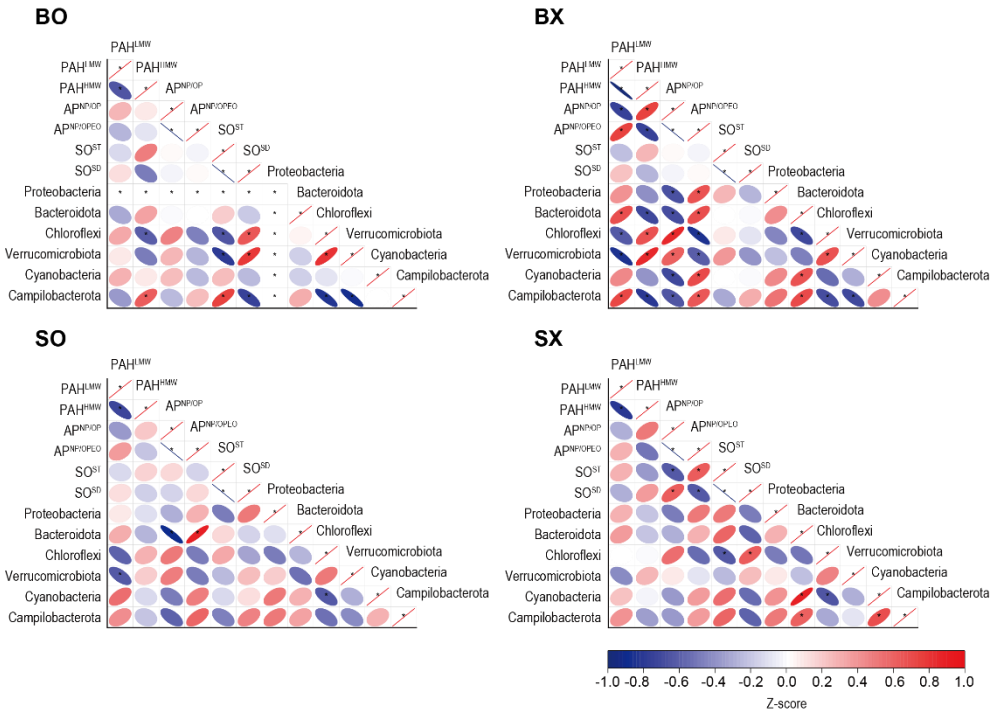

Figure 4.10
Correlation plot between bacterial community and chemical compounds in each treatment.

The bacterial community dynamics showed that the most abundant *Chloroflexi* and *Verrucomicrobia* may play a vital role in the early degradation of parent compounds, particularly HWM^{PAHs}, $NP\text{-}OP^{APs}$, and ST^{SOs}. *Bacteroidota*, *Proteobacteria*, *Campilobacterota* and *Cyanobacteria* may be essential during metabolites (LWM^{PAHs}, $NP\text{-}OPEO^{APs}$, and SD^{SOs}) degradation as key players at later times in this study. Bio-irrigation and phytoremediation promoted the initial rapid reduction of parent compounds in BO and SO (Figure 4.11). At initial stage with abundant parent compounds, *Anaerolineales* and *Verrucomicrobiales* which are hydrocarbon degrading bacteria increased (Tan et al., 2013; Cecotti et al., 2018). With the increase of metabolites in the late period, *Campylobacterales* were dominant in the BO group and *Chloroplast* was dominant in the SO experiment group. *Campylobacterales* is suggested that this phylotype assimilates benzene-derived carbon in a syntrophic benzene-mineralizing consortium that uses sulfate as terminal electron acceptor (Carrier et al., 2020). And also, *Chloroplast*, which indicated the mitochondrial DNA of macrophyes, is related with the presence of moderate levels of nutrients in this type of effluents (Naidoo & Naidoo, 2016).

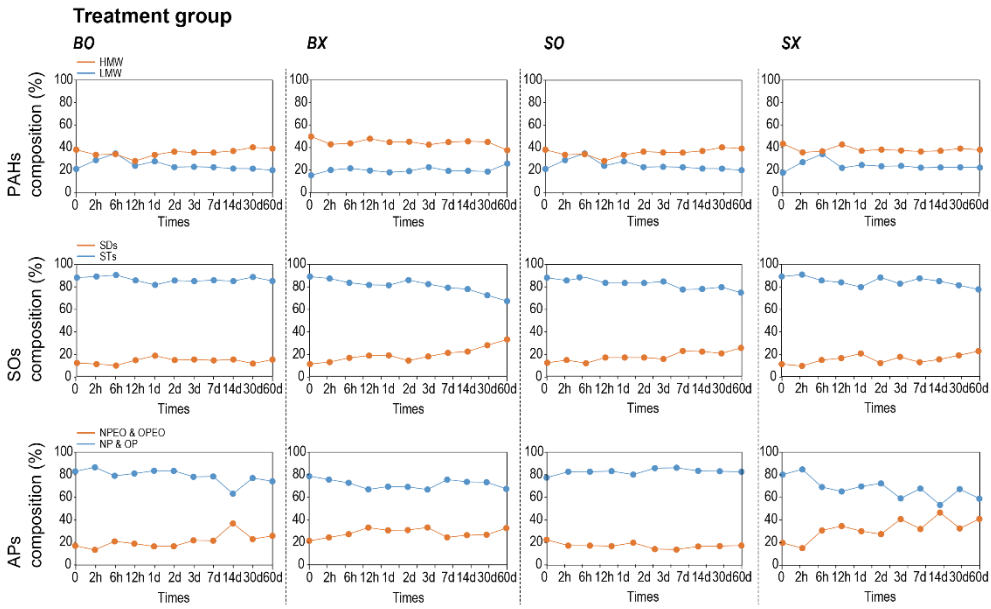

Figure 4.11

Change of each persistence toxic substances (polycyclic aromatic hydrocarbons: PAHs, styrene oligomers: SOs, and alkylphenols: APs+APEOs) in each treatment group

4.3.5. Evaluation to natural restoration of contaminated sediments & effect of bio-irrigation and phytoremediation in tidal flat by sediment quality triad approach (SQT)

The data obtained from chemical contamination, toxicity effect, and benthic community data (diversity) were integrated by use of the SQT approach to identify how bio-irrigation and phytoremediation effect for restoration of contaminated sediment within the groups changed in the 60 d. Comparing SQTs calculated for samples with respect to time (0 d vs. 60 d) and the groups (BX vs. BO and SX vs. SO) revealed an overall increase of SQTs (Figure 4.12).

In all groups, the recovery of benthic community increased over 2 times before that in 0 d. BO group showed an average recovery of 75.4% and more recovery than BX group (average: 61.5%) in all areas (chemistry: 17.9%p, toxicology: 23.7%p, and ecology: 79.1%p). Presumably, because of the effect of bio-irrigation by *Cyclina sinensis*, *Macrophthalmus japonicus*, it is promoting the quality to recover in the sediment. SO group showed an average of 74.1% recovery and SX showed 62.9%. Compared with SX, in SO, ecological factor by phytoremediation was recovered by 36.8%p more at 60 d, followed toxicological and chemical factors were recovered by 18.5%p and 15.2% more, respectively.

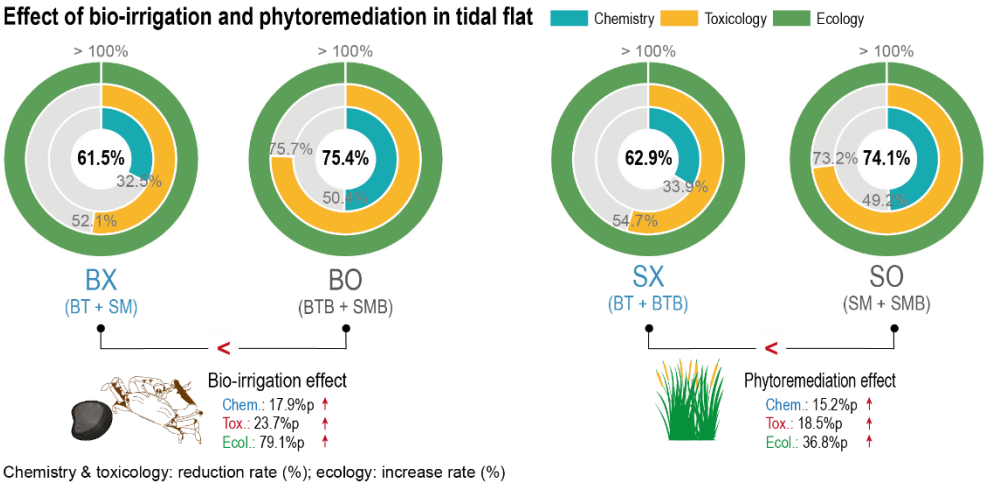

Figure 4.12

Comparison of effectiveness based on integrated approaches with eight target elements. The integrated approaches included: 1) PTSs reduction (PAHs and APs, and SOs concentration), 2) toxicology attenuation (%BaPmax from F2 and F3), and 3) benthic ecosystem recovery (Bacterial community, MPB individual, meiofaunal individual, and chlorophyll-a).

4.4. Conclusions

Here we present the first to provide an integrated assessment (SQT) of the bio-irrigation and phytoremediation effect in the tidal flat by implementation of in situ mesocosm. The following findings regarding the recovery of concentration of PTSs, AhR-mediated potencies, and the benthic community for evaluating the natural restoration of tidal flat were obtained: 1) Concentrations of target PTSs (PAHs, APs, SOs, and HMs) and the potential toxicity decreased significantly with an increase of benthic community for 60 days. 2) Greater reduction of concentrations in PTSs were found at the treatments with macro–fauna and –phyte, compared to other treatments, presumably due to the bio-irrigation and phytoremediation effect. 3) Bio-irrigation effect by macrofauna promoted the change of benthic community, and hydrocarbon degradation by bacterial succession. 4) Both bio-irrigation and phytoremediation make the bacterial community utilize the parent hydrocarbon compounds first, and it cause the rapid reduction of the AhR mediated potency in the sediments. 5) Through the integrated analysis of SQT (chemistry, toxicology, and benthic community), bio-irrigation showed higher recovery of 17.9%p, 23.7%p, and 79.1%p, respectively, chemically, toxicologically, and ecologically, and phytoremediation also showed higher recovery of 15.2%p and 18.5%p and showed a 36.8%p recovery. 6) Results of this study document relatively the natural restoratoin capacity in the tidal flat by an integrated analysis of environmental pollutants and associated biological responses in severely contaminated sediments.

CHAPTER 5.

INFLUENCE OF LIGAND'S DIRECTIONAL CONFIGURATION, CHRYSENES AS MODEL COMPOUNDS, ON THE BINDING ACTIVITY WITH AHR RECEPTOR

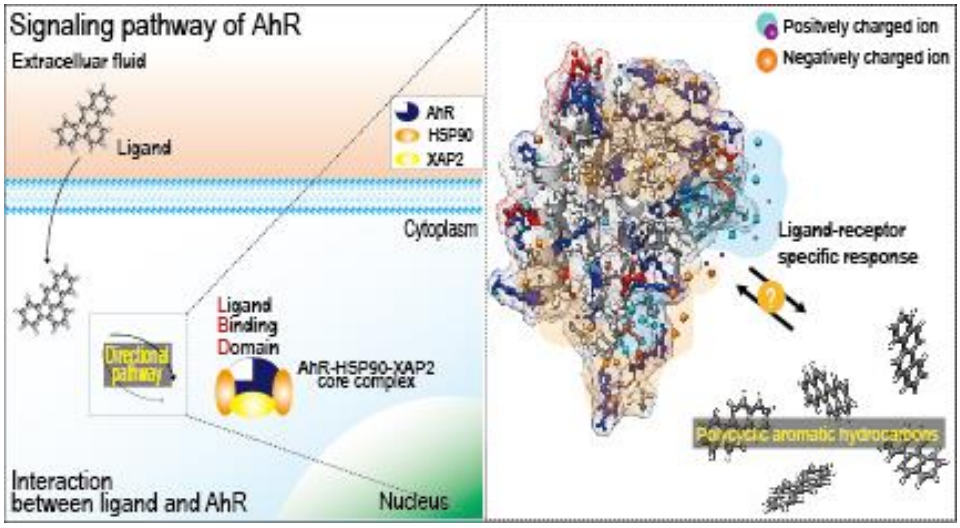

This chapter has been published in Scientific Reports.
Kim, T., Zhen J., Lee, J., Bauer, R., Lee, C., Kwon, B.-O., Kwon, B.-O., Cha K. H., Hong, S., Giesy, J. P., Chang, G. S., Khim, J. S. Influence of ligand's directional configuration, chrysenes as model compounds, on the binding activity with Ahr receptor. *Sci. Rep.* 2020, **10**, 13821. https://doi.org/10.1038/s41598-020-70704-9

5.1. Introduction

Protein receptors act as transcription factors that regulate expressions of genes and determine how cells in organisms respond to xenobiotics. When a receptor binds with exogenous substances (viz., ligand), ligand-receptor complexes are translocated to nuclei of cells where they regulate gene expressions. In the case of xenobiotics, this includes up-regulation of genes coding for enzymes, such as cytochrome P450 1A1 (CYP1A1), which transforms xenobiotics (Rothhammer et al., 2019). This receptor-mediated, enzyme regulation depends on ligand-specific binding affinity and especially since it is the first initiation event, provides the basis of toxicology. Although various receptors and signal transduction pathways are known, kinetics of how ligands interact with responsive receptors remains imperfect and is thus currently undergoing intensive research (Guo et al., 2016, Bernetti et al., 2017).

To understand such ligand-specific events involved in adverse outcome pathways (AOPs) or functioning of drugs knowledge of affinities of binding to receptors is fundamental (Ankley et al., 2010). There are a number of nuclear receptors, conserved in a wide range of vertebrates with which contaminants or drugs can interact as agonists or antagonists (Zhao et al., 2015). Variations among amino acid sequences of the ligand binding domain can explain differences in potencies of chemicals and sensitivities among species (Doering et al., 2015). Due to incomplete understanding of physico-chemical interactions involved in binding of ligands to protein receptors, accurate prediction of affinities of ligand-specific binding in addition to steric factors, predicting initiation of AOPs, and toxicities is challenging.

In ecotoxicology, assessment of toxic potencies has relied primarily on empirical observations of biological responses through in vivo and later developed in vitro systems (Legler et al., 2002). Aside from ethical issues involved in testing of whole animals and difficulty of studying threatened or endangered species or non-standard laboratory animals, the rapid upsurge in new chemicals either found in nature or synthesized in industry outpaces capacities of industries and governments to assess risks by use of traditional methods, which makes them impractical for routine screening and testing (Ferdowsian et al., 2011). In an effort to complement

traditional assays and efficiently screen new chemicals, this proliferation of new chemicals has led to increasing attention being given to in silico alternatives to empirical testing, especially in vivo (Cumming et al., 2013). Quantitative structure-activity relationships (QSAR) is one accepted alternative, in silico predictive method based on linear free energy models (LFEM) and statistical correlations between structure-related physico-chemical properties of ligands in the form of molecular descriptors (numerical quantities) and previously experimented bioactivity data. Multiple linear regression equations developed by the QSAR approach are then used to extrapolate target endpoints, such as toxic potencies of new chemicals (Figure 5.1a) (Kirchmair et al., 2015, Gramatica and Sangion, 2016, Chen et al., 2019). LFEMs include predictors of hydrophobic, electrical, and steric parameters. When structure-related properties are however, not linearly correlated to bioactivities, statistical inferences of target endpoints during semi-empirical modeling are not applicable (Cash, 1998, Ribeiro and Ferreira, 2005, Zvinavashe et al., 2008). Alternatively, recently, molecular docking models, based primarily on steric considerations, are being used to analytically estimate the binding affinity of ligands with receptors (Yang et al., 2010, Wang et al., 2013).

In a previous study, we introduced the directional reactivity factor to predict bioavailabilities of polychlorinated biphenyl congeners (PCBs) based on first principles. But physicochemical information of participating receptors, such as electronic charge state was not considered in the predictive equation, which makes it limited for predicting receptor-dependent bioactivity.18 Here, we report a novel, advanced directional reactive (DR) model that illustrates how physical properties of a ligand interplay to constitute optimal environments for biochemical interactions with respective receptors (Figure 5.1a). The DR approach identifies three, stepwise key parameters and optimal conditions affecting ligand-receptor activity: 1) dipole-driven electrostatic interactions between ligands and receptors; 2) molecular orientation induced by physical ligand-receptor interaction and 3) resulting directional configuration of reactive sites in ligands. As a proof of concept, the DR model was applied to a ligand class containing homologues of polycyclic aromatic hydrocarbon (PAH), chrysene interacting with cytosolic protein, the aryl

hydrocarbon receptor (AhR). Variation of the AhR-mediated toxic potencies across chrysene and its derivatives was well reproduced by the predictive model based on first-principles.

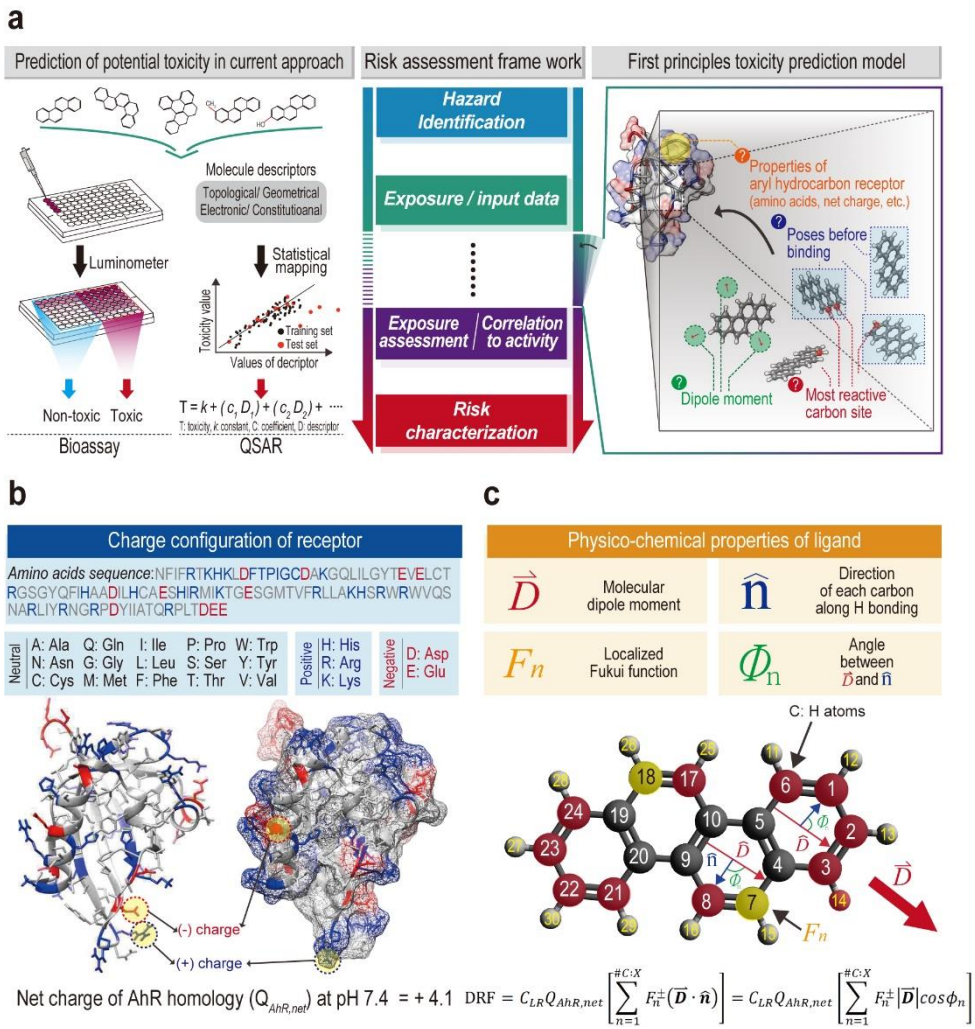

Figure 5.1.

Directional reactive modeling for AhR mediated potency. (a) Comparison between contemporary experimental approaches, quantitative structure-activity relationship (QSAR) and first principles potential toxicity prediction model; (b) Structural model of aryl hydrocarbon receptor (AhR) with ligand binding sites based on PDB ID: 4F3L and its amino acids sequence which is counted to 107. Net charge of AhR homology (QAhR,net) is determined to +4.1. (c) Physico-chemical properties of the model compound, chrysene, for the directional reactive factor (DRF).

5.2. Materials and Methods

5.2.1. Selection of Model Chemicals

As a first step toward identification of the major physical factors affecting toxic potencies, we selected the model chemicals considering four criteria: First, the selection began with a pool of high priority 16 PAHs regulated by the US Environmental Protection Agency which have played an exceptionally large role in environmental sciences. Second, candidates were narrowed to 7 PAHs exhibiting acute toxic potency since the DR model does not consider absorption, distribution, metabolism, and excretion, and thus the model compounds should show perceivable variation in the toxic potency for a short period of exposure (Kim et al., 2019). Third, for prediction of the binding activity with AhR receptor, the most potent AhR agonist in the environment would be desirable. Finally, various homologues of the selected AhR agonist were added in order to understand how the structural modification of ligand induces different binding activity with AhR receptor and resulting toxic potency. Following these steps, chrysene and its homologues were selected as the model compounds for application of our bio-physical communication model and comparison with experimental results of toxic potency testing. Chrysene homologues cover a broad set of compounds ranging from four- to six-membered benzene to methylated- and hydroxylated benzene; chrysene (Chr), benzo[a]chrysene (BaC), benzo[b]chrysene (BbC), benzo[c]chrysene (BcC), dibenzo[b,def]chrysene (DbdC), dibenzo[def,p] chrysene (DdpC), 1-methylchrysene (1MC), 2-methylchrysene (2MC), 3-methylchrysene (3MC), 1-hydroxychrysene (1HC), 2-hydorxychrysene (2HC), and 3-hydroxychrysene (3HC). Their full names, providers, and purities are present in the Supplementary information (Table 5.1).

Table 5.1. [a] Physico-chemical properties of aryl hydrocarbon receptors.

Single letter code	NFIFRTKHKLDFTPIGCDAKGQLILGYTEVELCTRGSGYQFIHAADILHCAESHIRMIKTGESGMTVFRLLAKHSRWRWV QSNARLIYRNGRPDYIIATQRPLTDEE
Number of residue	107
Molecular weight	12381.1 g mol^{-1}
Extinction coefficient	16500 M^{-1} cm^{-1}
Iso-electric point	pH 9.14
Net charge at pH 7.4	4.1
Estimated solubility	Good water solubility
[b]Equation for net charge	$\text{Net charge} = \sum_i N_i \frac{10^{pk_{a_i}}}{10^{pH} + 10^{pk_{a_i}}} - \sum_j N_j \frac{10^{pk_{a_i}}}{10^{pH} + 10^{pk_{a_j}}}$

[a] Data from Innovagen AB; [b]N_i are the number, and pKa_i are the pKa values, of the N-terminus and the side chains of Arginine, Lysine, and Histidine.

5.2.2. Density Functional Theory Calculations

Physical properties of chyrsene and its homologues to be implemented in the DR model were obtained from ab initio density functional theory (DFT) calculations, which were performed using the ORCA (version 4.1.1) program package (Neese, 2012). All stages of DFT computations were made by use of Becke three-parameter Lee-Yang-Parr (B3LYP) exchange functional with the polarized triple-zeta valence (def2-TZVPP) basis set. Meanwhile, very tight, self-consistent field (SCF) convergence (the energy change is 10-9 a.u.) and fine integration grid of 5.0 were employed. The first stage (spin-restricted) geometric optimizations were performed for all structures of the homologues of chrysene. Next, $\pm e$ charge was added to each compound as cationic or anionic case for the second stage (spin-unrestricted) optimizations. Based on the corresponding optimized structures, the molecular orbitals, Hirshfeld charge populations, density of orbital states, molecular dipole moments, and vibrational amplitudes for neutral, cationic and anionic states of each chrysene homologue were computed. The atom-condensed Fukui functions for all carbon atoms bonded with hydrogen or other functional groups in each homologue were determined by Hirshfield population analysis (Bultinck et al., 2007).

5.2.3. C 1s NEXAFS Spectroscopy

Since physical properties were determined from the DFT-calculated molecular orbitals of each model compound, the calculated molecular orbital structures were verified through comparison with experimental unoccupied molecular orbital structures measured by near edge X-ray absorption fine structure (NEXAFS) spectroscopy. Measurements of C 1s NEXAFS spectra were made at the 10D HR PES I/XAS KIST beamline of the Pohang Light Source in Korea. All NEXAFS spectra were measured in total electron yield (TEY) mode. After data acquisition, the spectra were energy calibrated with the Π* (C=C) transition at 285.6 eV of highly oriented pyrolytic graphite (HOPG). Samples were tested for radiation damage considering the sensitivity of carbon-based materials to X-ray radiation. Spectra were intensity-normalized to the incoming photon flux, as recorded by a photodiode.

5.2.4. H4IIE-luc transactivation bioassay for evaluating AhR-mediated potencies and calculation of EC50 of homologues of chrysene

H4IIE cell line derived from rat hepatoma has been reported to continuously express cytochrome P450 protein/mRNA. For this study, H4IIE cells transfected with the luciferase (Luc) reporter gene plasmid (pGudLuc1.1) were used, originally obtained from Jac Aarts, University of Wageningen, The Netherlands and further developed by John Giesy, University of Saskatchewan (Denison et al., 1993, Giesy et al., 2002). Upon ligand binding, AhR in H4IIE-luc is activated and translocated to the nucleus, where heat shock proteins are dissociated from the complex and they form a dimer with the AhR nuclear translocator (ARNT) protein. This complex binds to specific DNA sequences with high affinity, the dioxin-responsive element (DRE). The binding to the DRE results in DNA bending transcriptional activation of adjacent responsive genes. The detailed mechanism is provided in Figure 5.2.

Acute toxic potencies of chrysene homologues were determined based on an AhR-mediated activity using H4IIE-luc cells, by the method previously reported (Louiz et al., 2008). Since PAHs could be degraded by metabolic activity during the H4IIE-luc transactivation bioassay with longer exposure time, the 4 h exposure time was chosen for calculation of AhR-mediated toxic potency. After the exposure, the activity results were expressed as relative luminescence units that were quantified using a Victor X3 multi label plate reader (PerkinElmer, Waltham, MA). Benzo[a]pyrene was used as a positive control ligand. We converted responses of the H4IIE-luc bioassay to the percentages of the maximum response (%BaPmax) observed for a 50 nM BaP (=100 %BaPmax). All bioassays were repeated four times in triplicate (Table 5.2 for detail information of in vitro bioassay conditions). The half effective concentrations for the AhR-mediated effects of individual compounds were determined by use of H4IIE-luc bioassays. Compounds with 10 concentrations using 5-fold serial dilutions (viz., 100, 20, 4, 0.8, 0.16, 0.032, 0.0064, 0.00128, 0.000256, and 0.0000512 μg mL^{-1}) were tested. Estimations of EC50 values of target compounds from the dose-response relationships were basically assumed equal efficacy and parallelism between target compounds and reference compound (benzo[a]pyrene).

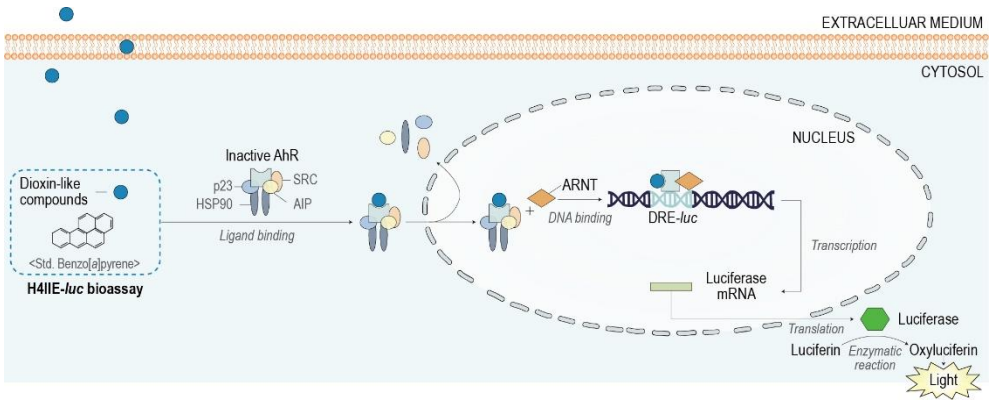

Figure 5.2.
The molecular mechanisms of activation of gene expression by the aryl hydrocarbon receptor (AhR) mediated responses in cell. B[a]P; Benzo[a]pyrene; HSP90; 90 kDa heat shock protein, AIP AhR-interaction protein (also known as XAP2), ARNT; AhR nuclear translocator, DRE; dioxin responsive element.

Table 5.2. In vitro bioassay conditions for evaluating toxicities of chemical compounds.

Cell line	H4IIE-*luc*
ATCC#	CRL-1548
Cell type	Recombinant (*luc*-gene)
Mode of Action	AhR-mediated potency
End point	Luciferase activity
Positive control	Benzo[*a*]pyrene
Culture condition	37 °C, 5% CO_2
Exposure time	4 h

5.2.5. In silico analysis: quantitative structure-activity relationship (QSAR) and molecular docking model

Prediction capability of current in silico models for chrysene homologues were tested with QSAR model and molecular docking analysis. VEGA-QSAR program and the GalaxyDock program were used for QSAR and molecular docking analysis, respectively. VEGA-QSAR has been performed and showed a large set of toxicological data and endpoints convincing to derive predictive toxicity according to the previous studies (Benfenati et al., 2013). In our case, EC50 values were obtained using SMLIES notation of VEGA-QSAR and obtained the toxicity data corresponding to Daphnia magna.

For molecular docking analysis, the GalaxyDock was used to simulate the optimized configuration of AhR receptor in the presence of model chemicals and determine the binding affinity for receptor-ligand docking at each ligand. The receptor-ligand docking was then simulated using the GalaxyDock in GalaxyWEB (Shin et al., 2012 and 2014). For each model chemical, 50 candidate configurations of the ligand-receptor docking were calculated and the configuration with the lowest formation energy was chosen as the optimal binding structure. Two aromatic residues of histidine 285 (H285) and phenylalanine 318 (F318) in the homology modeling were recognized as the most important for ligand binding (Lee et al., 2015). The distances between the nearest aromatic ring or residues of chrysene homologues and each of the ligand binding domains were calculated from the predicted binding pose generated by GalaxyDock. For calculations, the three-dimensional (3D) structure of the ligand binding domain (LBD) of the AhR was built from the sequence of amino acids in the rat AhR (GI: 7304873 in the NCBI sequence database) by the validation using the SWISS-MODEL, Rampage web servers, and ProSA-web (Wiederstein et al., 2007, Waterhouse et al., 2018). A crystal structure of 4F3L (identity = 27.8%, residues 252–357) was selected as a template. The structure model, built using Ramachandran plot from Rampage web server, was validated since 98% of the total residues were in the favored region with 2.4% of the residues in the allowed region. Furthermore, results from ProSA analyses showed the z-score for the 3D model to be within the range of score typically found for native proteins of the similar size.

5.3. Results and Discussion

5.3.1. Directional Reactive Modeling

For modeling interactions between ligands and receptor proteins, we explored two hypotheses; a) different binding activities of various ligands with the same kind of receptor (AhR receptor in this study) would solely depend on the ligand's physico-chemical properties and b) different binding activities would be resulted from the interaction of ligands with common properties of the receptor. These hypotheses suggest that a proper identification of physical properties of the ligand compounds and their interplay configuring the optimal interaction conditions with the common receptor would provide a probabilistic estimation of the ligand-specific binding activity. Then, the estimated ligand-receptor binding activity can be verified by comparison with statistical observation of receptor-mediated toxic potency.

When a ligand (drug or xenobiotic) is introduced into the cytosol of cells, it encounters various forces such as electrostatic, hydrogen bonding, π-π stacking, and van der Waals forces (Helm et al., 1991). Among these, electrostatic interaction is often the dominant force at large ligand-receptor separation before binding, while others are relatively weak or working over only small distances (Petukh et al., 2013). This electrostatic interaction is mediated by dipole moments of ligands and charge state contributed from charged amino acids in a receptor. Considering larger molecular weights of receptor proteins than that of ligand molecule, charges on receptors can be assumed to be fixed in space and result in rotation of the ligand to make its dipole moment vector align along the line of force action, while the ligand moves toward the receptor. This process would determine the relative orientation of a ligand to "active binding" sites of the receptor. Another necessary condition to be considered for optimal reactions, resulting in ligand-receptor binding, is distribution of "frontier molecular orbitals (FMOs)" of a ligand, that is, the highest occupied molecular orbital (HOMO) and the lowest unoccupied molecular orbital (LUMO). Spatial distributions of HOMO and LUMO are related to charge densities in FMOs and thus, suggest which constituent atoms in a molecule serve as preferred sites for nucleophilic or electrophilic interactions with charged amino acids in a receptor. The

DR model employs the atom-condensed Fukui function (F) as a FMO reactivity indicator. This approximation is valid for most cases of negligible orbital relaxation (Chattaraj, 2009). The optimal ligand-receptor reaction would then require the more reactive sites to be located at the front of the ligand, which is governed by the "dipole moment-driven alignment" (Figure 5.1a). Considering these physico-chemical processes, we developed directional reactivity factors (DRFs), which describe favorable orientation configurations between ligands and receptors, given the charge-dipole interaction (Equation 1).

$$\mathrm{DRF} = C_{LR} Q_{R,net} \left[\sum_{n=1}^{\#A:X} F_n^{\pm} \left(\vec{\boldsymbol{D}} \cdot \hat{\boldsymbol{n}} \right) \right] = C_{LR} Q_{R,net} \left[\sum_{n=1}^{\#A:X} F_n^{\pm} \left| \vec{\boldsymbol{D}} \right| cos\phi_n \right] \quad (1)$$

where QR,net is the receptor's net charge contributed from charged amino acids, F+ (F-) is the nucleophilic (electrophilic) Fukui function of each terminal atom bonded with hydrogen or other functional groups (#A:X) in the ligand, $\vec{\boldsymbol{D}}$ is the ligand's dipole moment vector, and $\hat{\boldsymbol{n}}$ is the bonding direction of the terminal atom. The correlation coefficient CLR is $1/4\pi\varepsilon_o\varepsilon_R r$ that represents Coulomb constant, relative permittivity of receptor cytosol (ε_R), and the inverse proportionality of charge-dipole interaction to the intermolecular distance (r). This coefficient becomes constant under the condition of equal ligand-receptor distance for the same type of receptor. The DRF equation takes into account contributions of all atom-condensed Fukui functions along the line of action ($\hat{\boldsymbol{D}}$). This describes reactive sites located behind the molecule ($\pi/2 < \phi_n < 3\pi/2$) with respect to the line of action that would reduce reaction affinity with the receptor. The use of either F+ or F- in the DRF calculation depends on the charged state of the responsive receptor. These quantities are computationally obtainable using the homology modeling method and the density functional theory (DFT) (Parr and Yang, 1995, Hirano et al., 2015).

5.3.2. DRF as an indicator of ligand-binding reactivity

The DR model was applied to predict AhR mediated toxic potencies of homologues of chrysene by examining the DRF, which represents the degree of optimal reaction configuration toward ligand-receptor binding. Cytosolic AhR is a widely used ligand-activated transcript factor regulating expression of CYP450, xenobiotic metabolizing enzymes, which occur in diverse species and cell types (Tagliabue et al., 2019). Chrysene is listed as one of 16 priority PAHs by the US EPA and has a variety of homologues (Zhang et al., 2017). The model compounds included 4 groups of differently modified chrysene homologues; benzo-, dibenzo-, methylated, and hydroxylated chrysenes. In each homologue group, 2−3 congeners were targeted to generally encompass homologous variations (Table 5.3 for full list of chrysene homologues). The net charge of AhR (QAhR,net) was obtained by building three-dimensional (3D) structures of the ligand binding domain (LBD) from the sequence of amino acids in the rat AhR (GI: 7304873 in the NCBI sequence database) using SWISS-MODEL (Waterhouse et al., 2018). The 3D AhR homology structure is composed of 107 amino acids in total and contains 5 histidines (His or H), 10 arginines (Arg or R), and 5 lysines (Lys or K), which possess positive charges at pH 7.4 (acidity condition of the in vitro bioassay in this study), and 5 aspartates (Asp or D) and 6 glutamates (Glu or E) of negatively charged acids (Figure 5.1b). These charged amino acids result in a total net charge of +4.1 at pH 7.4 (Figure 5.3, 5.4 and Table 5.3 for details of physico-chemical properties of receptor) (Lear et al., 2016).

Various physico-chemical properties of chrysenes, such as HOMO, LUMO, and molecular dipole moment, were determined by ab initio DFT calculations with Becke three-parameter Lee-Yang-Parr (B3LYP) exchange functional and the polarized triple-zeta valence (def2-TZVPP) basis set. The atom-condensed Fukui function was determined from the DFT-calculated Hirshfield charge population (Bultinck et al., 2007). Due to structural symmetry, when the chrysene base molecule is modified by electrophilic methyl and nucleophilic hydroxy groups while the base molecule has a weak dipole moment almost perpendicular to the molecule plane, the dipole moment changes dramatically, both in direction and magnitude (Figure 5.5 and Table 5.4). The additive rings (benzo- and dibenzo-chrysenes) also result in

rotation of dipole moment with small increase in magnitude. The hydroxy chrysene group has the largest dipole moment followed by the methyl group. The dipole moments of benzo and dibenzo groups are comparable to that of the base molecule. The electrophilic methyl and nucleophilic hydroxy groups substantially increase the dipole moment magnitude. Alternatively, frontier orbitals (HOMO and LUMO) responsible for intermolecular interaction are additionally contributed from orbitals around carbon sites in benzo- and dibenzo-chrysenes (Figure 5.5b and Figure 5.6).

Carbon in the methyl group does not possess LUMO and addition of the hydroxyl group suppress LUMO from nearby carbon atoms. The influence of molecular modification on frontier orbitals is supported by measurements of C 1s near-edge X-ray absorption fine structure (NEXAFS) (Figure 5.5c). Two spectral features about 284.8 and 285.6 eV correspond to C 1s $\rightarrow$ LUMO transitions from carbon atoms bonded with hydrogen or other functional groups (peak a) and those bonded with neighboring carbon atoms (peak b) (Fronzoni et al., 2014). Addition of a methyl group increases the spectral weight of a peak at the higher energy than LUMO of chrysene base molecule (284.8 eV) and thus the π^* state of carbon in the methyl group does not appear in the LUMO iso-surface. Suppression of the LUMO state due to the presence of the hydroxyl group is also supported by a decrease in the spectral weight of peak a, although there is no loss of a carbon atom through hydroxylation (Figure 5.6–5.8 for C 1s NEXAFS results for all chrysene homologues).

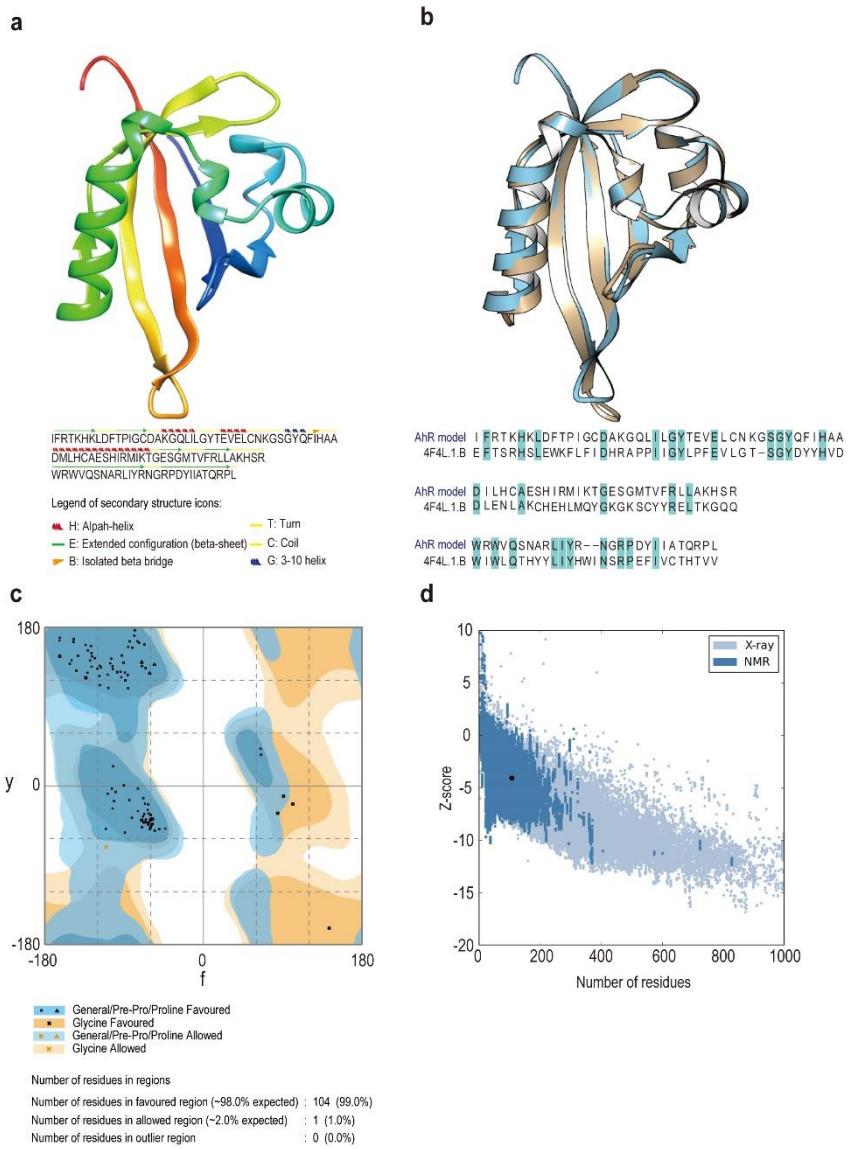

Figure 5.3.

Homology model and quality metrics of AhR LBD. (a) Modelled structure of AhR LBD with helices are shown in red, sheets are shown in yellow and loops are shown in green; (b) Superimposition of the template (light blue) with the AhR model (light brown) with an RMSD less than 1.0 Å and a structure overlap of 98.13; (c) Ramachandran plot showing ener-getically allowed regions for backbone dihedral angles y against f of amino acid residues in the AhR structure; (d) The ProSA analysis of the generated AhR structure in this study. 2 The figure represents the Prosa-web plot of template 4F3L chain A with a z-score value of -4.07.

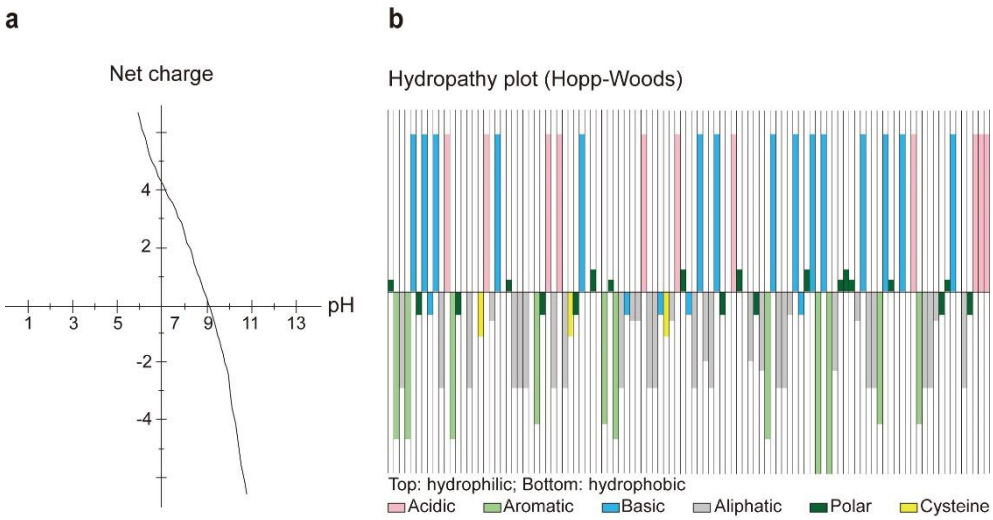

Figure 5.4

Calculated net charge and hydropathy plot in aryl hydrocarbon homology. (a) Expected net charge in AhR homology. AhR homology was expected to have a net charge of 4.1 in pH 7.43; (b) Hydropathy plot of AhR homology indicating its physico-chemical properties. The plot showed the degree of hydrophobicity or hydrophilicity of amino acids of AhR. The hydrophobic amino acids accounted for 42.05 of the total sequence in AhR homology, followed by 28.97% for the hydrophilic amino acids. Basic and acidic were 18.69% and 10.28% respectively.

Table 5.3. Chemical compounds information of chrysene homologues used in this study.

Compounds	Abb. [a]	Molecular formula	Number of benzene ring	Molecular weight	Log Kow	CAS RN	Purity (%)	Vendor
Chrysene	Chr	$C_{18}H_{12}$	4	228.294	5.81	218-01-9	> 98	Sigma-Aldrich (St. Louis, MO, USA)
Benzo[*a*]chrysene	BaC	$C_{22}H_{14}$	5	278.354	7.11	213-46-7	> 99	Tokyo Chemical Industry Ltd.
Benzo[*b*]chrysene	BbC	$C_{22}H_{14}$	5	278.354	7.11	214-17-5	> 98	Sigma-Aldrich (St. Louis, MO, USA)
Benzo[*c*]chrysene	BcC	$C_{22}H_{14}$	5	278.354	7.11	194-69-4	> 98	Sigma-Aldrich (St. Louis, MO, USA)
Dibenzo[*b*,*def*]chrysene	DbdC	$C_{24}H_{14}$	6	302.376	7.28	189-64-0	> 98	Tokyo Chemical Industry Ltd.
Dibenzo[*def*,*p*]chrysene	DdpC	$C_{24}H_{14}$	6	302.376	7.71	191-30-0	> 98	Sigma-Aldrich (St. Louis, MO, USA)
1-methylchrysene	1MC	$C_{19}H_{14}$	4	242.321	6.07[b]	3351-28-8	> 98	Sigma-Aldrich (St. Louis, MO, USA)
2-methylchrysene	2MC	$C_{19}H_{14}$	4	242.321	6.07[b]	3351-32-4	> 98	Sigma-Aldrich (St. Louis, MO, USA)
3-methylchrysene	3MC	$C_{19}H_{14}$	4	242.321	6.07[b]	3351-31-3	> 98	Sigma-Aldrich (St. Louis, MO, USA)
1-hydroxychrysene	1HC	$C_{18}H_{12}O$	4	244.287	5.04[b]	63019-38-5	> 98	Chiron
2-hydroxychrysene	2HC	$C_{18}H_{12}O$	4	244.287	5.04[b]	65945-06-4	> 98	Chiron
3-hydroxychrysene	3HC	$C_{18}H_{12}O$	4	244.287	5.04[b]	63019-39-6	> 98	Chiron

[a] Abb.: Abbreviations; [b] estimated

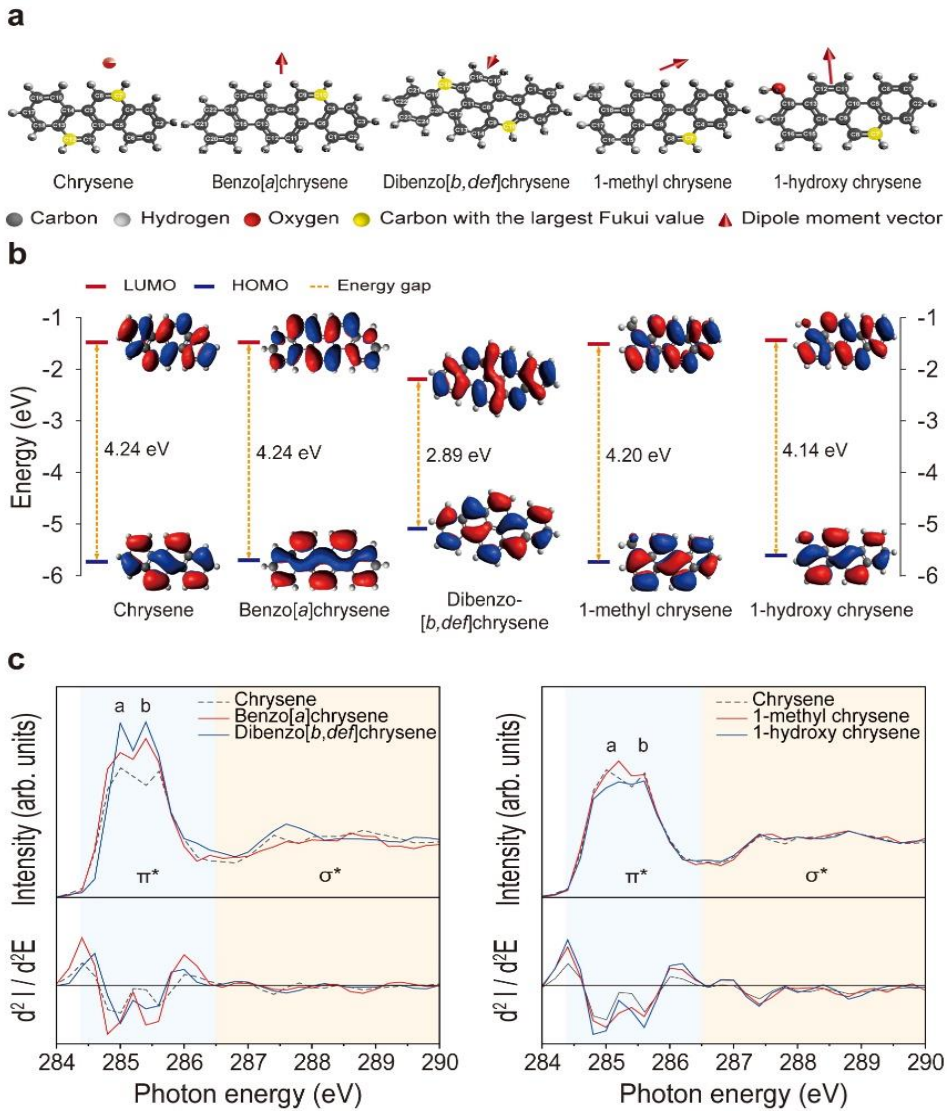

Figure 5.5

Molecular orbital structures of chrysene and its homologues (benzo, dibenzo, methyl and hydroxy chrysenes). (a) Change in dipole moment by addition of a benzene ring and functional group (methyl- and hydroxy-) of chrysene. Carbon atoms with the largest Fukui value in each chrysene homologue are highlighted in yellow and the red arrow denotes the direction and magnitude of dipole moment; (b) The HOMO and LUMO energies and corresponding orbital iso-surfaces for the chrysene homologues; (c) C 1s near-edge X-ray absorption fine structure (NEXAFS) spectra of chrysene homologues collected from pristine samples. Photon energy ranges exhibiting spectral features of carbon atoms bonded with hydrogen or other functional groups, C-H or C-X (peak a) and those bonded with neighboring carbon atoms, C-C (peak b).

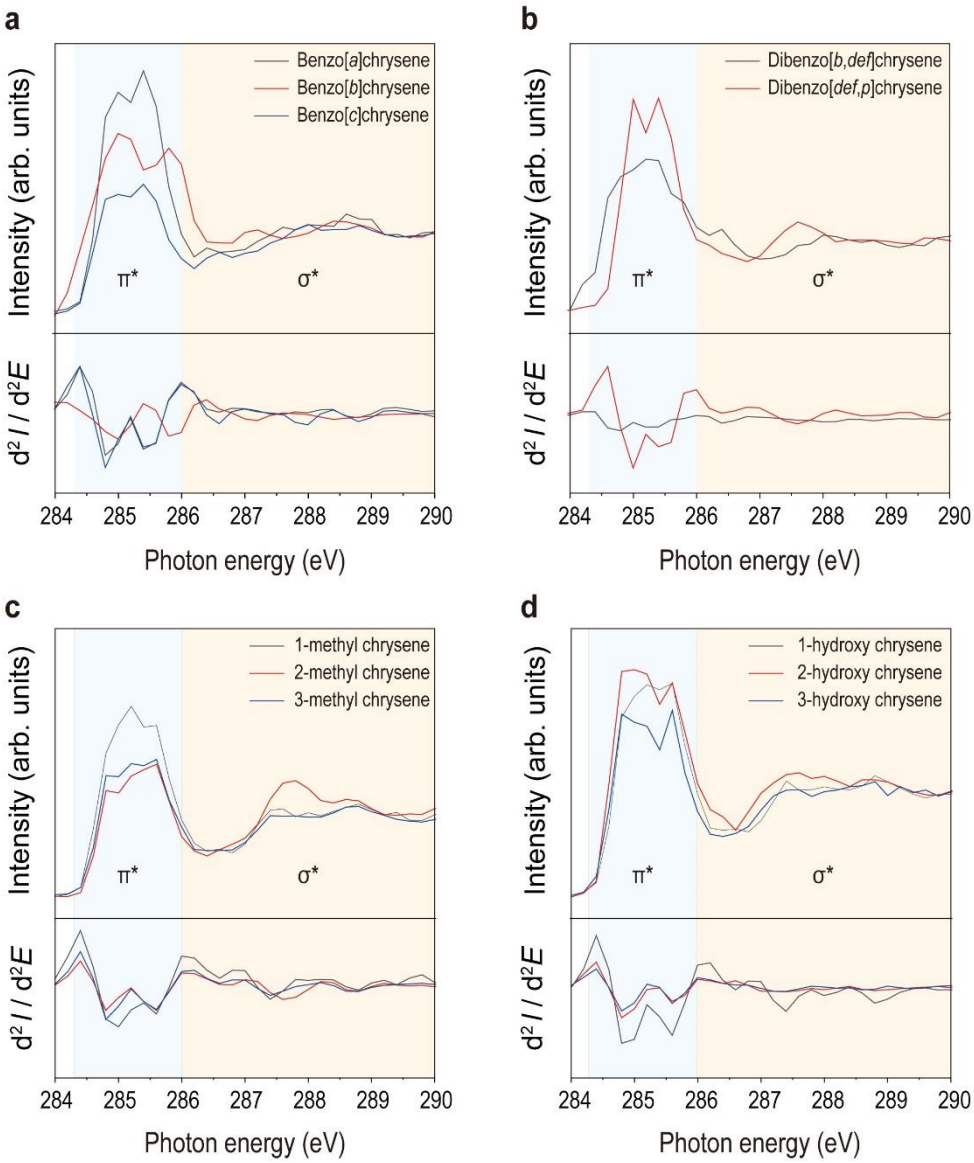

Figure 5.6

Carbon (1s) NEXAFS spectra of chrysene homologues of chrysene homologues. (a) benzo-chrysene, (b) dibenzo-chrysene, (c) methyl-chrysene, (d) hydroxyl-chrysene. The plotted spectra were collected from powder samples. LUMO orbitals were mainly localized around the carbon with hydrogen or other functional groups (peak a) and with neighboring carbon (peak b).

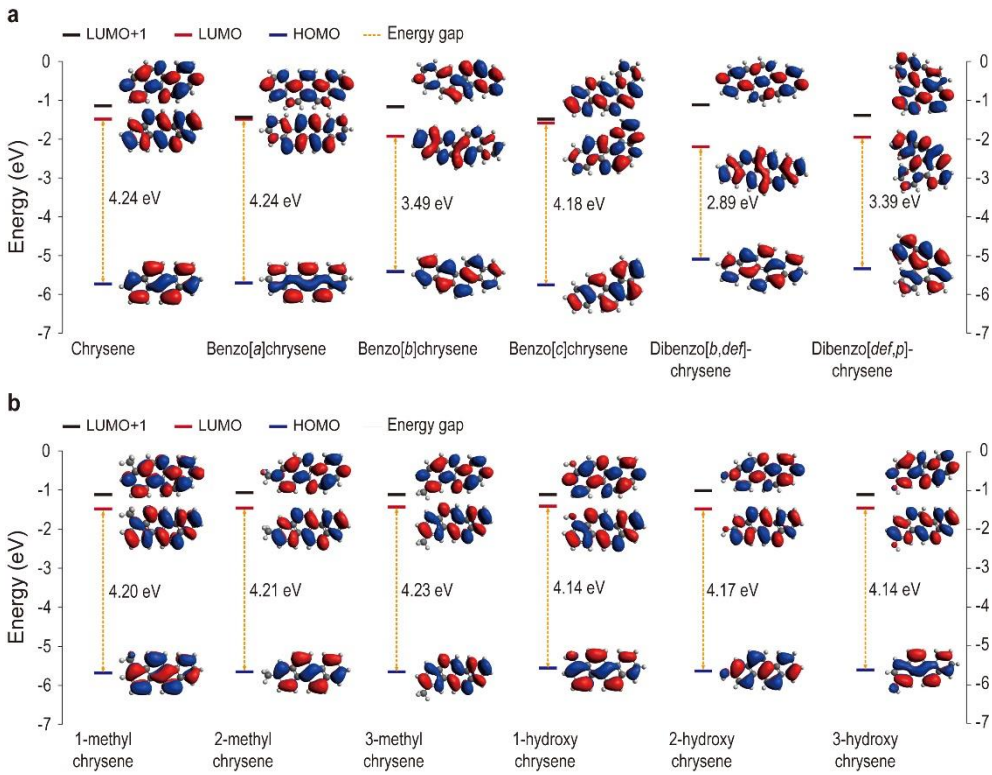

Figure 5.7

Visualization of the LUMO, LUMO +1 and HOMO orbital in chrysene homologues. (a and b) Presentation of the energy levels, HOMO-LUMO gap and orbital composition distribution of the HOMO and LUMO for chrysene and benzo-chrysene. The HOMO-LUMO gap is slightly difference in each congeners. LUMO orbitals were mainly localized around the C=H bond, but LUMO+1 orbitals showed the features of C=C.

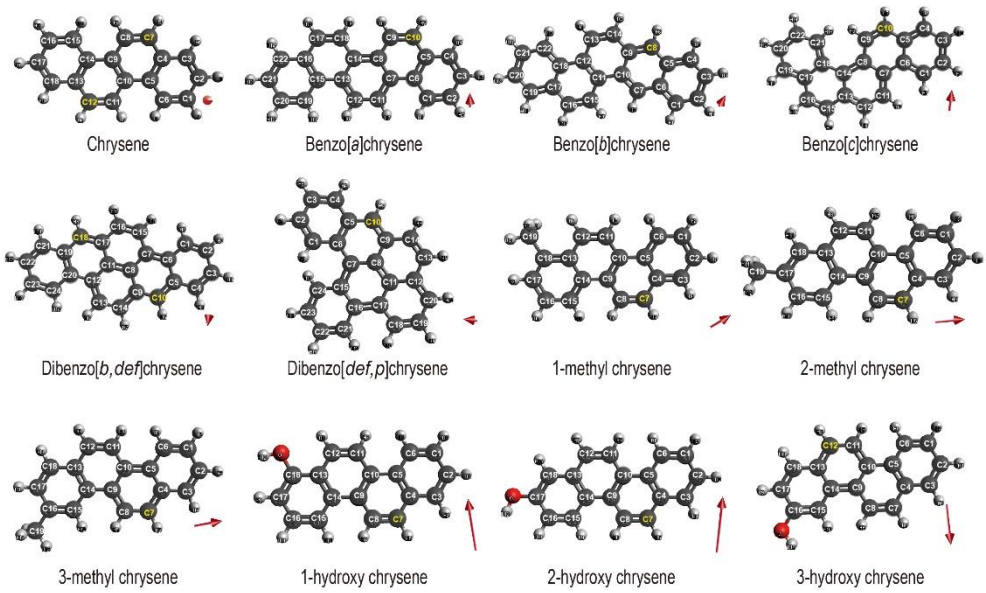

Figure 5.8

The information of physico-chemical properties in each chrysene homologue. Carbons in structure of chrysene homologues are shown in dark gray, hydrogens are shown in white and oxygen are shown in red color. A carbon with the highest Fukui value of chrysene homologues is shown in yellow, and dipole moments are shown in red arrow. The size of the arrow indicates the quantity of dipole moment. The carbon number of the chrysene homologues was randomly assigned.

Using DFT-calculated properties and total net charge of the AhR, DRF values for all 12 homologues of chrysene were obtained (Table 5.4). The charge-dipole interaction would occur in the cell cytosol containing dissolved ions such as Na+, K+, and Cl-, not in free space (Faundez and Hartzell, 2004). Results of a recent study suggested that these dissolved ions are attracted by and trapped in the vicinity of the charged amino acids in cytosolic proteins (Friedman, 2011). That is, Na+ and K+ ions are bound to negative Asp and Glu residues while Cl- ions are to positive Arg, Lys, and His residues. After being introduced into the cell cytosol, the ligand thus recognizes the electrostatic potential by these ions surrounding the charged amino acids, which can be approximated to opposite charge of the AhR protein (-QAhR,net). The dipole moment vector and Fukui functions resulting in the DRFs are selected in this regard. The most striking result is that hydroxy-chrysene has the smallest DRF values despite their strongest dipole moments. This is because carbons with the large Fukui functions are located on the opposite side of the ligand from the receptor (Figure 5.9 and Table 5.4 present as an example, the location of carbon with the largest Fukui value). Methyl chrysene exhibited the largest DRF values, followed by benzo-chrysenes. In each homolog group, DRF values depend on the dipole moment and relative location of reactive carbons to the dipole orientation. The DRF shows the large value (27.97) for 2-methylchrysene (2MC) and decreases to 6.79 for 1-methylchrysene (1MC). In the case of benzo[*c*]chrysene (BcC), the DRF is larger than that of 1MC, because of the favorable distribution of reactive carbon sites despite the smaller F+ and dipole moment.

Table 5.4. Structural and electronic configuration parameters of the chrysene homologues and the potential toxicity predicted by directional reactivity factor (DRF).

Compounds	HOMO (eV)	LUMO (eV)	HOMO-LUMO energy gap (eV)	Dipole moment magnitude (10^2 Debye)	Fukui value F^+	Carbon atoms with the largest Fukui value	Location of carbon* to AhR	Directional reactivity factor (DRF)
Chrysene	-5.75	-1.51	4.24	0.03	0.068	7C, 12C	P	-0.02
Benzo[*a*]chrysene	-5.73	-1.50	4.24	3.30	0.062	10C	B	-2.98
Benzo[*b*]chrysene	-5.43	-1.94	3.49	1.89	0.056	8C	F	1.60
Benzo[*c*]chrysene	-5.77	-1.59	4.18	10.10	0.060	10C	F	9.75
Dibenzo[*b*,*def*]chrysene	-5.11	-2.22	2.89	0.03	0.062	10C, 18C	B	-0.02
Dibenzo[*def*,*p*]chrysene	-5.36	-1.97	3.39	3.43	0.059	10C	B	-3.57
1-methylchrysene	-5.69	-1.49	4.20	39.58	0.069	7C	F	6.79
2-methylchrysene	-5.68	-1.47	4.21	61.40	0.067	7C	F	27.97
3-methylchrysene	-5.67	-1.44	4.23	57.52	0.067	7C	F	13.66
1-hydroxychrysene	-5.56	-1.43	4.14	131.50	0.070	7C	B	-33.19
2-hydroxychrysene	-5.66	-1.49	4.17	145.70	0.069	7C	B	-51.44
3-hydroxychrysene	-5.62	-1.48	4.14	94.04	0.059	12C	B	-58.75

* The carbon with the largest Fukui value; forward (F), perpendicular (P), and backward (B) to the AhR

5.3.3. AhR-mediated toxic potency of chrysene homologues

If the DR model describes the optimal configuration for ligand-receptor reaction properly, the DRF would be one promising indicator accurately estimating ligand-specific bioactivity. For robust validation of the DR model, a homogeneous set of AhR-mediated toxic potencies for chrysenes were examined experimentally by use of the in vitro, H4IIE-luc transactivation assay and compared with DRF values calculated from first-principles. The experimental dose-response curves for the groups of similarly structured chrysenes are presented (Figure 5.9a). AhR-mediated potencies of all chrysene homologues are evidenced in the range of 51–147%BaPmax, which indicated significant potential to cause toxicity and suggests selected target chemicals are as potent as benzo[*a*]pyrene, which is a well-known in vitro agonist of the AhR. By group, methyl chrysene exhibits the greatest potency, followed by benzo-chrysene, while dibenzo-chrysene and hydroxy chrysene both exhibited similar or lesser potencies, compared to that of the base compound of unsubstituted chrysene.

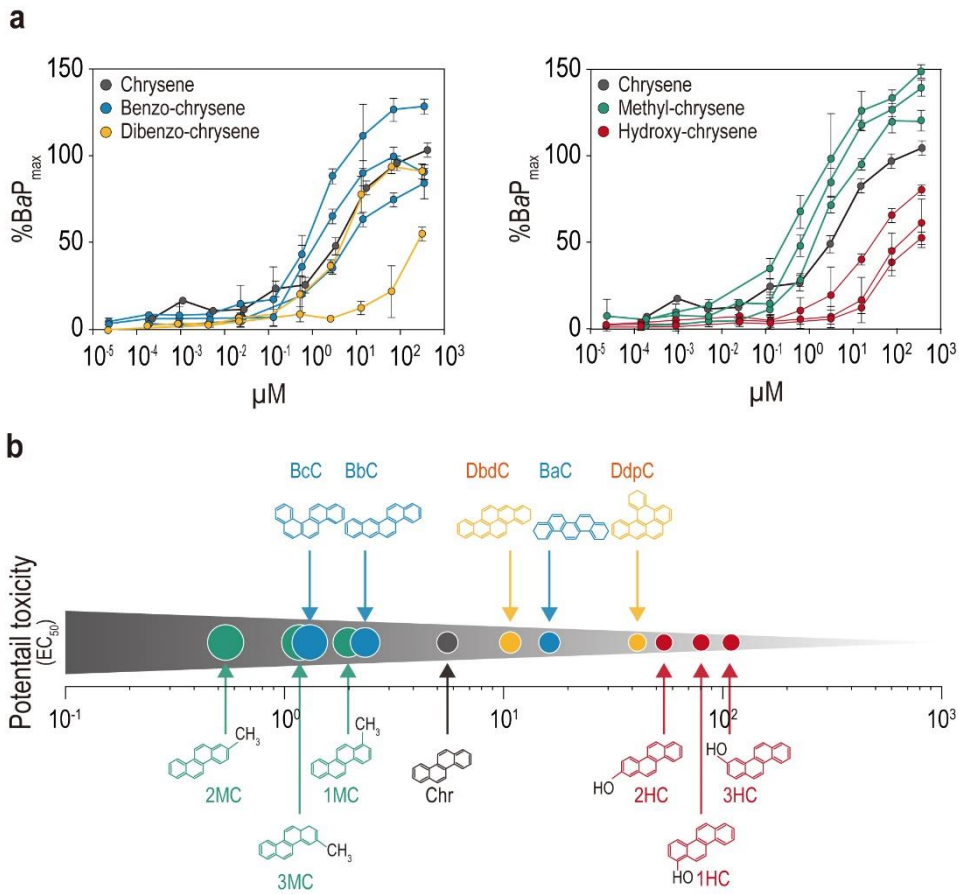

Figure 5.9

Experimental AhR-mediated potencies of chrysene homologues. (a) Dose-dependent activation of chrysene base compound and its homologues; benzo (n = 3), dibenzo (n = 2), methyl (n = 3), and hydroxy chrysenes (n = 3). Relative responses were normalized against the positive control (benzo[*a*]pyrene at the following concentrations; 100, 20, 4, 0.8, 0.16, 0.032, 0.0064, 0.00128, 0.000256, or 0.0000512 μg mL-1; set as 1.0 of potential toxicity). Dose expressed as nmol chrysene homologues/mL media (μM) present in the test well. EC50 are means of three or four independent experiments. Error bars represent the standard error; (b) The order of potential toxicity of chrysene homologue based on EC50 calculated for H4IIE-luc transactivation assay. Examined chrysene homologues were ranked in descending order of potential toxicity. The methyl chrysene group exhibits the highest potency followed by benzo chrysene one while dibenzo chrysene and hydroxy-chrysene groups show similar or lower potencies than other chrysene homologue groups.

For a detailed comparison with the DRF value for individual compounds, the half-maximal effective concentration (EC50) values were calculated (Figure 5.9b and Table 5.5). Among chrysene homologues tested, 2MC turns out to have the greatest toxic potency (EC50 = 6.6×10^{-1} μM) and 3HC was the least potent (EC50 = 1420.4×10^{-1} μM). Different EC50 values were also observed within each homologue group. The EC50 values of BaC, BbC, and BcC are 197.7×10^{-1} μM, 27.6×10-1 μM and 12.5×10^{-1} μM, respectively, despite having the same molecular formula, mass, and octanol-water partition coefficient (Log Kow; hydrophobicity). For the dibenzo-chrysene group, differences in EC50 values were between dibenzo[*b*,*def*]chrysene (DbdC) (143.4×10^{-1} μM) and dibenzo[*def*,*p*]chrysene (DdpC) (761.0×10^{-1} μM). A similar trend was observed for the methyl- and hydroxy-chrysene groups. The experimentally derived bioactivity data was consistent with the optimal ligand-receptor reaction predicted by the DR model for toxicity rank among homologue groups and among congeners within a homologue. This consistency suggests that accurate predictions of ligand-receptor binding and resulting ligand-specific bioactivity requires contributions involving not only physico-chemical properties but also interplay between and among them.

Table 5.5. Comparison of the directional reactivity (DR) model with other predictive models and experimental potential toxicity data.

Chemical	*In vitro* bioassay	QSAR [a]	Docking model [b]				Directional reactivity factor (DRF)
	H4IIE-*luc* EC_{50} (µM)	*Daphnia magna* EC_{50} (µM)	Free energy (kcal mol^{-1})	Binding distance to LBD (Å)			
				Total	H285 [c]	F318 [d]	
2-methylchrysene	6.6×10^{-1}	7.4×10^{-1}	-7.1	6.3	3.0	3.3	28.0
3-methylchrysene	11.4×10^{-1}	7.4×10^{-1}	-10.5	6.3	3.0	3.4	13.7
Benzo[*c*]chrysene	12.5×10^{-1}	5.4×10^{-1}	-8.0	7.4	3.6	3.8	9.8
1-methylchrysene	18.8×10^{-1}	7.4×10^{-1}	-9.8	6.6	3.1	3.4	6.8
Benzo[*b*]chrysene	27.6×10^{-1}	5.4×10^{-1}	-6.6	22.8	9.1	13.8	1.6
Chrysene	71.6×10^{-1}	9.1×10^{-1}	-9.7	6.6	3.2	3.4	-0.02
Dibenzo[*b*,*def*]chrysene	143.4×10^{-1}	4.2×10^{-1}	-6.1	23.2	9.2	14.0	-0.02
Benzo[*a*]chrysene	197.7×10^{-1}	5.4×10^{-1}	-5.6	25.1	10.6	14.5	-3.0
Dibenzo[*def*,*p*]chrysene	761.0×10^{-1}	4.2×10^{-1}	-7.8	33.0	18.4	14.6	-3.6
2-hydroxychrysene	586.7×10^{-1}	32×10^{-1}	-8.0	31.9	17.7	14.2	-51.4
1-hydroxychrysene	870.9×10^{-1}	32×10^{-1}	-8.9	32.3	17.7	14.6	-33.2
3-hydroxychrysene	1420.4×10^{-1}	32×10^{-1}	-8.1	6.7	2.9	3.8	-58.8

[a] Predicted data from VEGA-QSAR; [b] Galaxydock; [c] histidine 285 and [d] phenylalanine 318 in the AhR homology.

5.3.4. Comparison of predicted potencies: DR model vs. current in silico models

DRF values and experimental toxic potency data (inverse of EC50) were compared with the toxicity-relevant characteristics predicted by currently used in silico predictive models; QSAR (inverse of the median effective concentration, 1/EC50), a structure-based statistical regression method, and molecular docking models (free energy and binding distance), a structure-based analytical approach searching for the best ligand-receptor binding pose in terms of binding free energy (Cappelli et al., 2015, Du et al., 2016). Target toxicants can be input as the unambiguous notation of the structure such as SMILES in VEGA-QSAR. The results of predictive EC50 were obtained from the Instituto di Ricerche Farmacologiche Mario Negri (IRFMN) toxicity model (Daphnia magna acute) based on the training sets including aromatic hydrocarbons (Shin and Seok, 2012). The same AhR homology used in the DR model was employed for calculations with docking models. Overall, the results suggest that both QSAR and molecular docking models do not accurately estimate the experimental potencies determined by use of in vitro bioassays, say anti-empirical data.

The QSAR model predicted greatest toxic potency of dibenzo- and benzo-chrysene groups followed by chrysene base compound and methylated chrysenes. Different experimental toxicities within each homologue group are also not reproduced, rather the similar degree of toxicity among congeners was observed (benzo-chrysene: 5.4×10^{-1} μM; dibenzo-chrysene: 4.2×10^{-1} μM; methyl-chrysene: 7.4×10^{-1} μM; hydroxy-chrysene: 32×10^{-1} μM) (Figure 5.10a and Table 5.5). This results in statistically insignificant correlations between experimental 1/EC50 and QSAR-estimated 1/EC50 ($R^2 = 0.20$, $p > 0.05$), which implies considerable uncertainty in prediction accuracy of toxicity (Figure 5.10b). Unlike the QSAR approach, the docking analysis predicts different toxic potencies of congeners in each homologue group and high binding affinity behaviors (i.e., low free energy and short binding distance) of the group of methylated chrysene, which was consistent with empirical toxicity data (Figure 5.11).

Chrysene homologues composed of benzene rings (benzo- and dibenzo-

chrysene groups) exhibited lesser free energies than those of methyl- and hydroxy-chrysene groups. Another notable feature is that hydroxy-chrysenes show comparable free energy to methyl chrysenes while experimental toxic potency due to addition of the hydroxy group is least among chrysene homologues tested. Considering the fact that hydroxylated benzene compounds are usually known as metabolites by degradation or metabolism in abiotic and biotic responses, the docking model seems to overestimate toxicities of these model compounds (Table 5.6 presents a result of potential toxicity from other in silico models to predict toxic potencies) (Gissi et al., 2013). The statistical correlation between calculated optimal binding affinity and experimental 1/EC50 values is found to be insignificant (R2 = 0.09, $p > 0.05$) (Figure 5.10b). Meanwhile, although a positive correlation between 1/EC50 and total binding distance between the ligand and either of two binding domains (H285 and F318) was observed ($R^2 = 0.61$, $p < 0.01$), the short binding distances calculated for chrysene and 3HC compounds are inconsistent with experimental toxicity results.

Discrepancies of experimental bioactivity data from toxicity-relevant characteristics predicted by current in silico models are not unexpected. In fact, QSAR approaches are based on algorithms composed of a linear regression relationship between logarithms of aquatic toxicity of known chemicals and their structural molecular descriptors (training set). Effective toxic concentrations of individual chemicals were estimated by use of regression equations after training and the measure or calculated values of corresponding chemical from the descriptors.36 As a consequence, the congeners in each homologue group with the same molecular weight shows the same toxic potency according to the QSAR model.

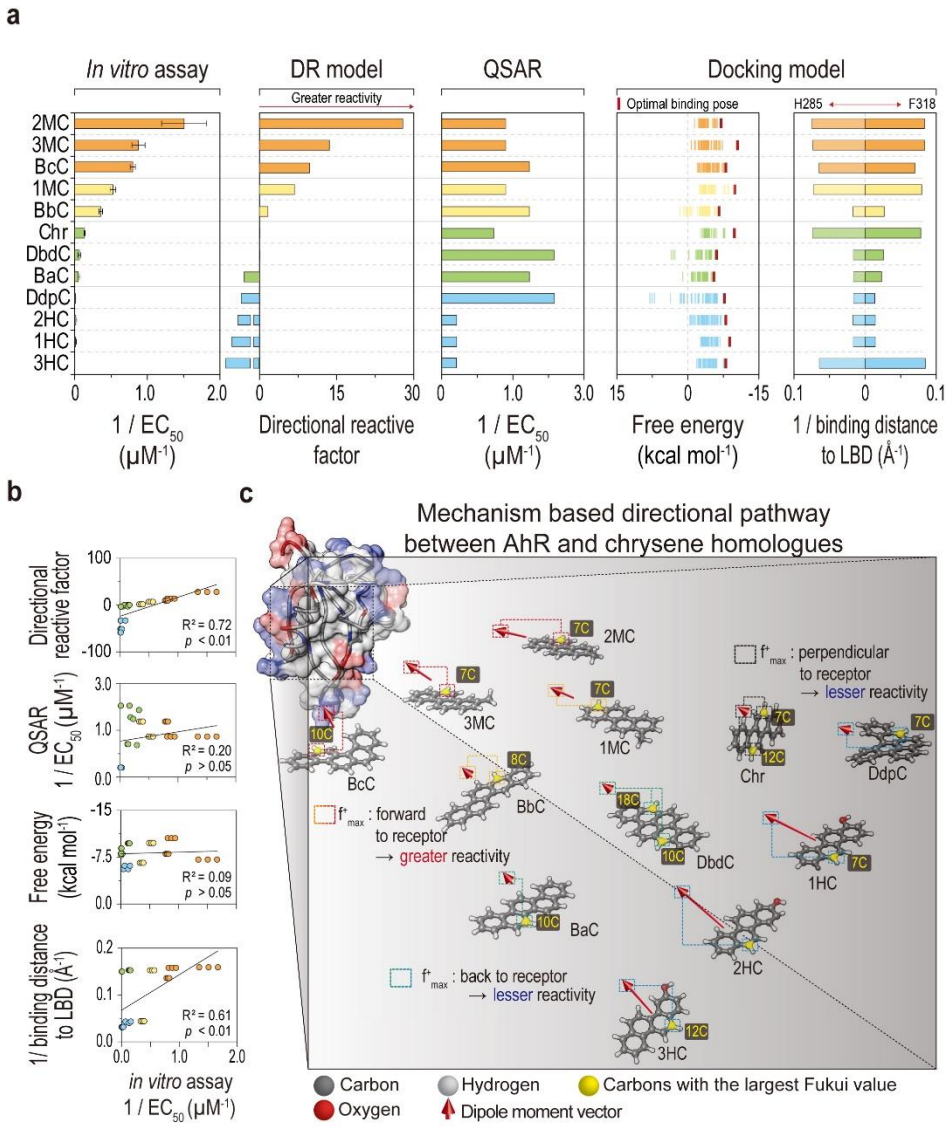

Figure 5.10

Prediction efficiency of DR model and other in silico assays. (a) Experimental potency results of in vitro bioassay (H4IIE-luc) and predicted toxicity-relevant characteristics by in silico models (QSAR, molecular docking model, and the DR model introduced here). The QSAR and the docking model calculations were made using VEGA-QSAR and GalaxyDock, respectively. Each toxicant in the graph was sorted in descending order of 1/EC50 value. (b) Predicted vs. observed values represented from each method and the regression coefficient, R2 with significance (*p*). (c) Visualization of first principles prediction model for AhR-mediated potency of chrysene homologues before their binding to AhR.

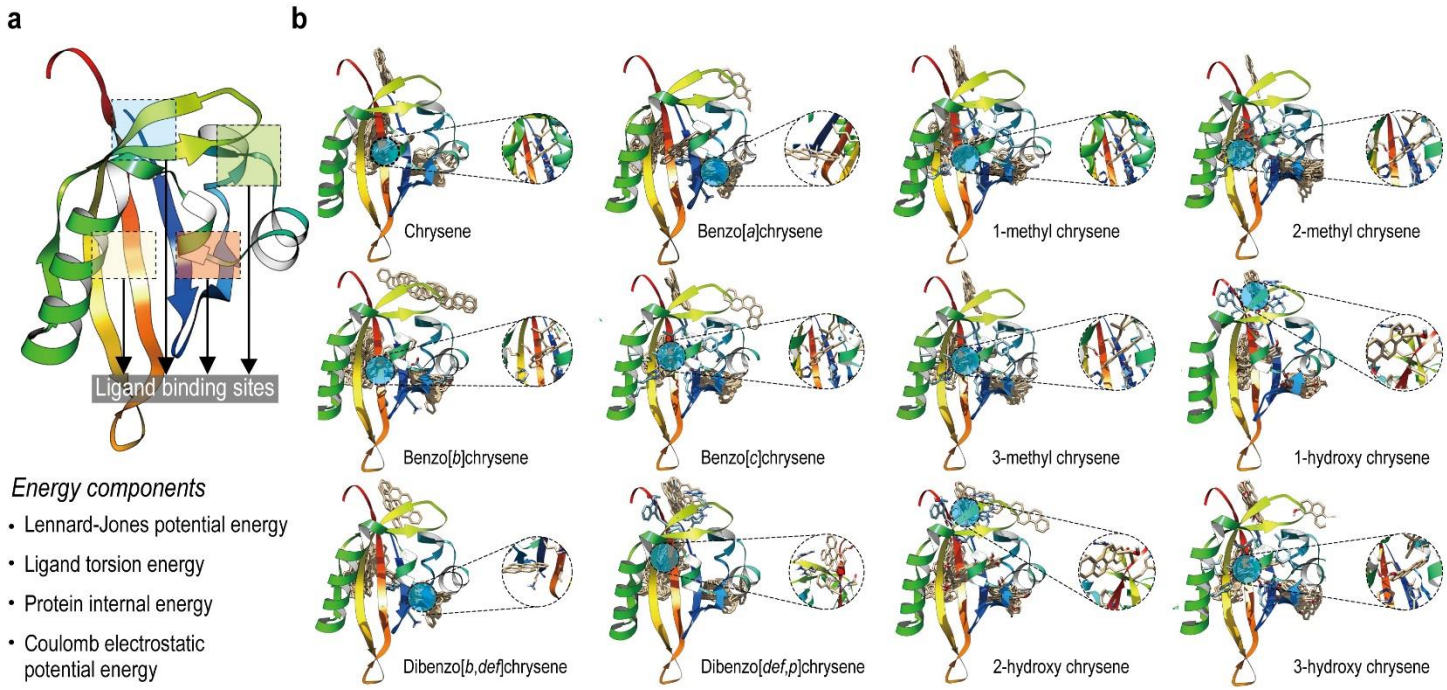

Figure 5. 11

AhR homology and binding poses in the docking model. (a) The docking model (galaxydock) used in this study calculated binding affinity by using various energy components such as Lennard-Jones potential energy, Ligand torsion energy, protein internal energy, and Coulomb electrostatic potential energy. (b) The docking results provided fifty possible binding poses between AhR and chrysene homologues and suggests the best optimized binding state which has the lowest binding affinity.

Table 5.6. Potential toxicity and binding affinity estimated in VirtualToxLab.

Compounds	AhR binding affinity (nM)	ToxPot
Chrysene	655	0.39
Benzo[*a*]chrysene	114	0.46
Benzo[*b*]chrysene	63.2	0.48
Benzo[*c*]chrysene	133	0.45
Dibenzo[*b*,*def*]chrysene	78.5	0.48
Dibenzo[*def*,*p*]chrysene	221	0.42
1-methylchrysene	593	0.39
2-methylchrysene	450	0.41
3-methylchrysene	501	0.40
1-hydroxychrysene	352	0.41
2-hydroxychrysene	466	0.41
3-hydroxychrysene	250	0.43

6.3.5. Conclusion

Toxicity testing has become central to hazard assessments of (in)organic substances associated with causal exposure in environments. Thus, accurate evaluation of adverse effects of chemicals on bio-organisms have been a profound problem in environmental and pharmaceutical toxicology (Krewski et al., 2010). Development of a model to reliably predict bioactivity complementing traditional bioassays is directly related with a fundamental question about how a chemical trigger the ligand-receptor binding that results in the following expression of xenobiotic metabolizing genes. Current computational approaches have focused on statistical correlations between structure-based physico-chemical properties and the observed bioactivity endpoints using multiple linear regression (i.e., QSAR), and characteristics of the ligand-receptor binding after minimization of free energy of binding (i.e., molecular docking) (Deng and Roux, 2006, Mobley et al., 2007, Floris et al., 2014). However, here, we have shown that structural similarity does not always guarantee that bioactivities will also be similar, but small structural differences, like different functionalization sites between 1MC and 2MC, can result in dramatic differences in toxic potency. Furthermore, since long-range dipole-charge interactions predetermine orientation and relative distribution of ligand's reactive sites before binding to the receptor, the best ligand-receptor binding pose with the minimum free energy must not be always plausible.

The DR model suggests that individual physico-chemical properties of specific ligands do not contribute independently to binding, but interplay between them is also important. This kinetic approach begins with consideration of the "molecular dipole moment" that is sensitive to functionalization, as the main property of ligand interacting with a receptor (mediated by trapped cytosolic ions) after a ligand is introduced into the cell cytosol. However, the favorable binding environment is achieved by combined influence from the molecular orientation and relative location of reactive sites driven by "alignment" of the dipole moment (Figure 5.10c). In this study, the DRF devised from the molecular level kinetic process could estimate the macroscopic toxic potency of chrysene homologues and therefore serve as a bioactivity indicator of chemicals. Once the amino acid sequence and constituent,

charged acids are identified, the DR model can be applied to investigate species-specific bioactivity.

Unlike other current models, this model does not predict toxicity through statistical methods, but predicts the possibility of toxic effects, assuming the pre-conjugation state in the case of toxicants combined with receptors. Based on this model, it was confirmed that the reactivity (Fukui value) of molecules in each ligand group was different depending on the position despite their structural similarity, and the contribution in dipole moment of the ligand was confirmed according to the position of the reactive molecule. Thus, we found that the shape and orientation configuration of toxicants before the ligand-receptor interaction were generally consistent with EC50 values. This model was based on a good understanding on the toxic mechanisms and could apply to compounds with different action mechanisms explaining different reactivity of similarly structured chemicals to AhR.

Computational studies have been increasing substantially in the last few years. Theses computational techniques with toxicity prediction model highly rely on QSAR analysis. While the DR model is an in silico-based approach like QSAR, but it employs more mechanism-driven consideration of toxic reaction rather than statistical inference and extrapolation. The DRF could bring up a topic of understanding the more scientifically robust basis for risk assessment by providing detailed mechanistic pathways and serve as a complementary to existing QSAR methodology. Using various efficient tools to calculate electronic excitation such as time dependent density functional theory (TDDFT), the DR model have the potential to extend to predict chemical interaction with biomolecules (e.g., fatty acids, DNA, RNA, and micro RNA) (Varsano et al., 2006). Therefore, further improvement of the DR model will keep pace with mutual advances in molecular biology and computational structural biology and provide a useful tool for discovery of drugs or predictive toxicology.

CHAPTER 6.

COMPREHENSION OF BIO-PHYSICAL COMMUNICATION FOR PREDICTING POTENTIAL TOXICITY OF 16 POLYCYCLIC AROMATIC HYDROCARBONS

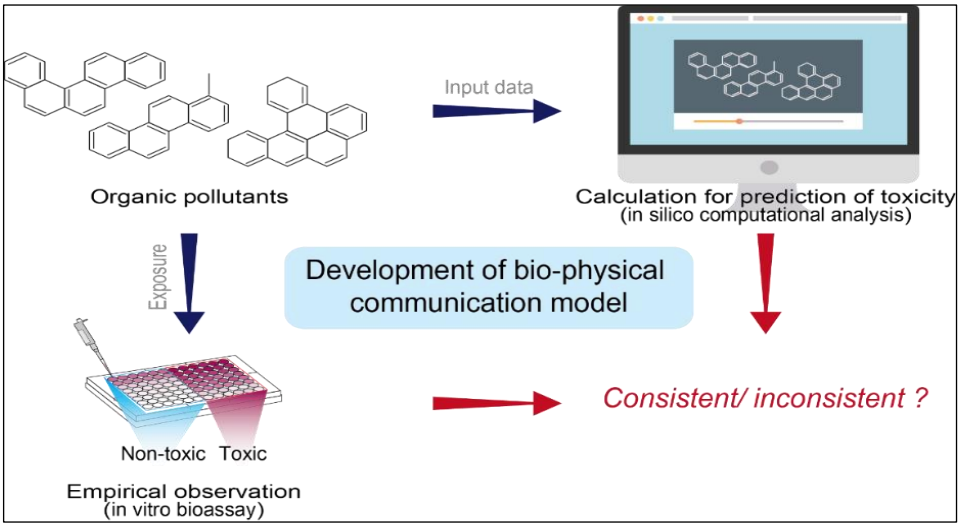

This chapter has been in preparation.
Kim, T., Zhen, J., Lee, J., Lee, C., Kwon, B.-O., Chae, K. H., Hong, S., Giesy, J. P., Chang, G. S., Khim, J. S. Comprehension of bio-physical communication for predicting potential toxicity of 16 polycyclic aromatic hydrocarbons.

6.1. Introduction

With increasingly the emerging persistent toxic substances (PTSs) from the influence of anthropogenic activities, PTSs have raised the potential acute or chronic toxicity in the marine environment. PTSs accumulated in the marine organisms by ingesting water, particles, or organisms, have major adverse effects, including cytotoxicity, endocrine disruption, immune abnormality, carcinogenesis, and lethality (Hader et al., 2020). Polycyclic aromatic hydrocarbons (PAHs) compounds are well known environmental PTSs that are present in various chemical forms across the terrestrial and marine environment. In fact, most of the work to understand the risk from exposure to PTSs involves the 16 PAHs on the US EPA Priority Pollutant List because of their several characteristics (easily measurable, occurred widely in the environment, and known to be carcinogenesis) (Andersson and Achten, 2015).

PTSs including 16 PAHs have long been of significant interest worldwide due to their potential adverse effects on bio-organisms. There have been various toxicity testing strategies for hazard identification of PTSs. Conventional toxicity-testing strategy for hazard identification of them is based on a complex set of whole-animal testing have difficulties addressing the wide variety of challenges today (Kim et al., 2020). Toxicity testing is under increasing pressure to meet several competing demands: i) test a large number of existing chemicals, many of which lack basic toxicity data; ii) test rapidly increasing number of new chemicals and novel materials; iii) reduce the use of animals; and iv) reduce the cost and time required for chemical safety evaluation (Krewski et al., 2010). However, the conventional strategy primarily relying on in vivo mammalian toxicity testing would be unable to meet those competing demands adequately (Figure 6.1a). The currently toxicity testing represents a paradigm shift from the use of experimental animals and apical endpoints toward the use of more efficient in vitro tests and in silico techniques. Furthermore, from cell-based in vitro studies to high-throughput computational techniques, newer approaches focusing on both hazard identification and exposure assessment have led to new understandings about the potential impacts of chemicals on the environment (Basketter et al., 2012).

From the 1960s until now, in vitro assays (76%) were the most studied among toxicity testing, followed by QSAR (13%) and docking models (11%) (Figure 6.1b). Since 1990s, in silico techniques such as QSAR and docking models have rapidly increased. Although in vitro bioassays have been well established for risk assessment and relatively less ethical issues than the animal testing, bioassays utilizing recombinant cells (e.g., H4llE-luciferase bioassay, H4llE-*luc*) are still cost- and labor intensive to meet the testing demand of upsurging hazardous substances. One of the most frequently asked questions in QSAR research is how large a training set is needed to ensure a reasonable predictive model. The answer to this question depends on many factors, among which the most important determinant is the quality of datasets. Without confirmation of the bioactivity mechanism of individual compounds, it is highly likely that the results from the linear relationship made by the dataset can be overestimated or underestimated (Alogheli et al., 2017). Unlike other two studies, the docking model utilizes physico-chemical properties of ligand and receptor to provide an optimized ligand binding status. In the absence of a comprehensive understanding of the relationships between each property of ligand and receptor, it relies solely on the results of the optimal binding status (Ribeiro and Ferreira, 2005).

The toxicity assessment in ecotoxicology has yet primarily relied upon empirical observation of biological responses through in vivo and later developed in vitro bioassays (Figure 6.1c). These bioassays determine the cause of the toxicity of individual compounds without understanding ligand identification and bioactivity mechanism analysis. In the case of QSAR, the results are produced by statistical inference through extrapolation and interpolation using experimental data to quickly screen many substances (Roy et al., 2013). As a result, the lack of observation in the mode of action (MOA) makes obtaining accurate data for the target substances difficult. A docking model can predict the binding state with the desired receptor by reflecting the molecular-specific tendency of the target substance, but it assumes an optimal state, so consideration of the state of the substance and the receptor before binding is insufficient (Moreira et al., 2010). Directional reactive factor (DRF) model which predicted the potential toxicity through the pre-binding state between

substances and receptors. In the DRF model, a follow-up study to confirm the actual binding state is needed because the predicted result value could not fully explain the binding because of the around charge generated by the net charge of the acceptor. To compensate for the binding state of each ligand, directional binding factor (DBF) model considered the binding probability of ligands and receptor. Finally, we developed a comprehensive toxicity prediction model which integrated a stepwise for toxicity response from pre-conjugation to the binding status by using the DRF and DBF model.

In the 21st century, this swift growth of new PTSs led to increasing attention garnered on the in silico alternatives in an effort to complement bioassays and screen a large number of substances. These alternatives make a paradigm from observational approach to the predictive approach in hazard identification, and then the prediction of toxicity was statistically inferred from many data. And recently, a toxicity prediction method employing a probabilistic approach was developed to overcome the shortcomings of statistical reasoning, and it was possible to confirm the cause of the toxic reaction by focusing more on the mechanism than the existing method (Figure 6.1d). Directional reactive and binding factor (DRBF) model can present important perspectives and results in response to the need for a mechanism-based and probabilistic toxicity prediction model for screening the ever-increasing number of compounds.

Here, we report a model based on ligand-receptor mechanism and suggest a probabilistic approach of predicting toxicity, deviating from the statistical analysis used in the alternatives (QSAR and docking model). Here, as an example, we applied our method to the 16 polycyclic aromatic hydrocarbons (PAHs) (see Table 6.1), with a well-known potential toxicity, interacting with the aryl hydrocarbon receptor (AhR). The approach in this study suggest transition from statistical interpretation of observation to analytical prediction of bio-physical communication during prediction the potential toxicity of persistent toxic substances.

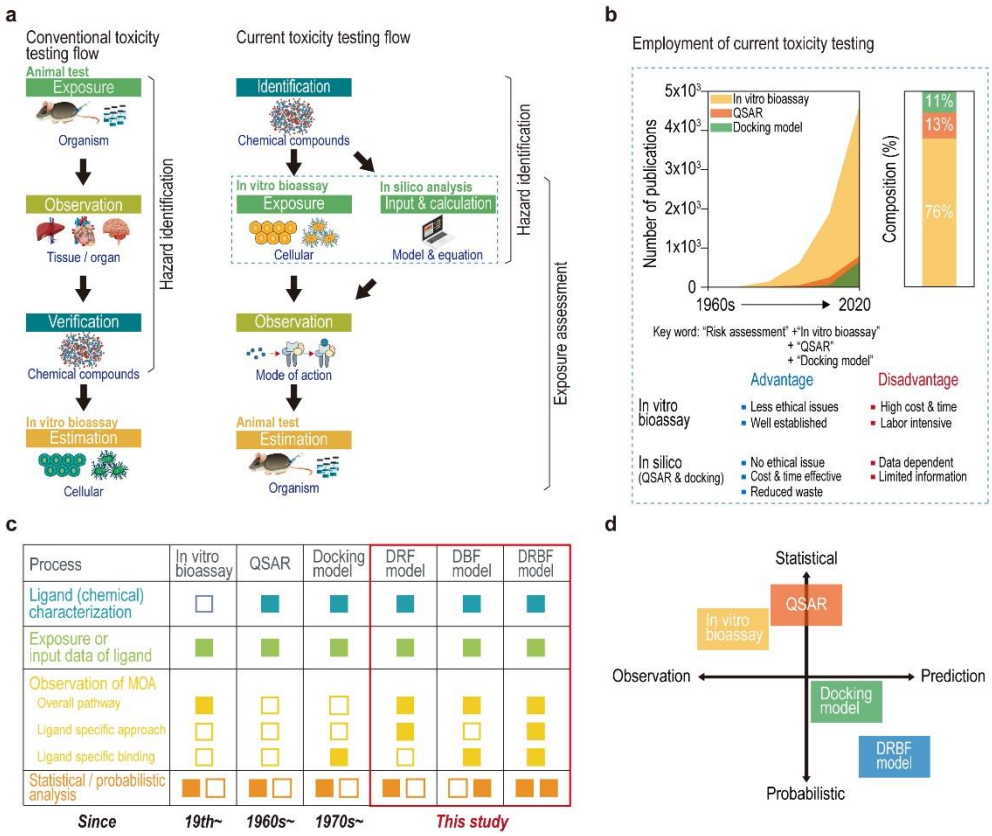

Figure 6.1

Overview of the methodologies used for the conventional and proposed next generation risk assessment of persistent toxic substances (PTSs) (a) Comparison between conventional toxicity testing and proposed next generation of toxicity testing; (b) Study effort for predicting the potential toxicity of PTSs by in silico method since 1960s. (c) Differences in each of the next generation toxicity testing methods within the toxicity response mechanism process; (d) A quadrant plot for perspectives (Observation–mechanistic approach and empirical–hypothetical) in each toxicity prediction method.

Table 6.1. Chemical compounds information of homologues of chrysene used in this study.

Compounds	[a]Abb.	Molecular formula	Number of benzene rings	Molecular weight	Log Kow	CAS RN	Purity (%)	Vendor
Naphthalene	Na	C10H8	2	128.17	3.30	91-20-3	> 98	Sigma-Aldrich (St. Louis, MO, USA)
Acenaphthene	Ace	C12H10	3	154.21	3.92	83-32-9	> 99	Sigma-Aldrich (St. Louis, MO, USA)
Acenaphthylene	Acl	C12H8	3	152.19	3.93	208-96-8	> 98	Sigma-Aldrich (St. Louis, MO, USA)
Fluorene	Flu	C13H10	3	166.22	4.18	95270-88-5	> 98	Sigma-Aldrich (St. Louis, MO, USA)
Phenanthrene	Phe	C14H10	3	178.23	4.46	85-01-8	> 98	Sigma-Aldrich (St. Louis, MO, USA)
Anthracene	Ant	C14H10	3	178.23	4.45	120-12-7	> 98	Sigma-Aldrich (St. Louis, MO, USA)
Fluoranthene	Fl	C16H10	4	202.25	5.16	206-44-0	> 98	Sigma-Aldrich (St. Louis, MO, USA)
Pyrene	Py	C16H10	4	202.25	4.88	129-00-0	> 98	Sigma-Aldrich (St. Louis, MO, USA)
Benzo[*a*]anthracene	BaA	C18H12	4	228.3	5.76	56-55-3	> 98	Sigma-Aldrich (St. Louis, MO, USA)
Chrysene	Chr	C18H12	4	228.3	5.73	218-01-9	> 98	Sigma-Aldrich (St. Louis, MO, USA)
Benzo[*b*]fluoranthene	BbF	C20H12	5	252.3	5.78	205-99-2	> 98	Sigma-Aldrich (St. Louis, MO, USA)
Benzo[*k*]fluoranthene	BkF	C20H12	5	252.3	6.11	207-08-9	> 98	Sigma-Aldrich (St. Louis, MO, USA)
Benzo[*a*]pyrene	BaP	C20H12	5	252.3	6.13	50-32-8	> 98	Sigma-Aldrich (St. Louis, MO, USA)
Dibenzo[*a,h*]anthracene	DbahA	C22H14	5	278.3	6.50	53-70-3	> 98	Sigma-Aldrich (St. Louis, MO, USA)
Benzo[*g,h,i*]perylene	BghiP	C22H12	6	276.3	6.63	191-24-2	> 98	Sigma-Aldrich (St. Louis, MO, USA)
Indeno[*1,2,3-c,d*]pyrene	IcdP	C22H12	6	276.3	6.70	193-39-5	> 98	Sigma-Aldrich (St. Louis, MO, USA)

[a] Abb.: Abbreviation

6.2. Materials and Methods

6.2.1. Selection of model chemicals

As the model compounds testing our model, United States Environmental Protection Agency (US EPA) 16 priority pollutants PAHs (16 PAHs) of special concern are selected considering their environmental persistence, bioaccumulation, and toxicity. These pollutants are emitted to atmosphere as byproducts of an incomplete combustion of fossil fuel, volcanic eruption, forest fires, and vehicle emissions (Lee et al., 2021). The model compounds represent a broad set of substances ranging from two to six rings of 5- and 6-members; naphthalene (Nap), acenaphthene (Ace), acenaphthylene (Acl), phenanthrene (Phe), fluorene (Flu), anthracene (Ant), fluoranthene (Fla), pyrene (Pyr), benzo[*a*]anthracene (BaA), chrysene (Chr), benzo[*a*]pyrene (BaP), benzo[*b*]fluoranthene (BbF), benzo[*k*]fluoranthene (BkF), dibenzo[*a*,*h*]anthracene (DahA), indeno[*1*,*2*,*3*-*cd*]pyrene (IcdP), and benzo[*g*,*h*,*i*]perylene (BghiP).

6.2.2. Density functional theory calculations

Physico-chemical properties of 16 PAHs were calculated by the ORCA program package based on Ab initio density functional theory (DFT) (Neese, 2011). Every stage of DFT computations was done employing Becke three-parameter Lee-Yang-Parr (B3LYP) exchange functional with the polarized triple-zeta valence (def2-TZVPP) basis set. The first stage (spin-restricted) geometry optimizations were carried out for neutral structures and then ±e charge was added for cationic or anionic state of each molecule as the second stage (spin-unrestricted) optimizations. From the geometry-optimized structures, molecular orbitals (MO), charge populations (Mulliken and Hirshfeld), density of states (DOS), electric dipole moments (DM), and vibrational amplitudes (VA) were computed.

6.2.3. Molecular dynamics for calculating the probability of binding in ligand:AhR

The computational inputs for molecular dynamic (MD) simulation was prepared using CHARMM-GUI tools (Fronzoni et al., 2014). Especially, the ligands (PAHs) were parametrized by "Ligand Reader & Modeler" with CHARMM General Force Field (CGenFF) (Waterhouse et al., 2018). The crystal structure of CLOCK:BMAL1 (PDB ID: 4F3L) was obtained from RCSB with HOH molecule removed. Afterwards, thirty molecules of a ligand were randomly placed at the surrounding of a receptor, the volume fraction (solute) was controlled at 8% to facilitate movements of small molecules. The solution system is a cubic box with a side length about 90 nm, filled and neutralized with (solvent molecules) 20,000 TIP3P molecules and 0.15% of K+/Cl- ions. This procedure was repeated for 16 different PAHs.

The simulation was carried out using GROMACS/2019.3 and CHARMM36m force field (Lee et al., 2016). Van der Waal (VDW) cut-off was set to 1.2 nm. Particle-Mesh-Ewald (PME) was employed for electrostatic interactions and the coulomb cut-off at 1.2nm with Verlet method. Steep energy minimization was converged to 100 $kJ \cdot mol^{-1} \cdot nm^{-1}$ with hydrogen bonds constrained by LINCS. Temperature was coupled separately for solute and solvent using a Nose-Hoover extended ensemble, following by 400-ps NVT equilibration in which the reference temperature was 310 K. Parrinello-Rahman method and isotropic coupling type were chosen for 2-ns NPT runs and the reference pressure was 1.0 bar. Finally, the 20-ns production run was performed using leap-frog algorithm (md). The integration time steps were set to 0.002 ps and the energy was saved every 100 ps (totally 200 frames) for data analysis. The last frame of each simulation was used as the principal structure for further studies of ligand-receptor binding.

6.2.4. Aryl hydrocarbon receptor homology modeling

Three-dimensional (3D) structure of the ligand binding domain (LBD) of the aryl hydrocarbon receptor (AhR) was built from the sequence of amino acids in the rat AhR (GI: 7304873 in the NCBI sequence database) by the validation using the SWISS-MODEL, Rampage web servers, and ProSA-web (Wiederstein and Sippl, 2007). A crystal structure of 4F3L (sequence identity = 27.8%, residues 252–357) was selected as a template. The structure model built using Ramachandran plot from Rampage web server was validated from the fact that 98% of the total residues were in the favored region with 2.4% of the residues in the allowed region. Further, results from the ProSA analysis showed the Z-score for the 3D model within the range of score typically found for native proteins of the similar size.

6.2.5. H4IIE bioassay and calculation in median effective concentration

The experimental acute toxicity of 16 PAHs was determined based on an AhR-mediated activity using H4IIE-luc cells, as previously reported (Kim et al., 2020). Considering the degradability of PAHs due to metabolic activity for longer exposure time, the 4 h exposure time was chosen for AhR-mediated potency. After the exposure, the activity was expressed as relative luminescence units that were quantified using a Victor X3 multi label plate reader (PerkinElmer, Waltham, MA). Benzo[*k*]fluoranthene (BkF) was used as a positive control ligand. We converted the responses of H4IIE-luc bioassay to the percentages with respect to the maximum response (%BkFmax) observed for a 50 nM BkF (=100 % BkFmax). The bioassays were repeated four times in triplicate. A half effective concentration for AhR-mediated effects of individual compound was determined from the H4IIE-luc bioassays. Compounds with ten concentrations using five-fold serial dilution (viz., 1, 0.2, 0.04, 0.008, 0.0016, and 0.0032 μg mL^{-1}) were prepared. Estimation of the EC50 values from the dose-response relationship was basically assumed considering equal efficacy and parallelism between reference compound (BkF).

6.2.6. In silico toxicity prediction analysis

VEGA-QSAR and OpenVirtualtoxLabTM program packages were used for QSAR and molecular docking analysis, respectively. VEGA-QSAR has been performed and showed a large set of toxicological data and endpoints convincing to derive predictive toxicity according to previous studies. The EC50 values were obtained using SMLIES notation of VEGA-QSAR and obtained the toxicity data corresponding to Daphnia magna (Benfenati et al., 2013). Ligand:AhR binding affinities were estimated and calculated by OpenVirtualtoxLabTM (Vedani et al., 2012). Combined automated and flexible docking with multidimensional QSAR was used to simulate and quantify toxic potential and how chemicals bind to a set of currently implemented proteins that cause adverse effects.

6.3. Results and Discussion

6.3.1. A comprehensive driving force of ligand to receptor calculated from DR model based on first principles

Ligand-receptor protein binding is fundamental biological process involving toxic response, drug efficacy, immunization, and another crucial cell function occurring in bio-organism (Fröhlich, 2018). Ligand:receptor complex (consist of p23, SRC, HSP90, and AIP) is translocated into the cell nucleus and regulates the expression of xenobiotic metabolizing enzymes such as CYP1A1, a member of cytochrome P450 family (Red box in Figure 6.2a). This receptor-mediated enzyme regulation depends on ligand-specific binding affinity and provides the base of in vitro bioassays in environmental toxicology for assessment of the adverse bioactivity of target toxicants. Although the receptor signal transduction pathways have been revealed in detail, the kinetics of how a ligand physico-chemically reacts with the responsive receptor is an unsolved question being under intensive research (Di Ventura et al., 2006).

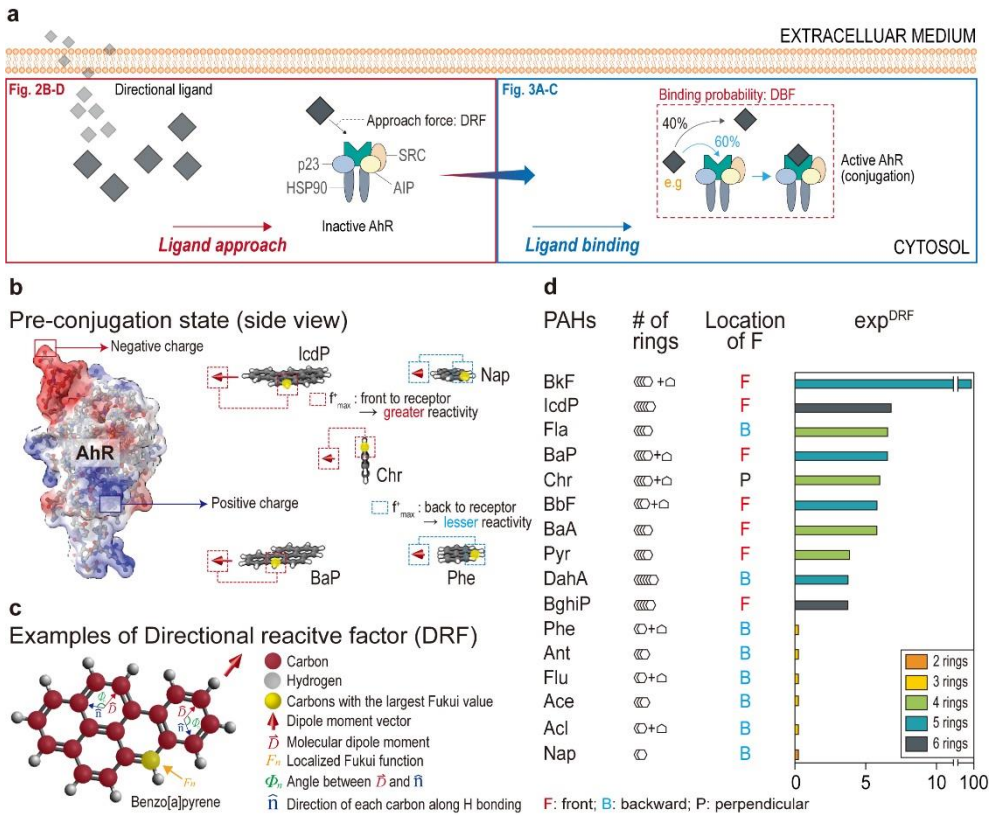

Figure 6.2

Directional reactive model for predicting a driving force of 16 PAHs to AhR (a) Schematic insight of mechanism-based approach for quantification to ligand approach and binding to AhR; (b) Visualization of first principles prediction model for AhR-mediated potency of 16 PAHs before their binding to AhR (c) Various factors for calculating the directional reactive factor (DRF). Carbon atoms with the largest Fukui value in each 16 PAH are highlighted in yellow and the red arrow denotes the direction and magnitude of dipole moment; (d) Predicted potential toxicity of 16 PAHs. Each color is the number of benzene rings that consist of 16 PAHs. F (forward), B (backward), and P (perpendicular) are indicated according to the position of the highest Fukui value in the carbon.

Each ligand is subjected to a variety of forces during the pre-conjugation state, including electrostatic, hydrogen bonding, and van der Waals forces. Given that receptor proteins are substantially larger than typical ligands (16 PAHs in this study), it is reasonable to assume that charges on receptors are fixed in space and the ligand would undergo a rotate to align its dipole moment vector with the line of force action as the ligand approaches the receptor. Therefore, they have their orientation status to the receptor (Figure 6.2b). This orientation status approach begins with consideration of their dipole moments (D) and Fukui values (F), as the ruling parameters of PAHs interacting with the receptor. Based on the molecular orbital structures obtained by ab initio density functional theory (DFT) calculation, physical properties of each PAHs were calculated (see Figure 6.3). The pre-conjugation status suggests that physico-chemical properties of PAHs do not contribute independently to binding to the receptor, but there is interplay between them (Figure 6.2c). Based on this consideration, an equation that describes the directional reactivity factor (DRF) was derived for a given AhR protein (see Figure 6.4, Table 6.2, 6.3 and 6.4) (Kim et al., 2020).

$$\mathrm{DRF} = C_{LR} Q_{R,net} \left[\sum_{n=1}^{\#A:X} F_n^{\pm} \left(\vec{\boldsymbol{D}} \cdot \hat{\boldsymbol{n}} \right) \right] = C_{LR} Q_{R,net} \left[\sum_{n=1}^{\#A:X} F_n^{\pm} \left| \vec{\boldsymbol{D}} \right| cos\phi_n \right] \cdots\cdots\cdots\cdots\cdots \quad (1)$$

C_{LR}: Coulomb constant $\left(\frac{1}{4\pi\varepsilon_o\varepsilon_R r}\right)$, relative permittivity of receptor cytosol (ε_R) including the inverse proportionality of charge-dipole interaction to the intermolecular distance (r); QR,net: the AhR's net charge from charged amino acids F^+ or F^-: each carbon bonded with hydrogen (#A:X) in PAHs; $\vec{\boldsymbol{D}}$: the ligand's dipole moment vector; $\hat{\boldsymbol{n}}$: the bonding direction of the terminal atom

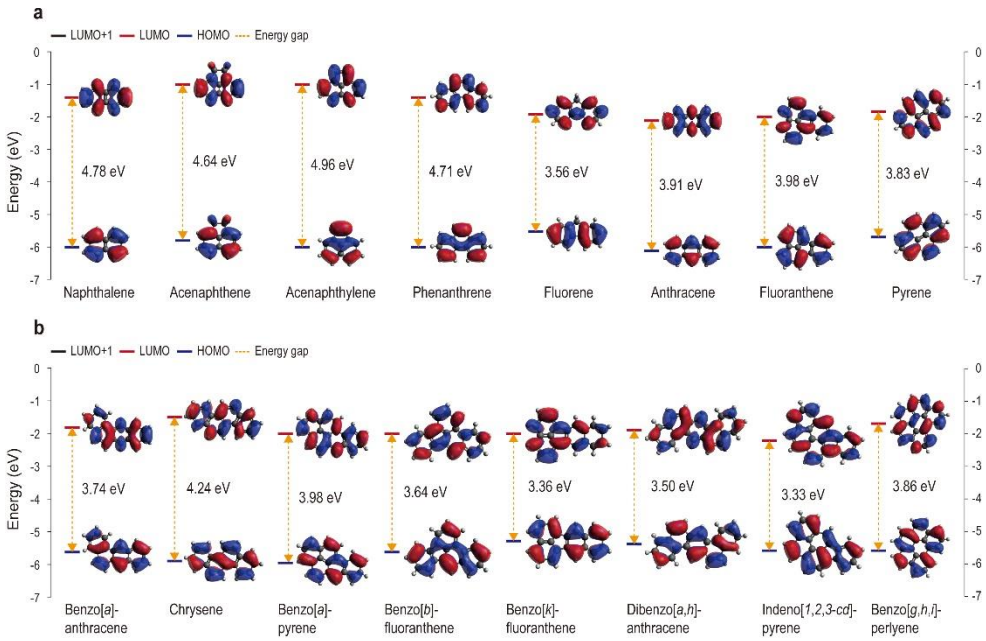

Figure 6.3

Visualization of the HOMO and LUMO orbital in chrysene homologues. (a and b) Presentation of the energy levels, HOMO-LUMO gap and orbital composition distribution of the HOMO and LUMO for chrysene and benzo-chrysene. HOMO-LUMO gap energy ranged from 2.89 eV to 4.24 eV. The HOMO-LUMO gap is slightly difference in each congener.

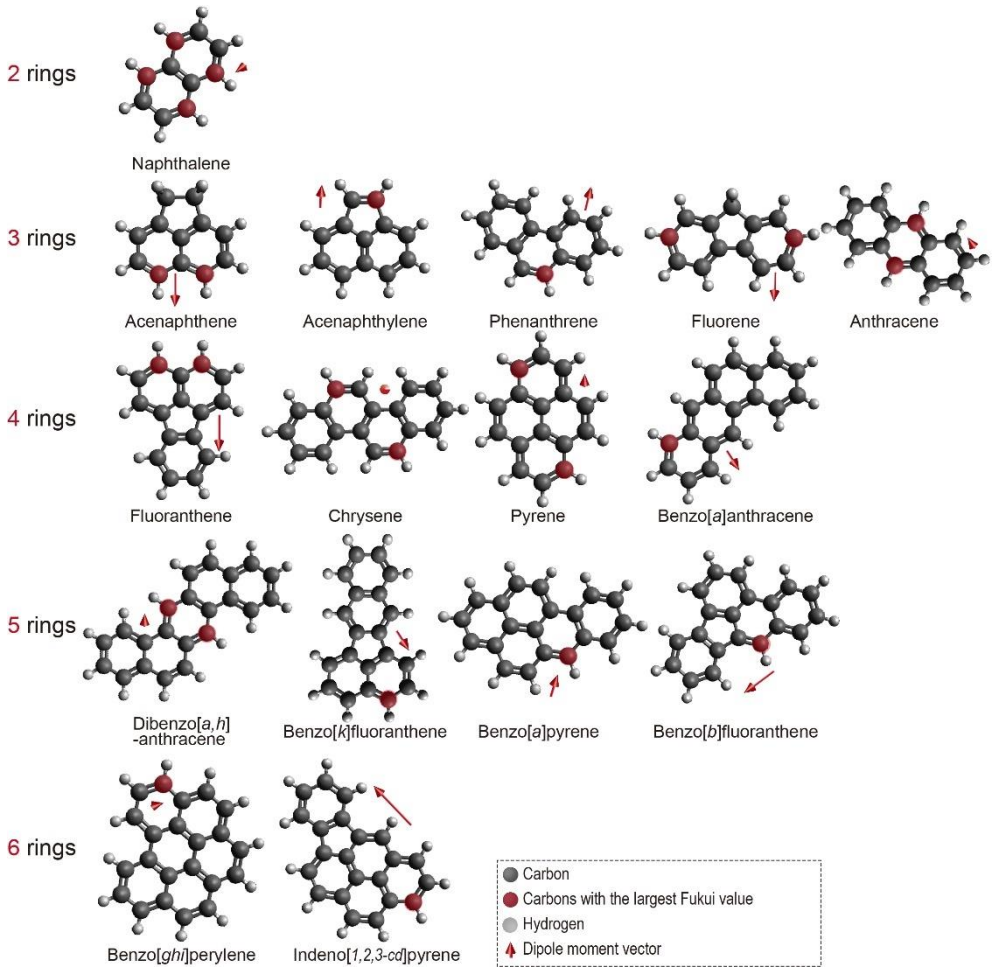

Figure 6.4

The information of physico-chemical properties in each 16 PAHs. Carbons in structure of chrysene homologues are shown in dark gray, hydrogens are shown in white and oxygen are shown in red color. A carbon with the highest Fukui value of chrysene homologues is shown in yellow, and dipole moments are shown in red arrow. The size of the arrow indicates the quantity of dipole moment.

Table 6.2. Structural and electronic configuration parameters of 16 PAHs and the potential toxicity predicted by directional reactivity factor (DRF).

Compounds	HOMO (eV)	LUMO (eV)	HOMO-LUMO energy gap (eV)	Dipole moment magnitude (10^2 Debye)	Fukui value F^+	Carbon atoms with the largest Fukui value	Location of carbon* to AhR	Directional reactivity factor (DRF)
Naphthalene	-6.0	-1.3	4.78	0.0	0.1	10C	B	-2.52
Acenaphthene	-5.7	-1.0	4.64	0.9	0.1	4C	B	-1.79
Acenaphthylene	-6.0	-1.0	4.96	0.5	0.1	9C	B	-2.24
Phenanthrene	-6.0	-1.3	4.71	0.0	0.1	8C	B	-1.10
Fluorene	-5.5	-1.9	3.56	0.0	0.1	7C	B	-1.64
Anthracene	-6.1	-2.1	3.91	0.3	0.1	2C	B	-1.58
Fluoranthene	-6.0	-2.0	3.98	0.3	0.1	14C	B	0.41
Pyrene	-5.6	-1.7	3.83	0.0	0.1	8C, 10C	F	0.27
Benzo[*a*]anthracene	-5.6	-1.8	3.74	0.0	0.1	9C	F	0.37
Chrysene	-5.8	-1.5	4.24	0.0	0.1	7C, 18C	P	0.40
Benzo[*a*]pyrene	-5.9	-2.0	3.98	0.4	0.1	2C	F	0.38
Benzo[*b*]fluoranthene	-5.6	-2.0	3.64	0.3	0.1	7C	F	0.37
Benzo[*k*]fluoranthene	-5.3	-2.0	3.36	0.0	0.1	7C	F	1.12
Dibenzo[*a*,*h*]anthracene	-5.4	-1.9	3.50	0.0	0.1	7C	B	0.27
Indeno[*1*,*2*,*3*-*cd*]pyrene	-5.6	-2.2	3.33	0.6	0.1	16C	F	0.41
Benzo[*g*,*h*,*i*]perlyene	-5.6	-1.7	3.86	0.0	0.1	10C	F	0.26

* The carbon with the largest Fukui value; forward (F), perpendicular (P), and backward (B) to the AhR.

Table 6.3. Searching for structure homologs of aryl hydrocarbon receptors.

Protein data Bank ID	Chain	GMQE	QMEAN	%Identity
4F3L	**B**	**0.67**	**-1.73**	**29.59**
4ZP4.1	B	0.65	-3.97	30.77
4ZP4.2	B	0.67	-2.54	30.77
4ZPH.1	B	0.67	-3.01	30.77
4ZPH.2	B	0.67	-2.54	30.77
4ZQD.2	B	0.67	-2.67	30.77
4ZQD.1	B	0.66	-3.21	30.77`
5KIZ.1	A	0.64	-4.24	31.07
6E3T.1	B	0.66	-2.62	30.77
5SY7.1	B	0.63	-2.22	25.70
4ZPR.1	B	0.59	-6.01	31.07
5SY5.1	B	0.61	-2.73	21.90
5SY5.2	B	0.62	-2.60	21.90
4H6J.1	A	0.60	-3.30	34.41
2A24.1	A	0.60	-3.99	30.77
4WN5.2	B	0.59	-2.66	24.27
4WN5.1	A	0.59	-2.40	24.27
4DJ3.1	A	0.57	-3.08	18.63

Table 6.4. Physico-chemical properties of aryl hydrocarbon receptors.

Single letter code	NFIFRTKHKLDFTPIGCDAKGQLILGYTEVELCTRGSGYQFIHAADILHCAESHIRMIKTGESGMTVFRLLAKHSRWR WVQSNARLIYRNGRPDYIIATQRPLTDEE
Number of residues	107
Molecular weight	12381.1 g mol^{-1}
Extinction coefficient	16500 M-1 cm^{-1}
Iso-electric point	pH 9.14
Net charge at pH 7.4	4.1
Estimated solubility	Good water solubility
[a] Equation for net charge	$\text{Net charge} = \sum_i N_i \frac{10^{pk_{a_i}}}{10^{pH} + 10^{pk_{a_i}}} - \sum_j N_j \frac{10^{pk_{a_i}}}{10^{pH} + 10^{pk_{a_j}}}$

[a]N_i is the number, and pKa_i are the pKa values, of the N-terminus and the side chains of Arginine, Lysine, and Histidine.

The DRF equation takes into account of the contribution of all atom-condensed Fukui functions along the line of action ($\widehat{\boldsymbol{D}}$). This reflects that the reactive sites located behind the molecule with respect to the line of action would reduce the reaction affinity with the receptor. The use of either F in the DRF calculation depends on the charge state of responsive receptor. Since the DRF represents the degree of the optimal reaction configuration toward the ligand-receptor binding, we applied the DR model to 16 PAHs to predict the AhR mediated toxic potency (Figure 6.2d). As a novel finding, carbon with the largest Fukui value in a ligand would be a preferred site when bound to the receptor. Therefore, the forward location of carbon with the largest Fukui value to the receptor would be a desirable orientation when ligand is diffing toward the receptor in a cell. Exponential DRF values (expDRF) were calculated for comparison between 16 PAHs. The results of expDRF showed a variation in the number of benzene rings. Overall, the greater the number of benzene rings, the greater the DRF value, and 2–3 benzene rings PAHs showed the lowest values. Of note, the carbon with the highest Fukui value is located to the forward to the receptor in 4–6 benzene rings PAHs, indicating the greater DRF value. Fla, which is known to have low toxicity, showed a high value in DRF, which indicated that another factor can affect when it binds with AhR.

Recent studies have focused on the kinetics of ligands and receptors rather than using the statistical analysis to the correlation between the properties and toxicity of ligands. It suggests further consideration of physio-chemical properties of the molecular which might affect the binding are needed before assuming the optimal binding configuration (Kim et al., 2020). Based on this model, it was confirmed that the reactivity (e.g., F) of molecules in each ligand group was different depending on the position, despite their structural similarity, and the contribution in dipole moment of the ligand was confirmed according to the position of the reactive molecule. As a result, we demonstrate that structural similarity does not always equate to similar bioactivity, and that even a modest structural difference, such as different functionalization locations, can cause a significant shift in results.

6.3.2. Probability of 16 PAHs binding to AhR and determination of potential toxicity for 16 PAHs

In the pre-conjugation state, the DRF from the ligand's physico-chemical properties would represent the factor driving the ligard toward the receptor protein. However, it is important to ascertain the state of the actual coupling because it is uncertain whether the driving force such as DRF directly affects the ligand:AhR complex. To overcome these problems, we used a molecular dynamics (MD) simulation method that utilizes the final binding state of PAHs-AhR (Blue box in Figures 6.2a and 6.5a). Through the MD results, the positions where 16 PAHs are mainly bound to AhR were divided into 18 sites in total (Figure 6.6). The result shows the ligand-receptor binding simulation as an example for Pyr. A Per-Arnt-Sim (PAS) domain comprises two structural repeats which are also involved in the dimerization with ARNT (PAS A: K, L, M, N, O, P, Q, and R) but which also allows the ligand binding (PAS B: A, B, C, D, E, F, G, H, I, and J). In this study, only the binding state of PAS B and ligand, which is favorable for potential toxicity, was considered (Tagliabue et al., 2019). The results suggest that MD simulations show the probability of PAHs-AhR binding state to assess the contribution of the potential toxicity through a solvent-mediated mechanism. Thus, it enables atomic-scale observation of ligand-binding processes within time scales accessible by standard MD (~20 ns). Directional binding factor (DBF) which was calculated as the probability of observing the ligand-binding in this type of MD simulation was estimated.

$$DBF = \frac{n(PAS\ B)_{binding}}{n(PAS\ B{+}PAS\ A)_{binding}} \quad \cdots\cdots (2)$$

where n(PAS B) binding and n(PAS A+PAS B) binding are the number of ligands binding to PAS B domain for transcription of carcinogenesis and the number of ligands binding to AhR including PAS A and PAS B, respectively.

In general, all 16 PAHs were confirmed to bind to PAS B regardless of the number of cyclic rings, suggesting that they can be carcinogenic as AhR agonists. In detail, the site of binding to AhR was different for each of the 16 PAHs (see Figure

6.7 and 6.8). As a result of MD simulation, 27 out of 30 DahA bound to the PAS domain, showing the highest binding rate among 16 PAHs (Figure 6.6b) BaP, which is known to be particularly toxic, 13 ligands (43% out of 30) were bound to the A site of PAS B. Among the 16 PAHs, Fla, Nat, Ace, and Flu, which had a small number of benzene rings, had a low number of bindings to AhR (particularly in PAS B) compared to other substances.

Before the ligand:receptor complex was translocated to the cell nucleus to regulate the expression of xenobiotic metabolizing enzymes, the ligand approach and receptor binding phenomena were quantitatively expressed as expDRF and DBF, respectively, and combined with directional reactive & binding factor (DRBF).

$$DRBF = exp^{DRF} \times DBF \quad \cdots\cdots (3)$$

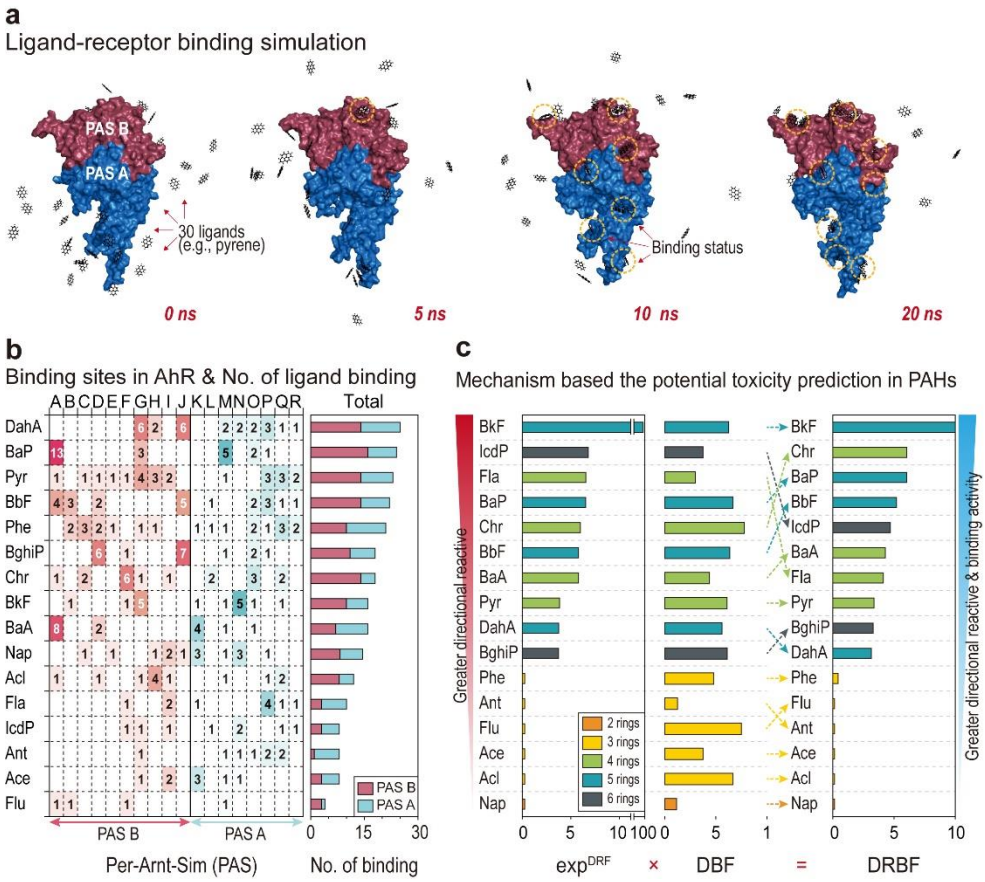

Figure 6.5

Ligand-receptor binding simulation by using molecular dynamic calculation (MD) and probabilistic approach for predicting the potential toxicity of 16 PAHs Prediction efficiency in silico assays (a) Molecular dynamics of 16 PAHs-AhR during 20 ns. There are PAS A and PAS B domains consisting of AhR, and PAS B contributes to carcinogenesis after the ligands binding; (b) Number and binding sites (PAS B: A, B, C, D, E, F, G, H, I, J; PAS A: K, L, M, O, P, Q, and R) of each 16 PAHs attached to AhR through MD simulation. PPAS B was calculated considering the number of bindings to PAS B in a total of 30 molecules: (c) Quantification of the predicted toxicity of 16 PAHs using the directional reactive and binding factor including DRF and DBF in the mechanism of Ligand-AhR. In the ligand approach state, DRF was calculated, and in the ligand binding state, directional reactive and binding factor (DBF) was quantified.

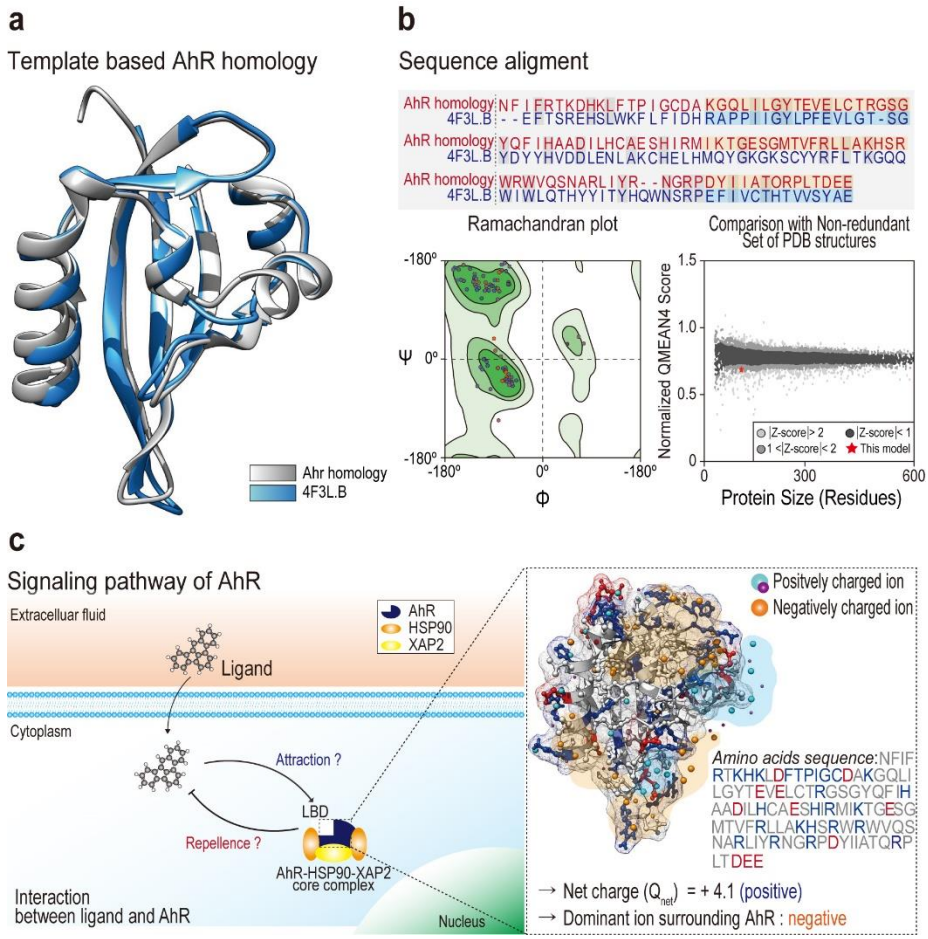

Figure 6.6

Homology model and quality metrics of AhR LBD. (a) Super-imposition of the template (light blue) with the AhR model (white); (b) Sequence alignment between the model and template. RMSD less than 1.0 Å and a structure overlap of 98.13. The ProSA analysis of the generated AhR structure in this study. 2 The figure represents the Prosa-web plot of template 4F3L chain A with a z-score value of − 4.07; (c) Signaling pathway of AhR and net charge of AhR homology model.

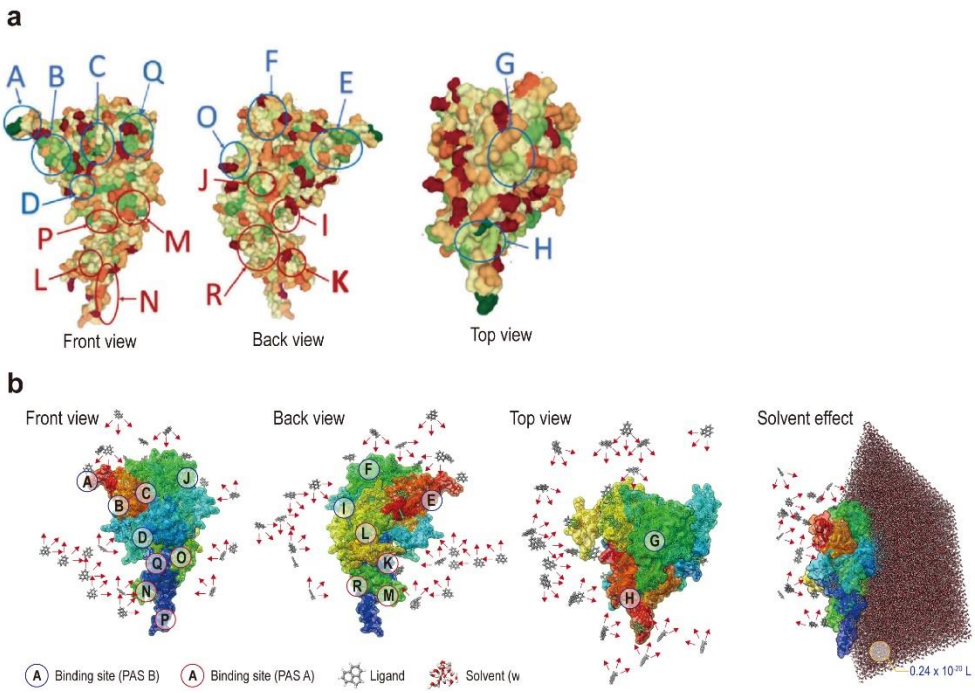

Figure 6.7

AhR Homology model and 16 PAHs binding sites. (a) Total 18 binding sites which were bound by 16 PAHs consisted of PAS A (red: A, B, C, D, E, F, G, H, and I) and PAS B (blue: J, K, L, M, N, O, P, Q, and R) domains. quality metrics of AhR LBD. (b) The number of total 30 ligands bound to AhR for 20 ns was measured, and the probability of binding to the PAS B domain was calculated.

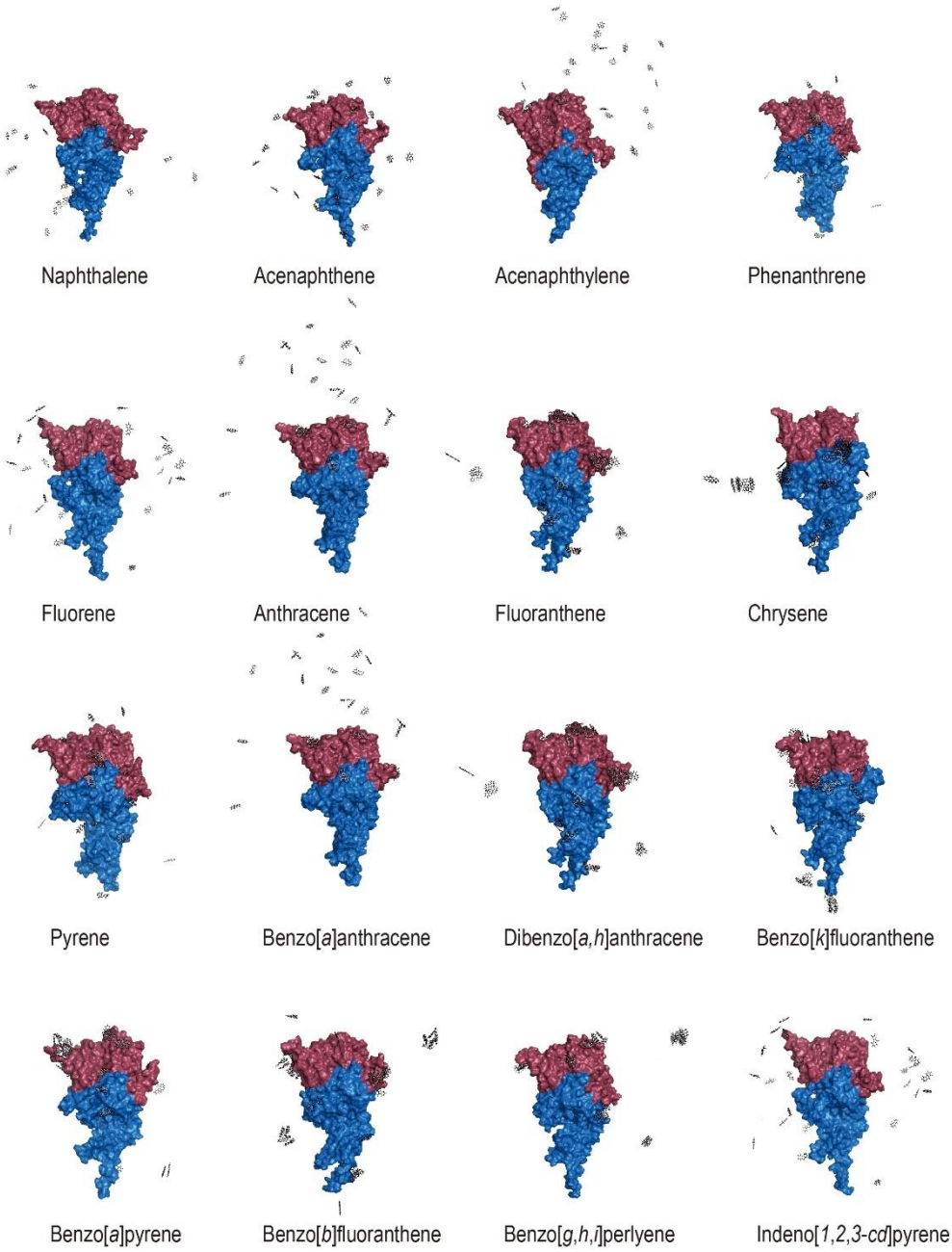

Figure 6.8
Molecular dynamics simulations of the binding of 16 PAHs (2–4 rings) to AhR in water solution. AhR homology consists of total two domains including PAS A (blue) and PAS B (red). The simulation was proceeded by the input of total each 30 PAHs to AhR. The results show that PAHs do not depend on only one binding site for binding to AhR.

Similar to the results of previous in vitro bioassay studies, the predicted potential toxicity of Fla with high $_{exp}$DRF was lesser, and the predicted toxicity of substances found to have greater toxicity such as Chr, BaP, BbF and BghiP increased (Figure 6.6c). Each of these stepwise quantification and probabilistic approaches not only emphasizes the importance of considering the mechanisms of toxic expression that could have been neglected, but also avoids statistical errors and can further increase the predictive rate of potential toxicity. Proteins often bind ligands in buried cavities that appear to be inaccessible based on static structures. The mechanisms and pathways by which ligands reach their binding sites in such cases are, thus, often unknown (Xing et al., 2012). Yet, ligand recognition by occluded cavities can happen rapidly, indicating there is no single dominant pathway (Cronin and Schultz, 2003). Therefore, the approach of probability in ligand-receptor binding can consider all the binding which can make the backward reaction such as carcinogenesis. We highlight the role of general movements for benzene to reach its binding cavity without the need for large-scale distortions of the protein structure, explaining the small activation energies. The observed consistency of our approach with the experimental and theoretical data available constitutes an initial framework for analyzing the ligand-binding mechanism in the structure and functions of the AhR. This probabilistic approach based on mechanism has shown that a variety of strategies can be chosen for the management of PTSs.

6.3.3. Experimental and predicted potential toxicity of 16 PAHs using in vitro and in silico testing

Figure 6.9a shows the experimental bioassay results of potential toxicity for 16 PAHs using the H4llE-luc cell lines (see Table 6.5). The experimental dose-response curves are categorized for the groups with the similar molecular weight and the number of aromatic rings. AhR-mediated potencies in 16 PAHs were greater as the number of cyclic rings increased. Compared with a positive control ligand of BkF (relative potency = 1), relative potency (ReP) values showed less than 0.01 in the 2–3 rings PAHs and relatively high values in 4–6 rings (< 0.85). Comparing with the results from the previous studies, the trend according to the increase in the number of benzene rings did not always coincide, and it was also confirmed that the AhR potency was different even if the number and molecular weight of the benzene rings were the same. The ligand-AhR complex of differential binding would be allowed by the structure of ligands and their conformational change in response to protein in the AhR (Sahai and Biggin, 2011, Rothhammer and Quintana, 2019).

Finally, the DRBF values and experimental toxic potency data (inverse of the Log EC50) were compared with the toxicity-relevant characteristics predicted by current in silico predictive models; QSAR model (1/LC50), a structure-based statistical regression method and molecular docking model (calculated as toxic potency score (ToxPot)) (Table 6.6). In DRBF model, IcdP, Chr, BaP and BkF showed lower DRF than Fla, but it was confirmed that the number of bindings to AhR was higher than Fla (Figure 6.9b). In PAHs consisting of 2–3 rings of benzene such as Phe, Flu, Ant, Ace, Acl, and Nap, although the calculation of the binding probability changed the ranking of potential toxicity, it does not significantly affect the overall trend. In particular, Chr, BaP, and BbF had DRBFs of 0.059, 0.049, and 0.046, which were predicted to have relatively higher potential toxicity than when only DRF was calculated. Of note, DRBF considering the binding probabilities showed a greater significant correlation (R^2=0.90 and $p<0.01$) (Figure 6.9c).

The overall results suggest that both QSAR and molecular docking models do not estimate the experimental toxic potencies of in vitro bioassays accurately. The QSAR model predicts the highest toxicity of depending on the greater number of

cyclic rings in PAHs. And also, the same toxicity between Ace and Acl was obtained (Fig. 4B). Most QSAR studies never calculate structure-dependent dependent two or more physico-chemical properties of substances, thus errors, including over/underestimating the potential toxicity, will be expected when extrapolation and interpolation are employed (Ginsberg et al., 2019). This results in the statistically significant correlation between experimental 1/Log EC50 and QSAR-estimated 1/LC50 ($R^2 = 0.57$, $p < 0.05$) (Figure 6.9c).

Overall, unlike the QSAR results, predicted greater potential toxicity results were evaluated for 16 PAHs composed of five benzene rings. As the number of rings and molecular weight increase, the toxicity is predicted to increase, and the results are significantly correlated to experimental results ($R^2 = 0.84$, $p < 0.05$) (Figure 6.9b and c). There are various factors affecting the binding status linked to bioactivation, such as the binding site of the ligand, the hydrophobic site of the receptor, and the arrangement of amino acids. However, the docking model may not always be able to achieve the optimum ligand-receptor binding posture with the lowest free energy because the long-range dipole-charge interaction sets the orientation and relative distribution of the ligand's reactive sites prior to binding to the receptor. For pre-conjugation of the ligand-receptor binding, the docking model cannot accommodate the probability of binding but the optimal binding state so that the potential toxicity of each ligand can be over/underestimated, so as to the QSAR approach (Cronin and Schultz, 2003).

When the results calculated as relative estimated toxicity (BkF=1) from in silico models including DRBF model suggested in the previous study were compared, it was confirmed that DRBF were more closely consistent to the experimental values than those of other models (Figure 6.9d and Table 6.7). From the relative predicted toxicity values of 16 PAHs presented through the DRBF model, the toxicity contribution of each PAH in the environmental sample (e.g., sediment and water) can also be calculated by a potency balance. In several previous studies using H4IIE-*luc* bioassays which were used in this study, it was confirmed that the mixture of PAHs exhibited AhR-mediated potencies additively. Since the homology modeling of AhR in this study utilized AhR of mice, it is necessary to understand and utilize

AhR sequences of fish in order to accurately understand the potential toxicity of organic pollutants in the marine environment.

The importance of mechanistic quantification of the dynamics between ligands and receptors can be exemplified by the influence of water molecules mediating interactions. Water molecules can have an effect to different binding modes within a receptor, ultimately dictated by the free energy of binding, but with many different contributions. In such a complex reaction, inferring only statistical reasoning and the presence or absence of combination rather than a mechanism-based approach can increase uncertainty (Cronin and Schultz, 2003). Moving away from the sole reliance on traditional approaches and information sources used in hazard, exposure, and risk assessment, toward the more expansive use of rapidly acquired chemical information via in vitro, in silico, and targeted testing strategies will require careful consideration of the information needed and values associated with a particular decision (Mondal et al., 2018). The information for the data collection should be obtained from the integrative consideration of quantifying the stage (approach and binding) of the toxic expression mechanism, stepping away from the convenience-seeking method (e.g., statistical estimation) for a moment.

Table 6.5. In vitro transactivation bioassay conditions for evaluating toxicities of chemical compounds.

Cell line	H4IIE-*luc*
ATCC#	CRL-1548
Cell type	Recombinant (*luc*-gene)
Mode of Action	AhR-mediated potency
Endpoint	Luciferase activity
Positive control	Benzo[*k*]fluoranthene
Culture condition	37 °C, 5% CO_2
Exposure time	4 h

Table 6.6. The predicted potential toxicity from in silico model

Compounds	QSAR *(Daphnia magna)*		Docking model [b)]
	LC_{50} (μM)	ReP	ToxPot
Naphthalene	2.95	0.04	0.20
Acenaphthene	1.09	0.12	0.22
Acenaphthylene	1.09	0.12	0.22
Phenanthrene	0.76	0.17	0.31
Fluorene	1.52	0.08	0.29
Anthracene	0.73	0.18	0.33
Fluoranthene	0.41	0.32	0.35
Pyrene	0.32	0.40	0.30
Benzo[*a*]anthracene	0.22	0.58	0.42
Chrysene	0.24	0.55	0.40
Benzo[*a*]pyrene	0.10	1.27	0.40
Benzo[*b*]fluoranthene	0.12	1.11	0.45
Benzo[*k*]fluoranthene	0.13	1.00	0.45
Dibenzo[*a*,*h*]anthracene	0.08	1.68	0.49
Indeno[*1*,*2*,*3*-*cd*]pyrene	0.05	2.35	0.45
Benzo[*g*,*h*,*i*]perlyene	0.05	2.39	0.39

Table 6.7. Comparison of the directional reactivity (DR) model with experimental potential toxicity data.

Chemical	*In vitro* bioassay (H4IIE-*luc*)		Mechanistic quantification model (This study)			
	Log(1/EC_{50}) (μM)	ReP [a)]	DRF [b)]	R_{DRF}	DRBF [c)]	R_{DRBF}
Naphthalene	0.06	6.65E-14	-2.52	3.24.E-07	1.99.E-05	1.77.E-07
Acenaphthene	0.09	3.40E-07	-1.79	6.60.E-06	5.76.E-04	5.13.E-06
Acenaphthylene	0.09	9.28E-08	-2.24	1.02.E-06	1.18.E-04	1.05.E-06
Phenanthrene	0.14	5.50E-04	-1.10	1.10.E-04	1.07.E-02	9.54.E-05
Fluorene	0.12	1.11E-04	-1.64	1.23.E-05	1.53.E-03	1.36.E-05
Anthracene	0.10	2.45E-06	-1.58	1.55.E-05	9.65.E-04	8.60.E-06
Fluoranthene	0.15	2.59E-03	0.41	5.39.E-02	4.30.E+00	3.83.E-02
Pyrene	0.16	8.08E-03	0.27	3.04.E-02	3.37.E+00	3.00.E-02
Benzo[*a*]anthracene	0.20	1.18E-01	0.37	4.59.E-02	4.29.E+00	3.82.E-02
Chrysene	0.23	5.44E-01	0.40	5.18.E-02	6.61.E+00	5.88.E-02
Benzo[*a*]pyrene	0.23	5.22E-01	0.38	4.75.E-02	5.53.E+00	4.92.E-02
Benzo[*b*]fluoranthene	0.21	2.51E-01	0.37	4.59.E-02	5.20.E+00	4.64.E-02
Benzo[*k*]fluoranthene	**0.24**	**1.00E+00**	**1.12**	**1.00.E+00**	**1.12.E+02**	**1.00.E+00**
Dibenzo[*a*,*h*]anthracene	0.15	4.61E-03	0.27	2.97.E-02	3.14.E+00	2.80.E-02
Indeno[*1*,*2*,*3-cd*]pyrene	0.24	8.52E-01	0.41	5.38.E-02	4.70.E+00	4.19.E-02
Benzo[*g*,*h*,*i*]perlyene	0.15	2.27E-03	0.26	2.97.E-02	3.29.E+00	2.93.E-02

[a)] Relative potency; [b)] directional reactive factor; [c)] directional reactive and binding factor.

6.4. Conclusion

Overall, this study has shown that a mechanistic approach to the potential toxicity of 16 PAHs based on dynamical relationship between ligands and receptor can both predict and evaluate their potential toxicity. We find this case example points out two factors that can help build confidence in emerging method: i) An approach independent on inferences from statistics and optimization, ii) the ability to construct the potential toxicity upon a mechanism-based adverse outcome pathway (AOP). The predictions have a relatively great coincidence with the experimental data and does not proceed under any statistical and limiting assumption but reflect the ligand-receptor binding process quantitatively. The combination of the probabilistic model with the mechanistic interpretation allowed us to understand the variation both the potential toxicities and their causes in ligand-receptor response. The principles employed, particularly quantification of pre-conjugation and binding state, have an importance beyond the immediate field of toxicity screening, for example in studies of drug efficacy and monitoring of human subjects in clinical trials. Therefore, further improvement of the DR model will keep pace with advances in molecular biology and computational structural biology and represent a significant step on the road to providing reliable and mechanistic interpretation screening systems for preclinical toxicology.

CHAPTER 7.

CONCLUSIONS

7.1. Summary

In the present study, the restoration capacity and ecotoxicological effects of organic pollutants were evaluated with enclosed experimental ecosystems and scales (microcosm, mesocosm, and in silico method). One of the greatest challenges of the present study was to evaluate quantitatively the restoration capacity for organic pollutants in a tidal flat and determine a novel factor contributing to the potential toxicity in marine organisms. This study confirmed the reaction relationship between the marine environment, living organisms, and organic pollutants step by step from a macro-microscopic approach.

In **Chapter 2**, a mesocosm study was performed to assess the restoration capacity of nutrient (TP, TN, and COD) contamination and short-term changes in seawater. The results were as follows: 1) the restoration capacity for organic pollutants in tidal flats was evaluated by a tide-simulated mesocosm; 2) enriched waterborne organic matters and nutrients rapidly decreased (~2 d) in the bare tidal flat; 3) the salt marsh showing a greater restoration capacity than the tidal flat indicated a vegetation effect, and 4) the removal capacity max. for COD & TP in Bongam was estimated to be 114 and 4.3 kg d^{-1}, respectively.

In **Chapter 3**, an artificial tidal control system was utilized for determination of benthic community responses after exposure of sedimentary oil contamination over a period of 90 days during which semi-field bioremediation experiments were conducted. The results revealed the following: 1) the mesocosm study first to adopt SQT revealed a varying oil cleanup efficiency among the methods; 2) physical cleanup effectively removed oils, but adverse ecological impacts were observed initially; 3) mixed biological methods maximized the oil removal efficacy across multiple SQT components; 4) “No treat” revealed a similar recovery efficacy to the “Treated,” highlighting natural attenuation, and 5) physical removal by hand wiping plus bioremediation achieved the greatest oil recovery.

In **Chapter 4**, an in situ mesocosm was used to evaluate the natural restoration of a tidal flat for persistent toxic substances in contaminated sediments with the characteristics of bio-irrigation and phytoremediation by macrofauna and

macrophyte. The key findings included 1) a reduction of AhR-mediated potencies and the recovery of benthic communities following lower PTS concentrations and 2) greater PTS concentration reductions in habitat types with macrofauna and macrophytes compared to habitat types without, and 3) bio-irrigation from macrofauna drove the change in benthic community and hydrocarbon degradation by bacterial succession.

In **Chapter 5**, an experiment-free approach was developed by proposing the driving factor contributing the potential toxicity when predicting potencies of a wide range of classes of chemicals acting through a range of mechanisms. The results included 1) simple, accurate models to predict binding of ligands to AhR, 2) identification of "dipole moment-aligned reactions" for ligands with the AhR, 3) development of a directional reactivity factor (DRF) as a prediction indicator and 4) greater accuracy than conventional toxicity prediction models (QSAR and docking model), and 5) the model highlighted a more profound mechanism of chemical toxicity.

In **Chapter 6**, a mechanistic approach to the potential toxicity of 16 PAHs based on the dynamical relationship between ligands and receptor can both predict and evaluate their potential toxicity. The results included 1) quantitatively calculations of the dynamical mechanism between AhR and 16 polycyclic aromatic hydrocarbons (16 PAHs), 2) the directional reactivity binding factor (DRF) as a mechanistic probabilistic prediction indicator linking molecular ligand-receptor binding to in vitro toxicity, 3) deviating from the existing statistical toxicity prediction method, predicting potential toxicity through probabilistic inference and 4) an analytical framework for predicting molecular bioactivity in silico which complements conventional observation-based bioassays.

To summarize the results of the above studies, the restoration capacity and ecotoxicological effects on the Korean coasts were evaluated, for which the data collectively include the introduction of various organic pollutants. First, for the restoration of organic pollutants, the results showed a reduction of organic pollutants as an exponential decay during the experimental periods (14–60 days) (Figure 7.1). When organic pollutants are introduced into coastal sediments, the concentration

becomes higher than the background concentration, but bacterial activity (degradation), bio-irrigation, and phytoextraction proceed rapidly, promoting degradation and dilution of organic pollutants. Although the initial rate of decrease in the concentration of organic pollutants varied according to the type of habitat, in general, the slope of the decrease rate became gentle and then reached the background concentration level after about 14 days. Thereafter, the rate of reduction can be different depending on the change in the environment and the initial concentration of the organic pollutants; however, if no special artificial restoration activity is carried out, it will naturally become similar to the background concentration after 300 days. In particular, a rapid decrease of parent compounds occurred in the early stage, and these substances have a higher DRF value than the metabolites and thus have a high reactivity with the medium (seawater, sediment, and organism), so it seems to have led to degradation.

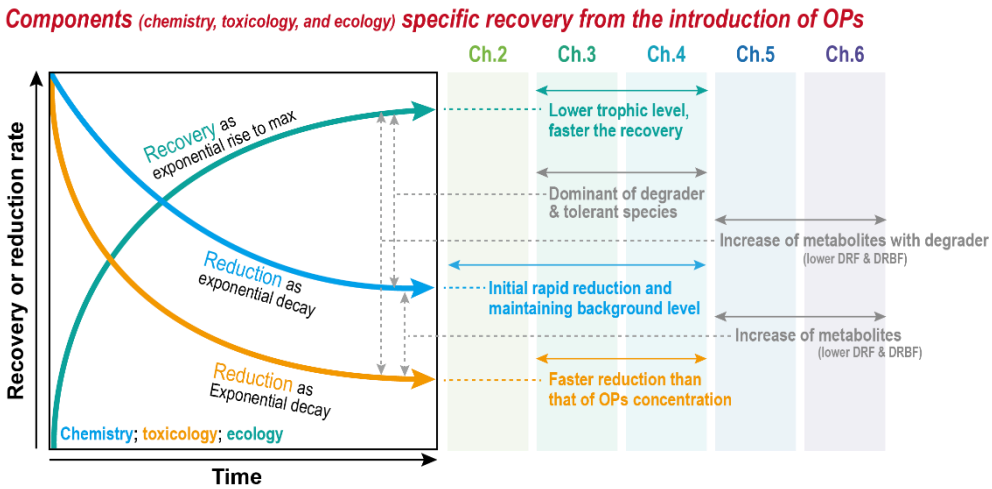

Figure 7.1

Components (chemistry, toxicology, and ecology) specific recovery from the introduction of organic pollutants.

Second, as natural restoration proceeds due to the inflow of organic pollutants into the intertidal zone, the potential toxicity of the sediment also decreases with exponential decay. The reduction of potential toxicity was completed in 200 days (a condition without an artificial remediation activity), and the reduction rate of the latent toxicity was faster than the rate of decrease of the concentration of organic pollutants. The reason for this difference in the reduction rate is that the parent material decreases, and metabolites increase during the restoration process of the sediments in the intertidal zone, so that the total concentration is maintained similarly (Wei et al., 2020). In this dissertation, it was confirmed that the difference in toxicity between the parent material and the metabolites was due to the difference in DRBF (reactivity) because of the unique characteristics (dipole moment and Fukui value) of each organic pollutant. There could be less of a toxic effect if more metabolites with low DRBF levels were made.

Third, as the concentration of the organic pollutants and the potential toxicity in the sediments decreased, the health of the benthic community also recovered as an exponential rise to its max. Among the animal colonies in the book, bacteria increased the fastest, followed by MPB and meiofauna. The increasing bacteria generally had many species that decomposed and utilized the land-driven organic pollutants and organic matter, and the increasing trend decreased around 14 days. Later, the succession of MPB and meiofauna took place, and their population increased. The rapid increase in benthic communities with an initial rapid decline in organic pollutants was the result of the emergence of degraders and tolerant species. The rapid increase in decomposers facilitated the decomposition of parent compounds, which led to an increase in metabolites with low DRBF, leading to an increase in organisms less resistant to pollution

7.2. Environmental implications and Limitations

One of the greatest challenges was to evaluate quantitatively the restoration capacity of organic pollutants and their ecotoxicological effect using the experimental scale design in this study in addition to the in silico approach. As a result, it was confirmed that, despite the contamination by severe organic pollutants, the tidal flat was rapidly restored due to its self-cleaning ability. The potential toxicity of the organic pollutants was reduced by the restoration capacity, and the benthic community structure in the habitat was changed. It was also confirmed that the cause of the dynamic change of the chemical, toxicological, and ecological factors was due to the physico-chemical properties of the organic pollutants (d'Errico et al., 2021). Each organic pollutant has its own characteristics, contributing to the response to the medium and even potential toxicity. Therefore, a molecular focused discussion could be necessary to screen for the effects of the introduction of organic pollutants in a marine environment.

The highlight of this dissertation was integrating chemistry, toxicology, and ecology for interpreting the effects in a marine environment to the introduction of organic pollutants. In this dissertation, the recovery of all of bacteria, meiofauna, and macrofauna were evaluated during the restoration of the contaminated sediment in the tidal flat, and this result provides detailed information for determining the sedimentary quality with a change in the benthic community health. This integrative approach improved the value of the results for the marine environment; however, detailed interactions between the chemicals, sediments, and organisms could not be explained. Thus, it is necessary to investigate other specific interactions and mechanisms that potentially exist in the marine environment. Calculation of the physicochemical properties using DFT analysis demonstrated the benefits of interpreting the more complicated interactions of each component (chemistry, toxicology, and ecology) in the mechanism-based assessment. In addition, this dissertation demonstrated that the DRF of the organic pollutants contributed not only to their reactivity but also predicted the potential toxicity. Overall, the results for this study can provide basic data necessary for coastal management (diagnosis,

evaluation, prediction, management, and application) and reassess the value of marine ecosystems in the future (Figure 7.2).

Nevertheless, this study has some limitations. First, other pollutant specific restorations for various organic pollutants were not considered, such as polychlorinated biphenyls, perfluorinated compounds, etc. To quantitatively estimate the value of the purification service in the intertidal zone, it is useful to select organic pollutants that are included in a management guideline in Korea (Hong et al., 2006). However, this study rarely evaluated the effect of all organic pollutants among the potential hazardous organic pollutants in Korea.

Second, the SQTs performed in this study were based on integrating the average of the recovery rate, which might be limited in reflecting detailed relationships (other pollutants and organisms). In particular, the approach is difficult to defend technically because of the lack of data on biological effects and the relatively subjective choice of various endpoints (Chapman, 2000). And now, the representative value expressing the state of the sediments through SQT is used as the recovery average of each component. Recent studies have presented chemistry, toxicology, and ecology components by comparing their similarities to those of reference sites (Zhang et al., 2020). Because the marine ecosystem includes various environments and each environment has different characteristics, the components should be weighted differently. To confirm the degree of recovery of each marine environment from pollution in detail, it is necessary to identify the characteristics of the medium and organisms and selectively identify factors that can reflect the environment. Third, in silico analyses were used to determine the physicochemical properties of organic pollutants in this dissertation. However, because the results from the in silico analysis were not considered in the real marine environment, more site-specific diagnostic approaches and criteria are required, particularly with respect to identifying and confirming stressors that can be reactive to various media in the marine environment (Gentleman, 2002, Valerio Jr., 2009). This approach requires a large set of simulations that can reflect the marine environment through complicated computer calculations. Future research directions for sediment assessment are suggested in the next section based on the current knowledge and limitations.

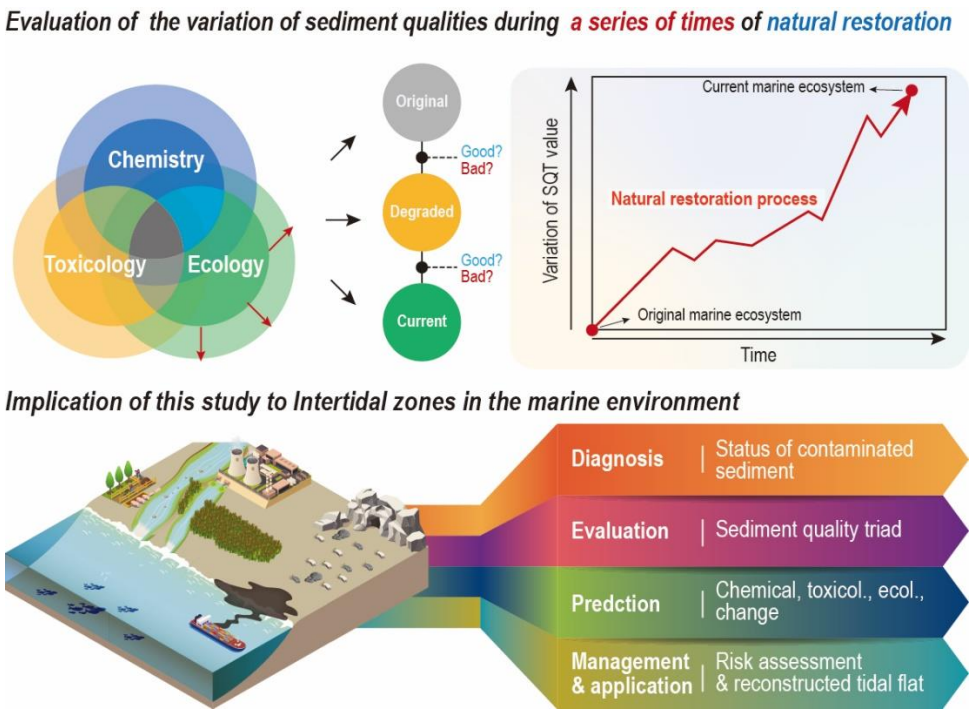

Figure 7.2
Implication of providing basic data from this study necessary for coastal management and rethinking the value of marine ecosystems in the future.

7.3. Future research directions

In this study, the SQT approach and in silico analysis were implemented to evaluate the restoration capacity of organic pollutants and their ecotoxicological effect in the marine environment, including instrumental analysis, bioassay, and analysis of the benthic community. The approach performed well at addressing the interaction between the chemical, toxicological, and ecological factors during the restoration with the contaminated sediments. However, many areas require further research to extend the current approach.

Future studies should establish concentration guidelines for the targeted organic pollutants, such as threshold effect levels and probable effect levels. These guidelines can contribute to the detailed calculation of the quantitative restoration capacity in the marine environment and the assessment of its impact. Consequently, it is important to evaluate concretely the risk of organic pollutants to the benthic community (Yoon et al., 2020). Different organic pollutants interact with each other and with biotic and abiotic factors such as sediments and marine organisms which generally affect these interactions differently in natural habitats (Tornero and Hanke, 2016).

SQGs were derived by concurrently collecting data from the mesocosm study with the measurements of the sediment samples. Because the quality of the sediments depends on various marine environments, future studies should investigate total organic carbon, particle size, and composition of the sediment which can affect the fate of organic pollutants (Hyland et al., 2005). For example, it is important to discriminate the restoration capacity of the interaction between the organic pollutants and the environment from each site. Such information could be used to determine site-specific restoration capacity and identify the responses of chemistry, toxicology, and ecology from the organic pollutants.

Moreover, an in silico study calculating the physicochemical properties of the organic pollutants was used to demonstrate the reason for the difference in recovery based on chemistry, toxicology, and ecology factors in this dissertation. Such information could be used to delineate the recovery of components and identify the

relative importance of each property. This information also suggests that we should take pertinent measures to purify contaminated sediments (Zimmerman et al., 2004). However, because there is a sense of difference between in silico and actual marine environment conditions, it is necessary to develop a new method that can consider the real marine environment. Although it is difficult to predict the effects of organic pollutants on various habitats and living organisms by calculating their properties, it is necessary to focus on marine ecosystem research.

The use of a multidisciplinary approach for the evaluation of the restoration capacity and ecotoxicological effects of organic pollutants is recommended because of its usefulness but still is a challenging practice. To understand the characteristics of organic pollutants and the response of the marine ecosystem due to their introduction, it is necessary to efficiently share the unresolved problems in each discipline (Cunliffe et al., 2013, Castiglioni et al., 2022). Through this approach, a quantitative weight of evidence for the integration of extensive data obtained from various methods should be considered by elaborating on each result. Each result should provide basic and useful data on the fate of organic pollutants for marine environment management based on the interpretation of the restoration and ecotoxicological effect occurring in the marine environment.

BIBLIOGRAPHY

Acir, I.-H., Guenther, K. Endocrine-disrupting metabolites of alkylphenol ethoxylates–a critical review of analytical methods, environmental occurrences, toxicity, and regulation. Sci. Total Environ. 2018, **635**, 1530–1546.

Adams, R. H., Dominguez-Rodriguez, V. I., Zavala-Cruz, J. Vibrio fischeri bioassay for determination of toxicity in petroleum contaminated soils from tropical southeast Mexico. Sains Malays. 2015, **44**, (3), 337–346.

Ahn, C., Mitsch, W.J. Scaling considerations of mesocosm wetlands in simulating large created freshwater marshes. Ecol. Eng. 2002, **18**, 327–342.

Allen D. C and Vaughn, C. C. Burrowing behavior of freshwater mussels in experimentally manipulated communities. J. N. Am. Benthol. Soc. 2009, **28**, 93–100

Alogheli, H., Olanders, G., Schaal, W., Brandt, P., Karlén, A. Docking of macrocycles: comparing rigid and flexible docking in glide. J. Chem. Inf. Model. 2017, **57**, 190–202.

Andersson, J.T., Achten, C. Time to say goodbye to the 16 EPA PAHs? Toward an up-to-date use of PACs for environmental purposes. Polycyclic Aromatic Compounds 2015, **35**, 330–354.

Ankley, G. T., Bennett R. S., Erickson R. J., Hoff D. J., Hornung M. W., Johnson R. D., Mount D. R., Nichols J. W., Russom C. L., Schmieder P. K., Serrrano J. A., Tietge J. E., Villeneuve D. L. Adverse outcome pathways: a conceptual framework to support ecotoxicology research and risk assessment. Environ. Sci. Pollut. Res. Int. 2010, **29**, 730–741.

APHA-AWWA-WPCF. Standard methods for the examination of water and wastewater. 1981, 15th ed., American Public Health Association, Washington, D.C.

Atkins, J.P., Burdon, D., Elliott, M., Gregory, A.J. Management of the marine environment: integrating ecosystem services and societal benefits with the DPSIR framework in a systems approach. Mar. Pollut. Bull. 2011, **62**, 215–226.

Austin, D.C., Lohan, E. Tidal vertical flow wastewater treatment system and method. Google Patents. 2005.

Azubuike, C. C., Chikere, C. B., & Okpokwasili, G. C. Bioremediation techniques–classification based on site of application: principles, advantages, limitations and prospects. World J. Microbiol. Biotechnol. 2016, **32**(11), 1–18.

Bach, Q.-D., Kim, S.-J., Choi, S.-C., Oh, Y.-S. Enhancing the intrinsic

bioremediation of PAH-contaminated anoxic estuarine sediments with biostimulating agents. J. Microbiol., 2005, **43**, (4), 319–324.38.

Bae, H., Ahn, I.-Y., Park, J., Song, S.J., Noh, J., Kim, H., Khim, J.S. Shift in polar benthic community structure in a fast retreating glacial area of Marian Cove, West Antarctica. Sci. Rep. 2021, **11**, 1–10.

Bae, H., Lee, J.-H., Song, S.J., Park, J., Kwon, B.-O., Hong, S., Ryu, J., Choi, K., Khim, J.S. Impacts of environmental and anthropogenic stresses on macrozoobenthic communities in Jinhae Bay, Korea. Chemosphere 2017, **171**, 681–691.

Bae, H., Park, J., Ahn, H., Khim, J. S., Bae, H., Park, J., Ahn, H., Khim, J. S. Shift in benthic diatom community structure and salinity thresholds in a hypersaline environment of solar saltern, Korea. Algae 2020, **35**, (4), 361–373.

Banta, G.T., Holmer, M., Jensen, M.H., Kristensen, E. Effects of two polychaete worms, Nereis diversicolor and Arenicola marina, on aerobic and anaerobic decomposition in a sandy marine sediment. Aquat. Microb. Ecol. 1999, **19**, 189–204.

Basketter, D., Clewell, H., Kimber, I., Rossi, A., Blaauboer, B., Burrier, R., Daneshian, M., Eskes, C., Goldberg, A., Hasiwa, N. Hoffmann, S., Jaworska, J., Knudsen, T. B., Landsiedel, R., Leist, M., Locke, P., Maxwell, G., McKim, J., McVey, E., Ouédraogo, G., Patlewicz, G., Pelkonen, O., Roggen, E., Rovida, C., Ruhdel, I., Schwarz, M., Schepky, A., Schoeters, G., Skinner, N., Trentz, K., Turner, M., Vanparys, P., Yager, J., Zurlo, J., Hartung, T. A roadmap for the development of alternative (non-animal) methods for systemic toxicity testing. 2012.

Benfenati E., A. Manganaro, G. Gini. VEGA-QSAR: AI inside a platform for predictive toxicology. Proceedings of the Workshop PAI, 2013, pp. 21-28

Bernetti, M., Cavalli, A. & Mollica, L. Protein–ligand (un) binding kinetics as a new paradigm for drug discovery at the crossroad between experiments and modelling. MedChemComm 2017, **8**, 534-550.

Billiard, S.M., Timme-Laragy, A.R., Wassenberg, D.M., Cockman, C., Di Giulio, R.T. The role of the aryl hydrocarbon receptor pathway in mediating synergistic developmental toxicity of polycyclic aromatic hydrocarbons to zebrafish. Toxicol. Sci. 2006, **92**, 526–536.

Borja, A., Dauer, D.M. Assessing the environmental quality status in estuarine and coastal systems: comparing methodologies and indices. Ecol. Indic. 2008, **8**, 331-337.

Bourlat, S.J., Borja, A., Gilbert, J., Taylor, M.I., Davies, N., Weisberg, S.B., et al. Genomics in marine monitoring: new opportunities for assessing marine health

status. Mar. Pollut. Bull. 2013, **74** (1), 19–31.

Brils, J. M., Huwer, S. L., Kater, B. J., Schout, P. G., Harmsen, J., Delvigne, G. A., Scholten, M. C. T. Oil effect in freshly spiked marine sediment on *Vibrio fischeri*, *Corophium volutator*, and *Echinocardium cordatum*. Environ. Toxicol. Chem. 2002, **21**(10), 2242–2251.

Bultinck, P., Van Alsenoy, C., Ayers, P. W. & Carbó-Dorca, R. Critical analysis and extension of the Hirshfeld atoms in molecules. J. Chem. Phys. 2007, **126**, 144111.

Byroade, J. D., Twedell, A. M., LeBoff, J. P. Handbook for Oil Spill Protection and Cleanup Priorities. Municipal Environmental Research Laboratory, Office of Research and Development. 1981, **81**.

Cappelli, C. I., Benfenati, E. & Cester, J. Evaluation of QSAR models for predicting the partition coefficient (log P) of chemicals under the REACH regulation. Environ. Res. 2015, **143**, 26–32.

Carpenter, S.R. Microcosm experiments have limited relevance for community and ecosystem ecology. Ecology. 1996, **77**, 677–680.

Carrier, V., Svenning, M.M., Gründger, F., Niemann, H., Dessandier, P.-A., Panieri, G., Kalenitchenko, D. The impact of methane on microbial communities at marine arctic gas hydrate bearing sediment. Front. Microbiol. 2020, **1932**.

Cash, G. Prediction of chemical toxicity to aquatic organisms: ECOSAR vs. Microtox® Assay. Environ. Toxic. Water 1998, **13**, 211–216.

Castiglioni, M., Rivoira, L., Ingrando, I., Meucci, L., Binetti, R., Fungi, M., El-Ghadraoui, A., Bakarim Z., Bubba, M. B., Bruzzoniti, M. C. Biochars intended for water filtration: A comparative study with activated carbons of their physicochemical properties and removal efficiency towards neutral and anionic organic pollutants. Chemosphere. 2022, **288**, 132538.

Cecotti, M., Coppotelli, B.M., Mora, V.C., Viera, M., Morelli, I.S. Efficiency of surfactant-enhanced bioremediation of aged polycyclic aromatic hydrocarbon-contaminated soil: Link with bioavailability and the dynamics of the bacterial community. Sci. Total Environ. 2018, **634**, 224–234.

Cha, J., Hong, S., Gwak, J., Kim, M., Lee, J., Kim, T., Han, G.M., Hong, S.H., Hur, J., Giesy, J.P. Identification of novel polar aryl hydrocarbon receptor agonists accumulated in liver of black-tailed gulls in Korea using advanced effect-directed analysis. J. Hazard. Mater. 2022, **429**, 128305.

Cha, J., Hong, S., Lee, J., Gwak, J., Kim, M., Kim, T., Hur, J., Giesy, J.P., Khim, J.S. Novel polar AhR-active chemicals detected in sediments of an industrial area using effect-directed analysis based on in vitro bioassays with full-scan high resolution mass spectrometric screening. Sci. Total Environ. 2021, **779**, 146566.

Chang, W. K., Ryu J., Yi, Y., Lee W-C., Lee C-W., Kang D., Lee C-H., Hong S., Nam J., Khim J. S. Improved water quality in response to pollution control measures at Masan Bay, Korea. Mar. Pollut. Bull. 2012, **64**, 427–435.

Chapman, P.M. Presentation and interpretation of sediment quality triad data. Ecotoxicology 1996, **5**, 327–339.

Chapman, P.M. The sediment quality triad approach to determining pollutioninduced degradation. Sci. Total Environ. 1990, **97**, 815–825.

Chattaraj, P. K. Chemical reactivity theory: a density functional view. CRC press. 2009

Chen, J., Zhang, W., Wan, Z., Li, S., Huang, T., Fei, Y. Oil spills from global tankers: Status review and future governance. J. Clean. Prod. 2019, **227**, 20–32.

Chen, L., Weng, D., Du, C., Wang, J., Cao, S. Contribution of frustules and mucilage trails to the mobility of diatom Navicula sp. Sci. Rep. 2019, **9**, 1–12.

Chen, Q., Wang X., Tan H., Shi W., Zhang X., Wei S., Giesy J. P., Yu H. Molecular Initiating Events of Bisphenols on Androgen Receptor-Mediated Pathways Provide Guidelines for in Silico Screening and Design of Substitute Compounds. Environ. Sci. Technol. Lett. 2019, **6**, 205–210.

Chen, R., Barko, J. Effects of freshwater macrophytes on sediment chemistry. J. Freshw. Ecol. 1988, **4**, 279–289.

Cicero-Fernández, D., Peña-Fernández, M., Expósito-Camargo, J. A., & Antizar-Ladislao, B. Role of Phragmites australis (common reed) for heavy metals phytoremediation of estuarine sediments. Int. J. Phytoremediation, 2016, **18**(6), 575–582.

Clements, W.H., Cherry, D.S., Cairns Jr, J. Impact of heavy metals on insect communities in streams: a comparison of observational and experimental results. Can. J. Fish. Aquat. Sci. 1988, **45**, 2017–2025.

Cole, J. R., Wang, Q., Fish, J. A., Chai, B., McGarrell, D. M., Sun, Y., Brown, C. T., Porras-Alfaro, A., Kuske, C. R., Tiedje, J. M. Ribosomal Database Project: data and tools for high throughput rRNA analysis. Nucleic Acids Res. 2014, **42**(D1), D633–D642.

Couillard, C. M., Lee, K., Légaré, B., King, T. L. Effect of dispersant on the composition of the water-accommodated fraction of crude oil and its toxicity to larval marine fish. Environ. Toxicol. Chem. 2005, **24**(6), 1496–1504.

Council, N.R. Toxicity testing in the 21st century: a vision and a strategy. National Academies Press, 2007.

Cronin, M.T., Schultz, T.W. Pitfalls in QSAR. J. Mol. Struct. 2003, **622**, 39–51.

Cumming, J. G., Davis, A. M., Muresan, S., Haeberlein, M. & Chen, H. Chemical predictive modelling to improve compound quality. Nat. Rev. Drug Discov. 2013, **12**, 948–962.

Cunliffe, M., Engel, A., Frka, S., Gašparovic, B., Guitart, C., Murrell, J. C., Slater, M., Stolle, C., Upstill-Goddard, R., Wurl, O. Sea surface microlayers: a unified physicochemical and biological perspective of the air–ocean interface. Prog. Oceanogr. 2013, **109**, 104–116.

D'Hondt, A.-S., Stock, W., Blommaert, L., Moens, T., Sabbe, K. Nematodes stimulate biomass accumulation in a multispecies diatom biofilm. Mar. Environ. Res. 2018, **140**, 78–89.

Dai, J., Sun, M-Y., Culp, R. A. A laboratory study on biochemical degradation and microbial utilization of organic matter comprising a marine diatom, land grass, and salt marsh plant in estuarine ecosystems. Aquat. Ecol. 2009, **43**, 825–841.

Das, N., and Chandran, P. Microbial degradation of petroleum hydrocarbon contaminants: an overview. Biotechno. Res. Int. 2011,

Dave, D., Ghaly, A. E. Remediation technologies for marine oil spills: A critical review and comparative analysis. Am. J. Environ. Sci. 2011, **7**(5), 423.

de Lima Ribeiro, F.A., Ferreira, M.M.C. QSAR model of the phototoxicity of polycyclic aromatic hydrocarbons. J. Mol. Struct., 2005, **719**, 191–200.

De Vogelaere, A. P., Foster, M. S. Damage and recovery in intertidal Fucus gardneri assemblages following the Exxon Valdez oil spill. Mar. Ecol. Prog. Ser. 1994, **106**, (3), 263–271.

Deng, Y. & Roux, B. Calculation of standard binding free energies: Aromatic molecules in the T4 lysozyme L99A mutant. J. Chem. Theory Comput. 2006, **2**, 1255–1273.

Dhaka, A., and Chattopadhyay, P. A review on physical remediation techniques for treatment of marine oil spills., J. Environ. Manage. 2021, **288**, 112428.

Di Ventura, B., Lemerle, C., Michalodimitrakis, K., Serrano, L., 2006. From in vivo to in silico biology and back. Nature **443**, 527–533.

Ding, C., He, X. K-means clustering via principal component analysis, Proceedings of the twenty-first international conference on Machine learning, 2004, p. 29.

Doering, J. A., Farmahin R., Wiseman S., Beitel S. C., Kennedy S. W., Giesy J. P., Hecker M. Differences in activation of aryl hydrocarbon receptors of white sturgeon relative to lake sturgeon are predicted by identities of key amino acids in the ligand binding domain. Environ. Sci. Technol. 2015, **49**, 4681–4689.

Donadi, S., Westra, J., Weerman, E.J., van der Heide, T., van der Zee, E.M., van de Koppel, J., Olff, H., Piersma, T., van der Veer, H.W., Eriksson, B.K. Non-trophic

interactions control benthic producers on intertidal flats. Ecosystems 2013, **16**, 1325–1335.

Drira, Z., Kmiha-Megdiche, S., Sahnoun, H., Tedetti, M., Pagano, M., Ayadi, H. Copepod assemblages as a bioindicator of environmental quality in three coastal areas under contrasted anthropogenic inputs (Gulf of Gabes, Tunisia). J. Mar. Biol. Assoc. U. K. 2018, **98**, 1889–1905.

Du, X., Li Y., Xia Y-L., Ai S-M., Liang J., Sang P., Ji X-L., Liu S-Q. Insights into protein–ligand interactions: mechanisms, models, and methods. Int. J. Mol. 2016, **17**, 144.

Duarte, B., Almeida, P., R. and Caçador I. *Spartina maritima* (codrdgrass) rhizosediment extracellular enzymatic activity and its role in organic matter decomposition processes and metal speciation. Mar. Ecol. 2009, **30**, 65–73.

Dubinsky, E. A., Conrad, M. E., Chakraborty, R., Bill, M., Borglin, S. E., Hollibaugh, J. T., Mason, O. U., M. Piceno, Y., Reid, F. C., Stringfellow, W. T. Succession of hydrocarbon-degrading bacteria in the aftermath of the Deepwater Horizon oil spill in the Gulf of Mexico. Environ. Sci. Technol. 2013, **47**(19), 10860–10867.

Edgar, R. C. Search and clustering orders of magnitude faster than BLAST. Bioinformatics 2010, **26**, (19), 2460–2461.

ElNaker, N.A., Elektorowicz, M., Naddeo, V., Hasan, S.W., Yousef, A.F. Assessment of Microbial Community Structure and Function in Serially Passaged Wastewater Electro-Bioreactor Sludge: An Approach to Enhance Sludge Settleability. Sci. Rep. 2018, **8**, 7013.

Eom, H.-J., Kim, H., Kim, B.-M., Chon, T.-S., Choi, J. Integrative assessment of benzene exposure to Caenorhabditis elegans using computational behavior and toxicogenomic analyses. Environ. Sci. Technol. 2014, **48**, 8143–8151.

Eriksson, B.K., Westra, J., van Gerwen, I., Weerman, E., van Der Zee, E., van der Heide, T., van de Koppel, J., Olff, H., Piersma, T., Donadi, S. Facilitation by ecosystem engineers enhances nutrient effects in an intertidal system. Ecosphere 2017, **8**, e02051.

Etkin, D. S. Presented at Arctic and Marine Oilspill Program (AMOP) Technical Seminar June. Analysis of Past Marine Oil Spill Rates and Trends For Future Contingency Planning. 2002.

Etkin, D. S., Welch, J. Development of an oil spill response cost-effectiveness analytical tool. 28th Arctic and Marine Oilspill Program Technical Seminar. Environment Canada: Ottawa ON 2005, 889–922.

Faundez, V. & Hartzell, H. C. Intracellular chloride channels: determinants of function in the endosomal pathway. Sci. Signal. 2004, re8–re8.

Fenchel, T. Worm burrows and oxic microniches in marine sediments. 1. Spatial and temporal scales. Mar. Biol. 1996, **127**, 289–295.

Feng, J., Zeng, Y., Ma, C., Cai, X., Zhang, Q., Tong, M., Yu, Bo, X., P. The surfactant tween 80 enhances biodesulfurization. Appl. Envrion. Microbiol. 2006, **72**(11), 7390–7393.

Ferdowsian, H. R. & Beck, N. Ethical and scientific considerations regarding animal testing and research. PloS One. 2011, **6**, e24059.

Fisher, J., Acreman, M. Wetland nutrient removal: a review of the evidence. HESS 2004, **8**, 673–685.

Floris M., Manganaro A., Nicolotti O., Medda R., Mangiatordi G. F. A generalizable definition of chemical similarity for read-across. J. Cheminfomatics. 2014, **6**, 39.

Fox, R. D. Physical/chemical treatment of organically contaminated soils and sediments. J. Air Waste Manag. Assoc. 1996, **46**, (5), 391–413.

Friedman, R. Ions and the protein surface revisited: extensive molecular dynamics simulations and analysis of protein structures in alkali-chloride solutions. J. Phys. Chem. B. 2011, **115**, 9213–9223.

Fröhlich, E., 2018. Comparison of conventional and advanced in vitro models in the toxicity testing of nanoparticles. Artif. cells Nanomed. Biotechnol. **46**, 1091–1107.

Fronzoni G., Baseggio O., Stener M., Hua W., Tian G., Apicella B., Alfe M., de Simone M., Kivimäki A., Coreno M. Vibrationally resolved high-resolution NEXAFS and XPS spectra of phenanthrene and coronene. J. Chem. Phys. 2014, **141**, 044313.

Fronzoni, G., Baseggio, O., Stener, M., Hua, W., Tian, G., Luo, Y., Apicella, B., Alfé, M., de Simone, M., Kivimäki, A., 2014. Vibrationally resolved high-resolution NEXAFS and XPS spectra of phenanthrene and coronene. J. Chem. Phys. **141**, 044313.

Furukawa, K. Case studies for urban wetlands restoration and management in Japan. Ocean. Coast. Manage. 2013, **81**, 97–102.

Gao, C. H., and Zekri, A. Applications of microbial-enhanced oil recovery technology in the past decade. Energy Sources A: Recovery Util. 2011, **33**(10), 972–989.

Geier M. C., Chlebowski A. C., Truong L., Simonich S. L. M., Anderson K. A., Tanguay R. L. Comparative developmental toxicity of a comprehensive suite of polycyclic aromatic hydrocarbons. Arch. Toxicol. 2018, **92**, 571–586.

Ginsberg, G.L., Pullen Fedinick, K., Solomon, G.M., Elliott, K.C., Vandenberg, J.J., Barone Jr, S., Bucher, J.R. New toxicology tools and the emerging paradigm shift

in environmental health decision-making. Environ. Health Perspect. 2019, **127**, 125002.

Gissi A., Nicolotti O., Carotti A., Gadaleta D., Lombardo A., Benfenati E. Integration of QSAR models for bioconcentration suitable for REACH. Sci. Total. Environ. 2013, **456**, 325–332.

Gramatica, P. & Sangion, A. A historical excursus on the statistical validation parameters for QSAR models: a clarification concerning metrics and terminology. J. Chem. Inf. Model. 2016, **56**, 1127–1131.

Guo, D., Heitman, L. H. & IJzerman, A. P. Kinetic aspects of the interaction between ligand and G protein-coupled receptor: the case of the adenosine receptors. Chem. Rev. 2016, **117**, 38–66.

Häder, D.-P., Banaszak, A.T., Villafañe, V.E., Narvarte, M.A., González, R.A., Helbling, E.W. Anthropogenic pollution of aquatic ecosystems: Emerging problems with global implications. Sci. Total Environ. 2020, **713**, 136586.

Hansen, K., Kristensen, E. The impact of the polychaete Nereis diversicolor and enrichment with macroalgal (Chaetomorpha linum) detritus on benthic metabolism and nutrient dynamics in organic-poor and organic-rich sediment. J. Exp. Mar. Biol. Ecol. 1998, **231**, 201–223.

Harada H., Akagi K., Tutioka T., Hashimoto A. Remediation of coastal sediments by addition of calcium nitrate and presence of benthos in a muddy tidal flat. J. Environ. Prot. 2014, **5**, 703–708.

Hasanudin, U., Fujita, M., Kunihiro, T., Fujie, K., Suzuki, T. The effect of clams (*Tapes philippinarum*) on changes in microbial community structure in tidal flat sediment mesocosms, based on quinone profiles. Ecol. Eng. 2004, **22**, 185–196.

Hayes, M. O., Michel, J., Betenbaugh, D. V. The intermittently exposed, coarse-grained gravel beaches of Prince William Sound, Alaska: comparison with open-ocean gravel beaches. J. Coast. Res. 2010, **26**(1), 4–30.

Helm, C. A., Knoll, W. & Israelachvili, J. N. Measurement of ligand-receptor interactions. 1991.

Hirano M., Hwang J-H., Park H-H., Bak S-M., Iwata H., Kim E-Y. In silico analysis of the interaction of avian aryl hydrocarbon receptors and dioxins to decipher isoform-, ligand-, and species-specific activations. Environ. Sci. Technol. 2015, **49**, 3795–3804.

Hong, S.-K., Koh, C.-H., Harris, R.R., Kim, J.-E., Lee, J.-S., Ihm, B.-S. Land use in Korean tidal wetlands: impacts and management strategies. Environ. Manage. 2010, **45**, 1014–1026.

Hong, S., Khim, J.S., Naile, J.E., Park, J., Kwon, B.-O., Wang, T., Lu, Y., Shim, W.J.,

Jones, P.D., Giesy, J.P. AhR-mediated potency of sediments and soils in estuarine and coastal areas of the Yellow Sea region: a comparison between Korea and China. Environ. Pollut. 2012, **171**, 216–225.

Hong, S., Yoon, S.J., Kim, T., Ryu, J., Kang, S.-G., Khim, J.S. Response to oiled wildlife in the management and evaluation of marine oil spills in South Korea: A review. Reg. Stud. Mar. Sci. 2020, **40**, 101542.

Hong, S.; Khim, J. S.; Ryu, J.; Park, J.; Song, S. J.; Kwon, B.-O.; Choi, K.; Ji, K.; Seo, J.; Lee, S. Two years after the Hebei Spirit oil spill: residual crude-derived hydrocarbons and potential AhR-mediated activities in coastal sediments. Environ. Sci. Technol. 2012, **46**(3), 1406–1414.

Hook, S. E., Osborn, H. L. Comparison of toxicity and transcriptomic profiles in a diatom exposed to oil, dispersants, dispersed oil. Aquat. Toxicol. 2012, **124**, 139–151.

Hope, J.A., Paterson, D.M., Thrush, S.F. The role of microphytobenthos in soft-sediment ecological networks and their contribution to the delivery of multiple ecosystem services. J. Ecol. 2020, **108**, 815–830.

Hou, L., Liu, M., Jiang, H., Xu, S., Ou, D., Liu, Q., Zhang, B. Ammonium adsorption by tidal flat surface sediments from the Yangtze Estuary. J. Environ. Geol. 2003, **45**, 72–78.

Howes, B.L., Dacey, J.W., King, G.M. Carbon flow through oxygen and sulfate reduction pathways in salt marsh sediments 1. Limnol. Oceanogr. 1984, **29**, 1037–1051.

Hsiao, S. I., Kittle, D. W., Foy, M. G., 1978. Effects of crude oils and the oil dispersant Corexit on primary production of arctic marine phytoplankton and seaweed. Environ. Pollut. **15**(3), 209–221.

Hu, J., Jia, G., Mai, B., Zhang, G. Distribution and sources of organic carbon, nitrogen and their isotopes in sediments of the subtropical Pearl River estuary and adjacent shelf, Southern China. Mar. Chem. 2006, **98**, 274–285.

Hwang, K., Lee, J., Kwon, I., Park, S.Y., Yoon, S.J., Lee, J., Kim, B., Kim, T., Kwon, B.-O., Hong, S. Large-scale sediment toxicity assessment over the 15,000 km of coastline in the Yellow and Bohai seas, East Asia. 2021, Sci. Total. Environ. **792**, 148371.

Imfeld, G., Braeckevelt, M., Kuschk, P., Richnow, H.H. Monitoring and assessing processes of organic chemicals removal in constructed wetlands. Chemosphere 2009, **74**, 349–362.

International Tanker Owners Pollution Federation Limited (ITOPF). Effects of oil pollution on the marine environment. 2011.

Jahn, A. E., Robilliard, G. A. Natural recovery: A practical natural resource restoration option following oil spills. International Oil Spill Conference 1997, 665–668.

Johann, S., Nüßer, L., Goßen, M., Hollert, H., Seiler, T. B. Differences in biomarker and behavioral responses to native and chemically dispersed crude and refined fossil oils in zebrafish early life stages. Sci. Total. Environ. 2020, **709**, 136174.

Jones V., Collins M. J., Penkman K. E. H., Jaffe´ R., Wolff G. A. An assessment of the microbial contribution to aquatic dissolved organic nitrogen using amino acid enantiomeric ratios, Org. Geochem. 2005, **36**, 1099–1107.

Jørgensen, B.B. The sulfur cycle of a coastal marine sediment (Limfjorden, Denmark) 1. Limnol. Oceanogr. 1977, **22**, 814–832.

Kadlec, R.H., Reddy, K., 2001. Temperature effects in treatment wetlands. Water Environ Res. **73**, 543–557.

Kahl, J.S., Norton, S.A., Fernandez, I.J., Nadelhoffer, K.J., Driscoll, C.T., Aber, J.D. Experimental inducement of nitrogen saturation at the watershed scale. Environ. Sci. Technol. 1993, **27**, 565–568.

Kalekar, P.S. Time series forecasting using holt-winters exponential smoothing. Kanwal Rekhi school of information Technology 2004, **4329008**, 1–13.

Kemp, W., Lewis, M., Cunningham, J., Stevenson, J., Boynton, W. Microcosms, macrophytes, and hierarchies: environmental research in the Chesapeake Bay. In: Giesy JP (ed) Microcosms in ecological research. National Technical Information Service, Springfield, 1980, pp 911–936

Khim, J.S., Park, J., Song, S.J., Yoon, S.J., Noh, J., Hong, S., Kwon, B.-O., Ryu, J., Zhang, X., Wang, T., Lu, Y., Giesy, J.P. Chemical-, site-, and taxa-dependent benthic community health in coastal areas of the Bohai Sea and northern Yellow Sea: a sediment quality triad approach. Sci. Total Environ. 2018, **645**, 743–752.

Kim J., Hong S., Cha J., Lee J., Kim T., Lee S., Moon H-B., Shin K-H., Hur J., Lee J-S., Giesy J. P., Khim J. S. Newly Identified AhR-Active Compounds in the Sediments of an Industrial Area Using Effect-Directed Analysis. Environ. Sci. Technol. 2019, **53**, 10043–10052.

Kim T-H., Waska H., Kwon E., Suryaputra I. G. A., Kim G. Production, degradation, and flux of dissolved organic matter in the subterranean estuary of a large tidal flat. Mar. Chem. 2012, **142–144**, 1–10.

Kim, H.-G., Song, S.J., Bae, H., Noh, J., Lee, C., Kwon, B.-O., Lee, J.-H., Ryu, J., Khim, J.S. Natural and anthropogenic impacts on long-term meiobenthic communities in two contrasting nearshore habitats. Environ. Int. 2020, **134**, 105200.

Kim, J.-E. Land use management and cultural value of ecosystem services in Southwestern Korean islands. J. Mar. Isl. Cult. 2013, **2**, 49–55.

Kim, J., Hong, S., Cha, J., Lee, J., Kim, T., Lee, S., Moon, H.-B., Shin, K.-H., Hur, J., Lee, J.-S. Newly identified AhR-active compounds in the sediments of an industrial area using effect-directed analysis. 2019, Environ. Sci. Technol. **53**, 10043–10052.

Kim, S.-J., Choi, D. H., Sim, D. S., Oh, Y.-S. Evaluation of bioremediation effectiveness on crude oil-contaminated sand. Chemosphere 2005, **59**(6), 845–852.

Kim, S., Hong, S., Lee, J., Kim, T., Yoon, S.J., Lee, J., Choi, K., Kwon, B.-O., Giesy, J.P., Khim, J.S. Long-term trends of persistent toxic substances and potential toxicities in sediments along the west coast of South Korea. Mar. Pollut. Bull. 2020, **151**, 110821.

Kim, T., Jeon, S., Hong, S., Song, S.J., Kwon, B.-O., Ryu, J., Khim, J.S. Spatiotemporal distributions of butyltin compounds in various intertidal organisms along the Samcheok and Tongyeong coasts of Korea. Chemosphere 2017, **172**, 268–277.

Kim, T., Lee, C., Lee, J., Bae, H., Noh, J., Hong, S., Kwon, B.-O., Kim, J.-J., Yim, U.H., Chang, G.S., Khim, J. S. Best available technique for the recovery of marine benthic communities in a gravel shore after the oil spill: A mesocosm-based sediment triad assessment. J. Hazard. Mater. 2022, **435**, 128945.

Kim, T., Noh, J., Kwon, B.-O., Lee, C., Kim, B., Kwon, I., Hong, S., Chang, G.S., Chang, W.K., Nam, J. Natural purification capacity of tidal flats for organic matters and nutrients: A mesocosm study. Mar. Pollut. Bull. 2020, **154**, 111046.

Kim, T., Zhen, J., Lee, J., Bauer, R., Lee, C., Kwon, B.-O., Chae, K.H., Hong, S., Giesy, J.P., Chang, G.S., Khim, J. S. Influence of ligand's directional configuration, chrysenes as model compounds, on the binding activity with aryl hydrocarbon receptor. Sci. Rep. 2020, **10**, 1–12.

Kimura, K., Ichimura, Y., Sakamaki, T., Nishimura, O., Inamori, Y., Kohata, K., Sudo, R. Analysis of the Effect of Artificial Tidal Flat on Water Purification Capacity. Proc. Coastal. Eng., 2002, **23**–**25**.

Kirchmair J., Göller A. H., Lang D., Kunze J., Testa B., Wilson I. D., Glen R. C., Schneider G. Predicting drug metabolism: experiment and/or computation? ev. Drug Discov. Today 2015, **14**, 387–404.

Kleindienst, S., Seidel, M., Ziervogel, K., Grim, S., Loftis, K., Harrison, S., Malkin, S. Y., Perkins, M. J., Field, J., Sogin, M. L. Chemical dispersants can suppress the activity of natural oil-degrading microorganisms. Proc. Natl. Acad. Sci. 2015, **112**(48), 14900–14905.

Kohonen, T. The self-organizing map. Proceedings of the IEEE 1990, **78**, 1464–1480.

Koo, B.J., Je, J.G., Woo, H.J. Experimental restoration of a salt marsh with some comments on ecological restoration of coastal vegetated ecosystems in Korea. Ocean Sci. J. 2011, **46**, 47.

Kowalska, J.B., Mazurek, R., Gąsiorek, M., Zaleski, T. Pollution indices as useful tools for the comprehensive evaluation of the degree of soil contamination–A review. Environ. Geochem. Health 2018, **40**, 2395–2420.

Krewski D., Jr Acosta D., Adersen M., Anderson H., Bailar III J. C., Boekelheide K., Brent R., Charnley G., Cheung V. G., Jr Green S., Kelsey K. T., Kerkvliet N. I., Li A. A., McCray L., Meyer O., Patterson R. D., Pennie W., Scala R. A., Solomon G. M., Stephens M., Yager J., Zeise L. Toxicity testing in the 21st century: a vision and a strategy. J. Toxicol. Env. Heal. B. 2010, **13**, 51–138.

Kwon, B.-O., Kim, H., Noh, J., Lee, S.Y., Nam, J., Khim, J.S. Spatiotemporal variability in microphytobenthic primary production across bare intertidal flat, saltmarsh, and mangrove forest of Asia and Australia. Mar. Pollut. Bull. 2020, **151**, 110707.

Lea-Smith, D. J., Biller, S. J., Davey, M. P., Cotton, C. A., Sepulveda, B. M. P., Turchyn, A. V., Scanlan, D. J., Smith, A. G., Chisholm, S. W., Howe, C. J. Contribution of cyanobacterial alkane production to the ocean hydrocarbon cycle. Proc. Natl. Acad. Sci. 2015, **112**(44), 13591–13596.

Lear, S. & Cobb, S. L. Pep-Calc. com: a set of web utilities for the calculation of peptide and peptoid properties and automatic mass spectral peak assignment. J. Comput. Aided. Mol. Des. 2016, **30**, 271–277.

Lee J., Hong S., Kwon B-O., Cha S. A., Jeong H-D., Chang W. K., Ryu J., Giesy J. P., Khim J. S. Integrated assessment of persistent toxic substances in sediments from Masan Bay, South Korea: Comparison between 1998 and 2014. Environ. Pollut. 2018, **238**, 317–325.

Lee S., Shin W-H., Hong S., Kang H., Jung D., Yim U. H., Shim W. J., Khim J. S., Seok C., Giesy J. P., Choi K. Measured and predicted affinities of binding and relative potencies to activate the AhR of PAHs and their alkylated analogues. Chemosphere 2015, **139**, 23–29.

Lee, C. W., Lee S. J., Jeon H. P. and Chang W. K. Local governance for ecosystem recovery of an urban tidal flat in Masan Bay, Korea. J. Int. Marit. Saf. Environ. Aff. Shipp. 2019, **3**, 1–2.

Lee, C., Hong, S., Noh, J., Lee, J., Yoon, S. J., Kim, T., Kim, H., Kwon, B.-O., Lee, H., Ha, S. Y. Comparative evaluation of bioremediation techniques on oil contaminated sediments in long-term recovery of benthic community health. Environ. Pollut. 2019a, **252**, 137–145.

Lee, C., Kwon, B.-O., Hong, S., Noh, J., Lee, J., Ryu, J., Kang, S.-G., Khim, J. S., Sub-lethal and lethal toxicities of elevated CO2 on embryonic, juvenile, and adult stages of marine medaka Oryzias melastigma. Environ. Pollut. 2018, **241**, 586–595.

Lee, J.-S.; Hong, S.; Lee, J.; Choi, T. S.; Rhie, K.; Khim, J. S. Evaluation of residual toxicity of hypochlorite-treated water using bioluminescent microbes and microalgae: Implications for ballast water management. Ecotoxicol. Environ. Saf. 2019, **167**, 130–137.

Lee, J. Kim, T. Yoon, S. J., Kim, S., Lee, A. H., Kwon, B.-O., Allam, A. A., Al-Khedhairy, A. A., Lee, H., Kim, J.-J. Multiple evaluation of the potential toxic effects of sediments and biota collected from an oil-polluted area around Abu Ali Island, Saudi Arabia, Arabian Gulf. Ecotoxicol. Environ. Saf. **183**, 2019, 109547.

Lee, J., Cheng, X., Swails, J.M., Yeom, M.S., Eastman, P.K., Lemkul, J.A., Wei, S., Buckner, J., Jeong, J.C., Qi, Y. CHARMM-GUI input generator for NAMD, GROMACS, AMBER, OpenMM, and CHARMM/OpenMM simulations using the CHARMM36 additive force field. J. Chem. Theory Comput. 2016, **12**, 405–413.

Lee, J., Hong, S., Kim, T., Lee, C., An, S.-A., Kwon, B.-O., Lee, S., Moon, H.-B., Giesy, J.P., Khim, J.S. Multiple bioassays and targeted and nontargeted analyses to characterize potential toxicological effects associated with sediments of masan bay: Focusing on AhR-mediated potency. Environ. Sci. Technol. 2020, **54**, 4443–4454.

Lee, J., Hong, S., Kim, T., Park, S.Y., Cha, J., Kim, Y., Gwak, J., Lee, S., Moon, H.-B., Hu, W., Wang, T., Giesy, J. P., Khim, J. S. Identification of AhR agonists in sediments of the Bohai and Yellow Seas using advanced effect-directed analysis and in silico prediction. J. Hazard. Mater. 2022, **435**, 128908.

Lee, J., Hong, S., Kwon, B.-O., Cha, S. A., Jeong, H.-D., Chang, W. K., Ryu, J., Giesy, J. P., Khim, J. S. Integrated assessment of persistent toxic substances in sediments from Masan Bay, South Korea: comparison between 1998 and 2014. Environ. Pollut. 2018b, **238**, 317–325.

Lee, J., Hong, S., Yoon, S.J., Kwon, B.-O., Ryu, J., Giesy, J.P., Allam, A.A., Al-Khedhairy, A.A., Khim, J.S. Long-term changes in distributions of dioxin-like and estrogenic compounds in sediments of Lake Sihwa, Korea: Revisited mass balance. Chemosphere 2017, **181**, 767–777.

Lee, J., Khim, J.S. Revisited a sediment quality triad approach in the Korean coastal waters: past research, current status, and future directions. Environ. Pollut. 2022, **29**, 118262.

Lee, J., Kim, T., Yoon, S.J., Kim, S., Lee, A.H., Kwon, B.-O., Allam, A.A., Al-

Khedhairy, A.A., Lee, H., Kim, J.-J. Multiple evaluation of the potential toxic effects of sediments and biota collected from an oil-polluted area around Abu Ali Island, Saudi Arabia, Arabian Gulf. Ecotoxicol. Environ. 2019, **183**, 109547.

Lee, J., Kwon, B.-O., Kim, B., Noh, J., Hwang, K., Ryu, J., Park, J., Hong, S., Khim, J.S. Natural and anthropogenic signatures on sedimentary organic matters across varying intertidal habitats in the Korean waters. Environ. Int. 2019, **133**, 105166.

Lee, J., Lim, J.-H., Park, J., Youn, S.-H., Oh, H.-J., Kim, J.-H., Kim, M.K., Cho, H., Yoon, J.-E., Kim, S. First Investigation of Microbial Community Composition in the Bridge (Gadeok Channel) between the Jinhae-Masan Bay and the South Sea of Korea. Ocean Sci. J. 2018, **53**, 251–260.

Lee, J., Tikhonov, D., Chopra, P., Maclot, S., Steber, A., Gruet, S., Allum, F., Boll, R., Cheng, X., Düsterer, S. Time-resolved relaxation and fragmentation of polycyclic aromatic hydrocarbons investigated in the ultrafast XUV-IR regime. Nat. Commun. 2021, **12**, 1–11.

Lee, J.G., Nishijima, W., Mukai, T., Takimoto, K., Seiki, T., Hiraoka, K., Okada, M. Factors to determine the functions and structures in natural and constructed tidal flats. Water Res. 1998, **32**, 2601–2606.

Lee, Y., Ryu, J., Hong, S., Khim, J.S. Temporal Trends of Persistent Toxic Substances and Benthic Community Responses in Special Management Areas of Korea: The Masan Bay and Lake Sihwa Cases, Persistent Organic Chemicals in the Environment: Status and Trends in the Pacific Basin Countries II Temporal Trends. ACS Publications, pp. 2016, 103–126.

Legler J., Zeinstra L. M., Schuitemaker F., Lanser P. H., Boderd J., Brouwer A., Vethaak A. D., de Voogt P., Murk A. J., Van der Burg B. Comparison of in vivo and in vitro reporter gene assays for short-term screening of estrogenic activity. Zeinstra L. M., Schuitemaker F., Lanser P. H., Bogerd J., Brouwer A., Vethaak A. D., de Voogt P., Murk A. J., Van der Burg B., 2002. Environ. Sci. Technol. **36**, 4410–4415.

Levin, L.A., Boesch, D.F., Covich, A., Dahm, C., ErsÚus, C., Ewel, K.C., Kneib, R.T., Moldenke, A., Palmer, M.A., Snelgrove, P. The function of marine critical transition zones and the importance of sediment biodiversity. Ecosyst. 2001, **4**, 430–451.

Li, P., Cai, Q., Lin, W., Chen, B., Zhang, B. Offshore oil spill response practices and emerging challenges. Mar. Pollut. Bull. 2016, **110**(1), 6–27.

Lima Ribeiro, F. A. & Ferreira, M. M. C. QSAR model of the phototoxicity of polycyclic aromatic hydrocarbons. J. Mol. Struc-THEOCHEM 2005, **719**, 191–200.

Lohrer, A., Halliday, N., Thrush, S., Hewitt, J., Rodil, I. Ecosystem functioning in a

disturbance-recovery context: contribution of macrofauna to primary production and nutrient release on intertidal sandflats. J. Exp. Mar. Biol. Ecol. 2010, **390**, 6–13.

Lönning, S., Hagström, B. E. Deleterious effects of Corexit 9527 on fertilization and development. Mar. Pollut. Bull. 1976, **7**(7), 124–127.

Louiz I., Kinani S., Gouze M-E., Ben-Attia M., Menif D., Bouchonnet S., Porcher J. M., Ben-Hassine O. K., Aït-Aïssa S. Monitoring of dioxin-like, estrogenic and anti-androgenic activities in sediments of the Bizerta lagoon (Tunisia) by means of in vitro cell-based bioassays: contribution of low concentrations of polynuclear aromatic hydrocarbons (PAHs). Sci. Total. Environ. 2008, **402**, 318–329.

Love, C. R., Arrington, E. C., Gosselin, K. M., Reddy, C. M., Van Mooy, B. A., Nelson, R. K., Valentine, D. L. Microbial production and consumption of hydrocarbons in the global ocean. Nat. Microbiol. 2021, **6**(4), 489–498.

Martínez-Gómez, C., Vethaak, A.D., Hylland, K., Burgeot, T., Köhler, A., Lyons, B.P., Thain, J., Gubbins, M.J., Davies, I.M. A guide to toxicity assessment and monitoring effects at lower levels of biological organization following marine oil spills in european waters. ICES J. Mar. Sci. 2010, **67**(6), 1105–1118.

McQuoid, M.R., Nordberg, K. The diatom Paralia sulcata as an environmental indicator species in coastal sediments. Estuar. Coast. Shelf Sci. 2003, **56**, 339–354.

Mearns, A. J. Recovery of shoreline ecosystems following the Exxon Valdez oil spill and subsequent treatment. Coastal Zone'93, ASCE. 1993, 466–479.

Meuleman, A.F., Van Logtestijn, R., Rijs, G.B., Verhoeven, J.T. Water and mass budgets of a vertical-flow constructed wetland used for wastewater treatment. Ecol. Eng. 2003, **20**, 31–44.

Michel, J. J. M., Byron, L. Shoreline assessment manual, Natioanl Oceanic and Atmospheric Administration (NOAA), **2013**. US Dept. of Commerce 62.

Milner, M. J., & Kochian, L. V. Investigating heavy-metal hyperaccumulation using Thlaspi caerulescens as a model system. Ann. Bot. 2008, **102**(1), 3–13.

MMAF (Ministry of Marine Affairs and Fisheries), Establishment of action plans for coastal environmental management areas. Seoul, Korea, 2002, 658 pp

Mobley, D. L., Graves A. P., Chodera J. D., McReynolds A. C., Shoichet B. K., Dill K. A. Predicting absolute ligand binding free energies to a simple model site. J. Mol. Biol. 2007, **371**, 1118–1134.

Mohr, S., Feibicke, M., Ottenströer, T., Meinecke, S., Berghahn, R., Schmidt, R. Enhanced Experimental Flexibility and Control in Ecotoxicological Mesocosm Experiments: A new outdoor and indoor pond and stream system. Environ. Sci.

Pollut. Res. 2005, **12**(1), 5–7.

Mondal, J., Ahalawat, N., Pandit, S., Kay, L.E., Vallurupalli, P., 2018. Atomic resolution mechanism of ligand binding to a solvent inaccessible cavity in T4 lysozyme. PLoS Comput. Biol. **14**, e1006180.

Montgomery, M., T., Osburn, C.L., Furukawa, Y., Gieskes, J.M. Increased capacity for polycyclic aromatic hydrocarbon mineralization in bioirrigated coastal marine sediments. Bioremediation J. 2008, **12**, 98–110.

Moore, J., Impacts of oil spills on shorelines. Good practice guidelines for incident management and emergency response personnel. IPIECA, 2016.

Moreira, I.S., Fernandes, P.A., Ramos, M.J., 2010. Protein–protein docking dealing with the unknown. J. Comput. Chem. **31**, 317–342.

Naidoo, G., Naidoo, K. Uptake of polycyclic aromatic hydrocarbons and their cellular effects in the mangrove *Bruguiera gymnorrhiza*. Mar. Pollut. Bull. 2016, **113**, 193–199.

Neese, F. The ORCA program system. Wiley Interdiscip. Rev. Comput. Mol. Sci. 2012, **2**, 73–78.

Nichols, D.S. Capacity of natural wetlands to remove nutrients from wastewater. Journal (Water Pollution Control Federation), 1983, 495–505.

Nikolopoulou, M., Pasadakis, N., & Kalogerakis, N. Enhanced bioremediation of crude oil utilizing lipophilic fertilizers. Desalination. 2007, **211**(1–3), 286–295.

Nixon, Z., Michel, J. A Review of distribution and quantity of lingering subsurface oil from the Exxon Valdez Oil Spill. Deep Sea Res. Part II: Top. Stud. Oceanogr. 2018, **147**, 20–26.

Odum, E.P. The mesocosm. BioScience 1984, **34**, 558–562.

Ohyama, K., Nagai, F., Tsuchiya, Y. Certain styrene oligomers have proliferative activity on MCF-7 human breast tumor cells and binding affinity for human estrogen receptor. Environ. Health Perspect. 2001, **109**, 699–703.

Okada, T., Mito, Y., Tokunaga, K., Sugino, H., Kubo, T., Akiyama, Y.B., Endo, T., Otani, S., Yamochi, S., Kozuki, Y. A comparative method for evaluating ecosystem services from the viewpoint of public works. Ocean Coast. Manag. 2021, **212**, 105848.

Paine, R. T., Ruesink, J. L., Sun, A., Soulanille, E. L., Wonham, M. J., Harley, C. D., Brumbaugh, D. R., Secord, D. L. Trouble on oiled waters: lessons from the Exxon Valdez oil spill. Annu. Rev. Ecol. Evol. Syst., 1996, **27**(1), 197–235.

Park, M., Lee, Y., Park, J., Kim, S., Kim, S., Lee, S. Changes in Water Quality in Masan Bay after the Introduction of the Total Pollution Load Management

System. J. Korean Soc. Mar. Environ. Energy 2018, **21**, 139–148.

Parr, R. G. & Yang, W. Density-functional theory of the electronic structure of molecules. Annu. Rev. Phys. Chem. 1995, **46**, 701–728.

Park, S., Lee, J., Hong, S., Kim, T., Yoon, S., Lee, C., Kwon, B.-O., Hu, W., Wang, T., Khim, J. Evaluation of ecotoxicological effects associated with coastal sediments of the Yellow Sea large marine ecosystem using the marine copepod *Tigriopus japonicus*. Mar. Pollut. Bull. 2022, **181**, 113937.

Patrick, R., Palavage, D. M. The value of species as indicators of water quality. Proc. Acad. Nat. Sci. Phila. 1994, 55–92.

Pearce, J.L., Waller, L.A., Chang, H.H., Klein, M., Mulholland, J.A., Sarnat, J.A., Sarnat, S.E., Strickland, M.J., Tolbert, P.E. Using self-organizing maps to develop ambient air quality classifications: a time series example. J. Environ. Health 2014, **13**, 1–14.

Perkins, R., Underwood, G., Brotas, V., Snow, G., Jesus, B., Ribeiro, L. Responses of microphytobenthos to light: primary production and carbohydrate allocation over an emersion period. Mar. Ecol. Prog. Ser. 2001, **223**, 101–112.

Petukh, M., Stefl, S. & Alexov, E. The role of protonation states in ligand-receptor recognition and binding. Curr. Pham. Des. 2013, **19**, 4182–4190.

Pezeshki, S., Hester, M., Lin, Q., Nyman, J. The effects of oil spill and clean-up on dominant US Gulf coast marsh macrophytes: a review. Environ. Pollut. 2000, **108**(2), 129–139.

Preparedness of Oil-polluted Shoreline cleanup and Oiled Wildlife interventions (POSOW). Oiled Shoreline Cleanup Manual. Centre of Documentation, Research and Experimentation on Accidental Water Pollution. 2013.

Procópio, L. Changes in microbial community in the presence of oil and chemical dispersant and their effects on the corrosion of API 5L steel coupons in a marine-simulated microcosm. Appl. Microbiol. Biotechnol. 2020, **104**, 6397–6411.

Rahsepar, S., Smit, M. P., Murk, A. J., Rijnaarts, H. H., Langenhoff, A. A. Chemical dispersants: oil biodegradation friend or foe? Mar. Pollut. Bull. 2016, **108**(1–2), 113–119.

Reed, M., Aamo, O. M., Daling, P. S. Quantitative analysis of alternate oil spill response strategies using OSCAR. Spill Sci. Technol. 1995, **2**(1), 67–74.

Reise, K. Sediment mediated species interactions in coastal waters. J. Sea Res. 2002, **48**, 127–141.

Romero, J.A., Brix, H., Comín, F.A. Interactive effects of N and P on growth, nutrient allocation and NH4 uptake kinetics by *Phragmites australis*. Aquatic. Bot. 1999, **64**, 369–380.

Rothhammer, V. & Quintana, F. J. The aryl hydrocarbon receptor: an environmental sensor integrating immune responses in health and disease. Nat. Rev. Immunol. 2019, **19**, 184–197.

Rothhammer, V., Quintana, F.J., 2019. The aryl hydrocarbon receptor: an environmental sensor integrating immune responses in health and disease. Nat Rev Immunol. **19**, 184–197.

Roy, K., Kar, S., Das, R.N., 2015. Statistical methods in QSAR/QSPR, A primer on QSAR/QSPR modeling. Springer, pp. 37–59.

Ryu, J., Khim J. S., Choi J-W., Shin H. C. An S., Park j., Kang D., Lee C-H., Koh C-H. Environmentally associated spatial changes of a macrozoobenthic community in the Saemangeum tidal flat, Korea. J. Sea. Res. 2011, 390–400.

Sachaniya, B. K., Gosai, H. B., Panseriya, H. Z., Vala, A. K., & Dave, B. P. Polycyclic aromatic hydrocarbons (PAHs): Occurrence and bioremediation in the marine environment. Marine pollution: Current status, impacts and remedies, 2019, **1**, 435–466.

Sahai, M.A., Biggin, P.C. Quantifying water-mediated protein–ligand interactions in a glutamate receptor: A dft study. J. Phys. Chem. B 2011, **115**, 7085–7096.

Sakshaug, E., Bricaud, A., Dandonneau, Y., Falkowski, P. G., Kiefer, D. A., Legendre, L., Morel, A., Parslow, J., Takahashi, M. Parameters of photosynthesis: definitions, theory and interpretation of results. J. Plankton. Res. 1997, **19**(11), 1637–1670.

Sandwell, D.R., Pilditch, C.A., Lohrer, A.M. Density dependent effects of an infaunal suspension-feeding bivalve (Austrovenus stutchburyi) on sandflat nutrient fluxes and microphytobenthic productivity. J. Exp. Mar. Biol. Ecol. 2009, **373**, 16–25.

Saros, J., Anderson, N. The ecology of the planktonic diatom Cyclotella and its implications for global environmental change studies. Biol. 2015, **90**, 522–541.

Schindler, D.W. Whole-ecosystem experiments: replication versus realism: the need for ecosystem-scale experiments. Ecosystems 1998, **1**, 323–334.

Shi, B., Wang, T., Yang, H., Zhou, Y., Bi, R., Yang, L., Yoon, S.J., Kim, T., Khim, J.S., 2021. Perfluoroalkyl acids in rapidly developing coastal areas of China and South Korea: Spatiotemporal variation and source apportionment. Sci. Total Environ. **761**, 143297.

Shin, W.-H. & Seok, C. GalaxyDock: protein–ligand docking with flexible protein side-chains. J. Chem. Inf. Model. 2012, **52**, 3225–3232.

Shin, W.-H., Lee, G. R., Heo, L., Lee, H. & Seok, C. Prediction of protein structure and interaction by GALAXY protein modeling programs. Bio. Design. 2014, **2**,

1–11.

Shrestha, P., Bellitürk, K., Görres, J.H. Phytoremediation of heavy metal-contaminated soil by switchgrass: a comparative study utilizing different composts and coir fiber on pollution remediation, plant productivity, and nutrient leaching. Int. J. Environ. Res. Public Health 2019, **16**, 1261.

Siva, J. L. Ecological impacts of oil spill cleanup: Are they significant? International Oil Spill Conference. American Petroleum Institute. 1979, 521–524.

Speirs, L., Rice, D.T., Petrovski, S., Seviour, R.J. The phylogeny, biodiversity, and ecology of the Chloroflexi in activated sludge. Front. Microbiol. 2019, **10**, 2015.

Street, L. Containment and Recovery Field Guide A guide to containment and recovery operations at sea. 2011.

Suzumura, M., Ingall, E.D. Distribution and dynamics of various forms of phosphorus in seawater: insights from field observations in the Pacific Ocean and a laboratory experiment. Deep Sea Research Part I: Oceanogr. Res. Pap. 2004, **51**, 1113–1130.

Swanberg, I.L. The influence of the filter-feeding bivalve Cerastoderma edule L. on microphytobenthos: a laboratory study. J. Exp. Mar. Biol. Ecol. 1991, **151**, 93–111.

Tagliabue, S. G., Faber, S. C., Motta, S., Denison, M. S. & Bonati, L. Modeling the binding of diverse ligands within the Ah receptor ligand binding domain. Sci. Rep. 2019, **9**, 1–14.

Tan, B., Dong, X., Sensen, C.W., Foght, J. Metagenomic analysis of an anaerobic alkane-degrading microbial culture: potential hydrocarbon-activating pathways and inferred roles of community members. Genome 2013, **56**, 599–611.

Thamdrup, B., Fossing, H., Jørgensen, B.B. Manganese, iron and sulfur cycling in a coastal marine sediment, Aarhus Bay, Denmark. Geochim. Cosmochim. Acta 1994, **58**, 5115–5129.

Thrush, S.F., Hewitt, J.E., Gibbs, M., Lundquist, C., Norkko, A. Functional role of large organisms in intertidal communities: community effects and ecosystem function. Ecosystems 2006, **9**, 1029–1040.

Tolhurst, T.J., Chapman, M., Murphy, R. The effect of shading and nutrient addition on the microphytobenthos, macrofauna, and biogeochemical properties of intertidal flat sediments. Front. Mar. Sci. 2020, **7**, 419.

Tremblay, J., Yergeau, E., Fortin, N., Cobanli, S., Elias, M., King, T. L., Lee, K., Greer, C. W. Chemical dispersants enhance the activity of oil-and gas condensate-degrading marine bacteria. Microb. Ecol. 2017, **11** (12), 2793–2808.

Tuler, S., Seager, T. P., Kay, R., Linkov, I.; Figueira, J. R. Defining and selecting

objectives and performance metrics for oil spill response assessment: A process design integrating analysis and deliberation. Durham, NH: Coastal Response Research Centre. 2007.

Turner, R.E., Swenson, E.M., Milan, C.S., OSWALD, T.A. Below-ground biomass in healthy and impaired salt marshes. Ecol. Res. 2004, **19**, 29–35.

United States Environmental Protection Agency Office of Emergency (EPA) Understanding oil spills and oil spill response. 1993, Vol. **9200**.

Uribe-Flores, M. M., Cerqueda-García, D., Hernández-Nuñez, E., Cadena, S., García-Cruz, N. U., Trejo-Hernández, M. R., Aguirre-Macedo, M. L., García-Maldonado, J. Q. Bacterial succession and co-occurrence patterns of an enriched marine microbial community during light crude oil degradation in a batch reactor. J. Appl. Microbiol. 2019, **127**(2), 495–507.

Valentine, D. L., Reddy, C. M. Latent hydrocarbons from cyanobacteria. Proc.Natl. Acad. Sci. 2015, **112**(44), 13434–13435.

Venosa, A. D., Zhu, X., Suidan, M., T., Lee K. Guidelines for the bioremediation of oil-contaminated salt marshes. United States Environmental Protection Agency (EPA), EPA/600/R-04-074. 2004.

Volkenborn, N., Woodin, S., Wethey, D., Polerecky, L. Bioirrigation in marine sediments. S.A. Elias (Ed.), Reference Module in Earth Systems and Environmental Sciences, Elsevier. 2016.

Walther III, H. R. Clean up techniques used for coastal oil spills: an analysis of spills occurring in Santa Barbara, California, Prince William Sound, Alaska, the Sea of Japan, and the Gulf Coast. Master's Projects and Capstones. 2014, **104**.

Wang, F., Dong, W., Wang, H., Zhao, Y., Zhao, Z., Huang, J., Zhou, T., Wu, Z., Li, W. Enhanced bioremediation of sediment contaminated with polycyclic aromatic hydrocarbons by combined stimulation with sodium acetate/phthalic acid. Chemosphere 2022, **291**, 132770.

Wang, X, Li X., Shi W., Wei S., Giesy J. P., Yu H., Wang Y. Docking and CoMSIA studies on steroids and non-steroidal chemicals as androgen receptor ligands. Ecotox. Environ. Safe. 2013, **89**, 143–149.

Wang, Z.; Fingas, M.; Li, K. Fractionation of a light crude oil and identification and quantitation of aliphatic, aromatic, and biomarker compounds by GC-FID and GC-MS, part II. J. Chromatogr. Sci. 1994, **32**(9), 367–382.

Wardrop, J. Chemical Dispersant Use in Oil Spill Management: Kill or Cure? The Controversy Persists. SPE Asia-Pacific Conference. 1991.

Waterhouse A., Bertoni M., Bienery S., Studer G., Tauriello G., Gumienny R., Heer F. T., de Beer T. A. P., Rempfer C., Bordoli L., Lepore R., Schwede T. SWISS-

MODEL: homology modelling of protein structures and complexes. Nucleic. Acids. Res. 2018, **46**, W296-W303.

Waterhouse, A., Bertoni, M., Bienert, S., Studer, G., Tauriello, G., Gumienny, R., Heer, F.T., de Beer, T.A.P., Rempfer, C., Bordoli, L., 2018. SWISS-MODEL: homology modelling of protein structures and complexes. Nucleic Acids Res. Spec. **46**, W296–W303.

Wathugala, A. G., Suzuki T. and Kurihara Y. Removal of nitrogen, phosphorus and COD from waste water using sand filtration system with *Phragmites australis*. Wat. Res. 1987, **21**, 1217–1224.

Wiederstein, M. & Sippl, M. J. ProSA-web: interactive web service for the recognition of errors in three-dimensional structures of proteins. Nucleic Acids Res. 2007, **35**, W407–W410.

Winberg, P.C., Lynch, T.P., Murray, A., Jones, A.R., Davis, A.R The importance of spatial scale for the conservation of tidal flat macrobenthos: an example from New South Wales, Australia. Biol. Conserv. 2007, **134**, 310–320.

Xing, Y., Nukaya, M., Satyshur, K.A., Jiang, L., Stanevich, V., Korkmaz, E.N., Burdette, L., Kennedy, G.D., Cui, Q., Bradfield, C.A., 2012. Identification of the Ah-receptor structural determinants for ligand preferences. ToxSci **129**, 86–97.

Yagi, A., Terai, H., 2001. Primary production and water purification in the Fujimae Tidal Flat. Verh. - Int. Ver. Theor. Angew. Limnol. **27**, 3394–3403.

Yamochi, S. Succession of macrobenthic fauna and nitrogen budget at two artificial tidal flats in Osaka Bay, Japan. Mar. Pollut. Bull. 2008, **57**, 137–141.

Yang, W., Liu X., Liu H., Wu Y., Giesy J. P., Yu H. Molecular docking and comparative molecular similarity indices analysis of estrogenicity of polybrominated diphenyl ethers and their analogues. Ecotox. Environ. Toxicol Chem. 2010, **29**, 660–668.

Yim, U. H., Ha, S. Y., An, J. G., Won, J. H., Han, G. M., Hong, S. H., Kim, M., Jung, J.-H., Shim, W. J. Fingerprint and weathering characteristics of stranded oils after the Hebei Spirit oil spill. J. Hazard. Mater. 2011, **197**, 60–69.

Yim, U. H., Hong, S., Lee, C., Kim, M., Jung, J.-H., Ha, S. Y., An, J. G., Kwon, B.-O., Kim, T., Lee, C.-H. Rapid recovery of coastal environment and ecosystem to the Hebei Spirit oil spill's impact. Environ. Int. 2020, **136**, 105438.

Yim, U. H., Kim, M., Ha, S. Y., Kim, S., Shim, W. J. Oil spill environmental forensics: the Hebei Spirit oil spill case. Environ. Sci. Tech. 2012, **46** (12), 6431–6437.

Yim, U. H.; Hong, S. H.; Shim, W.; Oh, J.; Chang, M. Spatio-temporal distribution and characteristics of PAHs in sediments from Masan Bay, Korea. Mar. Pollut. Bull. 2005, **50** (3) 319–326.

Yim, U.H., Hong, S., Lee, C., Kim, M., Jung, J.-H., Ha, S.Y., An, J.G., Kwon, B.-O., Kim, T., Lee, C.-H. Rapid recovery of coastal environment and ecosystem to the Hebei Spirit oil spill's impact. Environ. Int. 2020, **136**, 105438.

Yim, U.H., Khim, J.S., Kim, M., Jung, J.-H., Shim, W.J. Environmental impacts and recovery after the Hebei Spirit Oil Spill in Korea. Arch. Environ. Contam. Toxicol. 2017, **73**, 47–54.

Yoon, S.J., Hong, S., Kim, H.-G., Lee, J., Kim, T., Kwon, B.-O., Kim, J., Ryu, J., Khim, J.S. Macrozoobenthic community responses to sedimentary contaminations by anthropogenic toxic substances in the Geum River Estuary, South Korea. Sci. Total Environ. 2021, **763**, 142938.

Yoon, S.J., Hong, S., Kim, S., Lee, J., Kim, T., Kim, B., Kwon, B.-O., Zhou, Y., Shi, B., Liu, P., Hu, W., Huwang, B., Wang, T., Khim, J. S. Large-scale monitoring and ecological risk assessment of persistent toxic substances in riverine, estuarine, and coastal sediments of the Yellow and Bohai seas. Environ. Int. 2020, **137**, 105517.

Yoon, S.J., Hong, S., Kim, T., Lee, J., Kwon, B.-O., Allam, A.A., Al-Khedhairy, A.A., Khim, J.S. Occurrence and bioaccumulation of persistent toxic substances in sediments and biota from intertidal zone of Abu Ali Island, Arabian Gulf. Mar. Pollut. Bull. 2019, **144**, 243–252.

Yoon, S.J., Hong, S., Lee, C., Lee, J., Kim, T., Lee, J., Kim, B., Noh, J., Kwon, B.-O., Khim, J.S. 10 years long-term assessment on characterizing spatiotemporal trend and source apportionment of metal (loid) s in terrestrial soils along the west coast of South Korea. Sci. Total Environ. 2022, **826**, 154214.

You, S.-J., Kim, J.-G. Evaluation on the purification capacity of pollutants in the tidal flat. Korean J. Fish. Aquat. Sci. 1999, **32**, 409–415.

Zengel, S., Bernik, B. M., Rutherford, N., Nixon, Z., Michel, J. Heavily oiled salt marsh following the Deepwater Horizon oil spill, ecological comparisons of shoreline cleanup treatments and recovery. Plos one 2015, **10**(7), e0132324.

Zhang S., Yao H., Lu Y., Yu X., Wang J., Sun S., Liu M., Li D., Li Y-F., Zhang D. Uptake and translocation of polycyclic aromatic hydrocarbons (PAHs) and heavy metals by maize from soil irrigated with wastewater. Sci. Rep. 2017, **7**, 12165.

Zhang, J-Z., Huang, X-L. Effect of temperature and salinity on phosphate sorption on marine sediments. Environ. Sci. Technol. 2011, **45**, 6831–6837.

Zhang, Y., Li Q., Chen, Y., Dai Q., Hu, J. Dynamic change in enzyme activity and bacterial community with long-term rice cultivation in mudflats. Curr. Microbiol. 2019, **76**, 361–369.

Zhao, Y., Zhang, K., Giesy, J. P. & Hu, J. Families of nuclear receptors in vertebrate

models: characteristic and comparative toxicological perspective. Sci. Rep. 2015, **5**, 8554.

Zheng, Z., Peters, G. M., Arp, H. P. H., Andersson, P. L. Combining in silico tools with multicriteria analysis for alternatives assessment of hazardous chemicals: A case study of decabromodiphenyl ether alternatives. Environ. Sci. Technol. 2019, **53**(11), 6341–6351.

Zimmerman, J. R., Ghosh, U., Millward, R. N., Bridges, T. S., & Luthy, R. G. Addition of carbon sorbents to reduce PCB and PAH bioavailability in marine sediments: Physicochemical tests. Environ. Sci. Technol. 2004, **38**(20), 5458–5464.

Zvinavashe E., Van den Berg H., Soffers A. E. M. F., Vervoort J., Freidig A., Murk A. J., Rietjens I. M. C. M. QSAR models for predicting in vivo aquatic toxicity of chlorinated alkanes to fish. Chem. Res. Toxicol. 2008, **21**, 739–745.

ABSTRACT (IN KOREAN)

해양 환경은 육상 및 해양에서의 인간 활동으로 인해 광범위한 영향을 받는다. 해양 환경 중 조간대는 영양염류 (총질소 및 총인), 탄화수소 (유류 및 다환방향족탄화수소), 알킬페놀류, 스타이렌 올리고머를 포함한 유기 오염물질의 유입으로부터 육지와 바다 사이의 균형을 유지한다. 유기 오염물질의 거동은 물질의 물리화학적 특성에 크게 좌우된다. 더 큰 소수성 및 입자와의 반응성은 유기 오염물질이 퇴적물에 축적되게 만들고 그 결과, 퇴적물에서는 해수보다 몇 배나 더 큰 유기 오염물질의 농도를 유지한다. 해양 저서 퇴적물은 육상기인오염 물질의 최종 종착지이기 때문에 지속적인 해양 환경 생태서비스를 제공받기 위해서는 해양 환경의 유기 오염물 정화 능력과 생태독성 영향을 명확히 평가하는 것이 중요하다. 현재까지 조간대에서의 유기오염물질 정화 능력은 정량적으로 알려지지 않았고 정화 과정에서 발생하는 화학적, 독성학적, 생태학적 반응은 예측하기 어려웠다. 본 연구에서는 조간대 내 퇴적물이 정화되는 과정에서 발생하는 현상들을 실험적 규모 연구, 즉 메조코즘 연구를 통해 퇴적물의 생태위해성 평가법을 사용하여 정량적으로 확인하였다. 이를 위해 화학 분석, 생물 검정 및 저서 군집 구조 분석도 진행하였다. 그리고 인 실리고 연구를 통해 유기 오염물질의 물리화학적 특성을 분석하여 퇴적물의 정화 과정 속에서 발생하는 화학적, 독성학적, 그리고 생태학적 반응 원인을 제시하였다.

첫째로, 갯벌 퇴적물의 자정능을 평가하기 위해 $0.2m^3$ 부피의 유리 수조에 퇴적물을 이식하여 총인을 비롯한 고농도의 유기물질이 포함된 해수를 넣어 시간에 따른 변화 특성을 확인하였다. 갯벌 퇴적물은 총인 및 화학적 산소 요구량의 농도를 각각 2일 및 7일 만에 배경 농도 수준으로 제거하였다. 그리고 갯벌 퇴적물에 갈대를 심은 실험 구에서는 특히 용존 무기인을 빠르고 효율적으로 제거하였으며 이는 식생의 존재가 용존 유기 오염물질의 정화를 촉진하는 것을 의미한다. 또한 유기 오염물질의 침전은 생물학적 교란 효과가 작은 환경에서 우세한 것을 확인하였다.

둘째로, 자갈 조간대 내 유기 오염물질이 유입되었을 때를 가정하고 이를 회복하기 위한 물리적, 생물학적 기술들의 현황을 파악하고 효과를 분석하였다.

이를 위해 60일 동안의 메조코즘 연구로 잔류 유류 제거를 위한 물리적, 생물학적 기술, 그리고 자연정화능의 효과 및 영향을 비교하였다. 우선 고온고압 세척 처리는 잔류 유류를 최대 93% 제거하였다. 하지만 이와 같은 물리적 정화는 초기 정화 처리 기간 저서동물 군집에 악영향을 끼쳤다. 영양염, 유화제, 효소 활성제, 그리고 미생물 제제와 같은 생물학적 처리는 최대 66%의 잔류 유류를 제거하였다. '자연정화'는 다른 물리적 및 생물학적 기술들의 잔류 유류 제거 효과와 유사한 효율을 보여주었다. 특히 실험 기간은 미생물들의 천이를 확인하였으며 이는 시간에 따른 잔류 유류 성분의 변화 결과로 확인하였다. 자연정화는 다른 기술들만큼 유기 오염물질 제거에 효율적이었으며 특히 저서 군집에 대한 악영향을 최소화하는 특징이 있음을 확인하였다.

셋째로, 갯벌 퇴적물에서 잔류성 독성물질 특이적 정화와 생태독성 영향을 확인하기 위해 오염 퇴적물을 현장 갯벌에 이식하여 60일간 화학적, 독성학적, 그리고 생태학적 반응의 변화를 확인하였다. 그리고 머신 러닝을 통해 정화 과정 동안 오염 퇴적물의 특징을 4가지로 추출하였다. 대형저서동물과 식생이 함께 이식된 오염 퇴적물은 생물 관개 및 식물 정화 효과로 빠르게 회복되었다. 실험 기간은 잔류성 독성물질 내 다환방향족탄화수소, 알킬페놀류, 그리고 스타이렌 올리고머의 모물질들이 빠르게 감소하였는데 생물 관계 및 식물 정화로 인한 미생물의 활동으로 인한 결과임을 확인하였다.

넷째로, 매질 (해수, 퇴적물 및 해양 생물)에 대한 유기 오염물질의 반응성을 예측하기 위해 유기 오염물질의 물리화학적 성질을 분석하였습니다. 제1 원리를 활용한 밀도범함수이론을 통해 유기 오염물질과 매질 사이 반응을 정량적으로 확인할 수 있는 방향성 반응 인자를 고안하였다. 방향성 반응 모델은 유기 오염물질의 구조, 예로 벤젠 고리의 수, 메틸화 및 하이드록실화와 같은 구조적 변형이 있는 크라이센의 동족체를 대상으로 계산하였고 특히 아릴 탄화수소수용체와의 반응 관계 중심으로 적용하였다. 본 반응 모델의 결과는 크라이센 동족체의 생물검정 결과와 일치하였다. 제1 원리에 기반한 인실리코 연구는 유기 오염물질의 물리화학적 성질을 계산하였고 기존의 경험적 접근 방식을 보완하여 향후 해양 환경 내 매질 간의 반응성 예측에 활용할 수 있다.

끝으로, 독성 작용에 대한 반응 중심 접근 방법과 함께 16개의 다환방향족 탄화수소들의 생태독성 효과를 예측하기 위해 방향성 반응 모델을 응용하였다. 분자 역학 모델링 분석을 통해 아릴 탄화수소수용체와 다환방향족탄화수소의 결합 가능성을 확률적으로 계산하였고 이를 바탕으로 방향성 반응 모델과 연관시킨 방향성 반응-결합 인자를 고안하였다. 이 인자를 통해 유기 오염물질-수용체 결합을 예측할 수 있었고 나아가 생물검정 결과와 일치하는 것을 확인하였다. 잠재 독성 예측에 있어 방향성 반응-결합 인자는 유기 오염물질의 물리화학적 특성이 생물과의 독성 반응에 주요 요인이 될 수 있음을 요인이 될 수 있음 보여주었다. 향후 인 실리코 방법을 통한 유기 오염물질의 특성 분석은 생물뿐만 아니라 해수 및 퇴적물과 같은 해양 환경과의 반응 예측에 유의미하게 활용될 가능성을 확인하였다.

이상의 연구 결과를 종합해보면, 첫째, 먼저 조간대에 유입된 유기 오염물질의 농도는 초기 단계에서 전반적으로 급격한 감소를 했고, 모물질의 분해가 활발히 진행되었다. 둘째, 유기 오염물질 농도의 감소와 함께 퇴적물의 잠재 독성도 급격히 감소하였고, 유기 오염물질 농도의 감소 속도보다 더 빨랐다. 셋째, 저서 군집은 기하급수적으로 회복되었으며, 영양수준에 따라 각각의 회복 속도에 차이가 있었다. 넷째, 화학적, 독성학적, 생태학적 회복의 차이와 각 영향 관계는 유기 오염물질의 물리화학적 특성 영향에 기인한 것으로 확인되었다. 마지막으로, 본 연구의 방향성 반응 인자는 생물 내 잠재적인 독성을 예측하는 반응-결합 인자로 개발될 수 있으며 생물검정 결과와 상당히 일치한 것을 확인했다. 본 연구에서 활용한 통합적 접근은 해양 환경 내 유기 오염물질의 정화와 생태 독성학적 효과를 이해하는 데 있어 유용하게 사용될 수 있다. 앞으로 우리나라 해양 생태계 서비스의 가치를 재고하고 해안을 체계적으로 관리하기 위해서는 위와 같은 다학제적 접근이 지속해서 필요하다.

주제어: 유기 오염물질, 갯벌 정화능,
생태독성 영향, 저서 군집,
생태위해성 통합평가, 밀도범함수 이론

학 번: 2018-39302ㄴ